

***Stimuli-responsive Materials:
Developing Integrated Opto-molecular
Systems as Sensors and Actuators in
Micro-fluidic Devices***

Larisa Florea¹, B.Sc

Thesis submitted for the Degree of Doctor of Philosophy

Supervisor: Prof. Dermot Diamond¹

Dr. Fernando Benito-Lopez^{1,2}

¹CLARITY: Centre for Sensor Web Technologies, National Centre for Sensor Research, School of Chemical Sciences, Dublin City University, Dublin, Ireland;

²CIC microGUNE, Arrasate-Mondragón, Spain.

Dublin City University

June 2013



Declaration

I hereby certify that this material, which I now submit for assessment on the programme of study leading to the award of Doctor of Philosophy is entirely my own work, and that I have exercised reasonable care to ensure that the work is original, and does not, to the best of my knowledge, breach any law of copyright, and has not been taken from the work of others save and to the extent that such work has been cited and acknowledged within the text of my work.

Signed: _____

(Larisa Florea)

ID No.: _____

Date: _____

Acknowledgements

First of all I would like to thank Prof. D. Diamond for giving me the chance to work in his group, for his scientific help and for always encouraging and supporting me during my PhD. For believing in me. For being a great mentor.

I also want to thank Fernando for always seeing the best in me, in my research. For helping me with his knowledge and experience to realise my research projects. For always being there. Enthusiastic and inspiring. For being my supervisor and my friend.

A big thanks to all my other professors, mentors and supervisors for inspiring me along the years to become a researcher: Dr. E. Lahiff, Dr. R. Byrne, Prof. L. Poca, Prof. M. Peiu, Prof. V. Sitaru, Prof. F. Ilies, Prof. C. Csunderlick, Dr. M. Simon.

Thanks to Prof. D. Officer, Prof. G. Wallace, Prof. B. Paull, Prof. P. Nesterenko, Klaudia, Pawel, for all their scientific help, their kindness and for taking care of me during my research visits to Australia.

Thanks to Bartosz, Vincenzo, Cormac, Andy, Monika, Michele, Simon G, Simon C, Kevin, Caroline, Giusy, Deirdre, Mercedes, John, Claudio, Aoife, Kate, Jannick, Alexandre, David and all the people that within Clarity and NCSR helped me, each one in his own way, during my PhD.

I would like to thank my parents and my grandparents for their love and unconditional support that they have always showed me. For missing me everyday while I was in Ireland and always encouraging me.

Thanks to Ciprian for willing to join me on this island; for being my better half and my best friend.

Thanks to all my other friends: Remzi, Riki, Andreea G., Andreea M., Sorana, Raluca, Ale, Cristina, etc. For making me believe that somehow time stops. That nothing ever changes and we will be friends forever.

Mulțumiri

Aș dori să mulțumesc în primul rând Domnului Profesor D. Diamond, pentru că mi-a dat șansa să lucrez la el în grup și pentru că m-a încurajat în tot acest timp. Pentru că a crezut întotdeauna în mine și a fost un mentor excelent.

De asemenea aș dori să-i mulțumesc Domnului Dr. F. Benito-Lopez pentru că a văzut întotdeauna partea plină a paharului. Pentru că prin cunoștințele și experiența sa m-a ajutat să-mi realizez proiectele de cercetare. Pentru entuziasmul și inspirația sa. Aș dori să îi mulțumesc pentru că mi-a fost supraveghetor și prieten în același timp.

Multe mulțumiri celorlalți profesori, mentori și supraveghetori pe care am fost norocoasă să îi am pe parcursul acestor ani și care m-au inspirat să urmez o carieră în cercetare: Dr. E. Lahiff, Dr. R. Byrne, Prof. L. Poca, Prof. M. Peiu, Prof. V. Sitaru, Prof. F. Ilieș, Prof. C. Csunderlick, Dr. M. Simon. Nu va voi uita niciodată.

Multe mulțumiri profesorilor D. Officer, G. Wallace, B. Paull, P. Nesterenko, lui Klaudia și Pawel pentru tot ajutorul pe care mi l-au dat, pentru generozitatea lor și pentru că au avut grijă de mine pe parcursul șederii mele în Australia.

Aș vrea să le mulțumesc colegilor mei, Bartosz, Vincenzo, Cormac, Andy, Monika, Michele, Simon G, Simon C, Kevin, Caroline, Giusy, Deirdre, Mercedes, John, Claudio, Aoife, Kate, Jannick, Alexandre, David și tuturor celorlalți colegi din Clarity și NCSR care m-au ajutat, fiecare în felul său, pe parcursul doctoratului.

Multe mulțumiri părinților și bunicilor mei pentru dragostea lor și pentru susținerea necondiționată pe care mi-o arată întotdeauna.

Mersi iubii că m-ai însoțit pe această insulă friguroasă. Mulțumesc că ești alături de mine tot timpul, că mă faci fericită, că îmi ești partener și cel mai bun prieten.

Mulțumesc prietenilor mei: Remzi, Riki, Andreea G., Andreea M., Sorana, Raluca, Ale, Cristina, etc. Cu voi, viața e mai frumoasă.

List of Publications:

Peer-reviewed articles

- 1- **“Study of the N-methylcarbamylsuccinamic Acid Synthesis,”** Palani Adil, Larisa Florea, Evangelos Gerasimou, Carol Csunderlik, Monika Simon, *Revista de Chimie*, 61 (2010), 838-840.
- 2- **“Modified Polyaniline Nanofibres for Ascorbic Acid Detection,”** Larisa Florea, Emer Lahiff, Dermot Diamond, *MRS Proceedings 2011*, 1312, mrsf10-1312-hh09-03, doi:10.1557/opl.2011.672.
- 3- **“Photo-detection of Solvent Polarities using Non-invasive Coatings in Capillaries,”** Larisa Florea, Fernando Benito-Lopez, Alexandre Hennart, Dermot Diamond, *Procedia Engineering* 25 (2011) 1545 – 1548.
- 4- **“Synthesis and Characterisation of Spiropyran-polymer Brushes in Micro-capillaries: Towards an Integrated Optical Sensor for Continuous Flow Analysis,”** Larisa Florea, Alexandre Hennart, Dermot Diamond, Fernando Benito-Lopez, *Sensors and Actuators B: Chem.* 175 (2012) 92-99.
- 5- **“Photo-responsive Polymeric Structures based on Spiropyran,”** Larisa Florea, Dermot Diamond, Fernando Benito-Lopez, *Macromolecular Materials and Engineering*, 297 (2012) 1148-1159 (article featured on the cover).
- 6- **“Dynamic pH Mapping in Micro-fluidic Devices by Integrating Adaptive Coatings based on Polyaniline with Image Processing Techniques,”** Larisa Florea, Cormac Fay, Emer Lahiff, Dermot Diamond, Fernando Benito-Lopez, *Lab Chip* 13 (2013) 1079-1085.
- 7- **“Polyaniline Coated Micro-capillaries for Continuous Flow Analysis of Aqueous Solutions,”** Larisa Florea, Dermot Diamond, Fernando Benito-Lopez, *Analytica Chimica Acta* 759 (2013) 1-7 (article featured on the cover).
- 8- **“Temperature and pH triggered release characteristics of water: fluorescein from 1-ethyl-3-methylimidazolium ethylsulfate based ionogels,”** Simon Gallagher, Andrew Kavanagh, Larisa Florea, Douglas R. MacFarlane, Kevin J. Fraser and Dermot Diamond, *Chemical Communications*, 49 (2013), 4613-4615.
- 9- **“Spiropyran Polymeric Micro-capillary Coatings for Photo-detection of Solvent Polarity,”** Larisa Florea, Aoife McKeon, Dermot Diamond, Fernando Benito-Lopez, *Langmuir* 29 (2013) 2790-2797.
- 10- **“A merocyanine-based conductive polymer,”** Klaudia Wagner, Michele Zannoni, Anastasia B. S. Elliott, Pawel Wagner, Robert Byrne, Larisa E. Florea, Dermot Diamond, Keith C. Gordon, Gordon G. Wallace, David L. Officer, *Journal of Material Chemistry (C)*, 2013, accepted, DOI: 10.1039/c3tc30479e.
- 11- **“Self-protonating spiropyran-co-NIPAM-co-acrylic acid hydrogels as reversible photoactuators,”** Bartosz Ziółkowski, Larisa Florea, Jannick Theobald, Fernando Benito-Lopez and Dermot Diamond, *Soft Matter*, 2013, *submitted*.
- 12- **“Self-assembled Solvato-morphologically Controlled Photochromic Crystals,”** Larisa Florea, Fernando Benito-Lopez, Dermot Diamond, *Angewandte Chemie International Edition*, *submitted*.
- 13- **“Photo-activated Chemopropulsion of Organic Droplets,”** Larisa Florea, Klaudia Wagner, Pawel Wagner, David L. Officer, Gordon W. Wallace, Fernando Benito-Lopez, Dermot Diamond, *manuscript in preparation*.

- 14- **“Micro-capillary Systems Integrating Photo-controlled Molecular Cranes for Metal Ion Accumulation, Sensing and Release in Continuous Flow”**, Larisa Florea, Pavel Nesterenko, Brett Paull, Fernando Benito-Lopez, Dermot Diamond, *manuscript in preparation*.
- 15- **“Sensing the Flow: Adaptive Coating based on Polyaniline for Direct Observation of Mixing Processes in Micro-Fluidic Systems”**, Larisa Florea, Mustafa Tutar, Kate Meagher, Fernando Benito-Lopez, Dermot Diamond, *manuscript in preparation*.
- 16- **“Reversible photo-actuated porous hydrogels for micro-fluidics applications”** Bartosz Ziolkowski, Larisa Florea, Jannick Theobald, Fernando Benito-Lopez and Dermot Diamond, *manuscript in preparation*.

Book Chapters

1. **“Opto-smart Systems in Microfluidics,”** Larisa Florea, Dermot Diamond, Fernando Benito-Lopez, book chapter - *Pan Stanford Publishing Pte Ltd*, 2013, *accepted*.

Patents

- 1- **“Self-protonating spiropyran-co-NIPAM-co-acrylic acid hydrogels as reversible photoactuators,”** Bartosz Ziolkowski, Larisa Florea, Jannick Theobald, Dermot Diamond – patent application filed.

Conference Presentations

- 1- **“Negative Phototaxis Behaviour of Organic Droplets in Channels”**, Larisa Florea, Klaudia Wagner, Pawel Wagner, David L. Officer, Gordon W. Wallace, Fernando Benito-Lopez, Dermot Diamond, 17th International Conference on Miniaturized Systems for Chemistry and Life Sciences, Micro Total Analysis Systems μ TAS, Freiburg, Germany, 27-31 October, 2013. (**abstract submitted**)
- 2- **Self-Assembled Solvato-Morphologically Controlled Photochromic Crystals**, Larisa Florea, Fernando Benito-Lopez, Dermot Diamond, XXII International Materials Research Congress, Cancún, Mexico, 11-15 August 2013 (**oral accepted**).
- 3- **“Crystal Moths, Exploding Capsules, Micro-Vehicles and Hairy Capillaries: Using Self-Assembly to Generate Functional Platforms”**, Larisa Florea, Fernando Benito-Lopez, Dermot Diamond, EuroNanoforum, Dublin, Ireland, 18-26 June, 2013. (**poster accepted**)
- 4- **“Multi-purpose Capillary-integrated Optical Sensors Based on Spiropyran”**, Larisa Florea, Fernando Benito-Lopez*, Dermot Diamond, EuroNanoforum, Dublin, Ireland, 18-26 June, 2013. (**poster accepted**)
- 5- **“Polyaniline Coated Micro-capillaries for Continuous Flow Analysis of Aqueous Solutions”**, Larisa Florea, F. Benito-Lopez, D. Diamond, ATWARM International Conference 2013 *“Water - The Greatest Global Challenge”*, Dublin, Ireland, 14-16 May, 2013. (**poster presentation**)
- 6- **“Investigations into the Use of Microcantilever Arrays Activated with Photoactive Spiropyran as a Model System to Measure Surface Stress Changes”**, C. Grogan, L. Florea, S. Scarmagnani, D. Diamond, F. Benito-Lopez, F. Lyng, F. Pedreschi, R. Raiteri, 10th International Workshop on Nanomechanical Sensing (NMC 2013), Stanford, USA, 49, 1-3 May, 2013. (**poster presentation**)
- 7- **“Micro-capillary systems integrating photo-controlled molecular cranes for metal ion accumulation, sensing and release in continuous flow”**, Larisa Florea,

Dermot Diamond, Fernando Benito-Lopez, The Sixteenth International Conference on Miniaturized Systems for Chemistry and Life Sciences (μ TAS 2012), Okinawa, Japan, October 28 - November 1, 2012. **(Shortlisted for best poster)**

- 8- **“Adaptive Polymeric Materials: Developing Integrated Opto-chemical Sensors in Micro-fluidic Devices”**, Larisa Florea, Dermot Diamond, Fernando Benito-Lopez, 2nd International Symposium on Functional Nanomaterials, Dublin, Ireland, 6-7 September, 2012. **(poster presentation)**
- 9- **“Functional Materials: Smart Solutions to Generate Useful Micro-fluidic Devices”**, Fernando Benito-Lopez, Larisa Florea, Vincenzo F. Curto, Monika Czugala, Dermot Diamond, 2nd International Symposium on Functional Nanomaterials, Dublin, Ireland, 6-7 September, 2012. **(oral presentation)**
- 10- **"Photo-responsive polymeric structures based on spiropyran"**, Larisa Florea, Dermot Diamond, Fernando Benito-Lopez, 4th International Conference "Smart Materials, Structures and Systems, Montecatini Terme, Italy, 10-12 June 2012. **(oral presentation)**
- 11- **“Photoswitchable Behaviour of New Spiropiran Derivatives”**, Dermot Diamond, Larisa Florea, Fernando Benito-Lopez, Vincenzo F. Curto, SmartSurfaces2012: Solar & BioSensor Applications, Dublin, Ireland, 6-9 March, 2012. **(oral presentation)**
- 12- **“Photo- and electro-active materials in micro-fluidic devices”**, 7th Annual International Electromaterials Science Symposium”, Larisa Florea, Emer Lahiff, Fernando Benito-Lopez, Dermot Diamond, Geelong, Australia, 15-17 February 2012. **(poster presentation)**
- 13- **“Adaptive Polymeric Materials: Developing Integrated Opto-chemical Sensors in Micro-fluidic Devices,”** Larisa Florea, Dermot Diamond, Fernando Benito-Lopez – Monash University, Melbourne, Australia, 13-14th February 2012. **(invited talk)**
- 14- **"Spiropyran modified micro-capillaries as photonically controlled self-indicating systems for metal ion accumulation and release,"** Larisa Florea, Dermot Diamond, Fernando Benito-Lopez, 11th Asia-Pacific International Symposium on Microscale Separations and Analysis, Hobart, Tasmania, Australia, 27 - 30 November 2011. **(oral presentation)**
- 15- **"Adaptive Coatings in Micro-Capillaries and Micro-Channels as New Means to Develop Integrated Micro-Fluidic Optical Sensors"**, Larisa Florea, Dermot Diamond, Fernando Benito-Lopez, Seminar in Micro-fluidics, University California Berkeley, California, USA, 10th Oct 2011. **(invited talk)**
- 16- **“Sensing the Flow: Adaptive Coating based on Polyailine for Direct Observation of Mixing Processes in Micro-Fluidic Systems,”** Larisa Florea, Emer Lahiff, Dermot Diamond and Fernando Benito-Lopez, MicroTas, Seattle, October 2-6, 2011. **(Shortlisted for best poster).**
- 17- **“Dynamic pH Sensing in Micro-Fluidic Devices using Adaptive Coatings Based on Polyaniline,”** Larisa Florea, Emer Lahiff, Dermot Diamond and Fernando Benito-Lopez, MicroTas, Seattle, October 2-6, 2011. **(Shortlisted for best poster)**
- 18- **“Photo-Detection of Solvent Polarities using Non-Invasive Coatings in Capillaries,”** Larisa Florea, Fernando Benito-Lopez, Alexandre Hennart, Dermot Diamond – Euroensors, Athens, Greece, 4-7 September, 2011. **(oral presentation)**
- 19- **“New Functional Materials for Fluid Control and Sensing in Microfluidic Devices”**, Fernando Benito-Lopez, Larisa Florea, Vincenzo F. Curto, Monika Czugala, Kevin J. Fraser, Shirley Coyle, Robert Byrne, Dermot Diamond, University California Berkeley, California, USA, 14th July 2011. **(invited talk)**

- 20- **“Adaptive Coatings Based on Polyaniline for Dynamic pH Sensing in Micro-Fluidic Devices,”** Larisa Florea, Emer Lahiff, Dermot Diamond and Fernando Benito-Lopez, 63rd Irish Universities Chemistry Research Colloquium 2011, Dublin, June 23-24, 2011. **(poster presentation)**
- 21- **“New Functional Materials for Fluid Control and Sensing in Microfluidic Devices,”** Larisa Florea, Vincenzo F. Curto, Monika Czugała, Robert Byrne, Shirley Coyle, Dermot Diamond, Fernando Benito-Lopez, University of Granada, Spain, 10th June 2011. **(invited talk)**
- 22- **“Use of a photo-actuated Microcantilever Array Sensing System to Investigate Surface Stress Changes of photo-activated molecular films,”** Catherine Grogan, Slavica Koprivica, Larisa Florea, Silvia Scarmagnani, Dermot Diamond, Fernando Benito Lopez, Fiona Lyng, Fran Pedreschi and Roberto Raiteri, 8th International Workshop on Nanomechanical Sensing, Dublin, Ireland, May 11-13, 2011. **(poster presentation)**
- 23- **“Functionalisation of glass fibres and micro-fluidic channels via polymer brushes,”** Larisa Florea, Fernando Benito-Lopez, Emer Lahiff, Dermot Diamond – Conference on Analytical Sciences Ireland 2011, 6th CASi, Dublin, 21-22 February 2011. **(poster presentation)**
- 24- **“Self-Doped Carboxylated Polyaniline Nanofibres,”** Larisa Florea, Emer Lahiff, Dermot Diamond, MRS Fall Meeting, Boston, November 29 - December 3, 2010. **(oral presentation)**
- 25- **“Self-Doped Polyaniline Nanofibres,”** Larisa Florea, Emer Lahiff, Dermot Diamond. UNCSR Symposium, Dublin, October 2010. **(poster presentation)**
- 26- **“Self-doping polyaniline nanofibres,”** Larisa Florea, Emer Lahiff, Dermot Diamond, EMRS Spring Meeting, Strasbourg, 7-11 June 2010. **(oral presentation)**
- 27- **“Self-Doped Carboxylated Polyaniline Nanofibres,”** Larisa Florea, Emer Lahiff, Dermot Diamond, MRS Fall Meeting, Boston, November 29 - December 3, 2010. **(oral presentation)**
- 28- **“Study of N-methylcarbamoyl succinamic acid synthesis,”** Larisa Florea, Ana-Maria Raduta, Monika Simon, Carol Csunderlik, Adil Palani, “Timisoara’s Academic Days- Chemistry Symposium”, XI-th Edition, 28-29 May 2009 **(poster presentation)**
- 29- **“Study of N-methylcarbamoyl succinamic acid synthesis,”** Larisa Florea, Ana-Maria Raduta, Monika Simon, Carol Csunderlik, “13-th International Symposium for students in Chemistry”, Timisoara, 21-22 November 2008. **(oral presentation)**
- 30- **“Condensation of succinamic anhydride with monosubstituted ureas,”** Larisa Florea, Ana-Maria Raduta, Monika Simon, Carol Csunderlik, “XXX-th Romanian chemistry conference”, Calimanesti-Caciulata, 8-10 October 2008. **(poster presentation)**
- 31- **“Solid state electrolytes based on Ionic Liquids,”** Larisa Florea, Robert Byrne, Dermot Diamond, National Centre of Sensor Research, Dublin City University, “DiaMonD UREKA programme – One-day Symposium”, 15 August 2008. **(oral presentation and poster presentation)**
- 32- **“Synthesis of oxazolidinones using bis(o-nitrophenyl) carbonate,”** Larisa Florea, Ildiko Kecseti, Ramona Onea, Valentin Dobre, Monika Simon, Carol Csunderlik, “C.D. Nenitescu” - Conference for Students in Chemistry, Bucharest 8-9 November 2007. **(oral presentation)**

Overall Aim and Thesis Structure

Overall Aim

The aim of this thesis is to explore the concept of optical sensing using micro-fluidics by coating the inner walls of a micro-channel or micro-capillary with stimuli-responsive polymeric materials based on polyaniline and spiropyran, respectively. The polymerisation techniques are discussed and the resulting coatings characterised with a variety of techniques. Analysis of these coatings, presented in Chapters 4 to 7, show that they are suitable for pH, ammonia (polyaniline based coatings), and solvent (spiropyran polymeric coatings) detection in micro-fluidic devices used in continuous flow mode.

In the last two experimental chapters, Chapter 8 and 9, for the first time we present the potential of using spiropyran for;

- Photo-initiation of chemopropulsion of organic droplets in fluidic channels, and;
- Solvato-morphological control of self-assembled spiropryan micro-structures.

The experimental chapters (Chapters 4 to 9) illustrate the progress made in the integration of stimuli-responsive materials within fluidic platforms for sensing or actuating purposes, and hopefully give the reader an overview of the exciting potential of this research for micro-fluidic applications.

Selected publications and author contribution

This thesis includes one literature survey chapter, one review article published in a peer reviewed journal, one book chapter accepted for publication, four original papers published in peer reviewed journals, two submitted publications and one future work and perspectives chapter. The core theme of the thesis is stimuli-responsive materials used for the development of sensors and actuators in micro-fluidic devices. The ideas, development and writing up of all the papers in the thesis were the principal responsibility of myself, the candidate, working within CLARITY: Centre for Sensor Web Technologies, National Centre for Sensor Research, School of Chemical Sciences, Dublin City University under the supervision of Professor Dermot Diamond and Dr. Fernando Benito-Lopez.

The inclusion of co-authors reflects the fact that part of the work came from active collaboration between researchers and acknowledges input into team-based research.

In the case of Chapters 2 to 9, my contribution to the work was as follows:

| Thesis Chapter | Publication title | Publication status* | Nature and extent of candidate's contribution |
|-----------------------|---|--|--|
| 2 | Photo-responsive Polymeric Structures based on Spiropyran | Published. <i>Macromolecular Materials and Engineering</i> , 297 (2012) 1148-1159 | First author, manuscript development and writing up. |
| 3 | Opto-smart Systems in Microfluidics | Accepted. book chapter - <i>Pan Stanford Publishing Pte Ltd</i> (2013) | First author, manuscript development and writing up. |
| 4 | Polyaniline Coated Micro-capillaries for Continuous Flow Analysis of Aqueous Solutions | Published. <i>Analytica Chimica Acta</i> 759 (2013) 1-7 | First author, key ideas, experimental design, data collection and analysis, manuscript development and writing up. |
| 5 | Dynamic pH Mapping in Micro-fluidic Devices by Integrating Adaptive Coatings based on Polyaniline with Image Processing Techniques | Published. <i>Lab on a Chip</i> 13 (2013) 1079-1085. | First author, key ideas, experimental design, data collection and analysis, manuscript development and writing up. |
| 6 | Synthesis and Characterisation of Spiropyran-polymer Brushes in Micro-capillaries: Towards an Integrated Optical Sensor for Continuous Flow Analysis | Published. <i>Sensors and Actuators B: Chem.</i> 175 (2012) 92-99. | First author, key ideas, data collection and analysis, manuscript development and writing up. |
| 7 | Spiropyran Polymeric Micro-capillary Coatings for Photo-detection of Solvent Polarity | Published. <i>Langmuir</i> 29 (2013) 2790-2797. | First author, key ideas, experimental design, data collection and analysis, manuscript development and writing up. |
| 8 | Photo-activated Chemopropulsion of Organic Droplets | In preparation | First author, key ideas, experimental design, data collection and analysis, writing up. |
| 9 | Self-assembled Solvato-morphologically Controlled Photochromic Crystals | Submitted, <i>Angewandte Chemie Int. Ed.</i> | First author, key ideas, experimental design, data collection and analysis, writing up. |

Signed:

(Candidate)



.....
(Co-Supervisor)

.....

(Principal Supervisor)

.....

Date

* For example, 'published'/'in press'/'accepted'/'returned for revision'/'submitted'

Chapter Overview

A detailed overview of each chapter together with particular contributions from research collaborators (where applicable), are given below:

Chapter 1: Literature Survey

This introduction chapter gives a detailed overview of the themes common to all papers included in the thesis and sets the following chapters in the context of existing literature. Important topics including: micro-fluidics, optical sensors, adaptive polymeric materials, polyaniline and spiropyran, are widely discussed in order to inform the reader on the concepts that will be further used in the experimental chapters (Chapter 4 to 9). Moreover, this chapter presents the context in which the experimental chapters below contribute to the scientific advancement of the research area.

Chapter 2: Photo-responsive Polymeric Structures based on Spiropyran

This review chapter discusses the most recent examples of using polymeric structures based on spiropyran and their potential for a variety of applications ranging from photochromism and actuation to sensing purposes. The chapter highlights that smart molecular engineering of spiropyran functionalised polymer offers unique, unprecedented control over the characteristics of the end-material, and indicates aspects where there is a need for further innovation in the field.

Chapter 3: Opto-smart Systems in Micro-fluidics

This work, accepted as a book chapter, illustrates the most advanced ways to achieve photo-control flow in micro-fluidic channels throughout the use of photo-responsive molecules. The possibility of controlling flow in closed microchannels, and manipulating discrete microliter-sized droplets by employing photo- and thermo-responsive materials incorporated in micro-fluidic units in the form of polymeric actuators, photo-responsive coatings or photo-sensitive surfactants is discussed.

Chapter 4: Polyaniline Coated Micro-capillaries for Continuous Flow Analysis of Aqueous Solutions

This work, published as an original article illustrates the coating of fused silica micro-capillaries for aqueous ammonia sensing in continuous flow. The coatings are characterised through a variety of spectroscopic and imaging techniques to confirm their chemical structure, their morphology and their doping-dedoping properties.

Chapter 5: Dynamic pH Mapping in Micro-fluidic Devices by Integrating Adaptive Coatings based on Polyaniline with Image Processing Techniques

This work, published as an original article, describes the coating of PDMS/glass and PDMS/PDMS micro-channels with adaptive materials based on polyaniline. These coatings are characterised *'in situ'* through different spectroscopic and imaging techniques and their potential for pH sensing in continuous flow is demonstrated. Moreover, as the entire coated micro-channel possessed pH sensing properties, gradient pH sensing is also verified. This work has been done in collaboration with the engineering department at the NCSR, in particular with Mr. Cormac Fay, who developed the imaging processing algorithms.

Chapter 6: Synthesis and Characterisation of Spiropyran-polymer Brushes in Micro-capillaries: Towards an Integrated Optical Sensor for Continuous Flow Analysis

In this work, published as an original article, it has been demonstrated for the first time, the coating of a micro-capillary with spiropyran polymeric brushes obtained by surface-initiated ring opening metathesis polymerisation. This approach opens a new direction in the field of polymeric brushes and illustrates the great photochromic properties of the spiropyran unit inside the coating. The high density of the photochromic unit suggests the possibility of using this type of capillaries for sensing purposes in continuous flow based on the inherited spiropyran properties.

Chapter 7: Spiropyran Polymeric Micro-capillary Coatings for Photo-detection of Solvent Polarity

This work, published as an original article, presents several improvements performed to the coatings presented in Chapter 6 and confirms their potential as spiropyran-polymeric coatings in micro-capillaries for solvent sensing in continuous flow.

Chapter 8: Photo-activated Chemopropulsion of Organic Droplets

This work represents the current state-of-the-art in droplet actuation. The innovative approach consists in the combination of pH sensitive surfactants and photo-stimulated pH pumps (spiropyran). This procedure offers photo-actuation of droplets with great speeds, about 14 times faster than previous reported photo-actuated droplets. This work has been realised in collaboration with IPRI, Wollongong, Australia, where the spiropyran derivative was synthesised.

Chapter 9: Self-assembled Solvato-morphologically Controlled Photochromic Crystals

This work, recently submitted as communication, describes, for the first time, intriguing solvato-morphological control of photochromic micro-structures based on spiropyran. By simply changing the ratio of the solvents forming the aqueous phase, selective control of the formation of molecular assemblies at the liquid/air interface as well as the morphology (flat crystals to ribbon-like structures) and the dimensions ($\sim 10\text{-}80\text{ }\mu\text{m}$) of the resulting 3D structures can be easily achieved. Moreover, these microstructures exhibit reversible photoisomerization upon light irradiation in the solid state. Finally, guided aggregation of these micro-structures was also demonstrated. The spiropyran derivative used in this study was synthesised by Dr. S. Scarmagnani.

Chapter 10: Future Work and Perspectives

This chapter suggests possible following paths of the work presented in this thesis. Several new strategies for the development of novel miniaturised sensing platforms and new means of droplet/micro-gel actuation are proposed.

Table of Contents

| | |
|--|-----------|
| THESIS ABSTRACT | 1 |
| LIST OF ABBREVIATIONS | 2 |
| CHAPTER 1 – LITERATURE SURVEY | 4 |
| 1.1 MICRO-FLUIDICS AND LAB ON A CHIP DEVICES | 5 |
| 1.2 OPTO-CHEMICAL SENSORS | 5 |
| 1.3 SURFACE FUNCTIONALISATION | 7 |
| 1.4 ADAPTIVE POLYMERIC MATERIALS | 9 |
| 1.4.1 CONDUCTING POLYMERS | 10 |
| 1.4.1.1 OVERVIEW | 10 |
| 1.4.1.1 POLYANILINE | 11 |
| 1.4.2 PHOTO-RESPONSIVE MATERIALS | 19 |
| 1.4.2.1 OVERVIEW | 19 |
| 1.4.2.1 SPIROBENZOPYRANS | 20 |
| 1.4.3 INTEGRATION IN MICRO-FLUIDIC DEVICES | 29 |
| 1.4.3.1 VALVES | 30 |
| 1.4.3.2 PUMPS | 34 |
| 1.4.3.3 COATINGS | 36 |
| 1.5 REFERENCES | 39 |
| CHAPTER 2 – PHOTO-RESPONSIVE POLYMERIC STRUCTURES BASED ON SPIROPYRAN | 47 |
| ABSTRACT | 49 |
| 2.1 INTRODUCTION | 50 |
| 2.2 SPIROPYRAN-BASED POLYMERS | 53 |
| 2.3 PHOTO-MODULATED WETTABILITY | 56 |
| 2.4 PHOTO-MODULATED PERMEABILITY | 58 |
| 2.5 PHOTO-ACTUATION | 60 |
| 2.6 PHOTO-MODULATED ELECTRICAL PROPERTIES | 62 |
| 2.7 SENSING CAPABILITIES | 64 |
| 2.8 MECHANOCROMIC MECHANOPHORES | 68 |
| 2.9 CONCLUSIONS | 69 |
| 2.10 REFERENCES | 70 |
| CHAPTER 3 – OPTO-SMART SYSTEMS IN MICRO-FLUIDICS | 76 |
| ABSTRACT | 77 |
| 3.1 INTRODUCTION | 78 |
| 3.2 OPTO-SMART SYSTEMS INTEGRATION IN MICRO-FLUIDIC DEVICES | 79 |
| 3.2.1 PHOTO-CONTROLLED POLYMERIC ACTUATORS | 81 |
| 3.2.2 PHOTO-CONTROL OF ELECTRO-OSMOTIC FLOW | 90 |
| 3.2.3 PHOTO-MANIPULATION OF DROPLETS | 93 |

| | |
|--|-------------------|
| 3.3 CONCLUSIONS | 97 |
| 3.4 REFERENCES | 98 |
| <u>CHAPTER 4 – POLYANILINE COATED MICRO-CAPILLARIES FOR CONTINUOUS FLOW ANALYSIS OF AQUEOUS SOLUTIONS</u> | <u>104</u> |
| ABSTRACT | 106 |
| 4.1 INTRODUCTION | 107 |
| 4.2 EXPERIMENTAL | 108 |
| 4.2.1 MATERIALS AND METHODS | 108 |
| 4.2.2 FUSED SILICA MICRO-CAPILLARIES COATING PROTOCOL | 109 |
| 4.2.3 POLYANILINE COATINGS IMAGING PROTOCOL | 110 |
| 4.3 RESULTS AND DISCUSSION | 111 |
| 4.3.1 POLYANILINE COATINGS | 111 |
| 4.3.1.1 MORPHOLOGICAL ANALYSIS | 111 |
| 4.3.1.2 STRUCTURAL ANALYSIS | 112 |
| 4.3.1.3 OPTICAL PROPERTIES OF THE COATING | 114 |
| 4.3.2 AMMONIA SENSING | 117 |
| 4.4 CONCLUSIONS | 119 |
| 4.5 REFERENCES | 120 |
| <u>CHAPTER 5 – DYNAMIC pH MAPPING IN MICRO-FLUIDIC DEVICES BY INTEGRATING ADAPTIVE COATINGS BASED ON POLYANILINE WITH COLORIMETRIC IMAGING TECHNIQUES</u> | <u>123</u> |
| ABSTRACT | 124 |
| 5.1 INTRODUCTION | 125 |
| 5.2 EXPERIMENTAL | 127 |
| 5.2.1 MICRO-FLUIDIC DEVICE FABRICATION | 127 |
| 5.2.2 MICRO-FLUIDIC DEVICE FUNCTIONALISATION | 127 |
| 5.2.3 MEASUREMENTS OF ABSORBANCE SPECTRA OF PANI COATINGS | 129 |
| 5.2.4 DIGITAL IMAGE CAPTURE | 130 |
| 5.2.5 IMAGE PROCESSING | 131 |
| 5.3 RESULTS AND DISCUSSION | 131 |
| 5.3.1 CHARACTERISATION OF THE PANI COATINGS | 131 |
| 5.3.2 pH MEASUREMENTS | 132 |
| 5.3.3 pH DETERMINATION VIA COLORIMETRIC IMAGING ANALYSIS | 135 |
| 5.3.4 GRADIENT pH MEASUREMENTS | 136 |
| 5.4 CONCLUSIONS | 139 |
| 5.5 REFERENCES | 140 |
| <u>CHAPTER 6 – SYNTHESIS AND CHARACTERISATION OF SPIROPYRAN-POLYMER BRUSHES IN MICRO-CAPILLARIES: TOWARDS AN INTEGRATED OPTICAL SENSOR FOR CONTINUOUS FLOW ANALYSIS</u> | <u>144</u> |
| ABSTRACT | 145 |
| 6.1 INTRODUCTION | 146 |
| 6.2 EXPERIMENTAL | 148 |

| | |
|---|-------------------|
| 6.2.1 MATERIALS | 148 |
| 6.2.2 PROCEDURES | 149 |
| 6.2.2.1 SYNTHESIS OF SPIROPYRAN FUNCTIONALISED NORBORNENE MONOMER | 149 |
| 6.2.2.2 CHARACTERISATION OF SPIROPYRAN FUNCTIONALISED NORBORNENE MONOMER | 150 |
| 6.2.2.3 FUSED-SILICA MICRO-CAPILLARIES COATING PROTOCOL | 150 |
| 6.2.2.4 ESTIMATION OF THE MOLAR EXTINCTION COEFFICIENT OF THE SP-M | 151 |
| 6.2.2.5 MORPHOLOGICAL CHARACTERISATION OF THE POLYMER BRUSHES | 151 |
| 6.2.2.6 OPTICAL CHARACTERISATION OF THE SPIROPYRAN COATINGS | 152 |
| 6.3 RESULTS AND DISCUSSION | 153 |
| 6.3.1 STRUCTURE CHARACTERISATION AND PHOTOINDUCED CONVERSION OF SP TO MC | 153 |
| 6.3.2 POLYMER BRUSHES LENGTH ANALYSIS | 155 |
| 6.3.3 PHOTO-PATTERNING OF SPIROPYRAN-MEROCYANINE FORMS IN THE CAPILLARY | 155 |
| 6.3.4 CHARACTERISATION OF SP-MONOMER IN SOLUTION AND SP-POLYMER BRUSHES IN THE CAPILLARY BY UV-VIS SPECTROSCOPY | 157 |
| 6.3.5 SWITCHING PROPERTIES OF THE SP-POLYMER BRUSHES IN THE CAPILLARY BY UV-VIS SPECTROSCOPY | 159 |
| 6.4 CONCLUSIONS | 161 |
| 6.5 REFERENCES | 161 |
| <u>CHAPTER 7 – SPIROPYRAN POLYMERIC MICRO-CAPILLARY COATINGS FOR PHOTO-DETECTION OF SOLVENT POLARITY</u> | <u>165</u> |
| ABSTRACT | 166 |
| 7.1 INTRODUCTION | 167 |
| 7.2 MATERIALS AND METHODS | 170 |
| 7.2.1 REAGENTS | 170 |
| 7.2.2 SYNTHESIS OF SPIROPYRAN FUNCTIONALISED NORBORNENE MONOMER (SP-M) | 170 |
| 7.2.3 SYNTHESIS OF SPIROPYRAN POLYMERIC BRUSHES (POLY(SP-M)) | 171 |
| 7.2.4 CHARACTERISATION | 171 |
| 7.2.5 LIGHT SOURCE | 172 |
| 7.2.6 PHOTOCHEMICAL METHODS | 172 |
| 7.3 RESULTS AND DISCUSSION | 173 |
| 7.3.1 (SP-M) POLYMERIC COATINGS | 173 |
| 7.3.2 SOLVENT SENSING | 174 |
| 7.3.3 KINETICS OF PHOTO-INDUCED RING OPENING | 180 |
| 7.4 CONCLUSIONS | 183 |
| 7.5 REFERENCES | 184 |
| <u>CHAPTER 8 – PHOTO-ACTIVATED CHEMOPROPULSION OF ORGANIC DROPLETS</u> | <u>188</u> |
| ABSTRACT | 189 |
| 8.1 INTRODUCTION | 190 |
| 8.2 MATERIALS AND METHODS | 191 |
| 8.2.1 MATERIALS | 191 |
| 8.2.2 CHANNEL FABRICATION | 191 |
| 8.3 RESULTS AND DISCUSSION | 191 |
| 8.4 CONCLUSIONS | 197 |
| 8.5 REFERENCES | 198 |

| | |
|--|------------|
| CHAPTER 9 – SELF-ASSEMBLED SOLVATO-MORPHOLOGICALLY CONTROLLED PHOTOCHROMIC CRYSTALS | 200 |
| ABSTRACT | 201 |
| 9.1 INTRODUCTION | 202 |
| 9.2 EXPERIMENTAL | 204 |
| 9.3 RESULTS AND DISCUSSION | 204 |
| 9.4 CONCLUSIONS | 210 |
| 9.5 REFERENCES | 210 |
| CHAPTER 10 – FUTURE WORK AND PERSPECTIVES | 214 |
| 10.1 SENSING THE FLOW: ADAPTIVE COATINGS BASED ON POLYANILINE FOR DIRECT OBSERVATION OF MIXING PROCESSES IN MICRO-FLUIDIC SYSTEMS | 216 |
| 10.1.1 INTRODUCTION | 216 |
| 10.1.2 DIRECT OBSERVATION OF MIXING PROCESSES IN MICRO-FLUIDIC SYSTEMS | 217 |
| 10.2 SPIROPYRAN FUNCTIONALISED MICRO-CAPILLARIES FOR METAL ION SENSING, ACCUMULATION, RELEASE AND EXTRACTION | 220 |
| 10.2.1 INTRODUCTION | 220 |
| 10.2.2 METAL IONS SENSING – QUALITATIVE STUDIES | 221 |
| 10.2.3 METAL IONS ACCUMULATION AND RELEASE – QUANTITATIVE STUDIES | 225 |
| 10.2.3.1 DETECTION OF THE PHOTO-RELEASE OF METAL IONS USING CAPACITIVELY COUPLED CONTACTLESS CONDUCTIVITY DETECTION | 225 |
| 10.2.3.2 DETECTION OF THE PHOTO-RELEASE OF METAL IONS USING POST-COLUMN DERIVATISATION | 226 |
| 10.2.4 METAL IONS EXTRACTION | 229 |
| 10.3 PHOTO-ACTIVATED PROPULSION OF IONOGEL BOATS | 230 |
| 10.3.1 INTRODUCTION | 230 |
| 10.3.2 FROM ORGANIC DROPLETS TO IONOGELS | 231 |
| 10.3.2.1 IONOGEL BOATS – FIRST GENERATION | 231 |
| 10.3.2.2 IONOGEL BOATS – SECOND GENERATION | 232 |
| 10.4 CONCLUSIONS | 234 |
| 10.5 REFERENCES | 236 |
| APPENDIX A | A1 |
| APPENDIX B | B1 |
| B.1 MATERIALS AND METHODS | B2 |
| B.2 DIGITAL IMAGE CAPTURE | B3 |
| B.3 CHARACTERISATION OF POLYANILINE (PANI) COATING BY RAMAN SPECTROSCOPY | B5 |
| B.4 pH MEASUREMENTS | B7 |
| B.5 pH DETERMINATION VIA COLORIMETRIC IMAGING ANALYSIS | B8 |
| B.6 REFERENCES | B9 |
| APPENDIX C | C1 |
| C.1 KINETICS OF PHOTO-INDUCED RING OPENING OF POLY(SP-M) COATINGS | C2 |
| C.2 KINETICS OF PHOTO-INDUCED RING OPENING OF SP-M MONOMER IN SOLUTION | C3 |

| | |
|---|------------|
| APPENDIX D | D1 |
| D.1 CHARACTERISATION OF SPIROPYRAN SULFONIC ACID (SP-SO₃H) | D2 |
| D.2 PHOTOIRRADIATION | D2 |
| D.3 SPECTRAL MEASUREMENTS | D2 |
| D.4 PENDING DROPLET METHOD | D2 |
| D.5 UV-VIS SPECTROSCOPY OF SP-SO₃H | D2 |
| D.6 KINETICS OF PHOTO-INDUCED RING CLOSING | D4 |
| D.7 UV-VIS SPECTROSCOPY OF CHROMOIONOPHORE I (C1) | D5 |
| D.8 SURFACE TENSION MEASUREMENTS | D6 |
| D.9 DROPLET BEHAVIOR UNDER DIFFERENT pH CONDITIONS | D8 |
| D.10 MECHANISM OF PHOTO-PROPELLED MOTION OF DROPLET | D8 |
| D.11 EXAMPLES OF PHOTOACTIVATED CHEMOPROPULSION | D10 |
| D.12 REFERENCES | D10 |
| APPENDIX E | E1 |
| E.1 SYNTHESIS AND CHARACTERIZATION OF SP-COOH | E2 |
| E.2 ABSORBANCE SPECTRA OF SP-COOH IN ETOH | E3 |
| E.3 PHOTOS OF SP-COOH SOLUTION IN ETOH (10⁻³ M) AND SP-COOH DISPERSIONS IN ETOH/WATER (25 % ETOH) | E4 |
| E.4 EQUILIBRIUM OF SP-COOH DERIVATIVE IN ETOH/WATER SOLUTION | E5 |
| E.5 INTERFACIAL SELF-ASSEMBLY | E7 |
| E.6 SCANNING ELECTRON MICROSCOPY | E8 |
| E.7 ABSORBANCE SPECTRA OF SP-COOH MICROSTRUCTURES | E11 |
| E.8 MICROSCOPY IMAGING OF SP-COOH 25 % MICROSTRUCTURES UNDER CROSS POLARIZERS | E12 |
| E.9 GUIDED INTERFACIAL AGGREGATION | E13 |
| E.10 REFERENCES | E13 |

Stimuli-responsive Materials: Developing Integrated Opto-molecular Systems as Sensors and Actuators in Micro-fluidic Devices

Thesis Abstract:

Micro-fluidic platforms have been conferred with inherent optical sensing capabilities by coating the walls of micro-fluidic channels or micro-capillaries with stimuli-responsive materials. These adaptive materials respond optically to environmental stimuli, such as changes in pH, solvent polarity, the presence of certain metal ions and light. This approach confers sensing capabilities along the entire length of the coated micro-channel or micro-capillary. Adaptive coatings based on two types of materials are presented:

1. Conductive polymer polyaniline - The optical properties of these coatings respond to changes in the pH of the solution that is passing through the micro-channel or micro-capillary, and therefore can be used for dynamic pH monitoring (pH 2-8) or for aqueous ammonia sensing.
2. Photochromic spiropyran - Photoswitchable coatings based on spiropyran are used to photo-detect solvents of different polarity when passing through the micro-capillary in continuous flow. This sensing behaviour can be switched on/off remotely using light.

Finally, it is reported, for the first time, the potential of using spiropyran as a pH pump in fluidic channels for photo-activated chemopropulsion of organic droplets and the solvato-morphological control of self-assembled micro-structures based on spiropyran.

List of abbreviations

| | |
|---------------------|--|
| ATR-FTIR | Attenuated Total Reflectance - Fourier Transform Infrared spectroscopy |
| ACN | Acetonitrile |
| APS | Ammonium persulfate |
| ATRP | Atom Transfer Radical Polymerisation |
| Ch1 | Chromoionophore 1 |
| C1-H ⁺ | Protonated chromoionophore 1 |
| DCC | Dicyclohexylcarbodiimide |
| DCM | Dichloromethane |
| DMAP | 4-(Dimethylamino)pyridine |
| DMF | Dimethylformamide |
| EOF | Electroosmotic flow |
| EB | Emeraldine base |
| ES | Emeraldine salt |
| EtOH | Ethanol |
| E _T (30) | Reichardt's empirical polarity scale |
| FTIR | Fourier Transform Infrared spectroscopy |
| HDA | 2-Hexyldecanoic acid |
| HOMO | Highest occupied molecular orbital |
| HPLC | High Performance Liquid Chromatography |
| HSV | Hue, saturation and value color spaces |
| IL | Ionic Liquid |
| IR | Infrared |
| ISNBP | Indolinespiro nitro-benzopyran |
| ISBP | Indolinespirobenzopyran |
| LE | Leucoemeraldine |
| LED | Light-emitting diode |
| LCST | Lower critical solution temperature |
| LOAC | Lab-on-a-chip |
| LUMO | Lowest unoccupied molecular orbital |
| MC | Merocyanine form |

| | |
|----------------------|--|
| MC-H ⁺ | Protonated merocyanine form |
| MeOH | Methanol |
| NIPAAm | <i>N</i> -isopropyl acrylamide |
| NIR | Near Infrared |
| NMR | Nuclear magnetic resonance |
| PAni | Polyaniline |
| PDMS | Polydimethylsiloxane |
| PG | Pernigraniline |
| PMMA | Polymethylmethacrylate |
| pSPNIPAAm | Copolymer of an acrylated SP and poly(<i>N</i> - isopropyl-acrylamide) |
| RGB | Red Green and Blue scale |
| ROMP | Ring opening metathesis polymerisation |
| SAMs | Self-assembled monolayers |
| SEM | Scanning electron microscopy |
| SI-ROMP | Surface-initiated ring opening metathesis polymerisation |
| SP | Spiropyran form |
| SP-COOH | 1'-(3-carboxypropyl)-3',3'-dimethyl-6-nitrospiro[2 <i>H</i> -1]-benzopyran- 2,2' -indoline |
| SP-M | Spiropyran-norbornene monomer |
| SP-SO ₃ H | Spiropyran-sulfonic acid derivative |
| THF | Tetrahydrofuran |
| μTAS | Micro-Total Analysis Systems |
| UV | Ultraviolet |
| Vis | Visible |

Chapter 1

Literature Survey

***Stimuli-responsive Materials:
Developing Integrated Opto-molecular Systems as
Sensors and Actuators in Micro-fluidic Devices***

1.1 Micro-fluidics and Lab on a Chip Devices

In many fields, advances in fabrication technology have led to a device size reduction by several orders of magnitude [1-5]. One area that benefits in particular from this trend is the area of micro total analysis systems (μ TAS), also called “lab-on-a-chip” (LOC) [1]. LOC devices integrate and scale down laboratory functions and processes to a miniaturised chip format. Many LOC devices are used in a wide array of biomedical and other analytical applications including rapid pathogen detection [6], clinical diagnosis [7], forensic science [8], electrophoresis [9], flow cytometry [10], blood chemistry analysis [11, 12], protein [12, 13] and DNA analysis [12, 14].

LOC devices can be fabricated using a variety of technologies from many types of materials including polymers, glass, or silicon, or combinations of these materials [1]. LOC systems have several common features as such a micro-fluidic structure and one or several sensing capabilities [1]. Micro-fluidics can incorporate flow control devices, like pumps, mixers and valves [15] while the more common sensing capabilities are usually optical [16] or electrochemical [17] and are often integrated within the micro-fluidic system.

1.2 Opto-chemical Sensors

Opto-chemical sensors represent a group of chemical sensors in which electromagnetic radiation is used to generate the analytical signal in a transduction element [18]. The interaction of this radiation (that can cover different regions of the spectra: UV, Visible, IR, NIR) with the sample is evaluated from the change of a particular optical parameter and it is related to the concentration of the analyte [19]. Typically, an optical chemical sensor consists of a chemical recognition phase (sensing element or receptor) coupled with a transduction element (Figure 1.1).

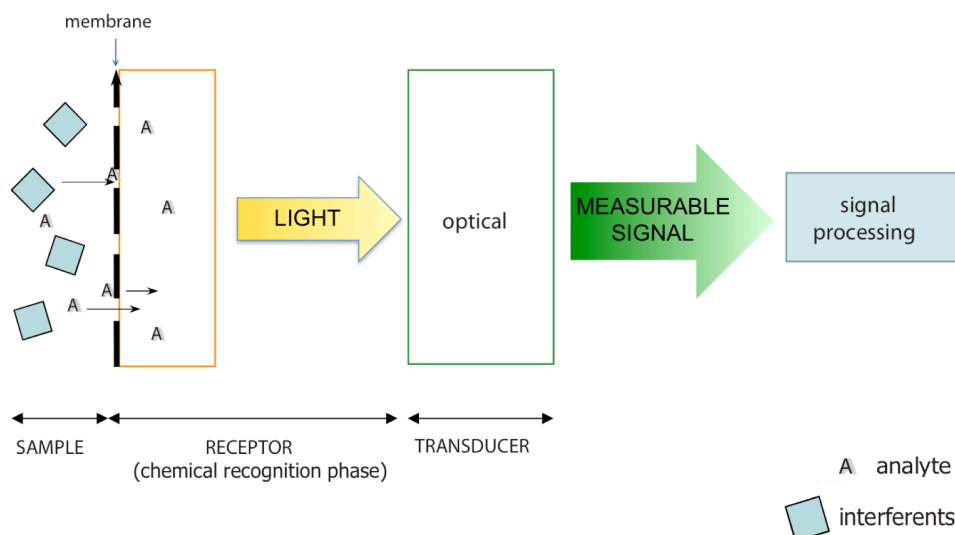


Figure 1.1. Schematic representation of the composition and function of an optical chemical sensor. (Reproduced from [18])

The optical signal processing is carried out using standard components and instrumentation to produce qualitative and meaningful data [20]. Optical chemical sensors provide the opportunity to continuously monitor chemical species and have found numerous applications in areas such as chemical industry [21], biotechnology [22], medicine [21, 23], environmental sciences [22, 24], among others. Some of the oldest and best-known applications include the use of pH indicator strips for sensing pH and oxygen measurements by quenching the phosphorescence of the dye tryptaflavin adsorbed on silica gel [20]. However, a major achievement occurred when conventional optical sensing techniques were coupled with optical fibres [20]. Although optical fibres were originally manufactured mainly for use in the communication industry they have been adapted to optical sensing devices. Optical fibres themselves allow transmission of light over long distances. Additionally, the development of high performance and high quality optical components, including light sources (lasers, light emitting diodes), photodetectors, amplifiers, that can be used in conjunction with optical chemical sensors, has promoted rapid progress and great interest in this sensing technology [18].

Chemical analysis is currently carried out in almost all areas of technology, and optical chemical sensors offer several advantages over conventional devices in a wide range of applications including process control, environmental and biomedical fields. Optical sensors are electronically passive and are not subjected to electrical

and electromagnetic interferences. They are also flexible, easily miniaturised, inexpensive and of rugged construction. They can be corrosion resistant and are capable of real-time monitoring of samples. As they are non-electrical, optical sensors are intrinsically safe and capable of operation in hostile environments. Optical sensors can be developed for chemical and biological analytes for which other sensing devices are not suitable or available [21, 25].

In terms of producing optical sensors, a relatively new and promising approach involves opto-fluidics where optic and fluidic functionalities are integrated at the micro- and nano-scale to leverage their combined advantages [26]. The micro-fluidic part, which bases on a fluidic platform, has many advantages because of its inherent small dimension. These include reduced consumption of reagents and analytes, improved time efficiency in the analysis, shrinkage in the size and weight of the systems, increased portability, reduced amount of harmful by-products, potentially low cost in fabrication [26].

Micro-channels functionalised with a sensing material have been previously reported and involve functionalisation of the inner wall of the micro-channel with antibodies for flow-through cell separation [27], fluorescent dyes for optical sensing of acidity [28] or monolayers with metal ion sensing properties [16, 29].

Chapters 4 to 7 of this thesis will focus on a new approach of producing optical chemical sensors in which adaptive polymeric materials inherently sensitive to a range of analytes are used as the optical sensitive layer in a micro-fluidic platform (where by micro-fluidic platform we refer either to micro-channels or to micro-capillaries).

1.3 Surface Functionalisation

As micro-fluidic devices are characterised by a high surface-to-volume ratio, surface effects become dominant in fluid handling and therefore surface properties play a crucial role in micro-fluidics-based applications. One straightforward method to generate modified surfaces is by using self-assembled monolayers (SAMs). As many of the micro-fluidic systems are based on glass or silicon, trichlorosilanes, triethoxysilanes, and trimethoxysilanes derivatives bearing functional groups at the other end of the molecule are regularly used for SAM coating. Deposition of SAMs

is easily achieved in micro-fluidic devices, since it only requires the flow of a solution or a gas stream of surface reacting molecules through the channels. SAMs have been used in glass micro-fluidic networks to engineer surface properties with the aim of controlling liquid motions [30], confining and aligning of biological macromolecules and liquid crystals [30], controlling electro-osmotic flow [31], preventing cell adhesion [32] and protein adsorption [33], and creating zones for specific immobilisation of proteins [34]. When derivatised with fluorescent groups, SAMs can function as optical sensors. This has been shown on flat surfaces [35-37], and also in micro-fluidic networks [38].

However, SAMs can also function as molecular scaffolds for more complicated polymeric architectures. Due to the high versatility of the silanisation agents, they can further serve to covalently anchor a variety of polymeric brushes to the substrate. Polymer brushes are polymer chains tethered by one end to a surface or an interface. At high grafting densities, *i.e.* when the distance between neighboring grafting points is small, steric repulsion leads to chain stretching and a brush-type conformation of the surface-tethered chains. More precisely, polymer brushes are more elongated near the attachment point and unstretched at the free end. This property made them appealing for a variety of applications in colloidal and interfacial phenomena, especially when applied to particles. In preventing flocculation, polymer chains (which prefer solvent to the colloidal particle surface) resist overlapping between neighboring particles resulting in colloidal stabilisation. The chemical grafting of polymer brushes can be accomplished by either “*grafting-to*” or “*grafting-from*” methods [39].

In the “*grafting-to*” approach, end-functionalised polymer molecules react with complementary functional groups located on the surface to form tethered chains (Figure 1.2a). This method can be performed relatively easily on flat surfaces, by spin or dip coating or solution casting of the appropriate polymer solutions. However, only a limited amount of the polymer can be tethered onto the substrates by the “*grafting-to*” approach. The attaching polymer chains have to overcome the activation barrier, which appears as soon as the earlier attached chains begin to overlap. This means that only low grafting densities and thin layers can be achieved (up to 10 nm)[40].

The second possibility to create polymer brushes is the “*grafting-from*” technique (Figure 1.2b). In this case, the polymerisation is initiated from the

substrate surface by already attached (usually by covalent bonds) initiating groups. Molecules of a monomer penetrate through the already grafted polymer layer much more easily compared with the polymeric chains in the “grafting to” approach, and high grafted amounts can be obtained [40]. This method utilises controlled polymerisation techniques like atom transfer radical polymerisation (ATRP) or ring-opening metathesis polymerisation (ROMP), among others. The working chapters of this thesis, from 4 to 7, will focus on the synthesis of polymer brushes from SAMs using mainly the “grafting from” approach.

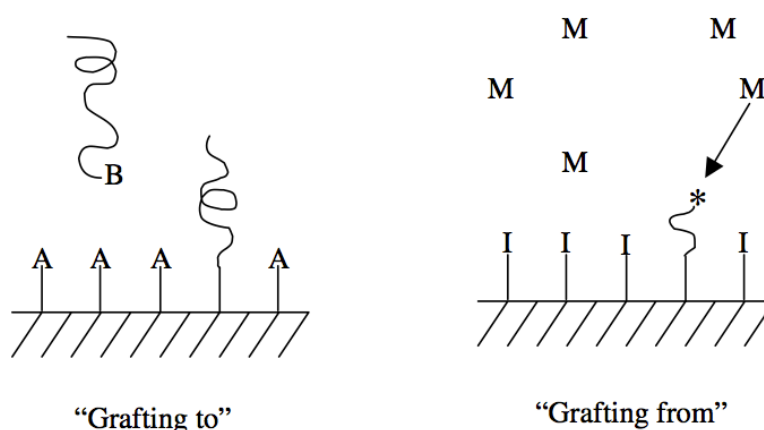


Figure 1.2. Preparation of polymer brushes using “grafting to” and “grafting from” approaches. (Reproduced from [39])

1.4 Adaptive Polymeric Materials

Adaptive materials, also described as “stimuli-responsive materials” or “molecular switches” are materials whose characteristics can dramatically change in response to external stimuli. The external stimuli can be of many natures: a change in pH, a change in temperature, a photo- mechano- or electrical stimulus among others, where some materials can respond to a combination of two or more stimuli [41-43].

A wide range of adaptive responsive materials, mostly involving polymers, has been reported in the recent years and they find applicability in fields ranging from medicine and biology to chemistry, physics, materials science, and engineering. Immobilisation of such adaptive materials in a micro-fluidic network could

potentially be used to probe solutions inside micro-fluidic networks, to monitor processes inside the channel, or to control processes in the channel.

If in the previous section several strategies were examined for producing polymer-functionalised surfaces, the following sections will describe in detail the adaptive materials that will be further used for the work described in the working chapters of this thesis (Chapters 4 to 9). These adaptive materials will be employed as coatings in micro-fluidic platforms for sensing applications or to photo-activate processes at the liquid/air interface, as such droplet actuation or photocromic performance). These materials will be photo or chemically switched between different modes of behaviour (*e.g.* passive or non-binding surface, and active or binding surface, in the case of spiropyran based polymers), using chemical or photonic stimuli.

This chapter presents the use of new opto-molecular systems as sensors and actuators in micro-fluidic devices, where the materials give an optical output (change in colour, change in their absorbance spectra) in response to an external stimulus. Two main systems will be employed: conducting polymers (polyaniline) and photo-responsive materials (spirobenzopyran).

1.4.1 Conducting Polymers

1.4.1.1 Overview

In general, conductive polymers are polymers with delocalised π -electron system with a wide band gap in their pristine state [44] and can be made electrically conducting by doping. Doping in conductive polymers refers to the oxidation or reduction of π -electronic system, p-doping and n-doping, respectively, and can be effected chemically or electrochemically [44]. To maintain electro-neutrality, doping requires incorporation of a counter ion. The doped and dedoped states have different electronic, optical, physical, chemical, and electrochemical aspects. Thus, reversible interchange between redox states or doped-dedoped states in conjugated polymers gives rise to changes in their properties including polymer conformation, conductivity and colour. These proprieties make conjugated polymers an important class of stimuli responsive materials suitable for a variety of applications, from

electrochromic devices [45], actuators [46, 47], to sensors [48]. In the recent years there has been a tremendous interest in developing nanostructures of these conducting polymers as they offer increased surface area, which translates to high sensitivities and short response times. When nanostructured conductive polymers are employed as sensing materials, the response time can be improved by several orders of magnitude in comparison with their bulk counterpart [49, 50]. Polyaniline (PAni), polypyrrole, polythiophene, and polyacetylene are some of the most explored conductive polymers [44].

1.4.1.2 Polyaniline

Among conjugated polymers, polyaniline has attracted great attention because of its electronic, electro-chemical, and optical properties, and especially because of its good environmental stability. Polyaniline can be reversibly switched between different oxidation states, and therefore can be used as a good material for electro-chemical sensor for redox active species. MacDiarmid *et al.* [51] showed that PAni can afford conduction by protonation of the emeraldine base (EB) leading to emeraldine salt (ES) through acid-base chemistry. This change is accompanied by a significant change in colour and in the UV-Vis spectra of the material, a property that offers the possibility to prepare optical pH sensors based on polyaniline. This phenomenon constitutes the bases of Chapter 4 and Chapter 5 and will be discussed in detail in the following section (“***Switching in Polyaniline***”) as it is important to understand which are the transitions that give rise to the distinct colours of EB and ES and which are the factors that determine these transitions. Although the electrical conductivity of polyaniline has been the subject of many comprehensive articles and reviews [52-56], this is not the focus of the research in this chapter and it will not be further discussed.

Polymerisation Techniques

During the synthesis process, polyaniline can be produced as nanogranular powders, nanotubes, nanowires, nanofibres, micromats or microspheres among others [57]. These morphologies can be obtained as precipitates during the oxidation, as colloidal

dispersions, or films and layers on a variety of supports. It is therefore not surprising that Professor A.G. MacDiarmid, Nobel Prize laureate for his work in the area of conductive polymers, has declared that “There are as many different types of polyaniline as there are people who synthesize it.” [58]. Although this has become an opinion often expressed in the literature, it should be mentioned, however, that the oxidation process is well defined and reproducible. This means that identical products are obtained in repeated syntheses following the same protocol.

The most common synthesis of polyaniline involves oxidative polymerisation, in which the polymerisation and doping occur concurrently, and may be accomplished either electrochemically or chemically [57]. Electrochemical methods tend to have lower yields than chemical methods. Furthermore, the chemical methods are far more amenable for large-scale production. A large number of chemical methods have been utilised to polymerise aniline; the majority of which take place in solution and may be categorised as monophasic or biphasic. Template and template-guided syntheses can also be employed for producing polyaniline [59, 60], but these methods will not be covered here.

The synthesis of PANi depends on many parameters (chemical nature of the oxidants, the nature of the acid protonating the aniline, the concentrations of the reactants and their molar proportions (especially of aniline and oxidant), temperature, solvent components (*e.g.* the organic component), the presence of additives (*e.g.* colloidal stabilisers, surfactants) and many others, which are important for the control of the properties and the PANi morphology. However, most often strongly acidic media, ($\text{pH} < 2.5$) is used for the fabrication of polyaniline, where ammonium peroxide is employed as the oxidant. In this case, the mechanism of oxidative chemical polymerisation generally accepted in literature is the one described in Figure 1.3 [61].

This mechanism starts with the protonation of aniline in strong acidic media ($\text{pK}_{\text{a aniline}} = 4.6$) followed by the formation of the resonance-stabilised radical cation. The next step involves coupling of the *N*- and *para*-radical cations (Figure 1.3 - A and B, respectively) and from here on “head-to-tail” coupling becomes predominant. Although coupling can occur also in the *ortho*-position, leading to defects in conjugation in the resultant polymer, this is happening only in small fractions. It has been shown that in polyaniline chains, more than 95 % of constitutional aniline units are linked in head-to-tail *para* positions [57].

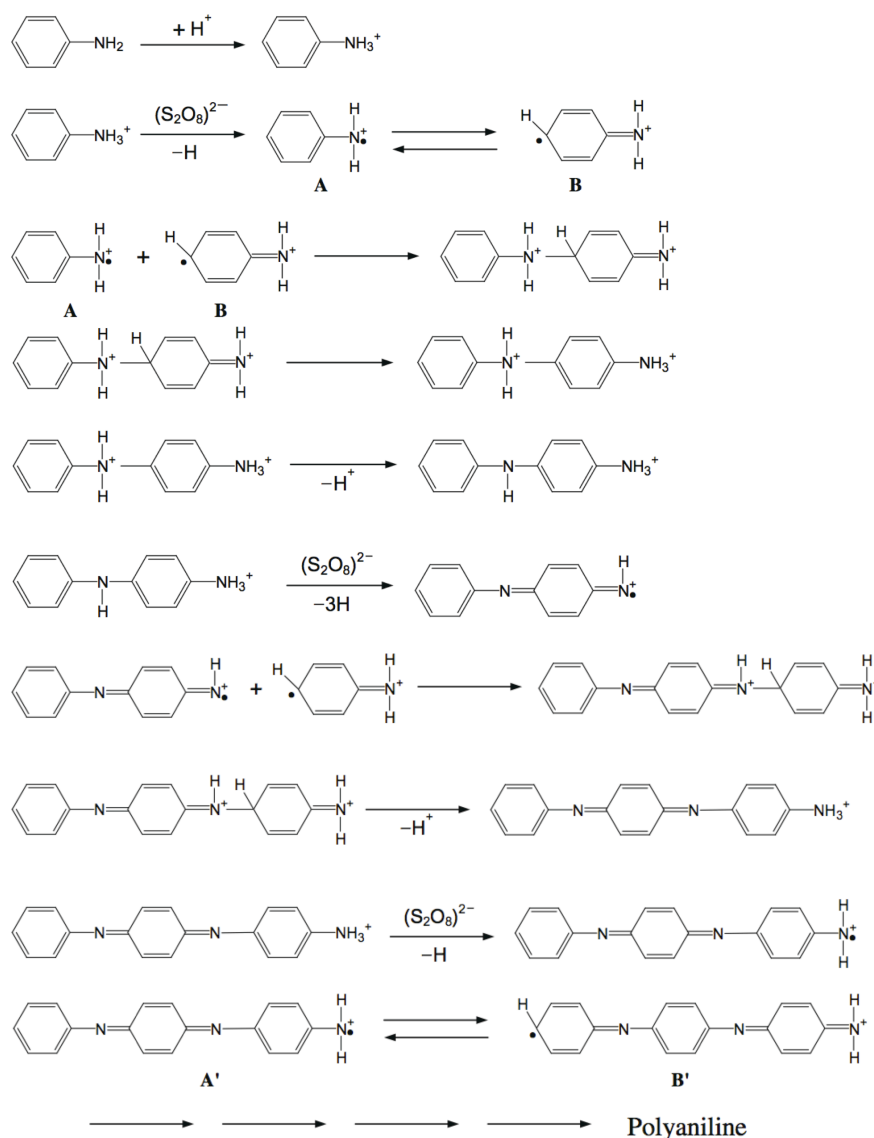


Figure 1.3. Mechanism of oxidative chemical polymerisation of aniline using $(\text{NH}_4)_2\text{S}_2\text{O}_8$ as the oxidant in a low-pH acidic aqueous medium ($\text{pH} \approx 0$). Reproduced from [61].

Most chemical methods employed to produce polyaniline are performed in solution in monophasic or biphasic systems.

Monophasic syntheses are usually carried out in aqueous acidic solution and involve the addition of an oxidant solution, most commonly ammonium persulfate or ferric salts, to a monomer solution. Syntheses have been carried out over a range of temperatures, from ambient down to -70°C and several oxidant/monomer ratios have been investigated. In most cases, however, the monomer and oxidant solutions are fairly dilute, as this rendered more control over the reaction. When all the factors influencing the aniline polymerisation such as temperature, concentration of

reactants, and oxidant/monomer ratio are taken into account, oxidative polymerisation of aniline is fairly straightforward, and proceeds in relatively high yield. Monophasic polymerisation of aniline will be further employed in Chapters 4 and 5 for producing polyaniline coatings in micro-capillaries and micro-channels.

Aniline polymerisation may also be controlled by the use of an initiator, where the initiator must be more easily oxidised than aniline [57]. Such an example is *N*-phenyl-1,4-phenylenediamine, an excellent initiator as it not only has a lower oxidation potential than aniline, but it is an intermediate in the oxidation of aniline. *N*-phenyl-1,4-phenylenediamine will preferentially react with the oxidant, thereby reducing side reactions. In this way, the obtained polymer was proven to be of improved homogeneity and the synthesis more reproducible with predicted chain length [62, 63]. Thus, throughout the use of such an initiator, and by controlling the ration between aniline (monomer) and dianiline (initiator) one may easily produce on demand short chain, highly soluble, moderately conductive polymers or long chain, highly conductive, polymers with limited solubility.

In our laboratories, we use this method to produce long polyaniline nanofibres. As it can be seen from the Scanning Electron Microscopy (SEM) images (Figure 1.4), the nanofibres obtained have diameters of about 100 nm and average lengths of approximately 30 μm .

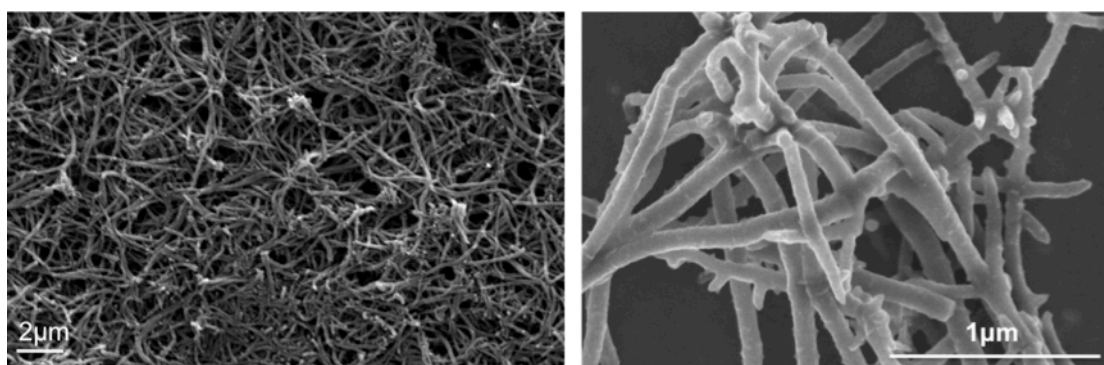


Figure 1.4. Scanning Electron Microscopy images of polyaniline nanofibres obtained through out monophasic polymerisation in the presence of *N*-phenyl-1,4-phenylenediamine.

Although monophasic synthesis has shown great potential to produce polyaniline in its nano-form, much research is focused on investigating the benefits of biphasic synthesis, in which the reactants exist in different solution phases

(organic and aqueous) and polymerisation occurs primarily at the interface [64]. In a typical interfacial polymerisation the aniline monomer is dissolved in the organic layer while the conventional low-pH acidic aqueous medium contains the oxidant. Since in these conditions the polyaniline product is synthesised in its hydrophilic emeraldine salt form, it diffuses away from the reactive interface into the aqua layer. This makes more reaction sites available at the interface and avoids further overgrowth. In this way, the nanofibers formed at the interface are collected in the water layer without severe secondary overgrowth. This is a well-documented method used in our laboratories to produce polyaniline nanofibres [65, 66]. Although many different organic layers can be employed, an example where the aniline is dissolved in toluene while the ammonium persulfate is dissolved in 1M HCl is presented in Figure 1.5. Green polyaniline (emeraldine salt form) appeared initially at the interface between the aqueous and the organic layer and then migrated into the aqueous phase. After reaction completion, the resulting product is normally purified by centrifugation and suspended as a colloid in deionised water or other solvents.

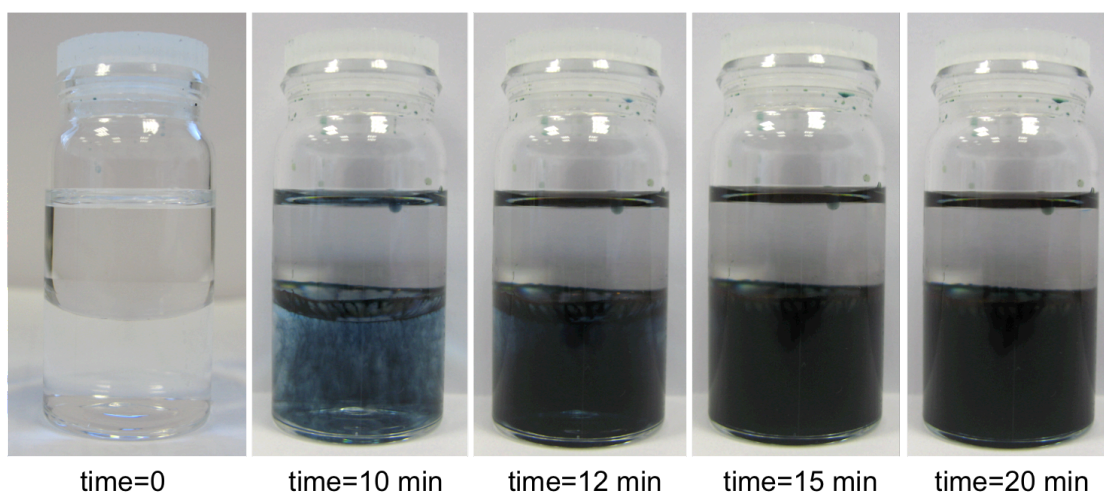


Figure 1.5. Photographs showing interfacial polymerisation of aniline in a toluene/water system. From left to right, the reaction times are 0, 10, 12, 15 and 20 min, respectively. The top layer is aniline dissolved in the organic solvent toluene while the bottom layer is an aqueous solution of 1.0 M hydrochloric acid containing the oxidant, ammonium persulfate.

This type of polymerisation produces homogeneous nanofibres with diameters between 40-80 nm and lengths from 500 nm to several micrometers, as

shown in the SEM image – Figure 1.6. These are considerably shorter than the ones obtained in the monophasic system in the presence of an initiator.

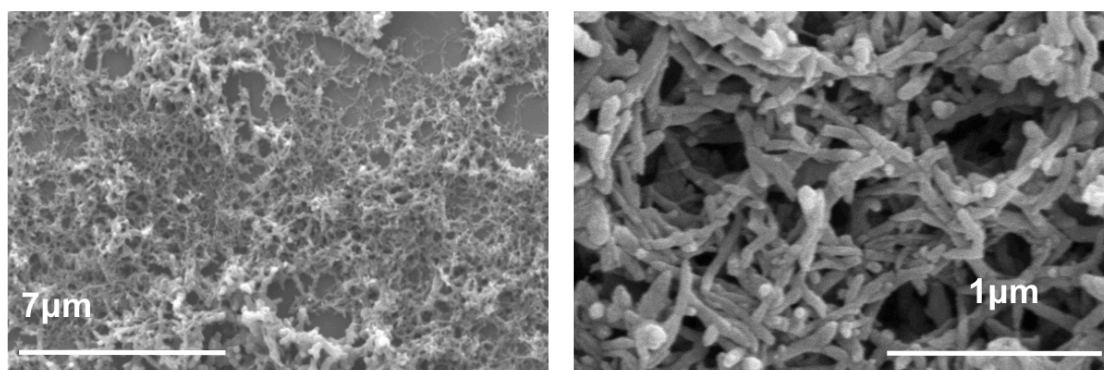


Figure 1.6. Scanning Electron Microscopy images of polyaniline nanofibres obtained through interfacial polymerisation.

Switching in Polyaniline

Polyaniline (Figure 1.7) consists of ‘ n ’ reduced (benzenoid diamine) and ‘ m ’ oxidised (quinoid diamine) repeating units, in which the oxidation state can be defined by the value of m [44].

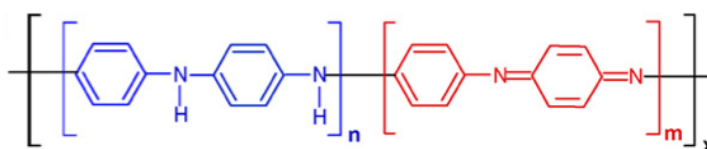


Figure 1.7. Structure of polyaniline.

Polyaniline may exist in three different redox forms (Table 1): Leucoemeraldine (LE) in its fully reduced state; pernigraniline (PG) fully oxidised state, with imine links instead of amine links, and the emeraldine form of polyaniline, often referred to as emeraldine base (EB), is either neutral or doped, with imine nitrogens protonated by an acid. EB is regarded as the most useful form of PANi due to its high stability at room temperature and because its doped form (emeraldine salt; ES) is electrically conducting. LE and PG are poor conductors,

even when doped with an acid. The three forms of polyaniline (LE, EB, PG) may be inter-converted by chemical and/or electrochemical oxidation or reduction [44].

Table 1. Different oxidation states of PAni.

| Form of PAni | Redox State | Oxidised groups | Reduced groups | Colour |
|-----------------|--------------------|-------------------|-------------------|-------------|
| | | (<i>m</i> value) | (<i>n</i> value) | |
| Leucoemeraldine | Fully reduced | 0 | 1 | White/Clear |
| Emeraldine | Partially oxidised | 0.5 | 0.5 | Blue/Green |
| Pernigraniline | Fully oxidised | 1 | 0 | Violet |

The reversible protonation/deprotonation reaction of the emeraldine form of polyaniline is of particular interest for the development of pH sensors and it has been used for constructing a wide variety of potentiometric [67, 68] and optical [69, 70] pH probes as the two species, EB and ES, possess dramatically different conductivities and optical properties.

The protonation process of EB occurs on the imine nitrogen atoms as shown in Figure 1.8, and ES is formed through successive formation of bipovalent species, bipolaron structure, and more stable polaron structure (Figure 1.8). This polaron structure is responsible for electrical conduction through hopping mechanism in its crystalline region and will give rise to different absorbance spectra [71].

Typically, emeraldine base exhibits an absorbance band at approximately 330 nm, due to the benzenoid π - π^* transition, and at approximately 635 nm, which is attributed to the quinoid exciton absorption [72]. This absorption is responsible for the blue colour of the emeraldine base (Figure 1.9). Upon doping, the quinoid transition disappears, and two new absorbances appear [73]. These new absorption bands are assigned to polaron and bipolaron transitions, at about 800 and 420 nm, respectively. The polaron transition occurs at a higher wavelength (thus lower energy) than the bipolaron transition.

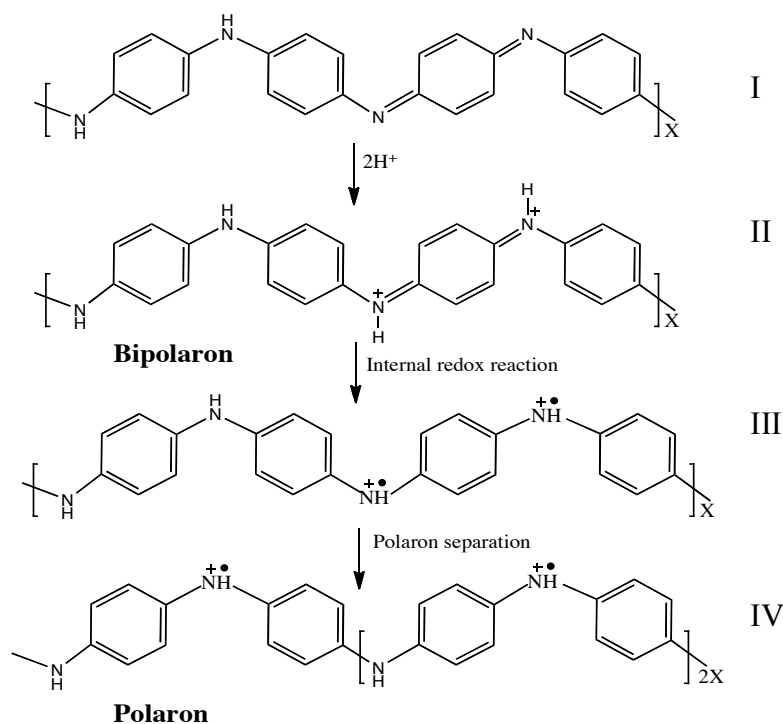


Figure 1.8. Chemical structures of emeraldine before protonation (I - emeraldine base) and after (II)–(IV) 50% protonation (emeraldine salt): (II-III) formation of bipolaron, and (IV) separation of two polarons. (Reproduced from [71])

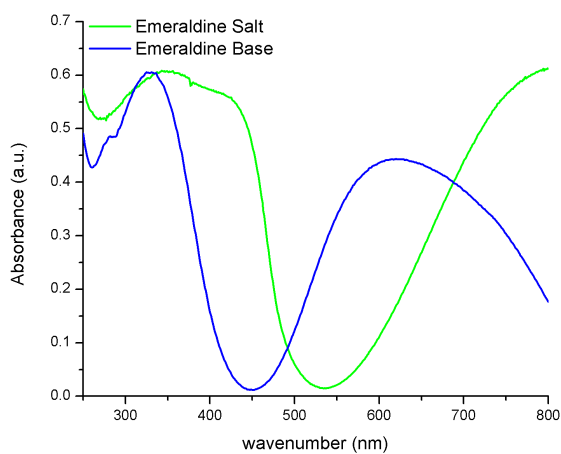


Figure 1.9. Typical absorption spectra of polyaniline dispersions in water solution in its two forms emeraldine salt and emeraldine base.

1.4.2 Photo-responsive Materials

1.4.2.1 Overview

Organic photochromic compounds are molecules of considerable interest as they are expected to offer routes to new functional materials that take advantage of polarity and geometrical changes induced by irradiation [74]. Photochromic molecules can be used to produce platforms with switchable behaviour where light irradiation can be used to induce reversible conformational transitions [75]. The colour changes induced by photoirradiation leads to their use in various photoresponsive devices such as light sensitive eyewear [76], optical memory [77, 78], molecular devices [79] and optical sensing applications, such as transport of metal ions [80], solvent [81] and metal ion detection [16, 82, 83].

Well-known families of photochromic include the spirobenzopyrans, spiropnaphthooxazine, naphthopyran, diarylethenes and furylfulgides [84]. They all undergo reversible photochromic behaviour: one isomer can be transformed into the other which then reverts back to the initial form in the dark (thermodynamically) or under a different light irradiation (photodynamically).

There has been an increasing interest in organic photochromic compounds as they represent bi-stable molecular systems, that exist in two stable molecular forms which can be converted from one to another, with a wide range of potential applications in electronic, photonics and computing [85]. Molecular sized switches, incorporated into a nanoscaled logic circuit are able to detect events and transmit signals in response to environmental stimulation [86].

Among the different families of photochromic compounds, spirobenzopyrans are probably the most widely studied [85, 87, 88] due to their high photosensitivity, very clear colour change and rapid switching kinetics between the two isomers. The first of these isomers, the closed spiropyran, is typically clear as it doesn't have an absorption in the visible region while the second one, open merocyanine, is strongly coloured. From these isomers, only the merocyanine presents solvatochromism and has a guest-binding site for certain metal ions [16, 74, 75, 81, 82]. These properties make possible the use of the spiropyran moiety in producing sensors where the sensing behavior could be switched ON/OFF using light. Moreover, in the "OFF" state, the binding sites are passivated hence the active surface is deactivated whereas

in the 'ON' state, the surface binding sites are activated and available. The use of this family of compounds could form the basis of new approaches for photoswitchable sensing, uptake and release of molecular guests or photocontrolled separations.

1.4.2.2 Spirobenzopyrans

The photochromic properties of spirobenzopyrans were first discovered by Fischer and Hirshberg in 1952 [89] where they observed that the irradiation of several solutions of spirobenzopyrans with UV-light (not exceeding 450 nm) produced colour modifications that could be reversed by exposing the same solutions to yellow light (containing no radiation below 500 nm).

Spirobenzopyrans refer in general to (substituted) *2H*-1-benzopyrans having a second ring system, usually (but not necessarily) heterocyclic, attached to the 2-carbon atom of the pyran in a spiro manner with a common tetrahedral carbon atom [85]. The two halves of the molecule are in two orthogonal planes (Figure 1.10). The benzopyran part is the common structure to all spiropyrans, except for different substitutions on the aromatic ring, while the heterocyclic part is variable and often is built upon mono or bi-heteroatomic azaheterocycles saturated or benzofused [85, 90].

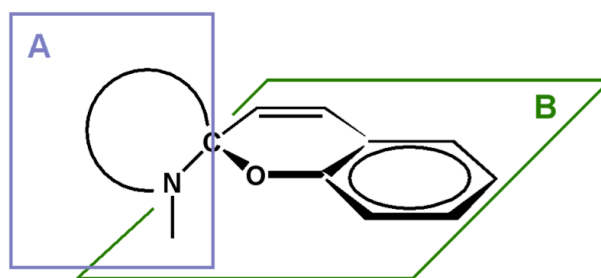


Figure 1.10. Schematic representation of the structure of spirobenzopyrans, showing the two orthogonal planes formed by the two halves of the molecule: the heterocyclic (A) and the benzopyran (B). (Reproduced from [90])

For the specific purpose of this discussion, from here on, we will be focused on a particular class of spiropyran: indolinespirobenzopyran (ISBP) (Figure 1.11).

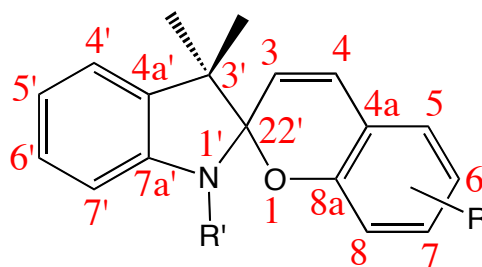


Figure 1.11. Schematic representation of indolinespirobenzopyran moiety and the positions of the atoms.

Photochromism

Spiropyrans exist in a closed, unpolar, orthogonal and colourless “spiro” form (SP), which is converted by exposure to ultraviolet (UV) light to an open, planar, conjugated, highly coloured “merocyanine” form (MC).

Upon irradiation, the C-O spiro bond in the SP form is cleaved heterolytically and the "spiro" carbon which was sp^3 -hybridised achieves sp^2 hybridisation and becomes planar (Figure 1.12) [85]. The aromatic group rotates, aligns its π -orbitals with the rest of the molecule, and it forms the conjugated system of the merocyanine form, with ability to absorb photons of visible radiation, therefore is strongly coloured. When the UV source is removed, the molecules relax to their ground state, the carbon-oxygen bond reforms, the spiro-carbon atom becomes sp^3 hybridised again and the molecule returns to its colourless state.

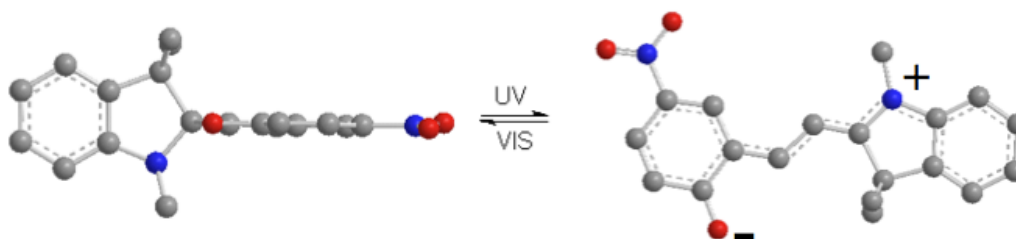


Figure 1.12. Indolinespiro nitro-benzopyran (ISNBP) conversion of the SP (left) to the MC form (right), by exposure to UV light and the reversible switching of the MC to the SP form, by exposure to visible light.

The photochromism of SP depends to a considerable extent on the energy of the $C_{\text{spiro}} - O$ bond and its polarity, the charge distribution on the atoms of the

pyran ring, and the degree of electronic interaction between the indoline and pyran sections of the molecule [91].

These factors, which all affect the photochemical properties of SPs, primarily depend on the structure of the initial spiropyrans, and therefore, to fully understand the photochromic behavior of the spiropyrans, it is necessary to focus on specific orbital interactions and structural features in the indoline spiropyran molecule in its ground electronic state. Only then it can one gain an understanding of why spiropyrans exhibits photochromism and which are the most important factors influencing this behavior.

A systematic X ray study of indolinespirobenzopyrans was the subject of a comprehensive review published by S. M. Aldoshin in 1990 [91]. Although the details of this study are not to be considered here, the main findings have to be outlined, as they are important for establishing the relationship between the structure and photochemical properties of ISBP.

X ray studies have shown that in spiropyrans, the indoline and benzopyran residues of the molecules are approximately at right angles to each other but are not planar (Figure 1.13). The indoline residue has the conformation of a flattened envelope with an inflection (dihedral angle) along the line of N(1') — C(3') in the range of 23-30°. This type of structure for an indoline heterocycle is due to an essentially pyramidal configuration of the N (1') nitrogen atom, which reduces the conjugation between the unshared electron pair (UEP) of the N(1') atom and the π system of the benzene ring. In fact, the UEP of the N atom have substantial sp^3 character, where the N(1') atom is situated approximately perpendicular to the plane formed by the first carbon atom of the R' substituent, C(7a') and C(22') atoms.

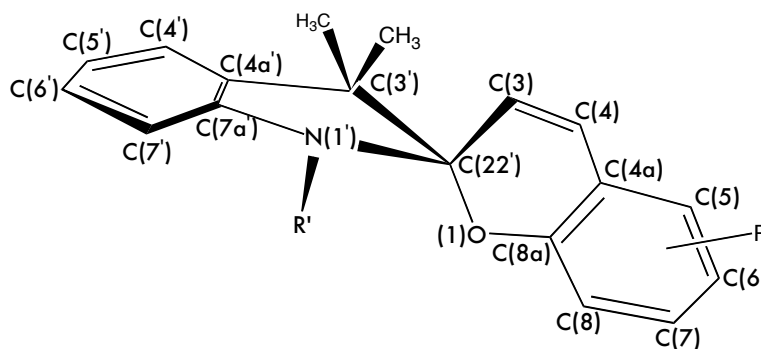


Figure 1.13. Schematic structure of SP molecules and the numbering. (Reproduced from [91])

The unshared electron pairs of the O atom are not equivalent; they have a π - and σ -character and have different configurations. Thus, the UEP σ -electron density is situated in the plane of the C(22')—O(1)—C(8a) atoms while the UEP π -electron density occurs perpendicular to this plane. With such a structure of the SP, the C_{spiro}—O bond of the pyran heterocycle occupies a *trans*-position relative to the UEP of the N(1') atom while the C_{spiro}—N(1') bond of the indoline heterocycle is in a *trans*-position relative to the π -UEP of the O atom. This type of structure can cause specific orbital interactions between the electronegative heteroatoms and the UEP of the N and O atoms bonded to a tetrahedral carbon atom. This interaction may be described in terms of an $n-\sigma^*$ interaction between the UEP (n) of the heteroatom and the antibonding σ^* orbital of the adjacent polar bond located mainly on the carbon atom of the spiro centre (Figure 1.14). Since the electro negativity of the oxygen atom is greater than that of the nitrogen atom, and the UEP energy of the O atom is lower than the UEP energy of the N atom, the antibonding σ^* orbital of the C_{spiro}—O bond will be lower in energy than the antibonding orbital of the C_{spiro}—N(1') bond, while the nonbonding orbital of the N(1') atom will be higher in energy than the nonbonding orbital of the O atom. Consequently interactions between the n -electrons of the N(1') atom and the σ^* orbital of the C_{spiro}—O bond are decisive in the spiro centre.

As a result of population of the antibonding orbital of the C_{spiro}—O bond, this type of interaction should lead to a strengthening of the C_{spiro}—N(1') bond and a weakening of the C_{spiro}—O bond, which appears respectively as a contraction and elongation of these bonds. In fact, the C_{spiro}—N(1') bond lengths shown by Aldoshin *et al.* [91][ref] are in the range of 1.432-1.453 Å and prove to be considerably shorter than the normal lengths of C(sp^3) — N(sp^3) bonds (1.47-1.48 Å) in five membered heterocycles, while the C_{spiro}—O bond lengths are in the range 1.452 -1.497 Å. Moreover, it proves to be considerably longer than normal C—O bonds (1.41-1.43 Å) in six membered heterocycles [85, 91].

This variation in the C_{spiro}—O bond length is critical in determining the overall photobehaviour of the molecule, as it has been found that under continuous irradiation conditions, all spiropyrans with C_{spiro}—O bond length longer than 1.42 Å undergo photochromism, while spiropyrans with C_{spiro}—O bond shorter than 1.42 Å do not [85].

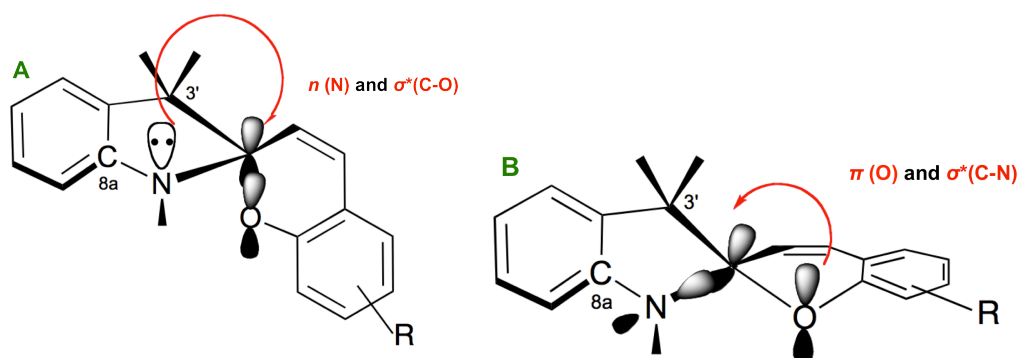


Figure 1.14. Scheme representing the two spatial interactions which may occur between the lone pair electrons on the nitrogen and oxygen and the σ^* antibonding between the C_{spiro} and the two heteroatoms. As the electronegativity of the oxygen is greater than the one of the nitrogen, the energy of the unshared electron pair in the nN is greater than the one in the nO and the energy level of the σ^*C-O is lower than the σ^*C-N . For these reasons, the interaction between the nN electrons and the σ^*C-O (**A**) is favoured compared to the lone pair nO electrons interactions with the σ^*C-N (**B**), determining a weakening of the $C_{\text{spiro}}-O$ bond and a strengthening of the $C_{\text{spiro}}-N$ bond. (reproduced from [91])

In these conditions, cleavage of the $C_{\text{spiro}}-O$ bond in the excited state may be, to a large extent, due to the further weakening and elongation of this bond during photoexcitation resulting from the same structural factors that caused the elongation and weakening of this bond in the ground state. Therefore, elongation of the $C_{\text{spiro}}-O$ bond in the ground state may serve as one of the criteria for photochemical activity in all spiropyrans [85, 91].

Transient spectroscopy methods have identified the presence of more than one merocyanine isomer upon irradiation with UV light [85, 92, 93]. Only the isomers having a central transoid segment represent a local energy minimum and are stable MC isomers as the cisoid configurations are at a relatively higher energy level due to internal steric hindrance [85]. The ring-opening reaction starts with cleavage of the $C-O$ bonds of the spiropyran, to give rise to sterically strained chiral - cisoid intermediate, which rapidly convert to nearly planar merocyanine isomers, labeled according to the configurations of the molecular fragments relative to the $N-C=C-C$, $C=C-C=C$, and $C-C=C-CO$ bonds (Figure 1.15).

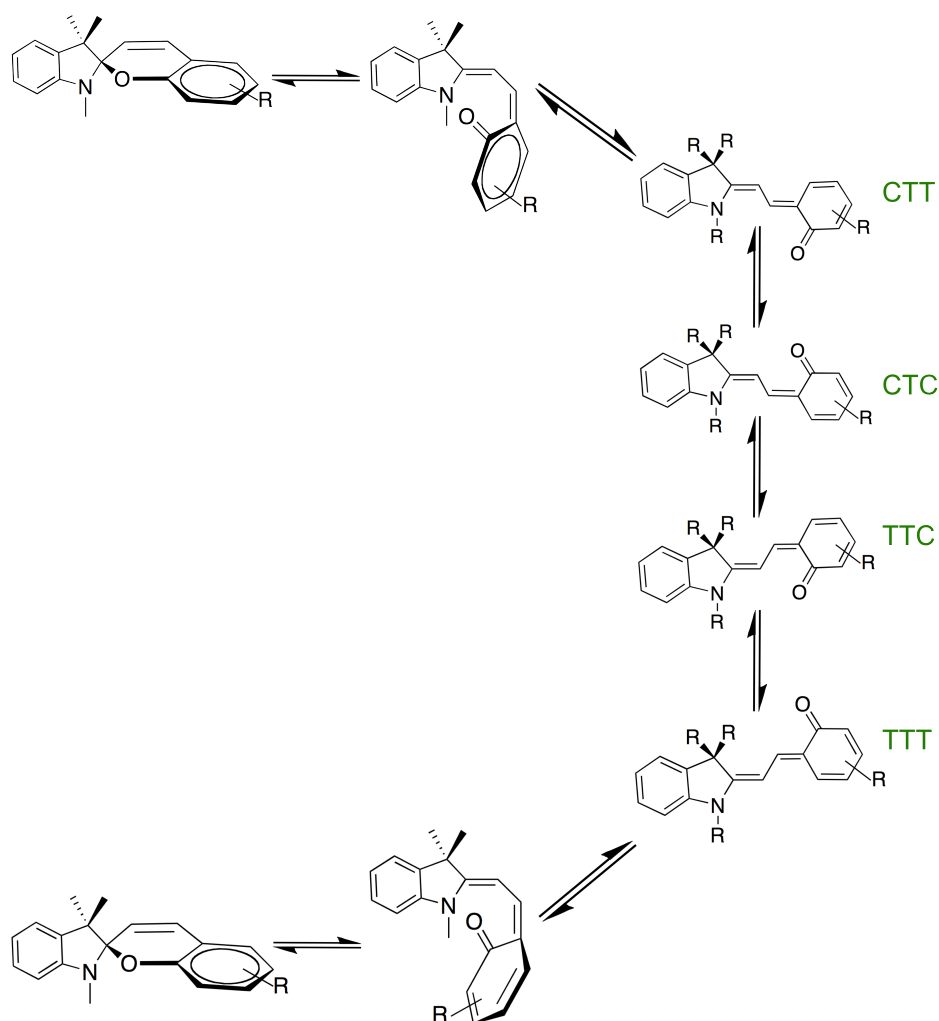


Figure 1.15. Schematic representation of different possible intermediate isomers induced by photoexcitation of the ring closed ISBP form, reproduced from [85].

The structure of the most stable isomers have been reported as TTC and CTC conformers as these possess a larger dipole moment according to theoretical modeling calculations [85].

Resonance Raman spectroscopy, laser photolysis and quenching experiments have shown that the primary step of the photochromic reaction of spiropyrans is the dissociation of a C-O bond in an electronic excited state [85, 90].

The mechanism suggested to describe the photochemical behavior of a series of indolinobenzopyrans with a nitro group in position 6 involves intersystem crossing to the short-lived triplet state of the ring-closed isomer 3Sp^* (Figure 1.16). This serves as a precursor of the triplet so-called “perpendicular” merocyanine form $^3\text{MC}^*_{\text{perp}}$ that may be correlated with the structure of sterically strained chiral intermediate from Figure 1.15. $^3\text{MC}^*_{\text{perp}}$ is in equilibrium with the triplet of the *trans*

isomer $^3\text{MC}^*_{\text{trans}}$. The reaction ends with quenching the triplet with oxygen and establishing a thermal equilibrium between the most stable merocyanine isomers, presumably CTC and TTC (Figure 1.15). In contrast, spiropyrans without the nitro group follow a singlet pathway rather than this mechanism [85, 90].

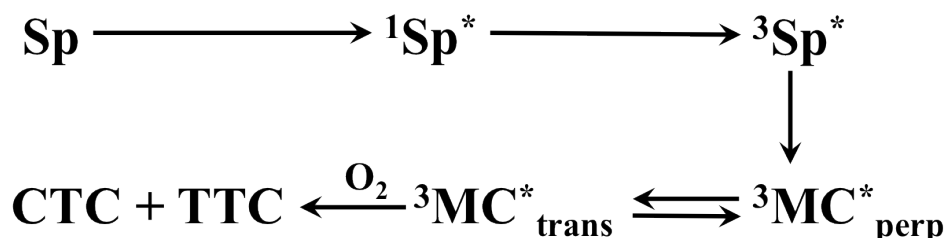


Figure 1.16. Mechanism suggested to describe the photo-chemical behavior for a series of indolinobenzopyrans with a nitro group in position 6. (Reproduced from [85])

After removal of UV-light irradiation, the enhanced colouration slowly reverts back to the original ring closed colourless spiro form. The relaxation time at room temperature depends significantly on the structure of the spiropyran and on the solvent polarity. This thermal decolouration of the MC has been demonstrated to follow a first order decay rate [85]. The reversion to the closed uncoloured spiro form can be also photochemically induced by white light irradiation [85].

Solvatochromism

The solvatochromic effect occurs where there is a strong dependence of the UV-Vis absorption bands of a compound on variations in the polarity of the solvent medium. It involves a change in the position and sometimes in the intensity of the absorption bands of the molecule when measured in different solvents. These changes are caused by intermolecular interactions between the solute and solvent that modify the energy gap between the ground and excited state of the absorbing species [85, 90]. Consequently, variations in the position, intensity, and shape of the absorption spectra can be direct measures of the specific interactions between the solute and solvent molecules.

Spiropyran compounds undergo solvatochromism, as the equilibrium between the ring closed spiro (SP) form and the ring open merocyanine (MC) form is

influenced by the external medium in which the molecule is dissolved. The solvatochromism of spiropyrans depends on three main factors: 1) solvent polarity 2) nature of the substituent groups, 3) concentration of the solution and it is governed by two mechanisms. The first mechanism is related to the shifting of the equilibrium between the SP and the MC form when the molecule is placed in solvent with different polarity. This effect is manifested by a shift in the absorption bands. The second is governed by the interactions that may occur between solvent and solute in solvents with different physical and chemical properties. In general for ISNBP as the polarity of the solvent increases, the maximum absorbance shifts to shorter wavelengths, higher frequency (*hypsochromic* or blue shift), while as the polarity decreases the maximum absorbance shifts to longer wavelengths, lower frequency (*bathochromic* or red shift) [90].

The coloured MC form is highly conjugated and characterised by a strong polar character, due to its zwitterionic character, which strongly contributes to the electronic distribution of the ground state. As a consequence, it is stabilised by polar solvents that decrease the thermal relaxation rate constant and the reversion MC→SP [85].

The colour of the MC form depends on the difference in polarity between the photo-excited MC form and the conjugated zwitterionic ground state. In polar solvents, the ground state of the MC form is stabilised relatively to the excited state, leading to a blue shift in the visible absorption band. In non-polar solvents, the energy difference between the ground and the excited state is much lower, because of the high energy level of the ground state. As a result the stabilisation of the conjugated zwitterionic MC form in polar solvents leads to a larger energy of activation and a slower conversion to the ring closed spiro form when compared to non-polar solvents (Figure 1.17).

The solvatochromic behaviour of spiropyrans will be further discussed in Chapter 7, where micro-capillary coatings based on spiropyran polymers will be examined for the optical detection of solvents of different polarities as they are passing inside micro-capillaries in continuous flow.

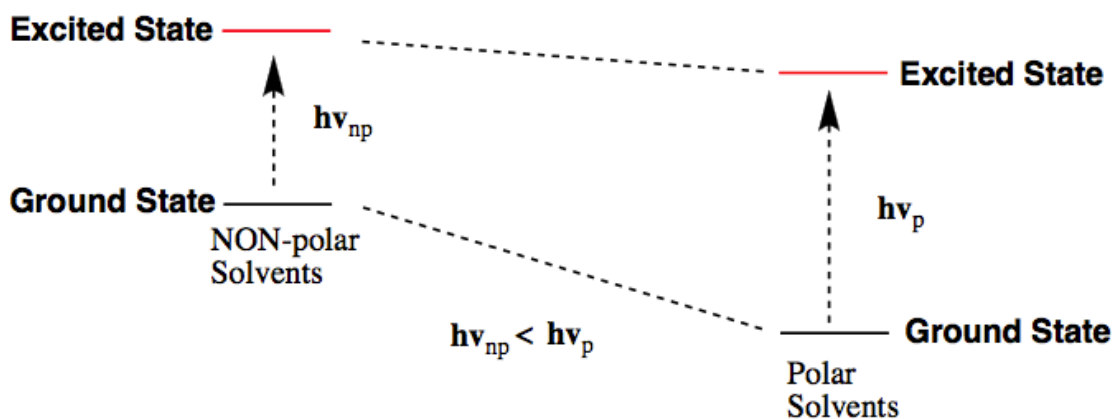


Figure 1.17. Schematic representation of the energy difference between the ground and the excited state of the MC form in polar and non-polar solvents. The colour of the MC form depends on the difference in polarity between the photo-excited MC form and the conjugated zwitterionic ground state. In polar solvents the ground state of the MC is stabilised relatively to the excited state, leading to a blue shift in the visible absorption band. In non-polar solvents, the energy difference between the ground state and the excited state is much lower, because of the high energy level of the ground state. (Reproduced from [90]).

Incorporation into Polymeric Materials

Since their discovery, photochromic spiropyrans (SP) have been incorporated into various materials *i.e.* surface bound monolayers [16, 81, 94, 95], Langmuir monolayers [96], Langmuir Blodgett films [96], polymeric brushes [97-100], photocontrollable surfactants [101], liquid crystalline materials [102], polymeric matrices [87, 98, 99, 103-119], organic/inorganic hybrid systems [120], colloidal particles [100, 121] and spiropyran initiators for radical polymerisations [122] and many others. Materials with photochromic spiropyrans have the advantage of reversibly photo-induce changes in their properties such as conductivity [106, 111, 123], wetting behaviour [87, 94, 97], optical properties [97, 105, 109, 114, 115, 118, 122], metal ion complexation [16, 82, 97, 110], cell adhesion [107], surface morphology [97], association/solubility [112, 113], mechanical effects [104, 119], colloidal system stability [100, 121], and membrane permeability [98, 99]. These properties have made spiropyran containing materials used for a variety of applications as such biological technologies [107], nonlinear optics [124], reversible optical memory [78, 106], optoelectronics [125] and chemical sensing [16, 81-83].

A comprehensive review discussing the incorporation of spiropyran derivatives into a variety of polymeric materials is given in Chapter 2 of this thesis. Specific examples are discussed in terms of the SP-incorporation techniques, influence of the SP's photochromic behaviour on the polymeric material and the applicability of the new-formed SP-containing polymers. Chapter 2 illustrates the great versatility and potential of polymeric materials incorporating spiropyran derivatives.

1.4.3 Integration in Micro-fluidic Devices

This section introduces the recent trends for the incorporation of stimuli-responsive polymers in micro-fluidic platforms, specifically micro-channels and micro-capillaries. It is structured in three main parts, based on the functionality of the stimuli-responsive polymers within micro-fluidic devices: pumps, valves and coatings.

The first two categories – specifically, pumps and valves, rely on the actuation propriety of some stimuli-responsive materials, able to convert external signals into a mechanical response. The most used actuators in micro-fluidics are hydrogels since they have the ability to undergo volumetric changes in response to an external stimulus, which is most often activated by a change in temperature, pH or a photo- or magneto-stimulus. The third category, coatings, relies on the intrinsic sensing proprieties of some stimuli-responsive polymers, able to detect analytes that are passing through the micro-fluidic platform. The inaccessibility of the coating makes, optical interrogation, one of the best approaches of collecting data that can be then related with the presence of a particular analyte. In these conditions, the “Coatings” section will cover stimuli-responsive materials, attached on the inner walls of a micro-channel or micro-capillary capable of changing their optical proprieties in response to the chemical/biological species that are transported through the micro-fluidic platform in continuous flow. Specific examples from recent literature, for each case will be outlined.

This section excludes adaptive materials that respond to optical stimulus as these are going to be extensively discussed in Chapter 3 of this Thesis – “Opto-Smart Systems in Microfluidics”.

1.4.3.1 Valves

Valves are one of the most important components within micro-fluidic systems, since they can regulate, direct or control the flow of a fluid and facilitate essential actions, such as sample/standard selection and addition of reagents. Incorporation of adaptive polymers allows control of the valve based on the intrinsic responsiveness of the adaptive polymer to thermal, chemical, electrical, optical or magnetic stimuli. Some examples of these valves will be further discussed here. Several reviews have outlined the fabrication and uses of polymer valves in micro-fluidics [126-128].

Satarkar and co-workers developed a nanocomposite hydrogel valve, in which magnetic nanoparticles were dispersed in temperature-responsive *N*-isopropylacrylamide (NIPAAm) polymer matrix [129] (Figure 1.18). The swelling and collapse of the resultant nanocomposite hydrogel valve was remotely controlled by application of an alternating magnetic field (AMF). When an AMF of 293 kHz is applied to the nanocomposite valve, this caused selective heating of the hydrogel nanocomposite above the lower critical solution temperature (LCST) of NIPAAm. As a consequence, the nanocomposite collapsed, leading to opening of the valve. Contrary, when the AMF was turned OFF, the cooling of the hydrogel nanocomposite resulted in recovery leading to closing of the valve. Application of multiple ON–OFF AMF cycles to the valve along with analysis of pressure at the inlet demonstrated that the valve could work for multiple cycles with good reproducibility.

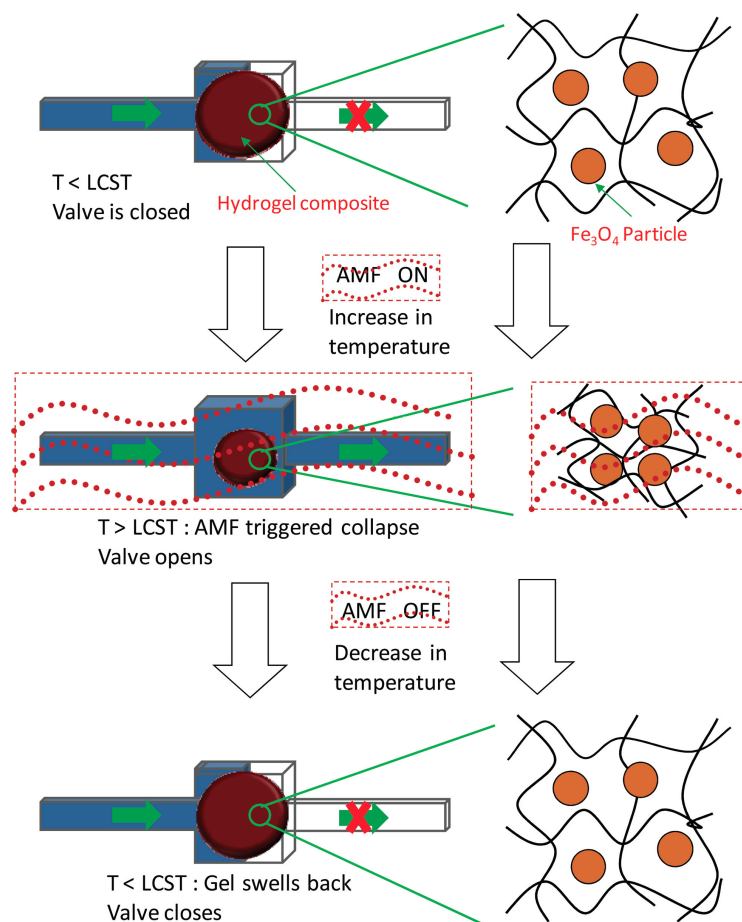


Figure 1.18. Scheme presenting the hydrogel nanocomposite valves performance with an alternating magnetic field (AMF). Application of the AMF results in collapse of the hydrogel, leading to opening of the valve. (Reproduced from [129])

In another example, Geiger *et al.* [130] presented a highly functional micro-fluidic device exhibiting an integrated thermally sensitive NIPAAm hydrogel valve. The valve was normally closed at room temperature. Upon heating above the LCST of 32°C, the polymer valve became hydrophobic, shrank while forming large pores, thus permitting the solution to flow. The valve has been actuated reliably over 100 times with no apparent degradation.

Chunder *et al.* [131] developed a superhydrophobic/hydrophilic switchable surface through the combination of layer-by-layer self-assembly and microfabrication techniques. This smart surface acted as a thermosensitive valve capable of controlling fluid flow by changing temperature. At 70 °C, the switchable surface is superhydrophobic and stops the water flow (closing status) while at room temperature, the surface becomes hydrophilic, and allows the flow (opening status).

Beebe *et al.* [132] designed and realised micro-valves by either patterning a pH-sensitive hydrogel along the walls of a channel or creating an array of the same hydrogel inside a micro-fluidic device. The swelling of these hydrogel structures blocked the channel when a high pH solution flowed into the channel, whereas when the pH value was appropriately decreased, the contracted state of hydrogel allowed the fluid to pass (Figure 1.19 A). Based on the valve mechanism described above, a pH-dependent flow sorter was also demonstrated (Figure 1.19 B) [132]. This device consisted of a “T” channel in which the entrance to each branch was gated with a hydrogel microstructure of different chemical compositions. The hydrogel for one branch expanded at high pH and contracted at low pH, while the hydrogel that gated the other branch exhibited an inverse behavior. Consequently, this device was capable of directing the flow from the centre channel through one branch or the other depending on the pH of the solution.

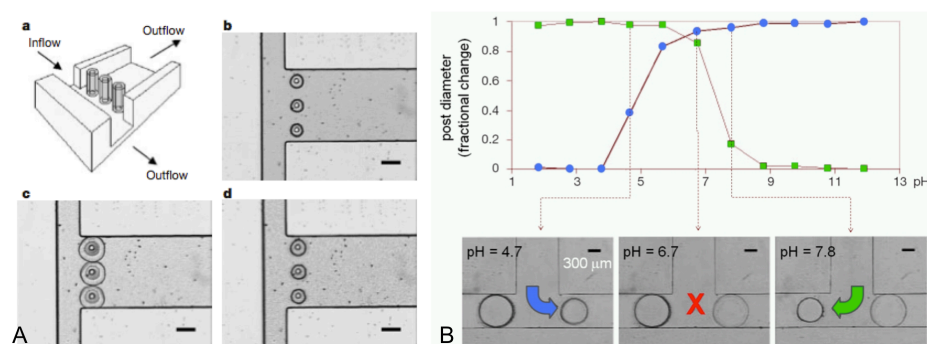


Figure 1.19. A) Prefabricated posts in a micro-channel serve as supports for hydrogel films, improving stability during volume changes. a) A diagram of the hydrogel films around the posts. b) The actual device after polymerisation of the hydrogel. c) The hydrogel films block the side channel branch in their expanded state. d) The contracted hydrogels allow fluid to flow down the side branch. B) The volume response of two different hydrogels with respect to the pH of the surrounding fluid. Top, the fractional change in diameter (f_D) of the hydrogels with respect to pH. Bottom, images showing a device that directs a fluid stream on the basis of its pH. The hydrogel gating the right branch (circles) expands in base and contracts in acid. The hydrogel gating the left branch (squares) behaves in the opposite manner (expands in acid and contracts in base). The fluid enters from the centre channel at a rate of 0.05 mL min^{-1} . At a pH of 7.8, the flow is directed down the left branch. At a pH of 4.7, the flow is directed down the right branch. Both hydrogels expand to shut off the flow when the pH is changed to 6.7. Scale bars, $300 \mu\text{m}$. (Reproduced from [132])

Kim *et al.* [133] developed a hydrodynamic fabrication method for pH-responsive microspheres based on acrylic acid, housed in a PDMS-based micro-fluidic valve, as reported in Figure 1.20. The analysis of volume-changes by alternating application of acidic and basic solutions showed a large and fast volume transition, which was stable and reproducible even under repeated motions.

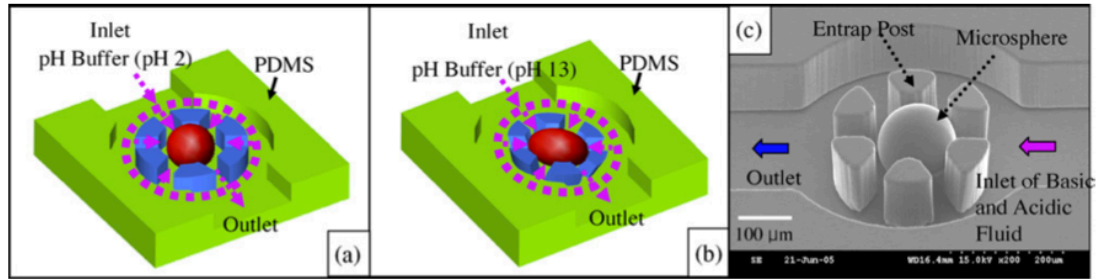


Figure 1.20. (a) Conceptual schematic (three-dimensional) of the shrinking motion of the microsphere inside the entrap posts (valve is in the “On” state). (b) Conceptual schematic (three dimensional) of the swelling motion inside the entrap posts (valve is in the “Off” state). (c) SEM image of the microsphere positioned inside the entrap posts. (Reproduced from [133])

Another pH responsive valve has been reported by Yu *et al.* [134]. The valve consisted of a pair of pH sensitive 2-hydroxyethyl methacrylate and acrylic acid 4:1 molar ratio (poly(HEMA-co-AA)) hydrogel strips overlapped by a pair of pH-insensitive strips (Figure 1.21). When exposed to pH 8 phosphate buffer, the pH-sensitive strips swelled while the pH-insensitive strips remained unchanged, causing the hydrogel bistris to extend and curve, thereby forming a check valve. Because of the geometry and orientation of the valve, forward flow pushes the bistris apart (Figure 1.21 c) while backward flow forces them together (Figure 1.21 d). Thus, the bistris operates like venous valves to control fluid flow. When acidic solution (pH = 3) enters the channel, the pH sensitive strips shrink, allowing both forward and backward flow. In comparison to traditional micro-fluidic valves where actuation occurs very rapidly, here the activation and deactivation times are quite slow, at 6 and 3 minutes respectively. Therefore, this slow operating valve can be successfully applied in drug delivery and bioassay devices, where timescales for events can be of the order of hours.

and 3 minutes respectively. However, this slow operating valve can be successfully applied in drug delivery and bioassay devices, where timescales for events can be of the order of hours.

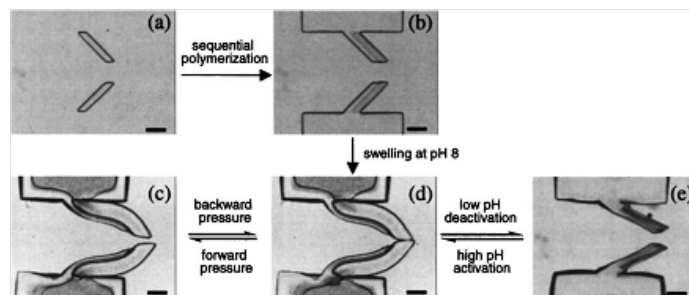


Figure 1.21. Fabrication and operation of a biomimetic valve based on a bistrup hydrogel. (a) Bistrup hydrogel is patterned by simultaneous photopolymerisation. (b) The anchor of the valve is formed using a non-responsive hydrogel. (c) When exposed to a basic solution, the bistrup hydrogels expand and curve to form a normally closed valve. (d) The bistrup valve is pushed open to allow flow in one direction (from left to right). (e) The flow is restricted in the opposite direction. (f) When exposed to acidic solutions, the valve is deactivated, returning to the permanently open state. Scale bars represent 500 μm . (Reproduced from [134])

1.4.3.2 Pumps

Several micro-pumps based on adaptive polymeric materials have been reported to date [135, 136]. Pumps in micro-fluidic devices allow the control of flows inside micro-channels in response to external stimuli. The main advantages of micro-pumps are low energy consumption, minimal sample carryover, and low-cost manufacture.

A diffusion micro-pump and a displacement pump, both based on the temperature-sensitive hydrogel poly(*N*-isopropylacrylamide) (PNIPAAm) have been reported by Ritcher *et al.* [137]. In the diffusion pump, if the swollen PNIPAAm actuator is heated, the micro-pump shrinks causing the solution to be released into the outlet and generate pumping pressure; when the hydrogel actuator is cooled down, the micro-pump swells by absorbing the liquid, leading to the deformation of an elastic membrane, which acts as pressure accumulator (Figure 1.22 a). The flow rate obtained for this device was $2.8 \pm 0.35 \mu\text{L min}^{-1}$.

In the displacement micro-pump reported by Ritcher *et al.* [137], unlike in diffusion type, the polymeric actuator generates pumping pressure when swelling, and the pressure is reduced when the pumping fluid fills the chamber, *i.e.* when the hydrogel is in the shrunk phase (Figure 1.22 b). This type of pump presents higher performance (flow rate of $4.5 \mu\text{L min}^{-1}$ and a back pressure of 1.28 kPa). Generally, these polymeric micro-pumps have a simple electrothermic control by means of resistive heating elements, which locally heat the thermo-responsive hydrogel. Inexpensive design, simple control and soft lithographic fabrication make these hydrogel pumps a significant advance towards the realisation of disposable micro-fluidic components.

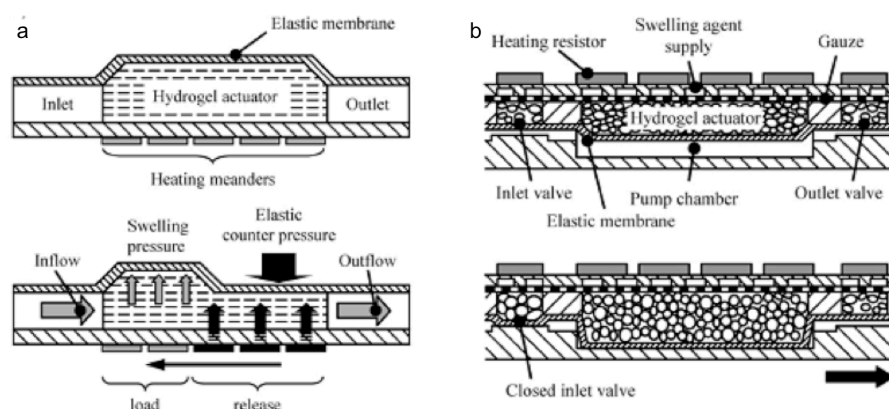


Figure 1.22. Schematic set-up and operating principle of diffusion micro-pump (a) and displacement micro-pump (b). (Reproduced from [137])

Magnetic stimulus responsive materials can be also used to generate flow. In this context, an innovative way of pumping fluid was demonstrated by Fahrni *et al.* [138] where ferromagnetic nanoparticles were incorporated into a PDMS copolymer and photo-polymerised in the channels to produce ‘artificial cilia’. The cilia moved in a rotating magnetic field, pumping liquid down the channel during the process. Flow visualisation experiments in a micro-channel indicated induced fluid velocities up to 0.5 mm s^{-1} .

Another example of micro-pump that used magnetic actuation was reported by Hatch *et al.* [139]. The operation of this pump used magnetically-actuated plugs of a ferrofluid (nanosize ferromagnetic particles suspended in an oil-based solvent). The ferrofluid was circulated in a circular channel with a permanent magnet. The motion of the ferrofluid plug caused portions of liquid to be pumped through the system.

Using a different approach, Kwon and co-workers [140] reported a valve-less micro-pump system based on the electroactive hydrogel 4-hydroxybutyl acrylate (4-HBA). The proposed micro-pump system (Figure 1.23), powered by a single 1.5 V commercial battery, expended very little energy (less than 750 mW per stroke) while pumping 0.9 wt % saline solution under a low voltage (less than 1 V), and remained fully functional after 6 months.

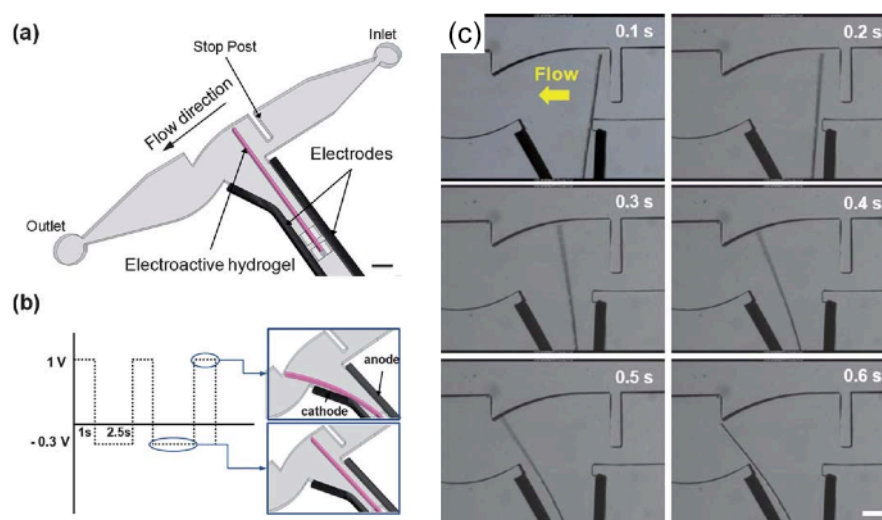


Figure 1.23. (a) Schematic illustration of the pumping system. The scale bar indicates 1 mm. (b) Electrical signal: the forward signal indicates hydrogel bending toward the cathode, and the backward signal indicates the hydrogel bending toward the anode. (c) Sequential photographs showing the gradual development of pumping at 1 V. The scale bar indicates 500 μ m. (Reproduced from [140]).

1.4.3.3 Coatings

Several coatings based on adaptive polymers have been reported in literature and their sensing capabilities have been evaluated.

Castelletti *et al.* [141] reported an integrated capillary electrophoresis sensor for L-ascorbic acid detection. The detection part of the micro-capillary column was modified with a thin film of polyaniline (Figure 1.24 A) and ascorbic acid was detected by monitoring the changes in the optical absorbance of the polyaniline film upon the reduction reaction. It was found that the sensor response (change in optical

absorbance at 650 nm) is directly proportional to the concentration of ascorbic acid (Figure 1.24 B), allowing detection of ascorbic acid over the range of 5–75 mg L⁻¹.

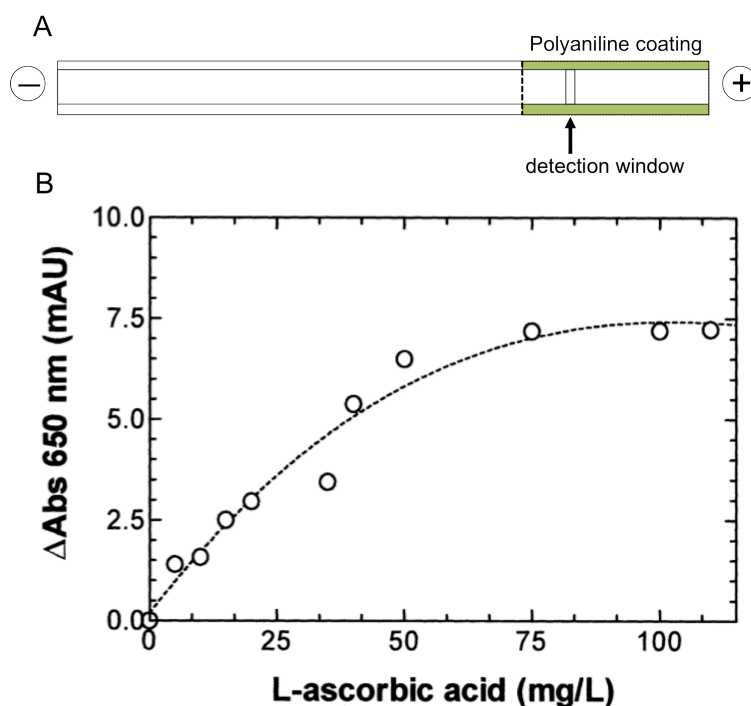


Figure 1.24. A - Scheme of polyaniline coated micro-capillary. B - Sensor response to ascorbic acid. The optical absorbance of polyaniline at the detection window was measured at 650 nm. Analysis was performed in 50 mM aspartic acid buffer. (Reproduced from [141])

In a different approach, Hisamoto *et al.* [142] coated square micro-capillaries with a PVC copolymer containing a calcium ionophore and a lipophilic dye. In this case the coating is not homogeneous all over the walls of the capillary but the cocktail material is deposited as ion-selective optode membranes at the four corners of the inner capillary (Figure 1.25 A). The membranes responded to Ca²⁺ in the concentration range 10⁻⁵ M – 1M (Figure 1.25 B). Using the same approach, the authors showed the immobilisation of a polymeric membrane containing Fluorescein isothiocyanate (FITC) that could be used for pH sensing.

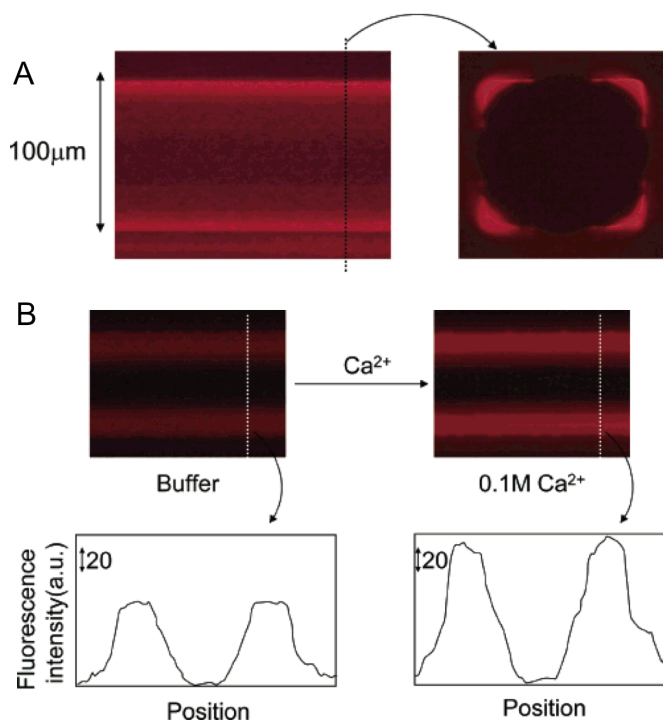


Figure 1.25. A- Top and cross sectional fluorescence images of PVC membrane-attached square capillary; B - Fluorescence response of the membrane-coating towards calcium ion. (Reproduced from [142])

Although the potential of these coatings can be easily appreciated, very few examples are presented to date in the literature. We believe that stimuli-responsive polymeric coatings grafted on the inner walls of a micro-channel or micro-capillary, that change their optical properties in response to the analyte passing inside, offer the possibility of building micro-fluidic integrated optical sensors. Having an inherently responsive micro-channel or micro-capillary means that specific analytes moving through the system can be detected dynamically along the entire channel length in real time, without the need to add reagents to the sample. On this basis, Chapters 4 to 7 of this thesis focus on the development of adaptive polymeric coatings in micro-fluidic devices. Applications of these coatings for pH, ammonia and solvent detection in continuous flow are presented.

1.5 References

1. West, J.; Becker, M.; Tombrink, S.; Manz, A., Micro total analysis systems: Latest achievements. *Analytical Chemistry* **2008**, *80*, 4403-4419.
2. Martinez, A. W.; Phillips, S. T.; Whitesides, G. M.; Carrilho, E., Diagnostics for the Developing World: Microfluidic Paper-Based Analytical Devices. *Analytical Chemistry* **2010**, *82*, 3-10.
3. Arora, A.; Simone, G.; Salieb-Beugelaar, G. B.; Kim, J. T.; Manz, A., Latest Developments in Micro Total Analysis Systems. *Analytical Chemistry* **2010**, *82*, 4830-4847.
4. Ohno, K.-i.; Tachikawa, K.; Manz, A., Microfluidics: Applications for analytical purposes in chemistry and biochemistry. *Electrophoresis* **2008**, *29*, 4443-4453.
5. Salieb-Beugelaar, G. B.; Simone, G.; Arora, A.; Philippi, A.; Manz, A., Latest Developments in Microfluidic Cell Biology and Analysis Systems. *Analytical Chemistry* **2010**, *82*, 4848-4864.
6. Muhammad-Tahir, Z.; Alocilja, E. C., Fabrication of a disposable biosensor for Escherichia coli O157 : H7 detection. *IEEE Sensors Journal* **2003**, *3*, 345-351.
7. Ziober, B. L.; Mauk, M. G.; Falls, E. M.; Chen, Z.; Ziober, A. F.; Bau, H. H., Lab-on-a-chip for oral cancer screening and diagnosis. *Head and Neck-Journal for the Sciences and Specialties of the Head and Neck* **2008**, *30*, 111-121.
8. Horsman, K. M.; Bienvenue, J. M.; Blasier, K. R.; Landers, J. P., Forensic DNA analysis on microfluidic devices: A review. *Journal of Forensic Sciences* **2007**, *52*, 784-799.
9. Harrison, D. J.; Fluri, K.; Seiler, K.; Fan, Z. H.; Effenhauser, C. S.; Manz, A., Micromachining a miniaturized capillary electrophoresis-based chemical-analysis system on a chip. *Science* **1993**, *261*, 895-897.
10. Yan, H.; Zhang, B.; Wu, H., Chemical cytometry on microfluidic chips. *Electrophoresis* **2008**, *29*, 1775-1786.
11. Borgatti, M.; Altomare, L.; Baruffa, M.; Fabbri, E.; Breveglieri, G.; Feriotto, G.; Maresi, N.; Medoro, G.; Romani, A.; Tartagni, M.; Gambari, R.; Guerrieri, R., Separation of white blood cells from erythrocytes on a dielectrophoresis (DEP) based 'Lab-on-a-chip' device. *International Journal of Molecular Medicine* **2005**, *15*, 913-920.
12. Gubala, V.; Harris, L. F.; Ricco, A. J.; Tan, M. X.; Williams, D. E., Point of Care Diagnostics: Status and Future. *Analytical Chemistry* **2012**, *84*, 487-515.
13. Hawtin, P.; Hardern, I.; Wittig, R.; Mollenhauer, J.; Poustka, A.; Salowsky, R.; Wulff, T.; Rizzo, C.; Wilson, B., Utility of lab-on-a-chip technology for high-throughput nucleic acid and protein analysis. *Electrophoresis* **2005**, *26*, 3674-3681.
14. Liu, S. R.; Shi, Y. N.; Ja, W. W.; Mathies, R. A., Optimization of high-speed DNA sequencing on microfabricated capillary electrophoresis channels. *Analytical Chemistry* **1999**, *71*, 566-573.
15. Dong, L.; Jiang, H., Autonomous microfluidics with stimuli-responsive hydrogels. *Soft Matter* **2007**, *3*, 1223-1230.
16. Benito-Lopez, F.; Scarmagnani, S.; Walsh, Z.; Paull, B.; Macka, M.; Diamond, D., Spiropyran modified micro-fluidic chip channels as photonically controlled self-indicating system for metal ion accumulation and release. *Sensors and Actuators B-Chemical* **2009**, *140*, 295-303.
17. Yamaguchi, A.; Jin, P.; Tsuchiyama, H.; Masuda, T.; Sun, K.; Matsuo, S.; Misawa, H., Rapid fabrication of electrochemical enzyme sensor chip using polydimethylsiloxane microfluidic channel. *Analytica Chimica Acta* **2002**, *468*, 143-152.
18. Lobnik, A.; Turel, M.; Korent Urek, Š., *Advances in Chemical Sensors*. InTech: 2012.

19. Schazmann, B.; Alhashimy, N.; Diamond, D., Chloride selective calix 4 arene optical sensor combining urea functionality with pyrene excimer transduction. *Journal of the American Chemical Society* **2006**, *128*, 8607-8614.
20. Narayanaswamy, R., Optical chemical sensors - Transduction and signal-processing. *Analyst* **1993**, *118*, 317-322.
21. Wolfbels, O. S., Fiber-optic chemical sensors and biosensors. *Analytical Chemistry* **2008**, *80*, 4269-4283.
22. Gauglitz, G., Direct optical sensors: principles and selected applications. *Analytical and Bioanalytical Chemistry* **2005**, *381*, 141-155.
23. Baldini, F.; Giannetti, A.; Mencaglia, A. A., Optical sensor for interstitial pH measurements. *Journal of biomedical optics* **2007**, *12*, 024024.
24. Baldini, F.; Bracci, S., Adsorption-based optical transduction in optical fibre chemical sensors for environmental and industrial applications. *Adsorption and Its Applications in Industry and Environmental Protection, Vol II: Applications in Environmental Protection* **1999**, *120*, 925-948.
25. Wilhelm, A. A.; Lucas, P.; DeRosa, D. L.; Riley, M. R., Biocompatibility of Te-As-Se glass fibers for cell-based bio-optic infrared sensors. *Journal of Materials Research* **2007**, *22*, 1098-1104.
26. Psaltis, D.; Quake, S. R.; Yang, C., Developing optofluidic technology through the fusion of microfluidics and optics. *Nature* **2006**, *442*, 381-386.
27. Miwa, J.; Suzuki, Y.; Kasagi, N., Adhesion-Based Cell Sorter With Antibody-Coated Amino-Functionalized-Parylene Surface. *Journal of Microelectromechanical Systems* **2008**, *17*, 611-622.
28. Mela, P.; Onclin, S.; Goedbloed, M. H.; Levi, S.; Garcia-Parajo, M. F.; van Hulst, N. F.; Ravoo, B. J.; Reinhoudt, D. N.; van den Berg, A., Monolayer-functionalized microfluidics devices for optical sensing of acidity. *Lab on a Chip* **2005**, *5*, 163-170.
29. Basabe-Desmonts, L.; Benito-Lopez, F.; Gardeniers, H. J. G. E.; Duwel, R.; van den Berg, A.; Reinhoudt, D. N.; Crego-Calama, M., Fluorescent sensor array in a microfluidic chip. *Analytical and Bioanalytical Chemistry* **2008**, *390*, 307-315.
30. Zhao, B.; Moore, J. S.; Beebe, D. J., Surface-directed liquid flow inside microchannels. *Science* **2001**, *291*, 1023-1026.
31. Sui, Z. J.; Schlenoff, J. B., Controlling electroosmotic flow in microchannels with pH-responsive polyelectrolyte multilayers. *Langmuir* **2003**, *19*, 7829-7831.
32. Kirby, B. J.; Wheeler, A. R.; Zare, R. N.; Fruetel, J. A.; Shepodd, T. J., Programmable modification of cell adhesion and zeta potential in silica microchips. *Lab on a Chip* **2003**, *3*, 5-10.
33. Munro, N. J.; Huhmer, A. F. R.; Landers, J. P., Robust polymeric microchannel coatings for microchip-based analysis of neat PCR products. *Analytical Chemistry* **2001**, *73*, 1784-1794.
34. Xiong, L.; Regnier, F. E., Channel-specific coatings on microfabricated chips. *Journal of Chromatography A* **2001**, *924*, 165-176.
35. Flink, S.; van Veggel, F.; Reinhoudt, D. N., Sensor functionalities in self-assembled monolayers. *Advanced Materials* **2000**, *12*, 1315-1328.
36. van der Veen, N. J.; Flink, S.; Deij, M. A.; Egberink, R. J. M.; van Veggel, F.; Reinhoudt, D. N., Monolayer of a Na⁺-selective fluoroionophore on glass: Connecting the fields of monolayers and optical detection of metal ions. *Journal of the American Chemical Society* **2000**, *122*, 6112-6113.
37. Crego-Calama, M.; Reinhoudt, D. N., New materials for metal ion sensing by self-assembled monolayers on glass. *Advanced Materials* **2001**, *13*, 1171-+.
38. Rudzinski, C. M.; Young, A. M.; Nocera, D. G., A supramolecular microfluidic optical chemosensor. *Journal of the American Chemical Society* **2002**, *124*, 1723-1727.
39. Zhao B, B. W., Polymer brushes: surface-immobilized macromolecules *Progress in Polymer Science* **2000**, *25*, 677-710.

40. Uhlmann, P.; Ionov, L.; Houbenov, N.; Nitschke, M.; Grundke, K.; Motornov, M.; Minko, S.; Stamm, M., Surface functionalization by smart coatings: Stimuli-responsive binary polymer brushes. *Progress in Organic Coatings* **2006**, *55*, 168-174.
41. Jin, Q.; Liu, G.; Ji, J., Micelles and Reverse Micelles with a Photo and Thermo Double-Responsive Block Copolymer. *Journal of Polymer Science Part a-Polymer Chemistry* **2010**, *48*, 2855-2861.
42. Garcia, A.; Marquez, M.; Cai, T.; Rosario, R.; Hu, Z.; Gust, D.; Hayes, M.; Vail, S. A.; Park, C.-D., Photo-, thermally, and pH-responsive microgels. *Langmuir* **2007**, *23*, 224-229.
43. Delcea, M.; Moehwald, H.; Skirtach, A. G., Stimuli-responsive LbL capsules and nanoshells for drug delivery. *Advanced Drug Delivery Reviews* **2011**, *63*, 730-747.
44. Wallace, G. G.; Spinks, G. M.; Kane-Maguire, L. A. P.; Teasdale, P. R., *Conductive electroactive polymers*. CRC Press LLC: 2003.
45. Beaujuge, P. M.; Reynolds, J. R., Color Control in pi-Conjugated Organic Polymers for Use in Electrochromic Devices. *Chemical Reviews* **2010**, *110*, 268-320.
46. Fuchiwaki, M.; Tanaka, K.; Kaneto, K., Planate conducting polymer actuator based on polypyrrole and its application. *Sensors and Actuators a-Physical* **2009**, *150*, 272-276.
47. Hutchison, A. S.; Lewis, T. W.; Moulton, S. E.; Spinks, G. M.; Wallace, G. G., Development of polypyrrole-based electromechanical actuators. *Synthetic Metals* **2000**, *113*, 121-127.
48. Hatchett, D. W.; Josowicz, M., Composites of intrinsically conducting polymers as sensing nanomaterials. *Chemical Reviews* **2008**, *108*, 746-769.
49. Berti, F.; Todros, S.; Lakshmi, D.; Whitcombe, M. J.; Chianella, I.; Ferroni, M.; Piletsky, S. A.; Turner, A. P. F.; Marrazza, G., Quasi-monodimensional polyaniline nanostructures for enhanced molecularly imprinted polymer-based sensing. *Biosensors & Bioelectronics* **2010**, *26*, 497-503.
50. Shirsat, M. D.; Bangar, M. A.; Deshusses, M. A.; Myung, N. V.; Mulchandani, A., Polyaniline nanowires-gold nanoparticles hybrid network based chemiresistive hydrogen sulfide sensor. *Applied Physics Letters* **2009**, *94*.
51. Macdiarmid, A. G.; Epstein, A. J., Polyanilines - A novel class of conducting polymers. *Faraday Discussions* **1989**, *88*, 317-+.
52. Lu, X. H.; Ng, H. Y.; Xu, J. W.; He, C. B.; He, B., Electrical conductivity of polyaniline-dodecylbenzene sulphonic acid complex: thermal degradation and its mechanism. *Synthetic Metals* **2002**, *128*, 167-178.
53. Campos, M.; Bello, B., Mechanism of conduction in doped polyaniline. *Journal of Physics D-Applied Physics* **1997**, *30*, 1531-1535.
54. Wnek, G. E., A proposal for the mechanism of conduction in polyaniline. *Synthetic Metals* **1986**, *15*, 213-218.
55. Syed, A. A.; Dinesan, M. K., Polyaniline - A novel polymeric material - Review. *Talanta* **1991**, *38*, 815-837.
56. Ameen, S.; Akhtar, M. S.; Husain, M., A Review on Synthesis Processing, Chemical and Conduction Properties of Polyaniline and Its Nanocomposites. *Science of Advanced Materials* **2010**, *2*, 441-462.
57. Sapurina, I.; Stejskal, J., The mechanism of the oxidative polymerization of aniline and the formation of supramolecular polyaniline structures. *Polymer International* **2008**, *57*, 1295-1325.
58. MacDiarmid, A. G., "Synthetic metals": A novel role for organic polymers (Nobel lecture). *Angewandte Chemie-International Edition* **2001**, *40*, 2581-2590.
59. Martin, C. R., Template synthesis of electronically conductive polymer nanostructures. *Accounts of Chemical Research* **1995**, *28*, 61-68.
60. Yang, L.-Y.; Liao, W.-B., Chemical synthesis of polyaniline inverse opals by templating colloidal crystals in the presence of dodecylbenzenesulfonic acid. *Macromolecular Chemistry and Physics* **2007**, *208*, 994-1001.

61. Wang, P.-C.; Venancio, E. C.; Sarno, D. M.; MacDiarmid, A. G., Simplifying the reaction system for the preparation of polyaniline nanofibers: Re-examination of template-free oxidative chemical polymerization of aniline in conventional low-pH acidic aqueous media. *Reactive & Functional Polymers* **2009**, *69*, 217-223.
62. Wei, Y.; Sun, Y.; Jang, G. Ä.; Tang, X., Effects of p,Äâaminodiphenylamine on electrochemical polymerization of aniline. *Journal of Polymer Science Part C: Polymer Letters* **1990**, *28*, 81-87.
63. Cameron, R. E.; Clement, S. K., Preparation of conductive polyaniline having controlled molecular weight. In Google Patents: 1991.
64. Zhang, X. Y.; Chan-Yu-King, R.; Jose, A.; Manohar, S. K., Nanofibers of polyaniline synthesized by interfacial polymerization. *Synthetic Metals* **2004**, *145*, 23-29.
65. Huang, J. X., Syntheses and applications of conducting polymer polyaniline nanofibers. *Pure and Applied Chemistry* **2006**, *78*, 15-27.
66. E. Lahiff; T. Woods; W. Blau; G. Wallace; Diamond, D., Synthesis and Characterisation of Controllably Functionalised Polyaniline Nanofibres. *Synthetic Metals* **In Press**.
67. Karyakin, A. A.; Vuki, M.; Lukachova, L. V.; Karyakina, E. E.; Orlov, A. V.; Karpachova, G. P.; Wang, J., Processible polyaniline as an advanced potentiometric pH transducer. Application to biosensors. *Analytical Chemistry* **1999**, *71*, 2534-2540.
68. Gill, E. I.; Arshak, A.; Arshak, K.; Korostynska, O., Investigation of Thick-Film Polyaniline-Based Conductimetric pH Sensors for Medical Applications. *IEEE Sensors Journal* **2009**, *9*, 555-562.
69. Jin, Z.; Su, Y. X.; Duan, Y. X., An improved optical pH sensor based on polyaniline. *Sensors and Actuators B-Chemical* **2000**, *71*, 118-122.
70. Grummt, U. W.; Pron, A.; Zagorska, M.; Lefrant, S., Polyaniline based optical pH sensor. *Analytica Chimica Acta* **1997**, *357*, 253-259.
71. Dhand, C.; Das, M.; Datta, M.; Malhotra, B. D., Recent advances in polyaniline based biosensors. *Biosensors & Bioelectronics* **2011**, *26*, 2811-2821.
72. Epstein, A. J.; Ginder, J. M.; Zuo, F.; Bigelow, R. W.; Woo, H. S.; Tanner, D. B.; Richter, A. F.; Huang, W. S.; Macdiarmid, A. G., Insulator-to-metal transition in polyaniline. *Synthetic Metals* **1987**, *18*, 303-309.
73. Chiang, J. C.; Macdiarmid, A. G., Polyaniline - Protonic acid doping of the emeraldine form to the metallic regime. *Synthetic Metals* **1986**, *13*, 193-205.
74. Byrne, R.; Benito-Lopez, F.; Diamond, D., Materials science and the sensor revolution. *Materials Today* **2010**, *13*, 9-16.
75. Byrne, R. J.; Stitzel, S. E.; Diamond, D., Photo-regenerable surface with potential for optical sensing. *Journal of Materials Chemistry* **2006**, *16*, 1332-1337.
76. Crano, J. C.; Flood, T.; Knowles, D.; Kumar, A.; VanGemert, B., Photochromic compounds: Chemistry and application in ophthalmic lenses. *Pure and Applied Chemistry* **1996**, *68*, 1395-1398.
77. Dvornikov, A. S.; Malkin, J.; Rentzepis, P. M., Spectroscopy and kinetics of photochromic materials for 3d optical memory devices. *Journal of Physical Chemistry* **1994**, *98*, 6746-6752.
78. Berkovic, G.; Krongauz, V.; Weiss, V., Spiropyran and spirooxazines for memories and switches. *Chemical Reviews* **2000**, *100*, 1741-1753.
79. Zhou, W.; Chen, D.; Li, J.; Xu, J.; Lv, J.; Liu, H.; Li, Y., Photoisomerization of spiropyran for driving a molecular shuttle. *Organic Letters* **2007**, *9*, 3929-3932.
80. Winkler, J. D.; Deshayes, K.; Shao, B., Photodynamic transport of metal-ions. *Journal of the American Chemical Society* **1989**, *111*, 769-770.
81. Rosario, R.; Gust, D.; Hayes, M.; Springer, J.; Garcia, A. A., Solvatochromic study of the microenvironment of surface-bound spiropyran. *Langmuir* **2003**, *19*, 8801-8806.

82. Fries, K. H.; Driskell, J. D.; Samanta, S.; Locklin, J., Spectroscopic Analysis of Metal Ion Binding in Spiropyran Containing Copolymer Thin Films. *Analytical Chemistry* **2010**, *82*, 3306-3314.
83. Fries, K. H.; Driskell, J. D.; Sheppard, G. R.; Locklin, J., Fabrication of Spiropyran-Containing Thin Film Sensors Used for the Simultaneous Identification of Multiple Metal Ions. *Langmuir* **2011**, *27*, 12253-12260.
84. Kobatake, S.; Irie, M., Synthesis and photochromism of diarylethenes with isopropyl groups at the reactive carbons and long pi-conjugated heteroaryl groups. *Chemistry Letters* **2003**, *32*, 1078-1079.
85. Minkin, V. I., Photo-, thermo-, solvato-, and electrochromic spiroheterocyclic compounds. *Chemical Reviews* **2004**, *104*, 2751-2776.
86. Raymo, F. M.; Giordani, S., Signal processing at the molecular level. *Journal of the American Chemical Society* **2001**, *123*, 4651-4652.
87. Anastasiadis, S. H.; Lygeraki, M. I.; Athanassiou, A.; Farsari, M.; Pisignano, D., Reversibly Photo-Responsive Polymer Surfaces for Controlled Wettability. *Journal of Adhesion Science and Technology* **2008**, *22*, 1853-1868.
88. Gerner, H., Photochromism of nitrospiropyrans: effects of structure, solvent and temperature. *Physical Chemistry Chemical Physics* **2001**, *3*, 416-423.
89. Fischer, E.; Hirshberg, Y., Formation of coloured forms of spirans by low-temperature irradiation. *Journal of the Chemical Society* **1952**, 4522-4524.
90. Dürr, H.; Bouas-Laurent, H., *Photochromism: Molecules and Systems*. Elsevier: 2003.
91. Aldoshin, S. M., Spiropyran - structural features and photochemical properties. *Molecular Crystals and Liquid Crystals Science and Technology Section a-Molecular Crystals and Liquid Crystals* **1994**, *246*, 207-214.
92. Chibisov, A. K.; Gerner, H., Photoprocesses in spirooxazines and their merocyanines. *Journal of Physical Chemistry A* **1999**, *103*, 5211-5216.
93. Aramaki, S.; Atkinson, G. H., Spirooxazine photochromism - Picosecond time-resolved raman and absorption-spectroscopy. *Chemical Physics Letters* **1990**, *170*, 181-186.
94. Dattilo, D.; Armelao, L.; Fois, G.; Mistura, G.; Maggini, M., Wetting properties of flat and porous silicon surfaces coated with a spiropyran. *Langmuir* **2007**, *23*, 12945-12950.
95. Rosario, R.; Gust, D.; Hayes, M.; Jahnke, F.; Springer, J.; Garcia, A. A., Photon-modulated wettability changes on spiropyran-coated surfaces. *Langmuir* **2002**, *18*, 8062-8069.
96. Tachibana, H.; Yamanaka, Y.; Matsumoto, M., Surface and photochemical properties of Langmuir monolayer and Langmuir-Blodgett films of a spiropyran derivative. *Journal of Materials Chemistry* **2002**, *12*, 938-942.
97. Samanta, S.; Locklin, J., Formation of photochromic spiropyran polymer brushes via surface-initiated, ring-opening metathesis polymerization: Reversible photocontrol of wetting behavior and solvent dependent morphology changes. *Langmuir* **2008**, *24*, 9558-9565.
98. Park, Y. S.; Ito, Y.; Imanishi, Y., Photocontrolled gating by polymer brushes grafted on porous glass filter. *Macromolecules* **1998**, *31*, 2606-2610.
99. Chung, D. J.; Ito, Y.; Imanishi, Y., Preparation of porous membranes grafted with poly(spiropyran-containing methacrylate) and photocontrol of permeability. *Journal of Applied Polymer Science* **1994**, *51*, 2027-2033.
100. Piech, M.; Bell, N. S., Controlled synthesis of photochromic polymer brushes by atom transfer radical polymerization. *Macromolecules* **2006**, *39*, 915-922.
101. Sakai, H.; Ebana, H.; Sakai, K.; Tsuchiya, K.; Ohkubo, T.; Abe, M., Photo-isomerization of spiropyran-modified cationic surfactants. *Journal of Colloid and Interface Science* **2007**, *316*, 1027-1030.

102. Lee, M. J.; Yoo, B. W.; Shin, S. T.; Keum, S. R., Synthesis and properties of new liquid crystalline compounds containing an indolinobenzospiropyranylazo group. Part 3. *Dyes and Pigments* **2001**, *51*, 15-24.
103. Adelmann, R.; Mela, P.; Gallyamov, M. O.; Keul, H.; Moeller, M., Synthesis of High-Molecular-Weight Linear Methacrylate Copolymers with Spiropyran Side Groups: Conformational Changes of Single Molecules in Solution and on Surfaces. *Journal of Polymer Science Part a-Polymer Chemistry* **2009**, *47*, 1274-1283.
104. Alonso, M.; Reboto, V.; Guiscardo, L.; San Martin, A.; Rodriguez-Cabello, J. C., Spiropyran derivative of an elastin-like bioelastic polymer: Photoresponsive molecular machine to convert sunlight into mechanical work. *Macromolecules* **2000**, *33*, 9480-9482.
105. Angiolini, L.; Benelli, T.; Giorgini, L.; Raymo, F. M., Optical and chiroptical switches based on photoinduced photon and proton transfer in copolymers containing spiropyran and azopyridine chromophores in their side chains. *Polymer* **2009**, *50*, 5638-5646.
106. Guo, X. F.; Zhang, D.; Gui, Y.; Wax, M. X.; Li, J. C.; Liu, Y. Q.; Zhu, D. B., Reversible photoregulation of the electrical conductivity of spiropyran-doped polyaniline for information recording and nondestructive processing. *Advanced Materials* **2004**, *16*, 636-+.
107. Higuchi, A.; Hamamura, A.; Shindo, Y.; Kitamura, H.; Yoon, B. O.; Mori, T.; Uyama, T.; Umezawa, A., Photon-modulated changes of cell attachments on poly(spiropyran-co-methyl methacrylate) membranes. *Biomacromolecules* **2004**, *5*, 1770-1774.
108. Irie, M.; Iwayanagi, T.; Taniguchi, Y., Photoresponsive polymers .7. Reversible solubility change of polystyrene having pendant spirobenzopyran groups and its application to photoresists. *Macromolecules* **1985**, *18*, 2418-2422.
109. Ivanov, A. E.; Ereemeev, N. L.; Wahlund, P. O.; Galaev, I. Y.; Mattiasson, B., Photosensitive copolymer of N-isopropylacrylamide and methacryloyl derivative of spirobenzopyran. *Polymer* **2002**, *43*, 3819-3823.
110. Kimura, K.; Nakamura, M.; Sakamoto, H.; Uda, R. M.; Sumida, M.; Yokoyama, M., Cation complexation, photochromism, and aggregation of copolymers carrying crown ether and spirobenzopyran moieties at the side chains. *Bulletin of the Chemical Society of Japan* **2003**, *76*, 209-215.
111. Kobayashi, N.; Sato, S.; Takazawa, K.; Ikeda, K.; Hirohashi, R., A new polymer electrolyte for reversible photoresponsive ionic-conduction. *Electrochimica Acta* **1995**, *40*, 2309-2311.
112. Kotharangannagari, V. K.; Sanchez-Ferrer, A.; Ruokolainen, J.; Mezzenga, R., Photoresponsive Reversible Aggregation and Dissolution of Rod-Coil Polypeptide Diblock Copolymers. *Macromolecules* **2011**, *44*, 4569-4573.
113. Lee, H.-i.; Wu, W.; Oh, J. K.; Mueller, L.; Sherwood, G.; Peteanu, L.; Kowalewski, T.; Matyjaszewski, K., Light-induced reversible formation of polymeric micelles. *Angewandte Chemie-International Edition* **2007**, *46*, 2453-2457.
114. Levy, D.; DelMonte, F.; Oton, J. M.; Fikshan, G.; Matias, I.; Datta, P.; Lopez-Amo, M., Photochromic doped sol-gel materials for fiber-optic devices. *Journal of Sol-Gel Science and Technology* **1997**, *8*, 931-935.
115. Lin, J. S.; Chiu, H. T., Photochromic behavior of spiropyran and fulgide in thin films of blends of PMMA and SBS. *Journal of Polymer Research-Taiwan* **2003**, *10*, 105-110.
116. Pennakalathil, J.; Hong, J.-D., Self-Standing Polyelectrolyte Multilayer Films Based on Light-Triggered Disassembly of a Sacrificial Layer. *Acs Nano* **2011**, *5*, 9232-9237.
117. Samoladas, A.; Bikiaris, D.; Zorba, T.; Paraskevopoulos, K. M.; Jannakoudakis, A., Photochromic behavior of spiropyran in polystyrene and polycaprolactone thin films - Effect of UV absorber and antioxidant compound. *Dyes and Pigments* **2008**, *76*, 386-393.

118. Stitzel, S.; Byrne, R.; Diamond, D., LED switching of spiropyran-doped polymer films. *Journal of Materials Science* **2006**, *41*, 5841-5844.
119. Lee, C. K.; Davis, D. A.; White, S. R.; Moore, J. S.; Sottos, N. R.; Braun, P. V., Force-Induced Redistribution of a Chemical Equilibrium. *Journal of the American Chemical Society* **2010**, *132*, 16107-16111.
120. Imai, Y.; Adachi, K.; Naka, K.; Chujo, Y., Photochromic organic-inorganic polymer hybrids from spiropyran-modified poly(N,N-dimethylacrylamide). *Polymer Bulletin* **2000**, *44*, 9-15.
121. Bell, N. S.; Piech, M., Photophysical effects between spirobenzopyran-methyl methacrylate-functionalized colloidal particles. *Langmuir* **2006**, *22*, 1420-1427.
122. Such, G. K.; Evans, R. A.; Davis, T. P., Rapid photochromic switching in a rigid polymer matrix using living radical polymerization. *Macromolecules* **2006**, *39*, 1391-1396.
123. Bardavid, Y.; Goykhman, I.; Nozaki, D.; Cuniberti, G.; Yitzchaik, S., Dipole Assisted Photogated Switch in Spiropyran Grafted Polyaniline Nanowires. *Journal of Physical Chemistry C* **2011**, *115*, 3123-3128.
124. Delaire, J. A.; Nakatani, K., Linear and nonlinear optical properties of photochromic molecules and materials. *Chemical Reviews* **2000**, *100*, 1817-1845.
125. Saragi, T. P. I.; Spehr, T.; Siebert, A.; Fuhrmann-Lieker, T.; Salbeck, J., Spiro compounds for organic optoelectronics. *Chemical Reviews* **2007**, *107*, 1011-1065.
126. Oh, K. W.; Ahn, C. H., A review of microvalves. *Journal of Micromechanics and Microengineering* **2006**, *16*, R13-R39.
127. Shoji, S.; Kawai, K., Flow control methods and devices in micrometer scale channels. *Topics in Current Chemistry* **2011**, *304*, 1-25.
128. Ziolkowski, B.; Czugala, M.; Diamond, D., Integrating stimulus responsive materials and microfluidics – The key to next generation chemical sensors. *Journal of Intelligent Material Systems and Structures* **2012**.
129. Satarkar, N. S.; Zhang, W.; Eitel, R. E.; Hilt, J. Z., Magnetic hydrogel nanocomposites as remote controlled microfluidic valves. *Lab on a Chip* **2009**, *9*.
130. Geiger, E. J.; Pisano, A. P.; Svec, F., A Polymer-Based Microfluidic Platform Featuring On-Chip Actuated Hydrogel Valves for Disposable Applications. *Journal of Microelectromechanical Systems* **2010**, *19*, 944-950.
131. Chunder, A.; Etcheverry, K.; Londe, G.; Cho, H. J.; Zhai, L., Conformal switchable superhydrophobic/hydrophilic surfaces for microscale flow control. *Colloids and Surfaces a-Physicochemical and Engineering Aspects* **2009**, *333*, 187-193.
132. Beebe, D. J.; Moore, J. S.; Bauer, J. M.; Yu, Q.; Liu, R. H.; Devadoss, C.; Jo, B. H., Functional hydrogel structures for autonomous flow control inside microfluidic channels. *Nature* **2000**, *404*, 588-590.
133. Kim, D.; Kim, S.; Park, J.; Baek, J.; Kim, S.; Sun, K.; Lee, T.; Lee, S., Hydrodynamic fabrication and characterization of a pH-responsive microscale spherical actuating element. *Sensors and Actuators a-Physical* **2007**, *134*, 321-328.
134. Yu, Q.; Bauer, J. M.; Moore, J. S.; Beebe, D. J., Responsive biomimetic hydrogel valve for microfluidics. *Applied Physics Letters* **2001**, *78*, 2589-2591.
135. Laser, D. J.; Santiago, J. G., A review of micropumps. *Journal of Micromechanics and Microengineering* **2004**, *14*, R35-R64.
136. Au, A. K.; Lai, H.; Utela, B. R.; Folch, A., Microvalves and Micropumps for BioMEMS. *Micromachines* **2011**, *2*, 179-220.
137. Richter, A.; Klatt, S.; Paschew, G.; Klenke, C., Micropumps operated by swelling and shrinking of temperature-sensitive hydrogels. *Lab on a Chip* **2009**, *9*, 613-618.
138. Fahrni, F.; Prins, M. W. J.; van Ijzendoorn, L. J., Micro-fluidic actuation using magnetic artificial cilia. *Lab on a Chip* **2009**, *9*, 3413-3421.
139. Hatch, A.; Kamholz, A. E.; Holman, G.; Yager, P.; Bohringer, K. F., A ferrofluidic magnetic micropump. *Journal of Microelectromechanical Systems* **2001**, *10*, 215-221.

140. Kwon, G. H.; Jeong, G. S.; Park, J. Y.; Moon, J. H.; Lee, S.-H., A low-energy-consumption electroactive valveless hydrogel micropump for long-term biomedical applications. *Lab on a Chip* **2011**, *11*, 2910-2915.
141. Castelletti, L.; Piletsky, S. A.; Turner, A. P. F.; Righetti, P. G.; Bossi, A., Development of an integrated capillary electrophoresis/sensor for L-ascorbic acid detection. *Electrophoresis* **2002**, *23*, 209-214.
142. Hisamoto, H.; Nakashima, Y.; Kitamura, C.; Funano, S.; Yasuoka, M.; Morishima, K.; Kikutani, Y.; Kitamori, T.; Terabe, S., Capillary-assembled microchip for universal integration of various chemical functions onto a single microfluidic device. *Analytical Chemistry* **2004**, *76*, 3222-3228.

Chapter 2

Photo-responsive polymeric structures based on spiropyran

Larisa Florea¹, Dermot Diamond¹ and Fernando Benito-Lopez^{1, 2 *}

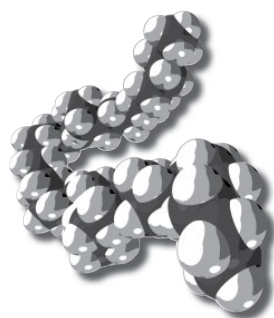
Macromolecular Materials and Engineering, 297 (2012) 1148-1159

ISSN:1438-7492; DOI: [10.1002/mame.201200306](https://doi.org/10.1002/mame.201200306)

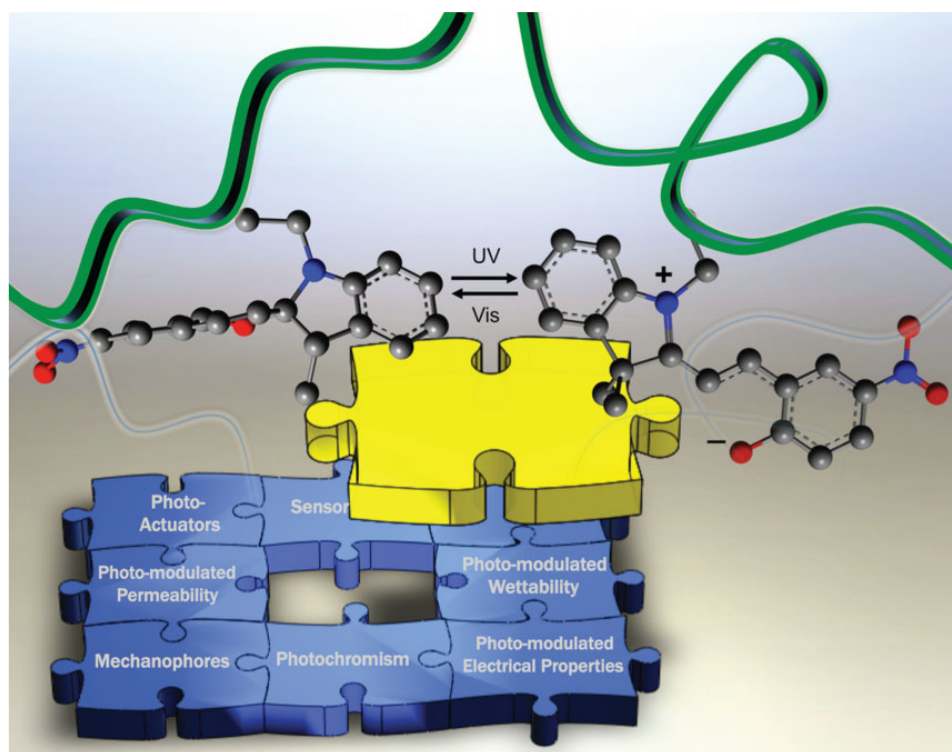
¹CLARITY: Centre for Sensor Web Technologies, National Centre for Sensor Research, School of Chemical Sciences, Dublin City University, Dublin, Ireland;

²CIC microGUNE, Arrasate-Mondragón, Spain, Tel.: +34 943710212

*Author to whom correspondence should be addressed;



Macromolecular Materials and Engineering

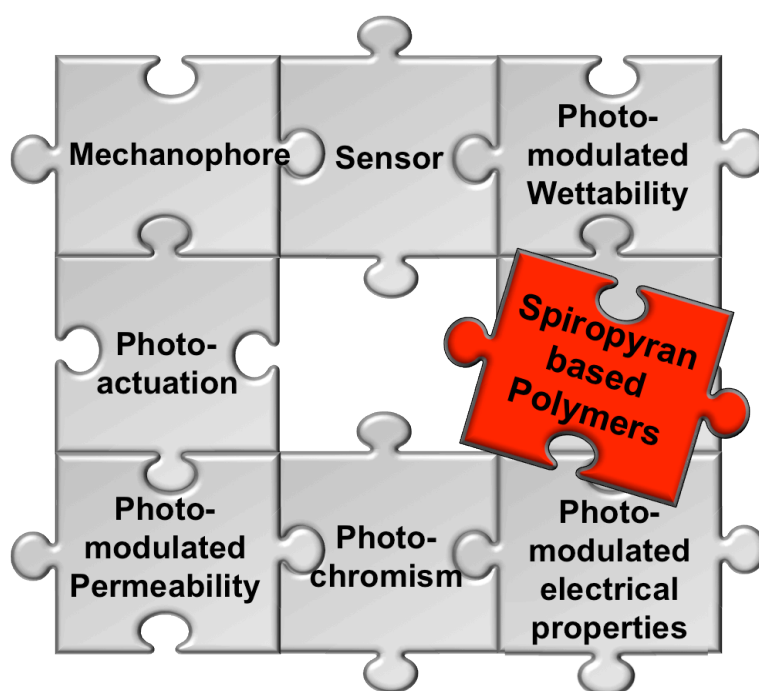


Special Issue:
Advances in Actively Moving Polymers
Guest-edited by Andreas Lendlein

12/2012

 WILEY-VCH

Abstract: Spiropyrans are one of the most popular classes of photochromic compounds that change their optical and structural properties in response to external inputs such as light, protons and metal ions, making them ideal molecules for the fabrication of multifunctional stimuli-responsive materials. Nowadays, the emphasis in polymeric materials incorporating spiropyran units, focuses on the effectiveness of their reversible response to external photonic stimuli. Photo-control of a range of key characteristics for flow systems, such as wettability, permeability, photo-modulation of flow by photo-actuation of valves, photonic control of uptake and release of guests using films and coatings, and colorimetric sensing of various species, are highlighted and discussed.



Keywords: adaptive materials; spiropyrans; photochromism; polymers;

2.1 Introduction

The photochromic properties of spirobenzopyrans were first discovered by Fischer and Hirshberg [1] in 1952 where they observed that the irradiation of several solutions of spirobenzopyrans with UV-light (not exceeding 450 nm) produced colour modifications that could be reversed by exposing the same solutions to yellow light (containing no radiation below 500 nm). The photochromism of spiropyran is due to the photo-cleavage of the C-O spiro bond upon irradiation with UV light [2, 3]. This cleavage allows a conformational rearrangement between a closed, colorless spiropyran form and an opened, colourful merocyanine (MC) form [3, 4] with an important absorption band in the visible spectral region (Figure 2.1). In contrast, the exposure of the MC to visible light produces the reversion to its closed spiropyran form (SP); therefore, it is possible to modulate its conformation using light irradiation. These two forms are characterised by an important change of charge and dipole moment. The opened MC form is characterised by a conjugation between the two extremities of the molecule and is stabilised in the presence of polar solvents [3, 4]. Another interesting property of the SP is its sensitivity towards pH [5, 6]. By adding acid, the opened MC gets protonated forming the protonated merocyanine (MCH^+) form (Figure 2.1). A metal ions-binding centre can also be generated by a spatial rearrangement of the opened MC form thus spiropyrans present a high interest for photo-reversible metal ion-complexation (Figure 2.1) [7-10]. Since the spiropyran derivatives are sensitive towards many external agents, they became in the recent years compounds of choice for the development of a new generation of stimuli-responsive materials and sensors.

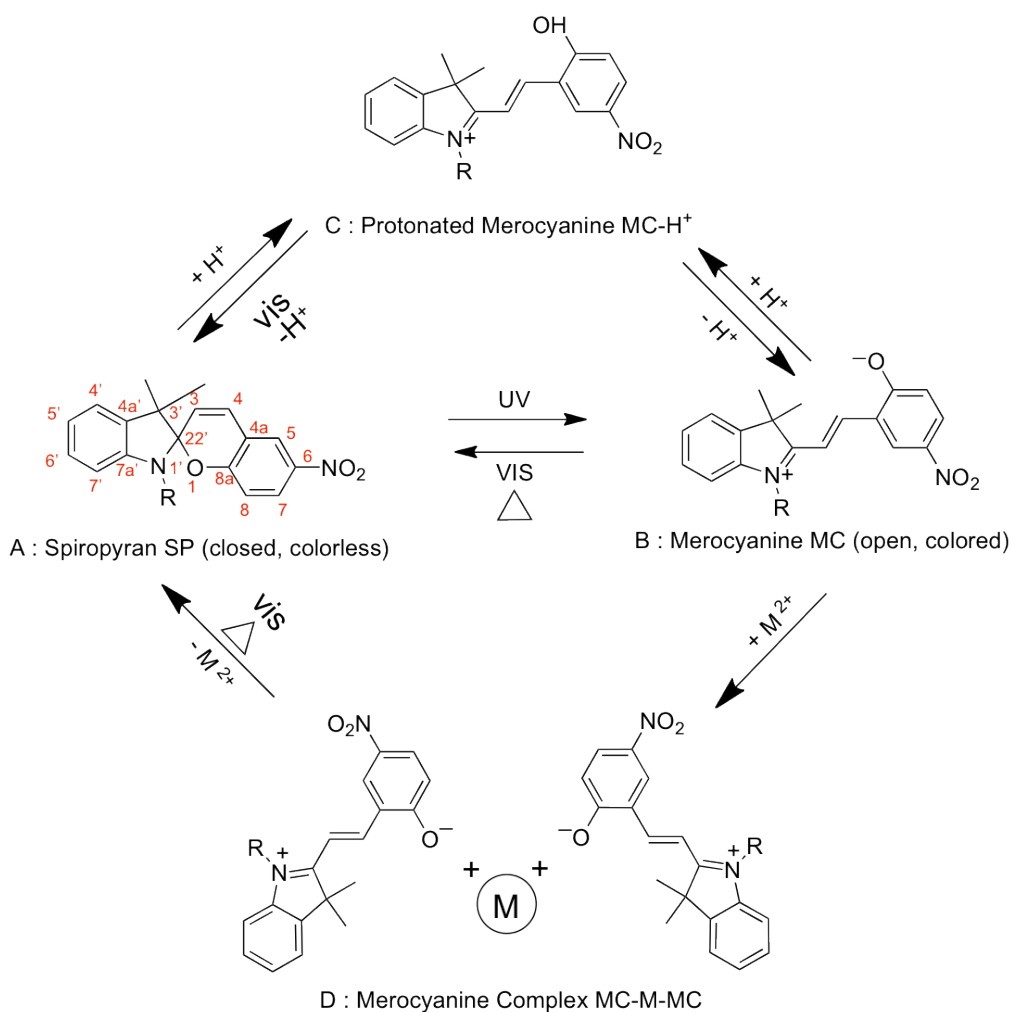


Figure 2.1. Reversible structural transformations of spiropyran derivatives in response to external inputs such as light, protons, and metal ions.

Since their discovery, photochromic spiropyran have been incorporated into various materials *i.e.* surface bound monolayers [7, 11-13], Langmuir monolayers [14], Langmuir Blodgett films [14], polymeric brushes [9, 15-17], photocontrollable surfactants [18], liquid crystalline materials [19], polymeric matrices [8, 15, 16, 20-36], organic/inorganic hybrid systems [37], colloidal particles [17, 38], ionic liquids [39-43] and initiators for radical polymerisations [44].

Materials with photochromic spiropyran have the advantage of reversibly photo-induce changes in their properties such as conductivity [24, 28, 45], wetting behaviour [9, 11, 22], optical properties [9, 23, 27, 31, 32, 35, 44, 46], metal ion complexation [7-10], cell adhesion [25], surface morphology [9], association/solubility [29, 30], mechanical effects [21, 36], colloidal system stability

[17, 38] and membrane permeability [15, 16]. Therefore the possibility to photo-induce such a variation in their physical and chemical properties, has made spiropyran-based materials widely utilised in biological applications [25], nonlinear optics [47], reversible optical memory [24, 48], optoelectronics [49] and chemical sensing [7, 10, 13, 46, 50]. The use of photo-stimulus is appealing because it can be applied precisely and in a non-invasive manner to different sections of a material or device, that otherwise, maybe unreachable. Stimuli-responsive polymers present all the advantages of polymeric materials, such as versatility, high response to weak stimuli, low cost, and compatibility with biological media. When photochromic spiropyran molecules are included in polymer matrices, new desired properties could be obtained. Stimuli-responsive polymers can introduce “on-demand” changes in volume [51-54], optical properties [23, 27, 31, 32, 34, 35, 44], permeability [15, 16] and surface chemistry [7, 55], which in turn activate different functions such as the capability of molecular recognition [7, 56] (including capture, release and detection of analytes), autonomous flow rate [52, 57], wettability switching [22] among others.

Although spiropyran systems have shown to have multiple advantages for a wide variety of applications, they still suffer from issues like photofatigue, insufficient selectivity and lack of sensitivity, which in turn hinders their applicability at a larger level, for real-life applications. Several reports show that by immobilising the spiropyran moiety in a polymer matrix, photofatigue (often encounter due to the formation of aggregates between individual merocyanine moieties) can be dramatically improved. By entrapping (covalently or non-covalently) the spiropyran unit, its degree of motion is reduced and therefore the possibility of interaction between MC molecules (formed upon irradiation with UV light) is reduced, having beneficial effects on decreasing the photo-fatigue [58]. Recent studies have shown that spiropyran fatigue resistance could be also improved by using light emitting diodes (LEDs) as light sources, most probably because they emit light in a narrow range of wavelengths that can be tuned to match the particular absorbance bands of the SP/MC forms of spiropyran [58]. For the use of spiropyran systems in sensing platforms, researchers are well aware that the phenolate group in the MC moiety is mild binding center for metal ions, and it does not express exceptional sensitivity and selectivity. However, several research groups have developed ligands based on the engineering of particular binding groups, typically in

the 1' or 8 positions [59, 60] of the spiropyran moiety (Figure 2.1) finding new opportunities in sensing that in the past seemed only idealistic.

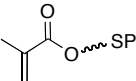
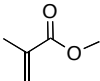
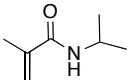
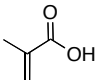
This chapter focuses on the incorporation of spiropyran derivatives into polymer matrices. Specific examples are discussed in terms of the SP-incorporation techniques, influence of the SP's photochromic behaviour on the polymeric material and the applicability of these new-formed SP-containing polymers. Although there is a great amount of literature that covers the area of stimuli-responsive polymers based on SP, here, we illustrate the great versatility and potential of SP-based polymeric systems. The purpose of this chapter is to present to the reader the vast possibilities of utilising spiropyran derivatives in polymeric materials emphasising the chemical design of the polymeric system and their applicability in many different areas of technology.

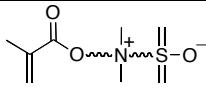
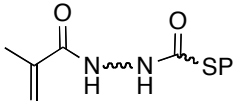
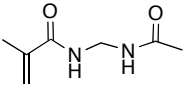
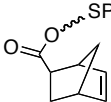
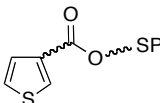
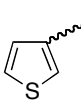
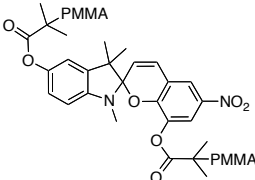
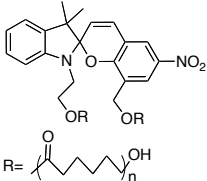
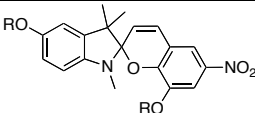
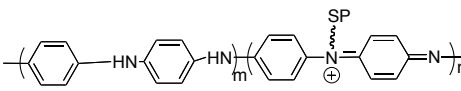
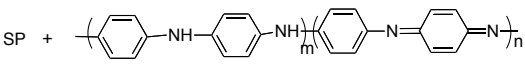
2.2 Spiropyran-based Polymers

Most protocols for the incorporation of spiropyran units into polymer matrices generally involve polymerisation of derivatised spiropyran monomers or copolymerisation of these species with compatible monomeric units, where the spiropyran moiety can be introduced as side chain or as a part of the main polymer chain [9, 10, 15, 16, 20, 33, 36, 50, 61-63]. Other methods include noncovalent doping/entrapment of spiropyran derivatives within various polymer matrices [24, 32, 34, 35] or functionalisation of pre-formed polymers with spiropyran pendant groups [45]. A number of examples of spiropyran based polymer most often present in recent literature are described in Table 2.1 and comprise a series of homo- and co-polymers obtained through various polymerisation techniques: radical polymerisation, atom-transfer radical polymerisation (ATRP), ring opening metathesis polymerisation (ROMP) and photo-polymerisation, among others. Other types of polymers in which the spiropyran is included as a pendant group post polymerisation or simply used as a dopant are also presented. Table 2.1 gives an overview of polymers containing spiropyran where the emphasis is on their structure. Spiropyran polymeric systems can be used for a variety of applications, showing that by combining the key advantages of the spiropyran moiety with the smart

engineering of spiropyran based polymers, new materials with designed macroscopic properties can be obtained. Various types of spiropyran polymers have been designed in order to acquire photo-control over specific characteristics of the material like permeability towards different analytes, wettability, sensing behaviour, actuation and electrical properties or to visualise mechanical stress. The following sections will discuss specific spiropyran polymeric systems based on their photo-modulated properties.

Table 2.1. Polymers containing spiropyran.

| No. | Homo- & Co- polymers of SP | | Application |
|-----|---|---|---|
| | SP monomer | Co-monomer | |
| 1 |  | - | Photo-controlled Wettability [63], Photo-modulation of Electrostatic Interactions [33] |
| 2 | |  | Metal Ions Sensing [61], Photo-controlled Wettability [61], Photo-controlled Permeability [15] |
| 3 | |  | Cyanide Anion Sensing [64], Photo-actuator [65-67], Photo-controlled Permeability [16], Photo-controlled Wettability [68] |
| 4 | |  | Metal Ions Sensing [69] |

| | | | |
|----|---|---|--|
| 5 | |  | Selective Cu ²⁺ Sensing [70] |
| 6 |  |  | Photo-actuator [71] |
| 7 |  | - | Photo-controlled Wettability [9], Solvent Sensing [72] |
| 8 |  |  | Cyanide Anion Sensing [73] |
| 9 |  | | Mechanophore [74-76] |
| 10 |  | | Mechanophore [77] |
| 11 |  | | Mechanophore [36] |
| | SP-functionalised polymers | | |
| 12 |  | | Photo-modulated conductivity [45] |
| | SP-doped polymers | | |
| 13 |  | | Photo-modulated conductivity [24] |

| | | |
|----|---|---------------------------------------|
| 14 | $\text{SP} + \left(\text{---} \text{C}(\text{CH}_3)_2 \text{---} \text{C}(\text{CH}_3) \text{---} \right)_x \left(\text{---} \text{C}(\text{CH}_3) \text{---} \text{C}(\text{CH}_3)_2 \text{---} \text{O---} \right)_y$ | Photo-controlled Wettability [22, 78] |
| 15 | $\text{SP} + \text{---} \text{C}(\text{C}_6\text{H}_{13}) \text{---} \text{C}(\text{S}) \text{---}$ | Photo-modulated conductance [79] |

* Unless specified SP monomeric units consist of a SP unit having the polymerisable group attached in position 1',6 or 8 (Figure 2.1); ~~~~~ - denotes an alkyl chain having from one to eight carbon atoms.

2.3 Photo-modulated Wettability

The wettability of surfaces depends on both, the surface chemistry and the surface morphology, in particular, on the micro-structures of the surface. Having the possibility to photo-control surface wettability has great implications in various fields as such micro-fluidics [80], self-cleaning surfaces [81, 82] and drug-delivery systems [81]. In this context, a lot of effort has been put on functionalising surfaces with spiropyran polymeric materials. The photo-control wettability of SP-modified surfaces is based on the change in the dipole moment of the photo-generated merocyanine in comparison with the closed spiropyran form (Figure 2.1). If confined to an interface, this change in dipole moment affects the surface free energy, which gives rise to a switch in wettability [9, 22, 61, 63, 78] (Table 2.1 – No 1, 2, 7, 15).

In 2008 Samanta *et al.* [9] synthesised a series of spiropyran functionalised norbornyl derivatives that were used to graft homopolymeric brushes using ROMP (Table 2.1 – No. 7) from silicon wafers and glass slides. The surface wettability was modulated using light as the external stimulus. The spiropyran-merocyanine photoinduced isomerisation gave a reversible contact angle change of 5-15 °. The degree of wettability was amplified by irradiation in the presence of Co^{2+} ions

obtaining a reversible contact angle variation of 35 °. At that time it was the largest change in photoinduced surface wettability observed for a flat substrate. A few months later, the same group reported another technique to graft photochromic brushes from glass surfaces [61] (Table 2.1 – No. 2) showing that in this conditions reversible contact angle variations as large as 70 ° when the films were irradiated in the presence of Fe²⁺ ions. Although impressive, these contact angle measurements were obtained under very specific conditions, involving a series of tedious processes such as:

- irradiation of the surface with UV light in the presence of 10 mM solution of metal salt in ethanol for 2 min;
- taking the contact angle measurement;
- irradiation (10 min) with visible light while immersed in toluene;
- drying and taking the second contact angle measurement.

Joseph *et al.* [68] reported a photo-responsive surface consisting on thin layers of crosslinked poly(*N*-isopropyl acrylamide) functionalised with photochromic spirobenzopyran (Table 2.1 – No.3) grafted from cyclic olefin copolymer (COC) substrate. The authors show that the wettability of the surface can be substantially decrease by white light irradiation and subsequently restore by storing the surface in an acidic solution (5 mM HCl) for 10 minutes. The contact angle change of the flat COC surface functionalised with the SP-poly(*N*-isopropyl acrylamide) cross-linked was 24 ° and can be augmented by the introduction of surface micro-structures (79 °) and even further enhanced by the incorporation of nanorods. The later showing a static contact angle change from 5 ° to 123 ° after irradiation with white light. This change in wettability upon irradiation with white light can be attributed to the synergistic effect between photoisomerization of the spirobenzopyran chromophore and the dehydration of the poly(*N*-isopropyl acrylamide) main chain can be explained as follow: light irradiation of the SP-poly(*N*-isopropyl acrylamide) cross-linked first induces photo- isomerization of spirobenzopyran chromophore to the hydrophobic SP closed-ring isomer causing the dehydration of the pNIPAAm polymer main chain. In the dark, in the presence of the acidic aqueous solution, the SP get protonated to MCH⁺ (Figure 2.1), positively charged, and more hydrophilic. This phenomenon induces the re-hydration of the SP-poly(*N*-isopropyl acrylamide)

copolymer. Even though the wettability of this type of surface can be repeatedly cycled with excellent reversibility for at least 5 cycles, still requires acidic treatment in between cycles in order to restore the surface hydrophilicity.

More recently, Wang *et al.* [63] grafted SP polymeric brushes on silicon substrates by atom transfer radical polymerisation (Table 2.1 – No.1). They reported a remarkable contact angle change of approximately 96 °, when the surface was exposed to cycles of UV (5 min) and visible light (20 min), with no intermediate surface treatment between measurements. The key point of this elevated wettability change comes from the combination of the SP properties with a microstructured, laser-etched, silicon substrate (Figure 2.2).

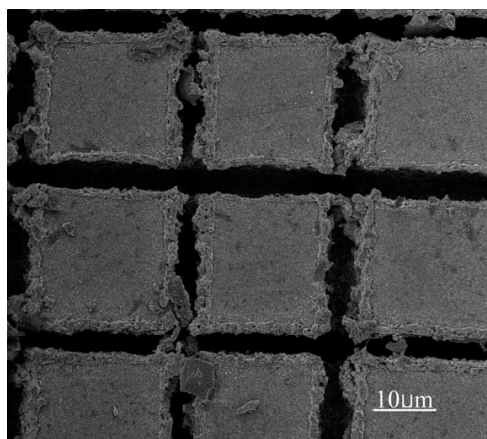


Figure 2.2. SEM image of the photo-responsive poly (SP) thin films on roughly etched silicon substrates. Reproduced with permission from ref [63].

At present this is the highest and fastest contact angle variation reported for surfaces containing SPs and shows that the combination of a high amount of SP units (*e.g.* through the use of polymeric brushes) with surface morphology optimisation is essential to obtain effective photo-induced reversible hydrophobic-hydrophilic surfaces.

2.4 Photo-modulated Permeability

The use of membranes for drug-delivery via photo-modulated permeability is of great interest, and has been extensively investigated for a considerable time. For

instance, Chung *et al.* [16] reported a polytetrafluoroethylene (PTFE) membrane grafted by conventional free radical polymerisation with a methacrylate-functionalised SP and acrylamide (Table 2.1- No. 3). Irradiation with UV light resulted in an increase in permeability of 125 % for a 10-volume % solution of water in methanol, suggesting that the pore sizes of the membrane are larger upon conversion to the MC form. The permeability of the membrane was reversed six times upon alternating exposure to UV and visible light with repeatable performances. In a similar manner, a photoresponsive membrane for organic solvents was produced by Park *et al.* [15], in which methacrylate-functionalised SP and methyl methacrylate (MMA) copolymer (SP-MA-*co*-MMA, Table 2.1 – No. 2) was grafted from a porous glass filter. Upon UV irradiation, the membrane was permeable to toluene, due to the collapse of the polymer chains (Figure 2.3 - up). Since both the SP and MC non-grafted polymers are soluble in dimethylformamide (DMF), the polymer-grafted filter showed no change in permeability for DMF upon irradiation (Figure 2.3 - bottom).

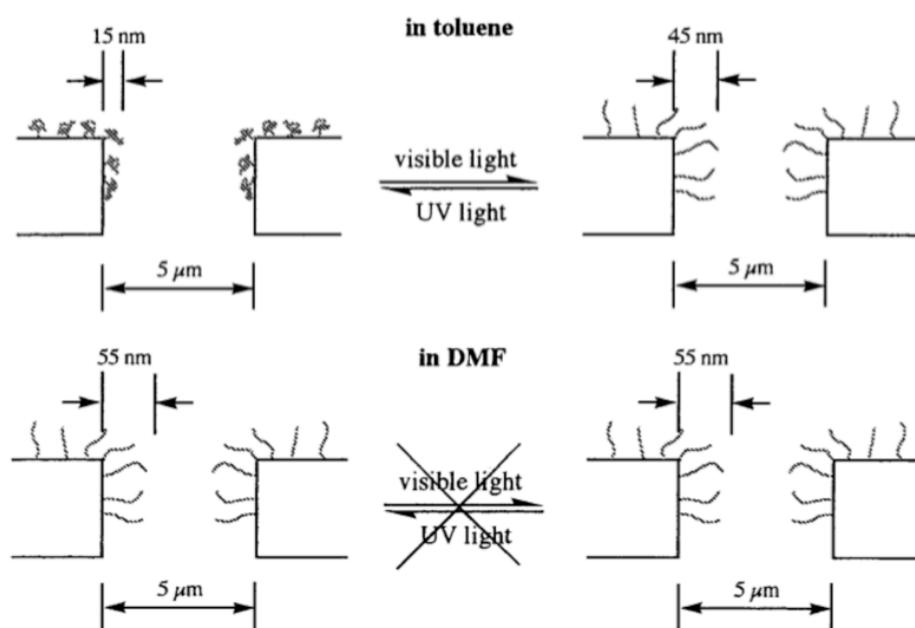


Figure 2.3. Schematic representation of the thickness of a (SP-MA-*co*-MMA) grafted layer. The shrunk grafted chains open pores to increase permeation, and extended chains cover pores to decrease permeation. Reproduced with permission from ref. [15] Copyright (1998) American Chemical Society.

2.5 Photo-actuation

Sugiura *et al.* [67] synthesised a poly(*N*-isopropyl acrylamide) co-acrylated spirobenzopyran (pSPNIPAAm) (Table 2.1 – No. 3) cross-linked with *N,N*-methylene-bis(acrylamide) capable of photo-actuation in acidic media. Micro-valves were fabricated based on this material through in situ polymerisation at desired positions in micro-channels and later opened by local light irradiation. The opening of the valve is due to the photo-induced shrinkage of the pSPNIPAAm gels and can be explained as follow: when the copolymer was immersed in an acidic (0.5 mM HCl) solution, the spiropyran present in the copolymer changed to the open protonated merocyanine form (Figure 2.1 - C). Then, when the polymer was irradiated with light at 422 nm, which matches the absorbance of the protonated merocyanine form, isomerisation of the chromophore to the closed-ring form takes place (Figure 2.1 - A); as a result, the hydrophobic SP isomer induces dehydration of the main polymer chain and shrinkage of the gel occurs. This process was found to be rather fast, with each valve opening within 18 to 30 s of light irradiation.

A similar approach was presented by Benito-Lopez *et al.* [65, 66], with the difference that in this case, an ionic liquid (IL) was incorporated within the pSPNIPAAm polymer matrix (Table 2.1 – No. 3) to produce micro-fluidic valves. Using various IL components within the gels allowed the valve actuation kinetics to be controlled through IL mediation of the rate of protonation/deprotonation, and related movement of counter ions and solvent (water). Different ionogels (IL + polymer matrix) were photo-polymerised *in situ* in the channels of a poly(methyl methacrylate) (PMMA) micro-fluidic platform. After immersion for 2 h in 0.1 mM HCl aqueous solution, to convert the ionogel to the protonated swollen state, the rate of photoinduced shrinking due to dehydration of the ionogel was measured. Results showed that trihexyl-tetradecylphosphonium dicyanamide based ionogel produced the fastest valve-opening kinetics, opening after 4s light irradiation (Figure 2.4).

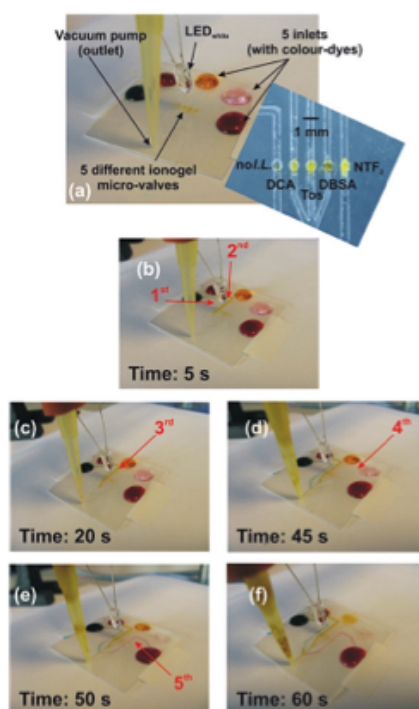


Figure 2.4. Performance of ionogel micro-fluidic valves: (a) micro-valves closed; the applied vacuum is unable to pull the dyes through the micro-channels. White light is applied for the time specified in each picture (b). ‘No I.L.’ valve is first to actuate followed by ionogels incorporating $[dca]^-$ (c), $[tos]^-$ (d), $[dbsa]^-$ (e), $[NTf_2]^-$ (f), all valves are open. Numbers and arrows indicate when the channel is filled with the dye because of micro- valve actuation [66]. Reproduced by permission of The Royal Society of Chemistry.

Recently, an improved reswelling time for spirobenzopyran-functionalised poly(*N*-isopropylacrylamide) hydrogels was reported by Satoh *et al.* [71] who used polymer type No. 6 (Table 2.1 - No. 6), with a SP unit which has a methoxy-group in position 8 (Figure 2.1). The electron donating methoxy group in position 8 increases the electron density of the oxygen (position 1) which reduces the activation free energy (ΔG^\ddagger), accelerating the ring-opening rate constant $k_{Sp \rightarrow MC-H^+}$ up to 19.8 compared to the unsubstituted spiropyran. The increased ring-opening rate of the methoxy spirobenzopyran caused the gel to spontaneously reswell in an acidic environment (5 mM HCl) from the light-induced shrunken state in approximately five minutes.

Although these SP-containing polymeric valves have interesting potential for micro-fluidic devices, mainly due to the fact that they offer the possibility of flow

control by photo-opening of the valves, to date they present drawbacks in that the closing mechanism of the valves is still very long compared with opening, and the valves can only be re-swollen in an acidic environment.

2.6 Photo-modulated Electrical Properties

Photo-control of electrical properties has been achieved by incorporating SP in conducting polymers through covalent bonding or doping, or by using SP containing polymers for polyelectrolytes multilayers.

Guo *et al.* [24] reported reversible photoswitchable proton-transfer processes between a molecular switch based on SP and the emeraldine salt form of polyaniline (SP-doped polyaniline Table 2.1 – No. 13) in the solid state and in solution. This process occurred as follows:

- 1) the MC form, generated by UV irradiation of SP (Figure 2.1), abstracted the protons from the conductive emeraldine salt form of polyaniline, forming protonated merocyanine (MCH^+) and led to a reduction in the degree of protonation of polyaniline;
- 2) upon visible-light irradiation, the MCH^+ form released protons, which were captured by the polyaniline, to restore the degree of protonation. As the degree of protonation dictates the conductivity of the polymer, the electrical conductivity of the SP-doped polyaniline thin-film was reversibly controlled by light irradiation (UV and visible light). Although the drop in conductivity of the polyaniline film could be realised quite rapidly (10 min UV light irradiation), exposure to white light irradiation for 8 hours was required to restore about 95% of the initial conductivity. However, the authors suggest that this can be seen as an advantage if the material is used for information recording (information can be written optically and read out electrically through conductivity measurements) as the slow conversion of MCH^+ to SP inside the polymer allows the stored information to be retained for at least 2 h in the dark.

Another example of a polymeric system comprising both polyaniline and spiropyran, but this time linked via a covalent bond (Table 2.1 – No. 12), was

presented by Bardavid *et al.* [45]. When the spiropyran pendant group was switched to the merocyanine form, the change in the dipole moment of the molecule led to a substantial (*ca.* 2 orders of magnitude) increase in conductance of the photochromic polyaniline nanowires. The transformation was found to be fully reversible with no significant signal loss.

Reversible changes in the dipole moment of SPs upon light irradiation (UV and visible light) were also exploited by Li *et al.* [79] who recently reported an organic field-effect transistor (OFET) that contains a spiropyran doped poly-(3-hexylthiophene) polymer (Table 2.1 – No. 15) as the active layer. In this OFET, the photo-induced, SP to MC and MC to SP conformational changes caused two distinct interaction strengths at the organic/organic interface and therefore the channel conductance could be reversibly modulated in a noninvasive manner.

A relatively new approach is the utilisation of spiropyran functionalised polymers for building polyelectrolytes multilayers. Pennakalathil *et al.* [33] recently showed that a stratum composed of poly(acrylate, merocyanine) (PMC) (Table 2.1 – No. 1) and poly-(diallyldimethylammonium chloride) (PDADMAC) bilayers can be easily disassembled in water upon irradiation with white light by converting the MC to SP (Figure 2.5). This phenomenon was ascribed mainly to the vanished electrostatic attractive interaction between the layer pairs, but also to the increased hydrophobicity of the PSP due to the photoisomerisation of zwitterionic ionic PMC to neutral PSP.

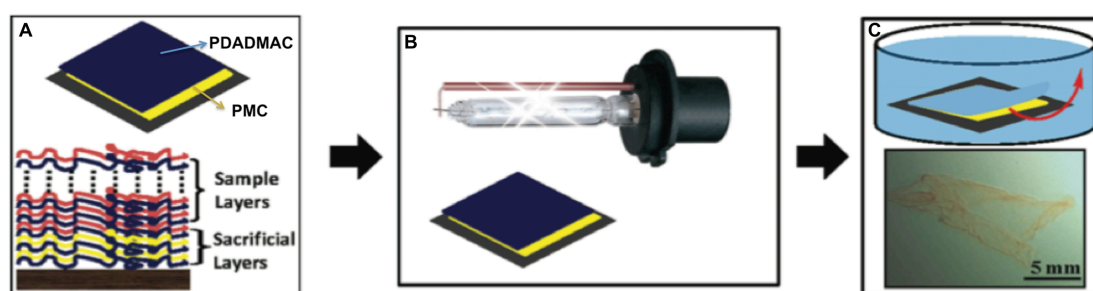


Figure 2.5. A- Schematic view of the sacrificial layer and the sample layer; B - Irradiation with white light; C - disassembly of the sacrificial layer in water after irradiation with white light. Reproduced with permission from ref. [33] Copyright (2011) American Chemical Society.

2.7 Sensing capabilities

In the area of sensing with spiropyran polymeric systems, a significant amount of research has focused on metal ion sensing, due to the ability of MC to employ the negatively charged phenolate group of the zwitterionic form in the binding of metal ions (Figure 2.1).

Controlled free radical polymerisation reactions, such as ATRP, have been used to graft copolymers of SP monomers with MMA (Table 2.1 – No. 2) onto surfaces to obtain photoswitchable planar substrates and colloids [17, 61]. An interesting example is the work of Fries *et al.* where polymer brushes were grafted [61] (or spin-coated [10, 50]) onto glass surfaces to create reversible photoswitchable optical sensors by utilising the complexation of the open MC zwitterion with metal ions (Figure 2.1). The irradiated polymers were exposed to 25 mM metal ion solutions and were air-dried [50, 61]. Upon complexation with different metal ions, the MC absorbance decreased, with an accompanying significant blue shift in the lambda maxima, which is metal ion dependent (Figure 2.6). When the complex was irradiated with visible light in a non-polar solvent, the metal ion was dissociated, and the ring closed to the inactive SP isomer. The system was reported to be reversible for at least three cycles, with good reproducibility of the contact angles. Using a similar type of polymer (Table 2.1 – No. 2) the same group also showed the possibility of detecting multiple divalent metal ions in binary solutions [50]. Several binary metal ion combinations of Sn^{2+} , Cu^{2+} , Fe^{2+} , Zn^{2+} , Co^{2+} , and Ni^{2+} were prepared at different concentration ratios and it was shown that depending on the binding affinity of the MC towards each individual metal ion, MC is capable of identifying one or both metal ions simultaneously (Table 2.2).

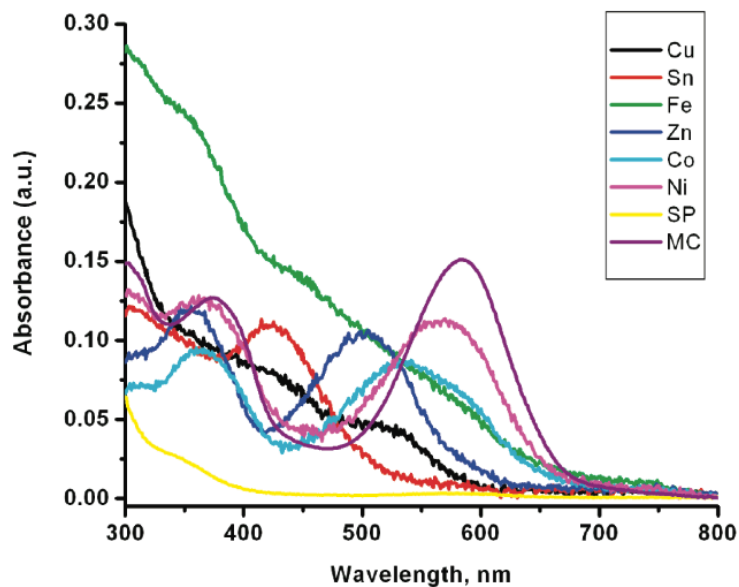


Figure 2.6. Absorbance spectra of SP-polymer layers (Table 2.1 – No. 2) in the presence of different metal ions. Reproduced with permission from ref. [50] Copyright (2011) American Chemical Society.

Table 2.2. Table showing the selectivity of the binding of spiropyran polymer in different binary metal ion solutions. Reproduced with permission from ref. [50] Copyright (2011) American Chemical Society.

| Metal Ion Mixtures | Ratios | | |
|--------------------|--------|-------|-------|
| | 10-90 | 50-50 | 90-10 |
| Sn-Co | Sn | Sn | Sn |
| Sn-Ni | Sn | Sn | Sn |
| Sn-Zn | Sn | Sn | Sn |
| Sn-Fe | Sn | Sn | Sn |
| Sn-Cu | both | both | both |
| Ni-Zn | Zn | Zn | Zn |
| Ni-Fe | Fe | Fe | Fe |
| Cu-Co | both | both | both |
| Cu-Ni | both | both | both |
| Cu-Fe | both | both | both |
| Cu-Zn | both | both | both |
| Co-Ni | both | both | both |
| Zn-Fe | both | both | both |
| Zn-Co | both | both | both |
| Co-Fe | both | both | both |

A similar polymer with potential for metal ion sensing was produced by Connal *et al.* [69] (Table 2.1 – No. 4) using highly ordered honeycomb materials

(Figure 2.7). They demonstrated that palladium ions could be integrated into the SP polymer chain, in solution, using the MC binding abilities and then incorporated into honey-comb films. Furthermore, by reducing the palladium in the film, palladium-based micro-ring structures were obtained, showing the potential of using SP-honeycomb films as templates for building hybrid organic/inorganic porous films.

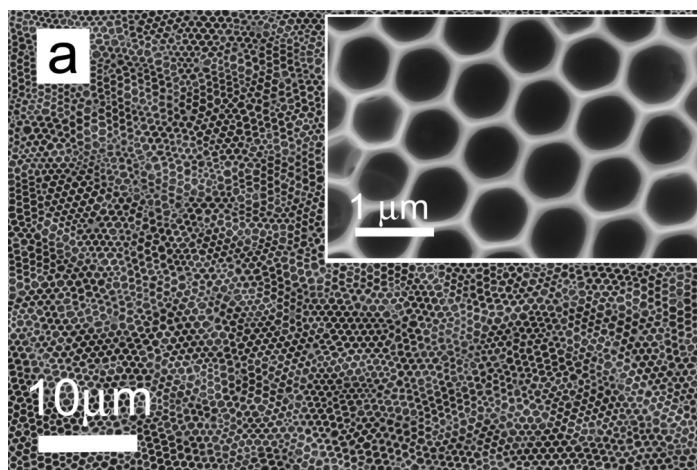


Figure 2.7. Scanning electron micrographs of photochromic honeycomb structures: (a) a low-resolution image of a honeycomb structure, with the inset showing a high-magnification image of the honeycomb structure. Reproduced with permission from ref. [69] Copyright (2010) American Chemical Society.

Although the poor selectivity of the SP-polymers is still considered as a drawback on these systems, good selectivity was reported in the case of Cu^{2+} when a sulfobetaine - methacrylate-functionalised SP copolymers, linear or covalently cross-linked (Table 2.1 – No. 5) were used [70]. However, even in this case, NaCl concentration in the system was found to play an important role, since high NaCl concentrations results in inefficient metal ion sensitivity. This effect could be due to the fact that the electrostatically cross-linked networks of the zwitterionic sulfobetaine units may be loosened by NaCl addition, resulting in easy entry of metal ions into the network.

Several photoswitchable fluorescent cyanide anion sensors based on SP-polymers, a copolymer consisting of *N*-isopropylacrylamide and coumarin-conjugated spiropyran units [64] (Table 2.1 – No. 3) and a spiropyran–polythiophene

conjugate [73] (Table 2.1 – No. 8), were recently reported. It was shown that the cyanide ion could be selectively detected (in the presence of anions such as F^- , Cl^- , Br^- , I^- , AcO^- , $H_2PO_4^-$, HSO_4^- , NO_3^- and ClO_4^-) by monitoring the formation of an adduct, derived from the nucleophilic addition of cyanide anion to the ring-opened MC form of the spiropyran (Figure 2.8).

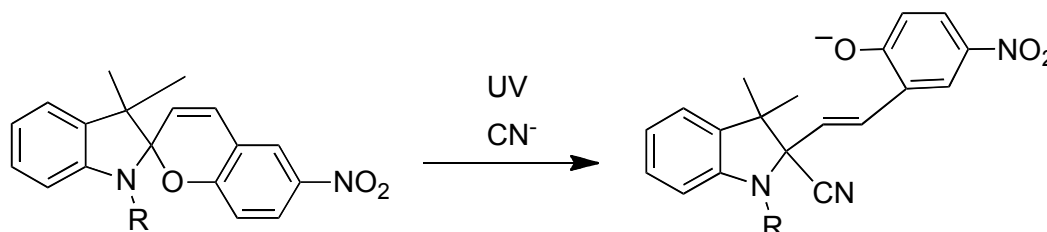


Figure 2.8. Scheme showing the reaction between the spiropyran and cyanide.

Another possibility of utilizing SP-polymers as sensors relies on the solvatochromic properties of the MC form. The colour of the MC form depends on the difference in polarity between the photo-excited MC form and the conjugated zwitterionic ground state. By utilising this property, we recently reported photochromic capillary coatings [72, 83] (Table 2.1 – No. 7) capable of detecting solvent of different polarities that are passing through a chemically modified capillary in continuous flow mode. In polar solvents, the ground state of the MC form is stabilised relative to the excited state, leading to a blue shift in the visible absorption band. In non-polar solvents, the energy difference between the ground and the excited state is much lower, because of the high energy level of the ground state. As a result, as the polarity of the solvent increases, the absorbance λ_{max} shifts to shorter wavelengths, (*hypsochromic* or blue shift), manifesting as a change in colour of the capillary coating (Figure 2.9).

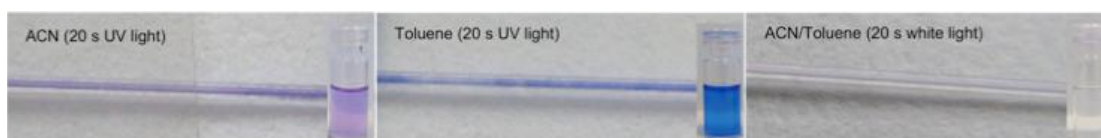


Figure 2.9. Photographs of the spiropyran monomer solutions and the spiropyran polymeric brushes (Table 2.1 – No. 7) functionalised capillary in acetonitrile (ACN) and toluene, respectively, after irradiation with UV and white light. Reproduced with permission from ref. [72] Copyright (2011) Elsevier.

An interesting approach of utilising the solvatochromic properties of the MC unit was reported by Shiraishi *et al.* [62], who showed the possibility of utilising a polymer consisting of poly-*N*-isopropylacrylamide (NIPAM) and SP units (poly-(NIPAM x -co-SP y) (x/y) 15/1), - No. 3) as a colorimetric thermometer in the range of 10-34 °C. The change in temperature induces a polarity change in poly-NIPAM from a more polar character at low temperature (coil conformation) to a less polar domain inside the polymer associated with polymer aggregation (globule), when temperature is increased. This change in polarity can be accurately sensed by the MC, present in the polymer matrix and interrogated by UV irradiation (Figure 2.10).

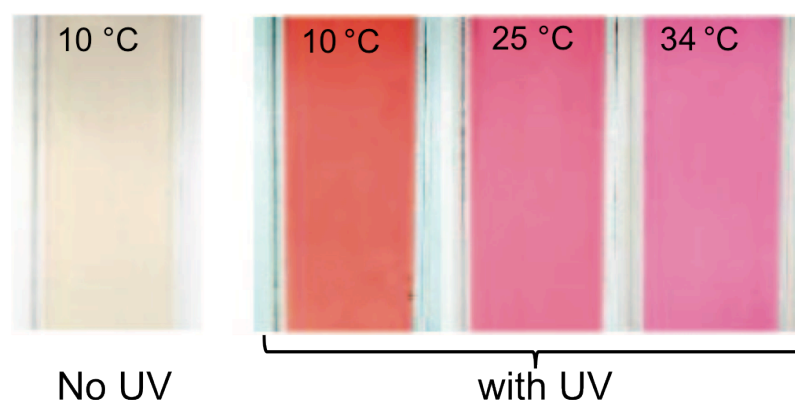


Figure 2.10. Photographs of the polymer solutions in different conditions. Reproduced with permission from ref. [62] Copyright (2009) American Chemical Society.

2.8 Mechanochromic Mechanophores

Mechanochromic mechanophores are mechanophores that change colour with the application of an external force. In the recent years, SPs have been incorporated into a range of polymeric materials and it was shown that they can provide visible detection and mapping of mechanical stresses through their mechanically induced transformation from SP to MC (Figure 2.11). The spiro C–O bond is the critical point for mechanically induced activation, and to ensure stress over the C–O junction, polymerisable groups or polymeric chains have to be placed on the SP unit on opposing sides of the spiro-junction. Mathematical modeling shows that positions 5' or 6' of the indole side and positions 7 or 8 of the benzopyran side (Figure 2.1),

preferentially stresses the spiro C–O bond over the spiro C–C bond, suggesting that these positions are the ideal linkage points between the SP and the polymer matrix for the production of mechanochromic materials. In this context, bifunctionalised SP units with polymerisable groups in these positions have been incorporated into poly-(methyl acrylate) (PMA) and poly-methylmethacrylate (PMMA) chains [74-76] (linear or crosslinked), polyurethanes [36] and polycaprolactone [77]. It was shown that, in all the above-mentioned examples, the C–O bond can be broken via a mechanical stress, resulting in a change in colour of the polymer before polymer failure. These results showed that 5', 6'- and 7,8 bifunctionalised SP units have great potential to produce smart polymers with self-sensing capabilities, damage detection and visual reporting of catastrophic failure prevention.

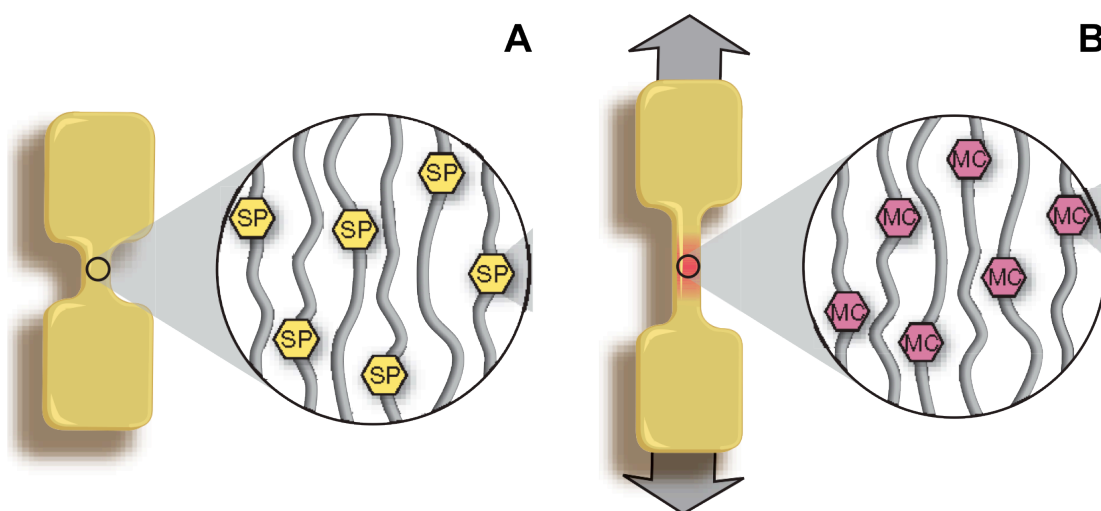


Figure 2.11. Schematic diagram of ‘dog bone’ specimens prepared from SP mechanochromic polymers. A: shows the initial state of the polymer; B: Upon application of tensile force, the conversion between the colourless spiropyran and coloured merocyanine forms of the mechanophore occurs. Reproduced with permission from ref. [76] Copyright (2009), Rights Managed by Nature Publishing Group.

2.9 Conclusions

The examples presented in this review undoubtedly demonstrate the versatility of spiropyrans with respect to routes for incorporation into polymeric matrices, and

great potential of the resulting switchable materials for many applications. For example, polymers can be doped or functionalised with SP post-polymerisation or directly linked during the polymerisation process. Moreover, derivatisation of SP with monomeric units at the 6-, the 8- or at the 1'- position (see Figure 2.1) can be achieved through the use of a spacer/linker group. Polymerisation of these SP-monomeric units or their copolymerisation with compatible monomeric units have produced a wide array of designer-polymers with tuneable properties. Smart engineering of SP-polymeric materials allows photo-modulation of the physical and chemical properties of these materials, ranging from phototchromic behaviour, to wettability, permeability, and electrical properties, to “on-demand” sensing behaviour (*i.e.*, that can be turned on or off using light). It seems to us that no other photochromic unit is capable of producing “stimuli-responsive” polymeric systems for such a wide variety of applications and we believe that these materials could form the basis of the new types of autonomous microfluidic based analytical devices that are much more biomimetic in nature.

Acknowledgements:

The project has been carried out with the support of the Irish Research Council - Embark Initiative and Science Foundation Ireland under the CLARITY award (07/CE/ I1147).

2.10 References

1. Fischer, E.; Hirshberg, Y., Formation of coloured forms of spirans by low-temperature irradiation. *Journal of the Chemical Society* **1952**, 4522-4524.
2. Hirshberg, Y., Reversible formation and eradication of colors by irradiation at low temperatures - a photochemical memory model. *Journal of the American Chemical Society* **1956**, 78, 2304-2312.
3. Minkin, V. I., Photo-, thermo-, solvato-, and electrochromic spiroheterocyclic compounds. *Chemical Reviews* **2004**, 104, 2751-2776.
4. Dürr, H.; Bouas-Laurent, H., *Photochromism: Molecules and Systems*. Elsevier: 2003.
5. Lee, C. W.; Song, Y. H.; Lee, Y.; Ryu, K. S.; Chi, K. W., Reversible photochromic switch ensemble and its photoimaging using H⁺ transfer between spiropyran and fluorescein in a polymer matrix. *Chemical Communications* **2009**, 6282-6284.
6. Doron, A.; Katz, E.; Tao, G. L.; Willner, I., Photochemically-, chemically-, and pH-controlled electrochemistry at functionalized spiropyran monolayer electrodes. *Langmuir* **1997**, 13, 1783-1790.

7. Benito-Lopez, F.; Scarmagnani, S.; Walsh, Z.; Paull, B.; Macka, M.; Diamond, D., Spiropyran modified micro-fluidic chip channels as photonically controlled self-indicating system for metal ion accumulation and release. *Sensors and Actuators B-Chemical* **2009**, *140*, 295-303.
8. Kimura, K.; Nakamura, M.; Sakamoto, H.; Uda, R. M.; Sumida, M.; Yokoyama, M., Cation complexation, photochromism, and aggregation of copolymers carrying crown ether and spirobenzopyran moieties at the side chains. *Bulletin of the Chemical Society of Japan* **2003**, *76*, 209-215.
9. Samanta, S.; Locklin, J., Formation of photochromic spiropyran polymer brushes via surface-initiated, ring-opening metathesis polymerization: Reversible photocontrol of wetting behavior and solvent dependent morphology changes. *Langmuir* **2008**, *24*, 9558-9565.
10. Fries, K. H.; Driskell, J. D.; Samanta, S.; Locklin, J., Spectroscopic Analysis of Metal Ion Binding in Spiropyran Containing Copolymer Thin Films. *Analytical Chemistry* **2010**, *82*, 3306-3314.
11. Dattilo, D.; Armelao, L.; Fois, G.; Mistura, G.; Maggini, M., Wetting properties of flat and porous silicon surfaces coated with a spiropyran. *Langmuir* **2007**, *23*, 12945-12950.
12. Rosario, R.; Gust, D.; Hayes, M.; Jahnke, F.; Springer, J.; Garcia, A. A., Photon-modulated wettability changes on spiropyran-coated surfaces. *Langmuir* **2002**, *18*, 8062-8069.
13. Rosario, R.; Gust, D.; Hayes, M.; Springer, J.; Garcia, A. A., Solvatochromic study of the microenvironment of surface-bound spiropyrans. *Langmuir* **2003**, *19*, 8801-8806.
14. Tachibana, H.; Yamanaka, Y.; Matsumoto, M., Surface and photochemical properties of Langmuir monolayer and Langmuir-Blodgett films of a spiropyran derivative. *Journal of Materials Chemistry* **2002**, *12*, 938-942.
15. Park, Y. S.; Ito, Y.; Imanishi, Y., Photocontrolled gating by polymer brushes grafted on porous glass filter. *Macromolecules* **1998**, *31*, 2606-2610.
16. Chung, D. J.; Ito, Y.; Imanishi, Y., Preparation of porous membranes grafted with poly(spiropyran-containing methacrylate) and photocontrol of permeability. *Journal of Applied Polymer Science* **1994**, *51*, 2027-2033.
17. Piech, M.; Bell, N. S., Controlled synthesis of photochromic polymer brushes by atom transfer radical polymerization. *Macromolecules* **2006**, *39*, 915-922.
18. Sakai, H.; Ebana, H.; Sakai, K.; Tsuchiya, K.; Ohkubo, T.; Abe, M., Photo-isomerization of spiropyran-modified cationic surfactants. *Journal of Colloid and Interface Science* **2007**, *316*, 1027-1030.
19. Lee, M. J.; Yoo, B. W.; Shin, S. T.; Keum, S. R., Synthesis and properties of new liquid crystalline compounds containing an indolinobenzospiropyranylazo group. Part 3. *Dyes and Pigments* **2001**, *51*, 15-24.
20. Adelmann, R.; Mela, P.; Gallyamov, M. O.; Keul, H.; Moeller, M., Synthesis of High-Molecular-Weight Linear Methacrylate Copolymers with Spiropyran Side Groups: Conformational Changes of Single Molecules in Solution and on Surfaces. *Journal of Polymer Science Part a-Polymer Chemistry* **2009**, *47*, 1274-1283.
21. Alonso, M.; Reboto, V.; Guiscardo, L.; San Martin, A.; Rodriguez-Cabello, J. C., Spiropyran derivative of an elastin-like bioelastic polymer: Photoresponsive molecular machine to convert sunlight into mechanical work. *Macromolecules* **2000**, *33*, 9480-9482.
22. Anastasiadis, S. H.; Lygeraki, M. I.; Athanassiou, A.; Farsari, M.; Pisignano, D., Reversibly Photo-Responsive Polymer Surfaces for Controlled Wettability. *Journal of Adhesion Science and Technology* **2008**, *22*, 1853-1868.
23. Angiolini, L.; Benelli, T.; Giorgini, L.; Raymo, F. M., Optical and chiroptical switches based on photoinduced photon and proton transfer in copolymers containing spiropyran and azopyridine chromophores in their side chains. *Polymer* **2009**, *50*, 5638-5646.

24. Guo, X. F.; Zhang, D.; Gui, Y.; Wax, M. X.; Li, J. C.; Liu, Y. Q.; Zhu, D. B., Reversible photoregulation of the electrical conductivity of spiropyran-doped polyaniline for information recording and nondestructive processing. *Advanced Materials* **2004**, *16*, 636-+.
25. Higuchi, A.; Hamamura, A.; Shindo, Y.; Kitamura, H.; Yoon, B. O.; Mori, T.; Uyama, T.; Umezawa, A., Photon-modulated changes of cell attachments on poly(spiropyran-co-methyl methacrylate) membranes. *Biomacromolecules* **2004**, *5*, 1770-1774.
26. Irie, M.; Iwayanagi, T.; Taniguchi, Y., Photoresponsive polymers .7. Reversible solubility change of polystyrene having pendant spirobenzopyran groups and its application to photoresists. *Macromolecules* **1985**, *18*, 2418-2422.
27. Ivanov, A. E.; Ereemeev, N. L.; Wahlund, P. O.; Galaev, I. Y.; Mattiasson, B., Photosensitive copolymer of N-isopropylacrylamide and methacryloyl derivative of spirobenzopyran. *Polymer* **2002**, *43*, 3819-3823.
28. Kobayashi, N.; Sato, S.; Takazawa, K.; Ikeda, K.; Hirohashi, R., A new polymer electrolyte for reversible photoresponsive ionic-conduction. *Electrochimica Acta* **1995**, *40*, 2309-2311.
29. Kotharangannagari, V. K.; Sanchez-Ferrer, A.; Ruokolainen, J.; Mezzenga, R., Photoresponsive Reversible Aggregation and Dissolution of Rod-Coil Polypeptide Diblock Copolymers. *Macromolecules* **2011**, *44*, 4569-4573.
30. Lee, H.-i.; Wu, W.; Oh, J. K.; Mueller, L.; Sherwood, G.; Peteanu, L.; Kowalewski, T.; Matyjaszewski, K., Light-induced reversible formation of polymeric micelles. *Angewandte Chemie-International Edition* **2007**, *46*, 2453-2457.
31. Levy, D.; DelMonte, F.; Oton, J. M.; Fikshan, G.; Matias, I.; Datta, P.; Lopez-Amo, M., Photochromic doped sol-gel materials for fiber-optic devices. *Journal of Sol-Gel Science and Technology* **1997**, *8*, 931-935.
32. Lin, J. S.; Chiu, H. T., Photochromic behavior of spiropyran and fulgide in thin films of blends of PMMA and SBS. *Journal of Polymer Research-Taiwan* **2003**, *10*, 105-110.
33. Pennakalathil, J.; Hong, J.-D., Self-Standing Polyelectrolyte Multilayer Films Based on Light-Triggered Disassembly of a Sacrificial Layer. *Acs Nano* **2011**, *5*, 9232-9237.
34. Samoladas, A.; Bikiaris, D.; Zorba, T.; Paraskevopoulos, K. M.; Jannakoudakis, A., Photochromic behavior of spiropyran in polystyrene and polycaprolactone thin films - Effect of UV absorber and antioxidant compound. *Dyes and Pigments* **2008**, *76*, 386-393.
35. Stitzel, S.; Byrne, R.; Diamond, D., LED switching of spiropyran-doped polymer films. *Journal of Materials Science* **2006**, *41*, 5841-5844.
36. Lee, C. K.; Davis, D. A.; White, S. R.; Moore, J. S.; Sottos, N. R.; Braun, P. V., Force-Induced Redistribution of a Chemical Equilibrium. *Journal of the American Chemical Society* **2010**, *132*, 16107-16111.
37. Imai, Y.; Adachi, K.; Naka, K.; Chujo, Y., Photochromic organic-inorganic polymer hybrids from spiropyran-modified poly(N,N-dimethylacrylamide). *Polymer Bulletin* **2000**, *44*, 9-15.
38. Bell, N. S.; Piech, M., Photophysical effects between spirobenzopyran-methyl methacrylate-functionalized colloidal particles. *Langmuir* **2006**, *22*, 1420-1427.
39. Byrne, R.; Coleman, S.; Gallagher, S.; Diamond, D., Designer molecular probes for phosphonium ionic liquids. *Physical Chemistry Chemical Physics* **2010**, *12*, 1895-1904.
40. Coleman, S.; Byrne, R.; Alhashimy, N.; Fraser, K. J.; MacFarlane, D. R.; Diamond, D., Photochromic imidazolium based ionic liquids based on spiropyran. *Physical Chemistry Chemical Physics* **2010**, *12*, 7009-7017.
41. Coleman, S.; Byrne, R.; Minkovska, S.; Diamond, D., Investigating Nanostructuring within Imidazolium Ionic Liquids: A Thermodynamic Study Using Photochromic Molecular Probes. *Journal of Physical Chemistry B* **2009**, *113*, 15589-15596.

42. Byrne, R.; Coleman, S.; Fraser, K. J.; Raduta, A.; MacFarlane, D. R.; Diamond, D., Photochromism of nitrobenzospiropyran in phosphonium based ionic liquids. *Physical Chemistry Chemical Physics* **2009**, *11*, 7286-7291.
43. Byrne, R.; Fraser, K. J.; Izgorodina, E.; MacFarlane, D. R.; Forsyth, M.; Diamond, D., Photo- and solvatochromic properties of nitrobenzospiropyran in ionic liquids containing the NTf₂⁻ anion. *Physical Chemistry Chemical Physics* **2008**, *10*, 5919-5924.
44. Such, G. K.; Evans, R. A.; Davis, T. P., Rapid photochromic switching in a rigid polymer matrix using living radical polymerization. *Macromolecules* **2006**, *39*, 1391-1396.
45. Bardavid, Y.; Goykhman, I.; Nozaki, D.; Cuniberti, G.; Yitzchaik, S., Dipole Assisted Photogated Switch in Spiropyran Grafted Polyaniline Nanowires. *Journal of Physical Chemistry C* **2011**, *115*, 3123-3128.
46. Darwish, T. A.; Evans, R. A.; James, M.; Malic, N.; Triani, G.; Hanley, T. L., CO₂ Triggering and Controlling Orthogonally Multiresponsive Photochromic Systems. *Journal of the American Chemical Society* **2010**, *132*, 10748-10755.
47. Delaire, J. A.; Nakatani, K., Linear and nonlinear optical properties of photochromic molecules and materials. *Chemical Reviews* **2000**, *100*, 1817-1845.
48. Berkovic, G.; Krongauz, V.; Weiss, V., Spiroprans and spirooxazines for memories and switches. *Chemical Reviews* **2000**, *100*, 1741-1753.
49. Saragi, T. P. I.; Spehr, T.; Siebert, A.; Fuhrmann-Lieker, T.; Salbeck, J., Spiro compounds for organic optoelectronics. *Chemical Reviews* **2007**, *107*, 1011-1065.
50. Fries, K. H.; Driskell, J. D.; Sheppard, G. R.; Locklin, J., Fabrication of Spiropyran-Containing Thin Film Sensors Used for the Simultaneous Identification of Multiple Metal Ions. *Langmuir* **2011**, *27*, 12253-12260.
51. Bassetti, M. J.; Chatterjee, A. N.; Aluru, N. R.; Beebe, D. J., Development and modeling of electrically triggered hydrogels for microfluidic applications. *Journal of Microelectromechanical Systems* **2005**, *14*, 1198-1207.
52. Beebe, D. J.; Moore, J. S.; Bauer, J. M.; Yu, Q.; Liu, R. H.; Devadoss, C.; Jo, B. H., Functional hydrogel structures for autonomous flow control inside microfluidic channels. *Nature* **2000**, *404*, 588-590.
53. Kwon, G. H.; Jeong, G. S.; Park, J. Y.; Moon, J. H.; Lee, S.-H., A low-energy-consumption electroactive valveless hydrogel micropump for long-term biomedical applications. *Lab on a Chip* **2011**, *11*, 2910-2915.
54. Richter, A.; Klatt, S.; Paschew, G.; Klenke, C., Micropumps operated by swelling and shrinking of temperature-sensitive hydrogels. *Lab on a Chip* **2009**, *9*, 613-618.
55. Garcia, A.; Marquez, M.; Cai, T.; Rosario, R.; Hu, Z.; Gust, D.; Hayes, M.; Vail, S. A.; Park, C.-D., Photo-, thermally, and pH-responsive microgels. *Langmuir* **2007**, *23*, 224-229.
56. Byrne, R. J.; Stitzel, S. E.; Diamond, D., Photo-regenerable surface with potential for optical sensing. *Journal of Materials Chemistry* **2006**, *16*, 1332-1337.
57. Dong, L.; Jiang, H., Autonomous microfluidics with stimuli-responsive hydrogels. *Soft Matter* **2007**, *3*, 1223-1230.
58. Radu, A.; Byrne, R.; Alhashimy, N.; Fusaro, M.; Scarmagnani, S.; Diamond, D., Spiropyran-based reversible, light-modulated sensing with reduced photofatigue. *Journal of Photochemistry and Photobiology a-Chemistry* **2009**, *206*, 109-115.
59. Stauffer, M. T.; Weber, S. G., Optical control of divalent metal ion binding to a photochromic catechol: Photoreversal of tightly bound Zn²⁺. *Analytical Chemistry* **1999**, *71*, 1146-1151.
60. Natali, M.; Soldi, L.; Giordani, S., A photoswitchable Zn (II) selective spiropyran-based sensor. *Tetrahedron* **2010**, *66*, 7612-7617.
61. Fries, K.; Samanta, S.; Orski, S.; Locklin, J., Reversible colorimetric ion sensors based on surface initiated polymerization of photochromic polymers. *Chemical Communications* **2008**, 6288-6290.

62. Shiraishi, Y.; Miyamoto, R.; Hirai, T., Spiropyran-Conjugated Thermoresponsive Copolymer as a Colorimetric Thermometer with Linear and Reversible Color Change. *Organic Letters* **2009**, *11*, 1571-1574.
63. Wang, D.; Jiao, P.; Wang, J.; Zhang, Q.; Feng, L.; Yang, Z., Fast photo-switched wettability and color of surfaces coated with polymer brushes containing spiropyran. *Journal of Applied Polymer Science* **2012**, *125*, 870-875.
64. Shiraishi, Y.; Sumiya, S.; Manabe, K.; Hirai, T., Thermoresponsive Copolymer Containing a Coumarin-Spiropyran Conjugate: Reusable Fluorescent Sensor for Cyanide Anion Detection in Water. *Acs Applied Materials & Interfaces* **2011**, *3*, 4649-4656.
65. Byrne, R.; Ventura, C.; Lopez, F. B.; Walther, A.; Heise, A.; Diamond, D., Characterisation and analytical potential of a photo-responsive polymeric material based on spiropyran. *Biosensors and Bioelectronics* **2010**, *26*, 1392-1398.
66. Benito-Lopez, F.; Byrne, R.; Raduta, A. M.; Vrana, N. E.; McGuinness, G.; Diamond, D., Ionogel-based light-actuated valves for controlling liquid flow in micro-fluidic manifolds. *Lab on a Chip* **2010**, *10*, 195-201.
67. Sugiura, S.; Sumaru, K.; Ohi, K.; Hiroki, K.; Takagi, T.; Kanamori, T., Photoresponsive polymer gel microvalves controlled by local light irradiation. *Sensors and Actuators a-Physical* **2007**, *140*, 176-184.
68. Joseph, G.; Pichardo, J.; Chen, G. F., Reversible photo-/thermo-responsive structured polymer surfaces modified with a spirobenzopyran-containing copolymer for tunable wettability. *Analyst* **2010**, *135*, 2303-2308.
69. Connal, L. A.; Franks, G. V.; Qiao, G. G., Photochromic, Metal-Absorbing Honeycomb Structures. *Langmuir* **2010**, *26*, 10397-10400.
70. Suzuki, T.; Hirahara, Y.; Bunya, K.; Shinozaki, H., Photo-reversible and selective Cu²⁺ complexation of a spiropyran-carrying sulfobetaine copolymer in saline solution. *Journal of Materials Chemistry* **2010**, *20*, 2773-2779.
71. Satoh, T.; Sumaru, K.; Takagi, T.; Kanamori, T., Fast-reversible light-driven hydrogels consisting of spirobenzopyran-functionalized poly(N-isopropylacrylamide). *Soft Matter* **2011**, *7*, 8030-8034.
72. Florea, L.; Benito-Lopez, F.; Hennart, A.; Diamond, D., Photo-detection of solvent polarities using non-invasive coatings in capillaries. *Procedia Engineering* **2011**, *25*, 1545 – 1548.
73. Park, I. S.; Jung, Y.-S.; Lee, K.-J.; Kim, J.-M., Photoswitching and sensor applications of a spiropyran-polythiophene conjugate. *Chemical Communications* **2010**, *46*, 2859-2861.
74. Beiermann, B. A.; Davis, D. A.; Kramer, S. L. B.; Moore, J. S.; Sottos, N. R.; White, S. R., Environmental effects on mechanochemical activation of spiropyran in linear PMMA. *Journal of Materials Chemistry* **2011**, *21*, 8443-8447.
75. Beiermann, B. A.; Kramer, S. L. B.; Moore, J. S.; White, S. R.; Sottos, N. R., Role of Mechanophore Orientation in Mechanochemical Reactions. *Acs Macro Letters* **2012**, *1*, 163-166.
76. Davis, D. A.; Hamilton, A.; Yang, J.; Cremar, L. D.; Van Gough, D.; Potisek, S. L.; Ong, M. T.; Braun, P. V.; Martinez, T. J.; White, S. R.; Moore, J. S.; Sottos, N. R., Force-induced activation of covalent bonds in mechanoresponsive polymeric materials. *Nature* **2009**, *459*, 68-72.
77. O'Bryan, G.; Wong, B. M.; McElhanon, J. R., Stress Sensing in Polycaprolactone Films via an Embedded Photochromic Compound. *Acs Applied Materials & Interfaces* **2010**, *2*, 1594-1600.
78. Lygeraki, M. I.; Tsiranidou, E.; Anastasiadis, S. H.; Fotakis, C.; Pisignano, D.; Cingolani, R.; Athanassiou, A., Controlling the reversible wetting capability of smart photochromic-polymer surfaces by micro patterning. *Applied Physics a-Materials Science & Processing* **2008**, *91*, 397-401.

79. Li, Y.; Zhang, H.; Qi, C.; Guo, X., Light-driven photochromism-induced reversible switching in P3HT-spiropyran hybrid transistors. *Journal of Materials Chemistry* **2012**, *22*, 4261-4265.
80. Zhao, B.; Moore, J. S.; Beebe, D. J., Surface-directed liquid flow inside microchannels. *Science* **2001**, *291*, 1023-1026.
81. LaVan, D. A.; McGuire, T.; Langer, R., Small-scale systems for in vivo drug delivery. *Nature Biotechnology* **2003**, *21*, 1184-1191.
82. Cheng, Y. T.; Rodak, D. E.; Wong, C. A.; Hayden, C. A., Effects of micro- and nano-structures on the self-cleaning behaviour of lotus leaves. *Nanotechnology* **2006**, *17*, 1359-1362.
83. Florea, L.; Hennart, A.; Diamond, D.; Benito--Lopez, F., Synthesis and characterisation of spiropyran-polymer brushes in micro-capillaries: Towards an integrated optical sensor for continuous flow analysis. *Sensors and Actuators B: Chemical* **2011**.

Chapter 3

Opto-Smart Systems in Micro-fluidics

Larisa Florea ¹, Dermot Diamond ¹ and Fernando Benito-Lopez ^{1, 2 *}

*"Opto-Nano-Mechanics: Material Systems, fundamentals, and applications" Edited
by E.M. Campo (Bangor University, UK), Pan Stanford Publishing-to be published
2013*

¹CLARITY: Centre for Sensor Web Technologies, National Centre for Sensor Research, School of Chemical Sciences, Dublin City University, Dublin, Ireland;

²CIC microGUNE, Arrasate-Mondragón, Spain, Tel.: +34 943710212

*Author to whom correspondence should be addressed;

Abstract: The possibility of using photo-stimulus to control flow in micro-fluidics devices is very appealing as light can provide contactless stimulation, is biocompatible and can be applied in a non-invasive and highly precise manner. One of the most popular ways to achieve photo-control flow in micro-fluidic channels is throughout the use of photo-responsive molecules. We review here the different principles and strategies of using photo-responsive molecules to induce or control liquid motion using light, which include the use of photo-controlled polymeric actuators, photo-sensitive coatings, or photo-sensitive surfactants. We further analyse the capability of these approaches to induce flow control throughout the photo-operation of valves, photo-control of electro-osmotic flows or photo-manipulation of discrete microliter-sized droplets.

3.1 Introduction

The intrinsic features of micro-fluidic devices ensure two main characteristics during an analytical process: low consumption of reagents and sample as well as rapid and repeatable analysis protocols [1]. However, to date, extensive chemical and biological tasks need to be carried out outside the micro-fluidic device to prepare and pre-process samples prior micro-fluidic manipulation as conventional lab-on-a-chip devices are not yet suitable for non-ideal sample analysis [2]. These tasks include sampling, pre-concentration, fluorescence labelling, filtration, mixing, sample analysis, as well as many other techniques that require manpower and are very time-consuming [3].

Therefore, the main aim is to realise downscaling of these conventional tasks within the micro-fluidic devices and consequently develop innovative systems capable of preparing and/or analysis of samples “on-chip”. If these functions could be integrated within the micro-fluidic device, then time and costs would be reduced and high throughput and high degree of automation would be realised [4]. For this purpose two main ways of investigation are considered: an “evolutionary” and a “revolutionary” approach.

The “evolutionary” approach involves tremendous downscale of conventional units, and their assembly level by level to achieve the desired functionalities [5-7]. However, micro-fluidic systems developed to date according to this approach, generally require complicated control systems and are by far from being trivial and widely accessible.

The “revolutionary” approach in the area of micro-fluidics is recently emerging and consists in the incorporation of stimuli-responsive materials into micro-fluidic devices, to obtain smart, functional, highly controllable components integrated in the micro-fluidic device [8-12]. For instance, the use of a light stimulus in micro-fluidic systems is appealing because it can be applied precisely in different sections within a microdevice, in a non-invasive manner.

The possibility of controlling flow in micro-fluidics using opto-stimulus will offer new platforms with unprecedented flexibility and improved versatility. Some recent reviews have already been devoted to specific aspects of this field [4, 8, 13, 14]. The use of holographic optical tweezers for optical manipulation, actuation and

sensing in lab-on-chip systems was described by Padgett and Di Leonardo [14]. Other recent review by Baigl [15] describes in detail strategies to photo-actuate micro-fluidic systems, such as the application of the chromocapillary effect, light-induced Marangoni effects, optically induced dielectrophoresis, digital optofluidics, light-induced electro-osmosis and optoelectrowetting, among others.

In this chapter the possibility of controlling flow in closed microchannels, and manipulating discrete microliter-sized droplets by employing photo- and thermo-responsive materials incorporated in micro-fluidic units in the form of polymeric actuators, photo-responsive coatings or photo-sensitive surfactants is reviewed.

3.2 Opto-Smart Systems Integration in Micro-fluidic Devices

The most widely used photo-sensitive molecules for photo-actuation of liquids in micro-fluidics are spiropyrans and azobenzenes. These are photochromic units that change their characteristics (conformation, polarity) reversibly in response to light of particular wavelengths. When incorporated in functional units, these changes in conformation/polarity of the photochromic unit induce in turn “on demand” changes in volume [16-19], surface chemistry [20-23], surface charge, wettability [23-25] or interfacial tension [26, 27]. Spiropyrans have been investigated extensively as active components in soft photo-actuators for micro-fluidic valves [11, 28]. The light-stimulated switching of spiropyran is due to the photo-cleavage of the C_{spiro}-O bond upon irradiation with UV light [29, 30]. This cleavage allows a conformational rearrangement between a closed, colourless spiropyran form and an opened, colourful merocyanine (MC) form [30, 31] with the colour arising from a strong absorption band in the visible spectral region (Figure 3.1 -A). In contrast, exposure of the MC isomer to visible light induces reversion to the closed spiropyran form (SP); therefore, it is possible to reversibly switch between the polar (or zwitterionic), coloured MC and colourless uncharged SP forms using light irradiation. Another interesting property of spiropyrans is its sensitivity towards pH [32, 33], under acidic conditions, the MC isomer is converted to the protonated merocyanine (MC-H⁺) form (Figure 3.1 - A).

Azobenzenes are another widely used class of photochromic molecules [34, 35]. Under dark conditions, azobenzene preferentially exists in its *trans*, less polar configuration. Under UV light irradiation (350–370 nm) it undergoes photoisomerisation to its *cis*, more polar form (Figure 3.1 - B). The reverse *cis* → *trans* isomerisation can be driven by visible light or occurs thermally in the dark. It is known that azobenzenes reversibly change their geometry from a planar to a non planar upon UV irradiation, generating a width decrease in the distance between the *para* carbon atoms from 9.9 Å to 5.5 Å and a corresponding increase in the dipole moment from 0.5 D to 3.1 D [36]. One of the most important advantages of azobenzenes is their stability over many illumination cycles, which makes them ideal components of numerous molecular devices and functional materials [37, 38]. Another approach to opto-actuation in micro-fluidics is through photo-thermal activation. The novelty of these systems relies on using light absorbance to generate localised heating [39-41].

This chapter will discuss recent trends for the incorporation of thermo- and photo-responsive moieties (in particular spiropyrans and azobenzene) into functional units in micro-fluidic devices capable of responding to an external opto-stimulus. The chapter will be structured into three main sections based on different micro-fluidic operations that can be controlled by light, *i.e.*:

- Photo-controlled polymeric actuators,
- Photo-controlled electro-osmotic flow,
- Photo-manipulation of droplets.

Specific examples will be discussed in terms of the technique used for integration of the photo- activated or photo-thermo- activated unit into the micro-fluidic device, the impact of the photo-stimulus and the applicability of these approaches for photo-actuation of liquids or droplets in micro-fluidics.

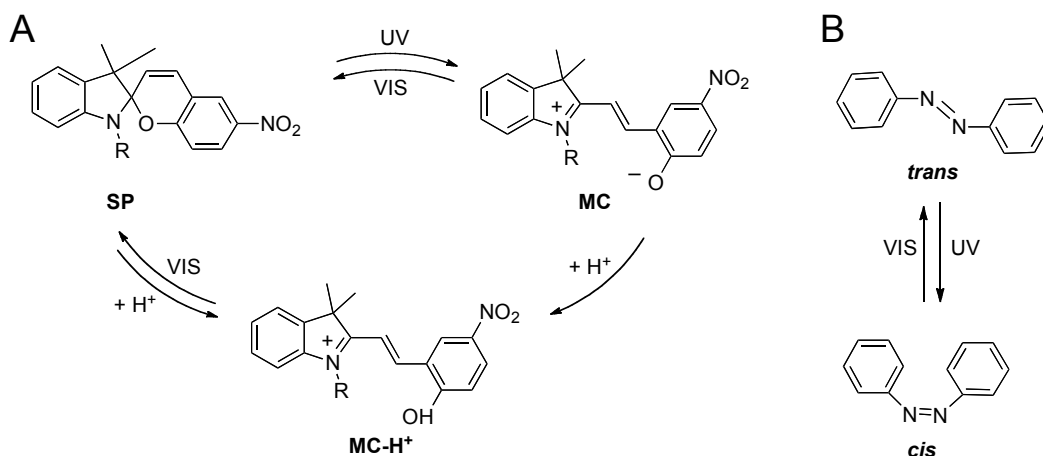


Figure 3.1. Reversible structural transformations of (A) spiropyran derivatives and (B) azobenzene in response to light.

3.2.1 Photo-controlled Polymeric Actuators

Stimuli-responsive polymers present all the advantages of polymeric materials, such as versatility, processability, low cost and amplified response to weak stimuli. Stimuli-responsive materials produce many useful effects in micro-fluidic systems, such as “on-demand” changes in volume [16-19], optical properties [42-48], permeability [49, 50] and surface chemistry [20, 21], which in turn activate/deactivate different functions such as the capability of molecular recognition [20, 51] (including capture, release and detection of analytes), autonomous control of flow rate and direction [17, 52], and wettability switching [24].

The most commonly used opto-actuators in micro-fluidics are photo-responsive hydrogels as they have the ability to undergo volumetric changes in response to an external light stimulus [11, 28]. A hydrogel is defined as a network of hydrophilic polymer chains that is able to swell and retain large amounts of water. In a fully-swollen hydrogel, up to 95 % of its mass can consist in water that was absorbed into its three dimensional network [53, 54]. Hydrogels possess excellent biocompatibility and a degree of flexibility, very similar to natural tissue, due to their significant water content [55, 56]. Photo-responsive engineered hydrogels can be made to collapse and thereby release a percentage of their water content upon light irradiation (Figure 3.2).

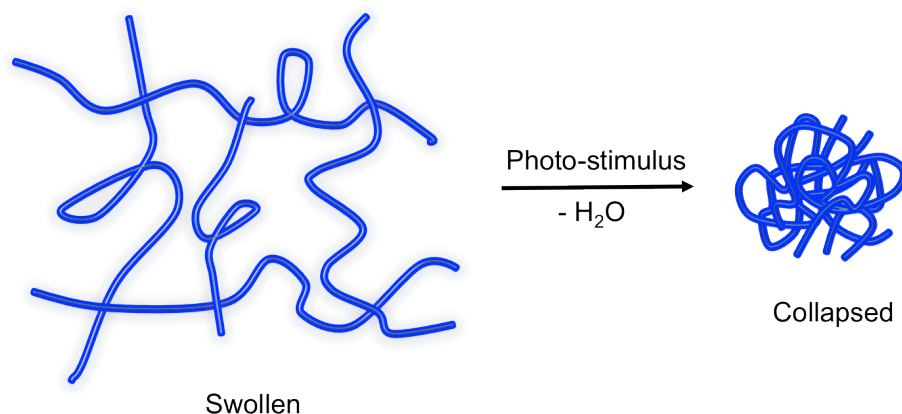


Figure 3.2. Photo-induced hydrogel shrinkage.

In this context, polymeric actuators are commonly employed in micro-fluidic devices to provide the functionality of micro-valves. Valves are central components within micro-fluidic systems, being essential for directional control and movement of flows while enabling important actions, such as flow regulation, flow diversion and addition of reagents. The micro-valves developed to date can be classified in two categories, active and passive, employing mechanical, non-mechanical and external control systems [57].

In the case of passive valves, which do not have any moving components and are easy to fabricate, hydrogel based materials have received special attention. These valves change volume in response to external stimuli to stop/open the flow [17, 39, 52, 58].

Incorporation of photo-responsive units within hydrogel-based valves allows non-invasive, external control of the valve based on the intrinsic responsiveness of the polymer to an optical stimulus. Photo-responsive polymer materials for micro-valve applications have been studied by many research groups, and many polymers and polymer gels functionalised with azobenzene [59], leukochromophore [60, 61], and spirobenzopyran [11, 28, 62, 63] have been examined.

This section is organised as follows: Firstly, we show how smart micro-valves can be actuated by light using a light-to-heat energy conversion mechanism. In this case, a localised temperature increase is caused by light irradiation, which in turn induces volume changes of the micro-valve (usually based on hydrogels). Then, we review how photo-responsive moieties like spiropyrans and azobenzenes are incorporated into polymers to achieve photo-precise manipulation of micro-valves.

Chen *et al.* [39] developed a light-actuated micro-valve via photoinitiated patterned polymerisation of *N*-isopropylacrylamide (NIPAAm) within micro-fluidic channels. PNIPAAm is one of the best-known temperature-sensitive hydrogels, having the ability to shrink and expand due to its lower critical solution temperature (LCST)[64-66]. Below the LCST (32 °C), PNIPAAm chains are hydrated by water due to the hydrogen bondings between the amide residue and on the polymer chains and the water molecules, and therefore the gel is swollen. Above this temperature hydrogen bonds between solvent molecules and water are gradually broken and polymer-polymer interactions become thermodynamically favored compared with polymer-solvent interactions. As a consequence, the PNIPAAm chains collapse sharply from a hydrophilic coil into a hydrophobic globule that precipitates in water [67, 68] and the PNIPAAm hydrogels shrink rapidly. The novelty of the approach used in Chen's PNIPAAm micro-valve relies on heating the valve from the absorption of light provided by a quartz halogen illuminator. The pressure-tolerance of the micro-valve can be tuned by changing the mechanical strength of the polymer monolith inside the microchannel through the choice of a suitable amount of monomer and crosslinker. In addition, the response time and pressure resistance of a PNIPAAm valve can be optimised by varying the tetrahydrofuran (THF) content in the polymerisation mixture. In these conditions, opening and closing response times of the valve can be modulated in the range of 4.0 to 6.2 s [39].

Using a different approach, Lo *et al.* [41] reported the performance of an IR light-responsive micro-valve. The valve consisted of PNIPAAm hydrogel nanocomposite incorporating glycidyl methacrylate functionalised graphene oxide (GO-GMA) sheets. The valve operated in two states – *OFF* (closed) - adopted when the IR source is turned off and the hydrogel completely blocks the channel, and *ON* (opened), adopted when the IR light is turned on, due to shrinking of the hydrogel upon absorbance of the IR light by the GO-GMA sheets. The *ON* state could be explained as follow: GO-GMA sheets absorbed the IR radiation converting it into heat. During this process, the temperature of the system is increased above the LCST of PNIPAAm, which triggers the hydrogel to contract, allowing for fluidic flow. When the IR light is switched off the heat dissipated to the surrounding environment, the hydrogel absorbed water and expanded its volume back to the original size, blocking the flow. A scheme of the performance of the hydrogel micro-valve is shown in Figure 3.3.

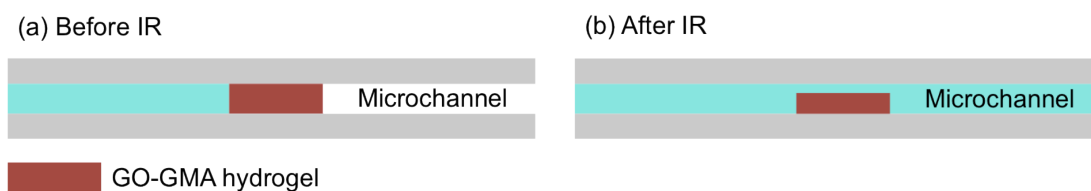


Figure 3.3. Schematic top-views of the micro-valve made of GO–GMA IR-responsive hydrogel. (a) GO–GMA hydrogel micro-valve before actuated by IR irradiation (OFF state) and (b) after exposure to IR light (ON state). Adapted from [41].

Independent optical control of micro-fluidic valves composed of optomechanically responsive nanocomposite hydrogels (poly-*N*-isopropylacrylamide-co-acrylamide) was achieved using strongly absorbing gold nanoparticles or nanoshells embedded in the actuator polymer (Figure 3.4) [69]. These nanocomposite materials respond to different wavelengths of light: while gold-colloid nanocomposite hydrogel collapses in response to green light, the gold-nanoshell nanocomposite hydrogel collapses in response to near-IR light. In both cases, the valves opened completely in less than five seconds. This approach has the advantage of allowing independent control of valves formed from composites with different nanoparticles depending on the illumination wavelength [69].

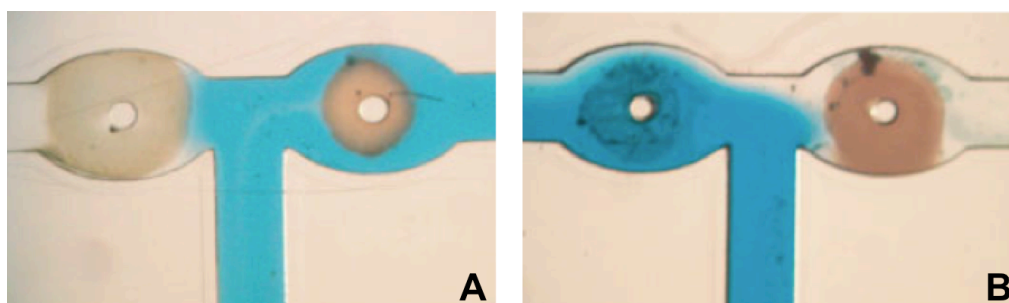


Figure 3.4. Two valves formed at a T-junction in a fluidics device, one made of a gold-colloid nanocomposite hydrogel and the other a gold-nanoshell nanocomposite hydrogel. The channels are 100 μm wide). A) When the entire device was illuminated with green light (532 nm, 1.6 W cm^{-2}), the gold colloid valve opened while the nanoshell valve remained closed. B) However, when the device was illuminated with near infrared light (832 nm, 2.7 W cm^{-2}), the opposite response was observed. In both cases, the valves opened within 5 s. [69]. Copyright © 2005 WILEY-VCH Verlag GmbH & Co.

A different optically addressable micro-actuator array (micro-fluidic “flash memory”) with latched operation was proposed by Hua *et al.* [40]. The micro-actuator array consists of individual phase-change based actuators addressed by localised heating through focused light patterns provided by a modified projector or high power laser pointer. After the initial light “writing” during which the phase is temporarily changed to a liquid form, the actuated status is self-maintained by the solid phase of the actuator without power and pressure inputs (Figure 3.5). The micro-fluidic flash memory can be re-configured by a new light illumination pattern and common pressure signal providing a flexible, energy-efficient, and low cost multiplexing solution for micro-fluidic applications based on physical displacements.



Figure 3.5. Schematic side view of a single actuator operated by a projector. (a) Large membrane deflection upon light illumination and pressure; (b) deflection erased by a second light illumination (no pressure applied). Adapted from [40].

While in all the examples described so far the key of the opto-stimulation is the conversion of photo-energy to thermal energy, photo-stimulation can also be achieved by incorporation of photo-responsive moieties in micro-fluidic units.

In 2004, Sumaru *et al.* [70] presented an actuation mechanism based on the lower critical solubility temperature (LCST) of spiropyran (3 mol %) copolymers of poly(*N*-isopropylacrylamide) (pSPNIPAM). Figure 3.6 shows the chemical structure of pSPNIPAM and the reversible isomerisation of the photochromic unit from the protonated merocyanine (MCH^+) to the closed spiropyran form (SP) under white light irradiation. In acidic conditions (0.26 mM HCl), the spiropyran unit present in the copolymer changed from SP to the MCH^+ form, which presents a strong absorption band around 422 nm. When the copolymer was irradiated with light matching the absorbance of MCH^+ , the MCH^+ is switched back to the closed hydrophobic SP form, releasing one proton in the process (Figure 3.6); As result of the formation of the more hydrophobic SP isomer, dehydration of the main polymer chain occurs. A correlated change in both absorbance at 422 nm (particular to

MCH⁺) and specific conductance was recorded when pSPNIPAAm aqueous solution (0.10 wt %) was repeatedly irradiated with white light over three cycles.

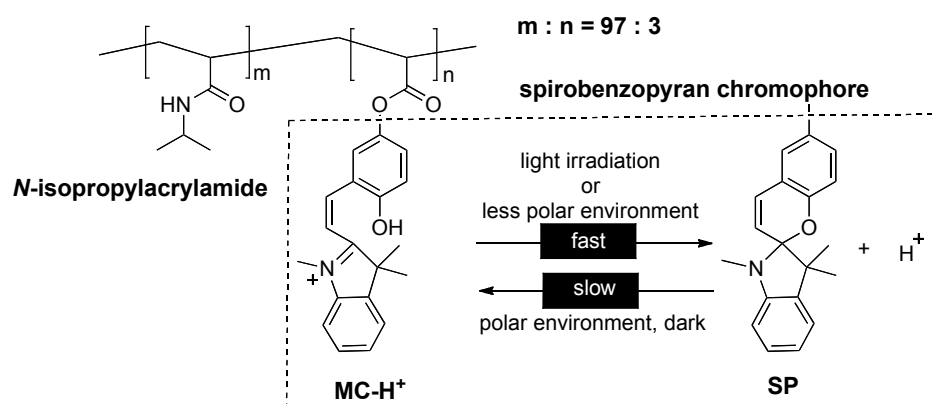


Figure 3.6. Chemical structure of pSPNIPAAm and characteristics of its components: pNIPAAm main chain and spiobenzopyran side chain [70]. Copyright (2004) American Chemical Society.

Independently controlled micro-valves made from such material, capable of photo-actuation in acidic media (0.5 mM HCl), were later demonstrated by Sagiura *et al.* [71]. These micro-valves (Figure 3.7) were fabricated through in situ polymerisation at desired positions in the micro-channels and later opened by local light irradiation. This process was found to be rather fast, with each valve opening within 18 to 30 s of light irradiation. The maximum pressure the pSPNIPAAm gel micro-valves could withstand was determined to be 30 ± 6.6 kPa. Over this pressure the gels deformed and leakage occurred.

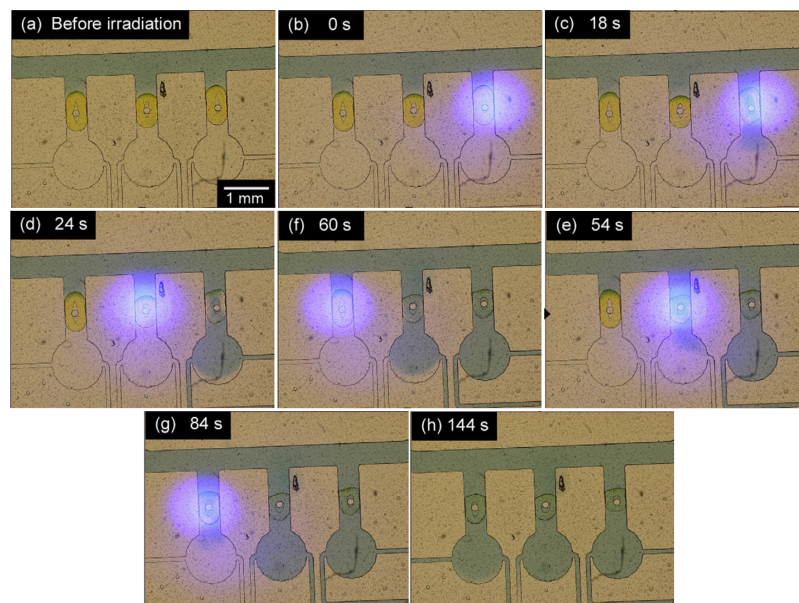


Figure 3.7. Independent control of multiple pSPNIPAAm gel micro-valves by means of local light irradiation. (a) A solution containing blue dye was introduced into the main microchannel. (b) Blue light was locally irradiated to the right side pSPNIPAAm gel micro-valve. (c) The right side micro-valve was opened after 18 s blue light irradiation. (d) Blue light was locally irradiated to the center micro-valve. (e) The center micro-valve was opened after 30 s blue light irradiation. (f) Blue light was locally irradiated to the left side micro-valve. (g) The left side micro-valve was opened after 24 s blue light irradiation. (h) After light irradiation, the chambers were filled with the blue dye solution. Reproduced with permission from ref. [71] Copyright (2007) Elsevier.

A similar approach was presented by Benito-Lopez *et al.* [11] in our laboratories, with the difference that in this case, an ionic liquid (IL) was incorporated within the pSPNIPAAm polymer matrix to produce micro-fluidic valves. Four different phosphonium based ionic liquids incorporating different anions (dicyanoamide ([dca]⁻), bis(trifluoro methanesulfonyl)-amide ([NTf₂]⁻), dodecylbenzenesulfonate ([dbsa]⁻), tosylate ([tos]⁻)) were used and the micro-valves were produced throughout *in situ* polymerisation of the ionogels (IL + pSPNIPAAm) in micro-channels fabricated in poly(methyl methacrylate) (PMMA). After immersion of the ionogels for 2 h in 0.1 mM HCl aqueous solution, in order to allow protonation of the photochromic unit to the MCH⁺ form and to obtain a fully swollen ionogel, photo-induced dehydration kinetics were measured. It was found that the incorporation of different ILs causes different actuation behaviours of the ionogels.

When used for the production of micro-valves, by simply varying the IL-component of the ionogel, different micro-valves can be tuned to open at different times using a single light source. Results showed that in the particular configuration used by the authors, the IL-free polymer gel micro-valve opens after 2 s of light irradiation, followed by the [dca]⁻ based ionogel (4 s.), the [tos]⁻ based ionogel (18 s) and the [dbsa]⁻ based ionogel (44 s). The slowest kinetics are given by the [NTf₂]⁻ based ionogel (49 s) (Figure 3.8).

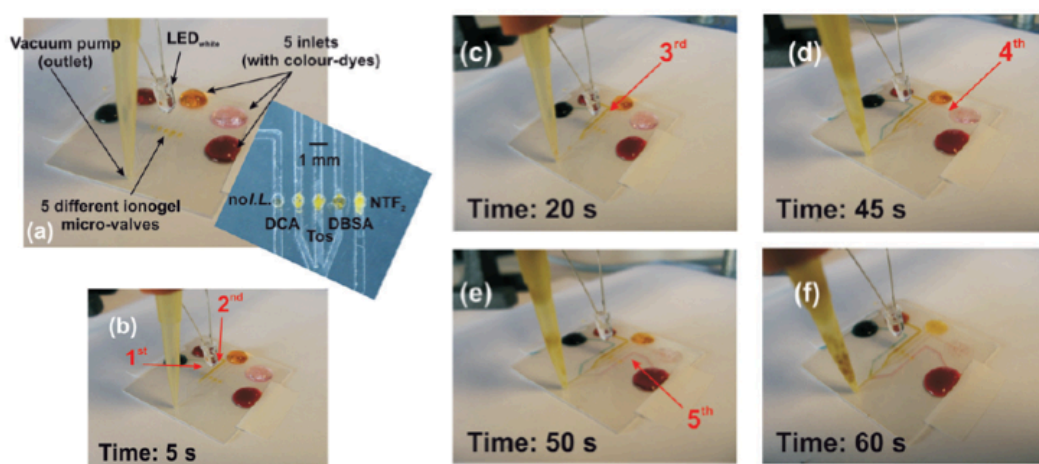


Figure 3.8. Performance of the ionogel micro-fluidic valves: (a) micro-valves closed; the applied vacuum is unable to pull the dyes through the microchannels. White light is applied for the time specified in each picture (b). ‘No I.L.’ valve is first to actuate followed by ionogels incorporating [dca]⁻ (c), [tos]⁻ (d), [dbsa]⁻ (e), [NTf₂]⁻ (f), all valves are open. Numbers and arrows indicate when the channel is filled with the dye because of micro-valve actuation [11]. Reproduced by permission of The Royal Society of Chemistry.

More recently, an original approach for photo-control of fluid in micro-fluidics incorporating pSPNIMAAm hydrogels was described by Sugiura *et al.* [72, 73]. The authors demonstrated on-demand formation of micro-channels with arbitrary pathways by micro-patterned light irradiation of a 200 μm thick pSPNIMAAm hydrogel sheet prepared by *in situ* free radical polymerisation. (Figure 3.9). The hydrogel layer was covalently attached to a glass slide while another glass slide containing multiple inlets and outlets was placed on top of the hydrogel sheet. Micro-patterned light irradiation was realised by means of computer-controlled maskless micro-pattern projection unit. As a result of micro-patterned light

irradiation, the pSPNIPAAm hydrogel gel in the irradiated area between adjacent inlet/outlet ports shrank, forming a micro-channel between the two glass plates and allowing for fluid to flow (Figure 3.9). The effect was repeated for several channel configurations – straight, bent or serpentine. Furthermore, authors also demonstrated, in the same publication, independent and parallel flow control in a polydimethylsiloxane (PDMS) micro-channel network through the opening of targeted microvalves created with the same photoresponsive hydrogel sheet. In this system, a micro-fluidic device containing multiple photoresponsive micro-valves was constructed by stacking a PDMS micro-channel chip and a glass slide with mechanically fabricated through-holes on pSPNIPAAm hydrogel sheet attached to a glass plate. Parallel control of multiple micro-valves was also successfully demonstrated as two micro-valves were simultaneously opened within several minutes by micro-patterned light irradiation. As this system works in “photon mode” in contrast with “heat mode”, no interference between adjacent micro-valves was observed. Although, the isomerisation of the SP unit is a reversible phenomenon, the reswelling of the gel is still diffusion limited due to the requirement for re-protonation of SP for valve closing. As a consequence, the reswelling process takes more than one hour and several strategies for the chemical modification of the SP unit or of the pNIPAAm polymer chain in order to improve the kinetics of the reswelling process are presently under investigation.

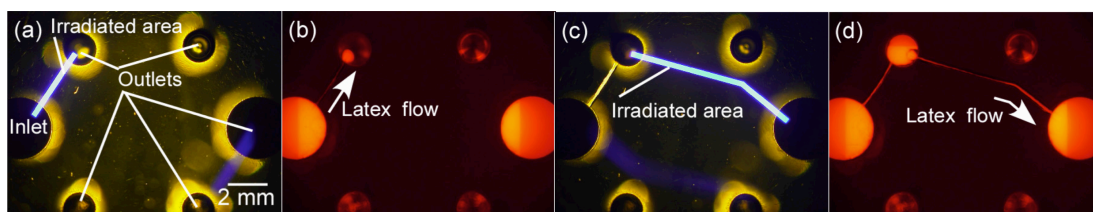


Figure 3.9. On-demand formation of microchannels with arbitrary pathways in a “universal” micro-fluidic system by micro-patterned light irradiation. White arrows indicate the flow direction of a fluorescently labelled latex bead suspension. (a) Microchannel formation by micro-patterned light irradiation of the pSPNIPAAm hydrogel sheet (b) Latex bead suspension flow through the microchannel after irradiation. Flow of the red coloured latex bead suspension from the inlet to the upper-left-side outlet is slightly visible. (c)–(d) A different sequence of micro-patterned light irradiation and microchannel formation. Adapted from [73].

In a different approach, a new micro-valve membrane actuator for micro-fluidic system applications was realised by using a crosslinked liquid-crystalline polymer (CLCP) incorporating azobenzene moieties [13]. It was found that under UV light irradiation the valve is open while under white light irradiation the valve is closed. The micro-valve operation is shown in Figure 3.10. The time to open and close the valve can be as short as 8 s and 6 s, respectively.

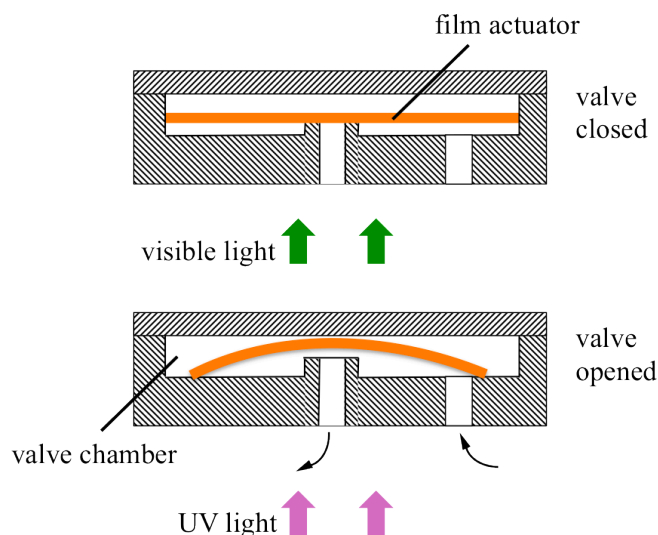


Figure 3.10. Cross-sections and working principle of the photo-activated micro-valve. Adapted from [13].

3.2.2 Photo-control of Electro-osmotic Flow

When an electric field is applied along a micro-channel or micro-capillary having a charged wall, the motion of mobile counter-ions in the diffuse counter-ion layer near the channel wall induces a spontaneous global liquid motion (Figure 3.11). This movement is called electro-osmotic flow (EOF)[74-76]. EOF constitutes an important component in certain chemical separation techniques, notably capillary electrophoresis [74, 75]. There has been an increased interest in EOF in the recent years, in parallel with the development of micro-fluidic systems and EOF has been exploited in micro-fluidics to provide a degree of flow control. This approach offers a range of advantages compared to more established pumps based technologies, such as peristaltic pumps, as it creates a constant pulse-free flow in which the magnitude

and direction of the flow are controlled externally, without the use of any mechanically moving parts.

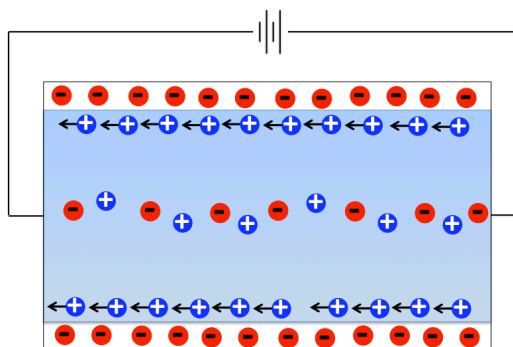


Figure 3.11. Schematic representation of the formation of electroosmotic flow when an external electric field is applied along the length of a microcapillary/ microchannel, in the case where the walls are negatively charged.

EOF is strongly sensitive to the *zeta* potential of the channel wall and the key requirement to realise photo-controlled EOF is the ability to optically change the *zeta* potential of the micro-channel/micro-capillary wall. Moorthy *et al.* [77] demonstrated this type of approach by using micro-channels (1000 μm wide, 20 μm deep) coated with titanium dioxide (TiO_2). TiO_2 is a direct semiconductor that exhibits a change in surface charge upon radiation with UV light, leading to variations in the *zeta* potential. In these conditions, electroosmotic flow modulation was recorded in the presence/absence of UV radiation. The magnitude of the change in electroosmotic flow rate due to UV irradiation was found to be pH dependent. Under optimal conditions (pH = 4.7), the authors report a change in EOF from 0 (no light) to $-242 \pm 60 \mu\text{m s}^{-1}$ (with light). Another strategy was later proposed by Oroszi *et al.* [78] who used micro-channels formed between PDMS and glass coated with cadmium sulfide (CdS) photoactive layer. Light illumination (provided by a mercury lamp filtered to 400 – 725 nm) resulted in a decreased electric field accompanied by a reduction of electroosmotic flow. Specifically, at a driving voltage of 100 V, photo-irradiation of the photo-conductor for periods of 30 s caused a decrease in the average flow velocity from $45 \mu\text{m s}^{-1}$ (in the dark) to $8 \mu\text{m s}^{-1}$ (under illumination). The same group later on demonstrated that introducing a pattern into the

photosensitive layer enables the generation of complex flow profiles upon illumination [79].

Spiropyrans have also been used to modify the electroosmotic flow. It has recently been demonstrated in our laboratories by Scarmagnani *et al.* [80] that, under acidic conditions, electroosmotic flow (EOF) generated in a spiropyran-modified acrylate based monoliths could be modulated using light irradiation (Figure 3.12). In an acidic environment (HCl 1 mM) The SP-modified acrylate based monolith gained a positively charged surface due to the protonation of the SP unit to MC-H⁺ (Figure 3.12A) and the micro-capillary adopted a yellow colour (Figure 3.12B). Upon irradiation with white light, MC-H⁺ converted back to the non-polar SP form (Figure 3.12A) indicated by the change in colour of the microcapillary to colourless (Figure 3.12 B). When the MC-H⁺ form is dominant, it produces a charged surface, which enables a relatively high flow rate (up to 1.6 $\mu\text{L min}^{-1}$) to be generated under electroosmotic conditions. Upon exposure to white light, the concentration of MC-H⁺ decreases due to the photo-conversion to the uncharged SP form, with up to 20 % reduction of the EOF. The process is reversible, and removal of the light source results in a flow increase back to the original rate. A schematic of the microchip used in these experiments is shown in Figure 3.12C.

The ability to alter flow rates in micro-fluidic channels using light has very significant implications, as it could dramatically simplify the manner in which micro-flow systems are controlled.

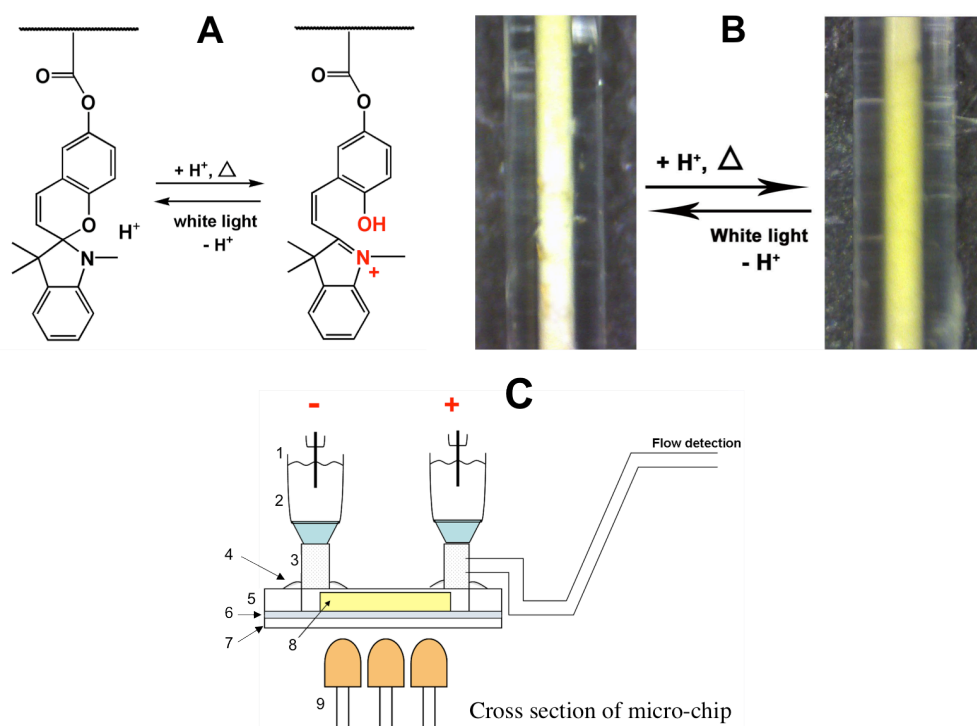


Figure 3.12. (A) SP acrylate switching in acidic environment between the MC-H⁺ form (right) and the SP form (left) when irradiated with white light. (B) Picture of the spiropyran acrylate monolith flushed with HCl 10⁻³ M switched between the MC-H⁺ form, in the absence of light exposure and the SP form when irradiated with white light. (C) Schematic representation of the cross section of the microchip: 1) Electrode; 2) 1.5 ml 10⁻³ M HCl reservoir; 3) PEEK tubing; 4) epoxy glue; 5) PMMA sheet 5 mm thickness; 6) layer of PSA; 7) second sheet of PMMA (0.5 mm thickness); 8) SP acrylate monolith 8 mm length; 9) white LEDs (430-760 nm) [80]. Copyright © 2010 Trans Tech Publications Inc.

3.2.3 Photo-manipulation of Droplets

Digital or droplet-based micro-fluidics involves the generation and manipulation of discrete droplets inside micro-devices [81] and unlike continuous-flow systems, droplet-based micro-fluidics allows for independent control of each droplet. Droplet micro-fluidics encompasses two different approaches;

- mechanisms that are much more similar to traditional micro-fluidics, in which droplets are carried by a carrier flow, and;
- more innovative mechanisms like electrowetting for droplet transport.

Photo-manipulation of droplets for micro-fluidic purposes can be realised through the use of photo-sensitive molecules incorporated in surface (channel) coatings or surfactants.

In 1992 Chaudhury and Whitesides [82] showed that a wettability gradient on a surface is able to induce droplet motion. In this context, if a wettability gradient of a micro-fluidic platform could be optically induced, then droplet movement could be realised. Given the fact that light intensity is easily manipulated, a gradient can be created by partially illuminating a substrate that exhibits photo-responsive wettability behaviour.

Photo-responsive surface wettability is usually achieved by functionalising with a photochromic moiety, most often azobenzenes and spiropyrans that dramatically change polarity upon photo-irradiation. Although a vast variety of photochromic coated substrates have shown to exhibit significant changes in wettability upon photo-stimulation [23, 24, 83-85], so far only a few have demonstrated droplet photo-manipulation.

Ichimura *et al.* [86] showed the movement of an oil droplet on a flat surface modified with calix[4]resorcinarene derivative having photochromic azobenzene units. Asymmetrical photo-irradiation of this surface with different UV and visible light fluxes caused a gradient in the surface free energy due to the isomerisation of the azobenzene-containing monolayer, leading to a directional droplet movement. Although the velocity of the droplet depended intrinsically on the intensity and gradient of the light, a typical speed of $35 \mu\text{L min}^{-1}$ was observed for the motion of a $2 \mu\text{L}$ olive oil droplet. Authors also demonstrated the photo-manipulation of fluid inside a surface-modified glass tube, showing the applicability of this technique for fluid manipulation in micro-fluidics. Although there is no theoretical limitation in movement distance for this approach, the surface-assisted method was only demonstrated for liquids that exhibited both small-hysteresis and large photo-induced changes in contact angles upon photo-isomerisation.

More recently, similar results were reported by Yang *et al.* [87] using a flat surface functionalised with an azobenzene monolayer, and also by Berna *et al.* [88], using a photo-sensitive rotaxane-modified substrate (flat or tilted by 12°). Although promising, these photo-droplet manipulations were only demonstrated for olive oil, a few organic compounds (benzonitrile, diiodomethane, 1-Methylnaphthalene, 1,1,2,2 - Tetrachloroethane), some nematic liquid crystals, but

never for water. At this stage, photo-manipulation of surface wettability cannot produce fast manipulation of a large number of individual droplets, which is required for delivering real-life applications of digital micro-fluidics.

Another interesting means of transporting μL -sized droplets that has been explored in recent years is the use of photo-sensitive surfactants [26, 27]. These are surfactants that incorporate a photochromic moiety, most often spiropyrans [89-93] or azobenzenes [26, 27, 94-96], although other photoswitchable moieties have also been investigated [94, 97].

For linear surfactants functionalised with spiropyrans or azobenzenes, UV irradiation induces isomerisation of the photochromic unit to the more polar form which causes an increase in air–water interfacial tension of up to 10 mN m^{-1} [15]. Diguët *et al.* [26] explored the use of a cationic photo-sensitive surfactant that incorporates an azobenzene unit for photo-manipulation of droplets. The first demonstration was performed with an oil droplet floating on a water bath containing a cationic photo-sensitive azobenzene trimethylammonium bromide surfactant AzoTAB (Figure 3.13A) that is initially in the trans configuration. Partial illumination of the solution containing AzoTAB with UV light, next to the droplet, resulted in a higher surface tension in the illuminated area and the droplet could be ‘pushed’ along by the UV light. Contrariwise, by changing the light source to blue light, the surface tension gradient formed is in the opposite direction, causing the droplet to be ‘pulled’ along by the blue light. This type of droplet manipulation can be performed repeatedly, with droplet velocities of up to $300 \mu\text{m s}^{-1}$. The authors also demonstrated that greater precision of droplet manipulation can be achieved by using simultaneous two-color illumination, wherein the center part of the droplet is under blue illumination (attraction) while the droplet periphery is surrounded by a UV light (repulsion). This two-color illumination creates a ‘trap’ for the droplet and therefore by moving the two-color source, the droplet can be moved at will around a desired trajectory. Figure 3.13 B shows a superposition of a set of images which follows the path of a single droplet as it is moved along a heart-shaped trajectory at a speed of about $300 \mu\text{m s}^{-1}$. This type of precise and fast droplet manipulation is very appealing for droplet-based analytical/micro-fluidic applications, as now one can imagine parallel and complex manipulation of a large number of individual μL -sized droplets using two-color location control.

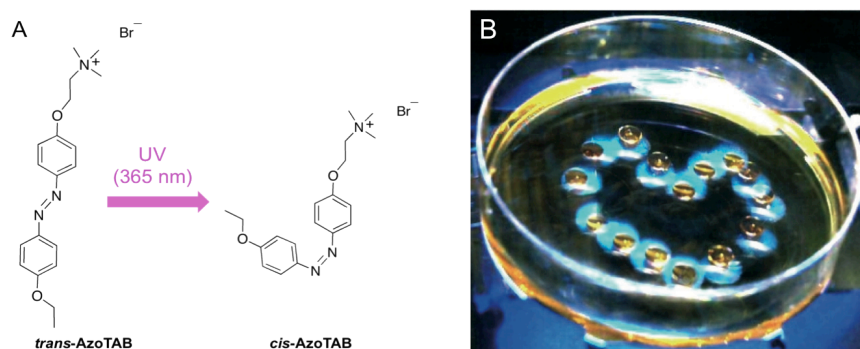


Figure 3.13. A-Molecular structure of the photo-sensitive surfactant AzoTAB. Upon illumination at 365 nm, trans-AzoTAB isomerises to cis configuration, resulting in a more polar tail [26]. B- Photomontages of the motion of a droplet along a heart shape trajectory. Adapted from www.baigllab.com.

Another fascinating way of using photo-sensitive surfactants to control liquid behavior was recently demonstrated by the same group. In this case, AzoTAB was used to provide photo-induced reversible switching between a continuous two-phase laminar flow and a droplet generating regime, in micro-fluidic devices employing a typical water-in-oil flow focusing geometry [27]. Based on the same principle, they demonstrated that interfacial energy between flowing liquids and the micro-fluidic substrate could be photo-modulated. When AzoTAB was added to the aqueous phase of a two-phase laminar-flow regime (water/oil) in a micro-fluidic system, UV light induced fragmentation of the flow, to a regime where mono-dispersed droplets were formed. When the light stimulus was removed, the system reverted to the laminar regime (Figure 3.14). This strategy was applicable to different device morphologies and allowed many cycles of reversible and rapid switches as well as spatio-temporal control of flow regime localisation.

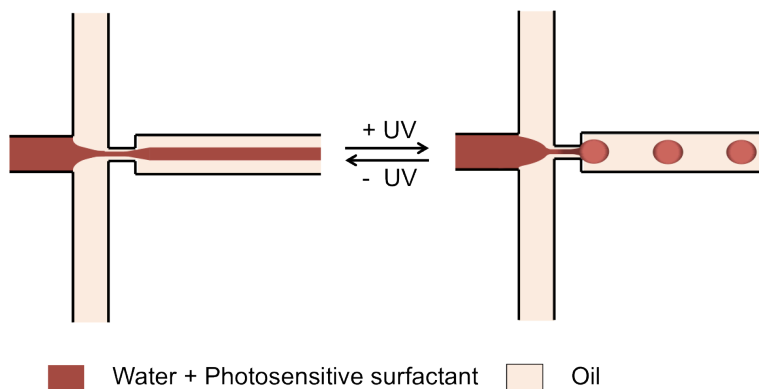


Figure 3.14. Snapshots from a video showing the photo-induced reversible switching between a continuous two-phase laminar flow and a droplet generating regime. The images show a water solution containing AzoTAB photo-sensitive surfactant that is flowing into a water-in-oil flow focusing device. Without UV, the water phase is wetting the micro-fluidic substrate and forms a stable continuous two-phase laminar flow “tube” regime (A). Application of UV induces a dewetting transition and the water phase enters a stable droplet-generating regime (B). Adapted from www.baigllab.com.

3.3 Conclusions

The examples presented here give some indication of the potential of using an optical stimulus for photo-modulation of flow behavior in micro-fluidics by incorporating photo-responsive units into polymeric actuators, coatings, or surfactants. Although these examples can only hint at the possibilities, such as photo-modulation of flows or photo-induced droplet formation in micro-fluidics, the reader can gain some knowledge of the tools now available to achieve these effects. Incorporation of photo-responsive or photo-thermo-responsive molecules in micro-fluidics together with smart engineering of the opto-functional unit can provide switchable characteristics that have great potential for many target applications. Opto-controlled micro-fluidics can open new possibilities based on unprecedented flexibility, versatility, reduced costs and simplicity. Moreover, advanced features such as parallel manipulation of multiple spatially resolved photo-responsive units through the use of patterned light exposure, variable light intensities, user selectable wavelengths, and excellent temporal control, become practically realisable. This clearly opens great advantages over standard actuation methods that rely on highly

complex arrays of actively moving components (pumps, valves) based on individually addressable electronic or pressure based control.

We believe that the use of opto-responsive units in micro-fluidics could form the basis of the new types of autonomous micro-fluidic-based analytical devices that are much more biomimetic in nature, and lower cost than current technologies. However, the future of opto-manipulated micro-fluidics relies on convincing demonstrations of their application to real scenarios in which their unique photo-controlled characteristics lead to truly disruptive platforms for studying chemical or biological processes compared to existing technologies.

3.4 References

1. Martinez, A. W.; Phillips, S. T.; Whitesides, G. M.; Carrilho, E., Diagnostics for the Developing World: Microfluidic Paper-Based Analytical Devices. *Analytical Chemistry* **2010**, *82*, 3-10.
2. Gonzalez Crevillen, A.; Hervas, M.; Angel Lopez, M.; Cristina Gonzalez, M.; Escarpa, A., Real sample analysis on microfluidic devices. *Talanta* **2007**, *74*, 342-357.
3. Argentiére, S.; Gigli, G.; Mortato, M.; Gerges, I.; Blasi, L., Advances in Microfluidics. In *Advances in Microfluidics*, Kelly, R., Ed. InTech: 2012.
4. Byrne, R.; Benito-Lopez, F.; Diamond, D., Materials science and the sensor revolution. *Materials Today* **2010**, *13*, 9-16.
5. Abgrall, P.; Gue, A. M., Lab-on-chip technologies: making a microfluidic network and coupling it into a complete microsystem - a review. *Journal of Micromechanics and Microengineering* **2007**, *17*, R15-R49.
6. Laser, D. J.; Santiago, J. G., A review of micropumps. *Journal of Micromechanics and Microengineering* **2004**, *14*, R35-R64.
7. Psaltis, D.; Quake, S. R.; Yang, C., Developing optofluidic technology through the fusion of microfluidics and optics. *Nature* **2006**, *442*, 381-386.
8. Czugala, M.; Ziolkowski, B.; Byrne, R.; Diamond, D.; Benito-Lopez, F. In *Materials science: the key to revolutionary breakthroughs in micro-fluidic devices*, 2011; Jaume, E.; Eugene, M. T.; Eva, M. C., Eds. SPIE: 2011; p 81070C.
9. Ziolkowski, B.; Czugala, M.; Diamond, D., Integrating stimulus responsive materials and microfluidics – The key to next generation chemical sensors. *Journal of Intelligent Material Systems and Structures* **2012**.
10. Florea, L.; Hennart, A.; Diamond, D.; Benito-Lopez, F., Synthesis and characterisation of spiropyran-polymer brushes in micro-capillaries: Towards an integrated optical sensor for continuous flow analysis. *Sensors and Actuators B: Chemical* **2012**, *175*, 92-99.
11. Benito-Lopez, F.; Byrne, R.; Raduta, A. M.; Vrana, N. E.; McGuinness, G.; Diamond, D., Ionogel-based light-actuated valves for controlling liquid flow in micro-fluidic manifolds. *Lab on a Chip* **2010**, *10*, 195-201.
12. Florea, L.; Diamond, D.; Benito-Lopez, F., Polyaniline Coated Micro-capillaries for Continuous Flow Analysis of Aqueous Solutions. *Analytica Chimica Acta*.

13. Chen, M.; Huang, H.; Zhu, Y.; Liu, Z.; Xing, X.; Cheng, F.; Yu, Y., Photodeformable CLCP material: study on photo-activated microvalve applications. *Applied Physics a-Materials Science & Processing* **2011**, *102*, 667-672.
14. Padgett, M.; Di Leonardo, R., Holographic optical tweezers and their relevance to lab on chip devices. *Lab on a Chip* **2011**, *11*, 1196-1205.
15. Baigl, D., Photo-actuation of liquids for light-driven microfluidics: state of the art and perspectives. *Lab on a Chip* **2012**, *12*, 3637-3653.
16. Bassetti, M. J.; Chatterjee, A. N.; Aluru, N. R.; Beebe, D. J., Development and modeling of electrically triggered hydrogels for microfluidic applications. *Journal of Microelectromechanical Systems* **2005**, *14*, 1198-1207.
17. Beebe, D. J.; Moore, J. S.; Bauer, J. M.; Yu, Q.; Liu, R. H.; Devadoss, C.; Jo, B. H., Functional hydrogel structures for autonomous flow control inside microfluidic channels. *Nature* **2000**, *404*, 588-590.
18. Kwon, G. H.; Jeong, G. S.; Park, J. Y.; Moon, J. H.; Lee, S.-H., A low-energy-consumption electroactive valveless hydrogel micropump for long-term biomedical applications. *Lab on a Chip* **2011**, *11*, 2910-2915.
19. Richter, A.; Klatt, S.; Paschew, G.; Klenke, C., Micropumps operated by swelling and shrinking of temperature-sensitive hydrogels. *Lab on a Chip* **2009**, *9*, 613-618.
20. Benito-Lopez, F.; Scarmagnani, S.; Walsh, Z.; Paull, B.; Macka, M.; Diamond, D., Spiropyran modified micro-fluidic chip channels as photonically controlled self-indicating system for metal ion accumulation and release. *Sensors and Actuators B-Chemical* **2009**, *140*, 295-303.
21. Garcia, A.; Marquez, M.; Cai, T.; Rosario, R.; Hu, Z.; Gust, D.; Hayes, M.; Vail, S. A.; Park, C.-D., Photo-, thermally, and pH-responsive microgels. *Langmuir* **2007**, *23*, 224-229.
22. Higuchi, A.; Hamamura, A.; Shindo, Y.; Kitamura, H.; Yoon, B. O.; Mori, T.; Uyama, T.; Umezawa, A., Photon-modulated changes of cell attachments on poly(spiropyran-co-methyl methacrylate) membranes. *Biomacromolecules* **2004**, *5*, 1770-1774.
23. Samanta, S.; Locklin, J., Formation of photochromic spiropyran polymer brushes via surface-initiated, ring-opening metathesis polymerization: Reversible photocontrol of wetting behavior and solvent dependent morphology changes. *Langmuir* **2008**, *24*, 9558-9565.
24. Anastasiadis, S. H.; Lygeraki, M. I.; Athanassiou, A.; Farsari, M.; Pisignano, D., Reversibly Photo-Responsive Polymer Surfaces for Controlled Wettability. *Journal of Adhesion Science and Technology* **2008**, *22*, 1853-1868.
25. Dattilo, D.; Armelao, L.; Fois, G.; Mistura, G.; Maggini, M., Wetting properties of flat and porous silicon surfaces coated with a spiropyran. *Langmuir* **2007**, *23*, 12945-12950.
26. Diguët, A.; Guillermic, R. M.; Magome, N.; Saint-Jalmes, A.; Chen, Y.; Yoshikawa, K.; Baigl, D., Photomanipulation of a Droplet by the Chromocapillary Effect. *Angewandte Chemie-International Edition* **2009**, *48*, 9281-9284.
27. Diguët, A.; Li, H.; Queyriaux, N.; Chen, Y.; Baigl, D., Photoreversible fragmentation of a liquid interface for micro-droplet generation by light actuation. *Lab on a Chip* **2011**, *11*, 2666-2669.
28. Sugiura, S.; Sumaru, K.; Ohi, K.; Hiroki, K.; Takagi, T.; Kanamori, T., Photoresponsive polymer gel microvalves controlled by local light irradiation. *Sensors and Actuators a-Physical* **2007**, *140*, 176-184.
29. Hirshberg, Y., Reversible formation and eradication of colors by irradiation at low temperatures - a photochemical memory model. *Journal of the American Chemical Society* **1956**, *78*, 2304-2312.
30. Minkin, V. I., Photo-, thermo-, solvato-, and electrochromic spiroheterocyclic compounds. *Chemical Reviews* **2004**, *104*, 2751-2776.
31. Dürr, H.; Bouas-Laurent, H., *Photochromism: Molecules and Systems*. Elsevier: 2003.

32. Lee, C. W.; Song, Y. H.; Lee, Y.; Ryu, K. S.; Chi, K. W., Reversible photochromic switch ensemble and its photoimaging using H⁺ transfer between spiropyran and fluorescein in a polymer matrix. *Chemical Communications* **2009**, 6282-6284.
33. Doron, A.; Katz, E.; Tao, G. L.; Willner, I., Photochemically-, chemically-, and pH-controlled electrochemistry at functionalized spiropyran monolayer electrodes. *Langmuir* **1997**, *13*, 1783-1790.
34. Gaonkar, S. R.; Kumar, G. S.; Neckers, D. C., Photochromism of azobenzene-containing polymers .4. effect of spacer groups. *Macromolecules* **1990**, *23*, 5146-5148.
35. Ide, T.; Ozama, Y.; Matsui, K., Photochemistry of azobenzene in sol-gel systems. *Journal of Non-Crystalline Solids* **2011**, *357*, 100-104.
36. Nicoletta, F. P.; Cupelli, D.; Formoso, P.; De Filpo, G.; Colella, V.; Gugliuzza, A., Light Responsive Polymer Membranes: A Review. *Membranes* **2012**, *2*, 134-197.
37. Singleton, T. A.; Ramsay, K. S.; Barsan, M. M.; Butler, I. S.; Barrett, C. J., Azobenzene Photoisomerization under High External Pressures: Testing the Strength of a Light-Activated Molecular Muscle. *Journal of Physical Chemistry B* **2012**, *116*, 9860-9865.
38. Hoffmann, K.; Resch-Genger, U.; Marlow, F., Photoinduced switching of nanocomposites consisting of azobenzene and molecular sieves: investigation of the switching states. *Microporous and Mesoporous Materials* **2000**, *41*, 99-106.
39. Chen, G.; Svec, F.; Knapp, D. R., Light-actuated high pressure-resisting microvalve for on-chip flow control based on thermo-responsive nanostructured polymer. *Lab on a Chip* **2008**, *8*, 1198-1204.
40. Hua, Z.; Pal, R.; Srivannavit, O.; Burns, M. A.; Gulari, E., A light writable microfluidic "flash memory": Optically addressed actuator array with latched operation for microfluidic applications. *Lab on a Chip* **2008**, *8*, 488-491.
41. Lo, C.-W.; Zhu, D.; Jiang, H., An infrared-light responsive graphene-oxide incorporated poly(N-isopropylacrylamide) hydrogel nanocomposite. *Soft Matter* **2011**, *7*, 5604-5609.
42. Angiolini, L.; Benelli, T.; Giorgini, L.; Raymo, F. M., Optical and chiroptical switches based on photoinduced photon and proton transfer in copolymers containing spiropyran and azopyridine chromophores in their side chains. *Polymer* **2009**, *50*, 5638-5646.
43. Ivanov, A. E.; Ereemeev, N. L.; Wahlund, P. O.; Galaev, I. Y.; Mattiasson, B., Photosensitive copolymer of N-isopropylacrylamide and methacryloyl derivative of spirobenzopyran. *Polymer* **2002**, *43*, 3819-3823.
44. Levy, D.; DelMonte, F.; Oton, J. M.; Fikshan, G.; Matias, I.; Datta, P.; Lopez-Amo, M., Photochromic doped sol-gel materials for fiber-optic devices. *Journal of Sol-Gel Science and Technology* **1997**, *8*, 931-935.
45. Lin, J. S.; Chiu, H. T., Photochromic behavior of spiropyran and fulgide in thin films of blends of PMMA and SBS. *Journal of Polymer Research-Taiwan* **2003**, *10*, 105-110.
46. Samoladas, A.; Bikiaris, D.; Zorba, T.; Paraskevopoulos, K. M.; Jannakoudakis, A., Photochromic behavior of spiropyran in polystyrene and polycaprolactone thin films - Effect of UV absorber and antioxidant compound. *Dyes and Pigments* **2008**, *76*, 386-393.
47. Stitzel, S.; Byrne, R.; Diamond, D., LED switching of spiropyran-doped polymer films. *Journal of Materials Science* **2006**, *41*, 5841-5844.
48. Such, G. K.; Evans, R. A.; Davis, T. P., Rapid photochromic switching in a rigid polymer matrix using living radical polymerization. *Macromolecules* **2006**, *39*, 1391-1396.
49. Chung, D. J.; Ito, Y.; Imanishi, Y., Preparation of porous membranes grafted with poly(spiropyran-containing methacrylate) and photocontrol of permeability. *Journal of Applied Polymer Science* **1994**, *51*, 2027-2033.

50. Park, Y. S.; Ito, Y.; Imanishi, Y., Photocontrolled gating by polymer brushes grafted on porous glass filter. *Macromolecules* **1998**, *31*, 2606-2610.
51. Byrne, R. J.; Stitzel, S. E.; Diamond, D., Photo-regenerable surface with potential for optical sensing. *Journal of Materials Chemistry* **2006**, *16*, 1332-1337.
52. Dong, L.; Jiang, H., Autonomous microfluidics with stimuli-responsive hydrogels. *Soft Matter* **2007**, *3*, 1223-1230.
53. Alvarez-Lorenzo, C.; Concheiro, A., Intelligent Drug Delivery Systems: Polymeric Micelles and Hydrogels. *Mini-Reviews in Medicinal Chemistry* **2008**, *8*, 1065-1074.
54. Yoshida, M.; Yang, J. S.; Kumakura, M.; Hagiwara, M.; Katakai, R., Artificially intelligent hydrogels responding to external stimuli such as temperature and pH. *European Polymer Journal* **1991**, *27*, 997-1005.
55. He, L.; Zuo, Q.; Xie, S.; Huang, Y.; Xue, W., Intelligent hydrogels for drug delivery system. *Recent patents on drug delivery & formulation* **2011**, *5*, 265-274.
56. Kim, B.; Shin, Y., pH-sensitive swelling and release behaviors of anionic hydrogels for intelligent drug delivery system. *Journal of Applied Polymer Science* **2007**, *105*, 3656-3661.
57. Oh, K. W.; Ahn, C. H., A review of microvalves. *Journal of Micromechanics and Microengineering* **2006**, *16*, R13-R39.
58. Geiger, E. J.; Pisano, A. P.; Svec, F., A Polymer-Based Microfluidic Platform Featuring On-Chip Actuated Hydrogel Valves for Disposable Applications. *Journal of Microelectromechanical Systems* **2010**, *19*, 944-950.
59. D. Kungwachakun, M. I., Photoresponsive polymers—photocontrol of the phase-separation temperature of aqueous-solutions of poly N-isopropylacrylamide-co-N-(4-phenylazophenyl)acrylamide. *Makromol. Chem. Rapid Commun.* **1988**, *9*, 243–246.
60. M.Irie, D. K., Photoresponsive polymers. 8. Reversible photo- stimulated dilation of polyacrylamide gels having triphenylmethane leuco derivatives. *Macromolecules* **1986**, *19*, 2476–2480.
61. M. Irie, M. H., Photoresponsive polymers—reversible solution viscosity change of poly(N,N-dimethylacrylamide) with pendant triphenyl- methane leucohydroxide residues in methanol. *Makromol. Chem. Rapid Commun.* **1985**, *6*, 533–536.
62. M. Irie, A. M., K. Hayashi, Photoresponsive polymers. reversible solution viscosity change of poly (methyl methacrylate) having spiroben- zopyran side groups. *Macromolecules* **1979**, *12*, 1176–1180.
63. A. Menju, K. H., M. Irie, Photoresponsive polymers. 3. Reversible solution viscosity change of poly(methacrylic acid) having spirobenzopy- ran pendant groups in methano. *Macromolecules* **1981**, *14*, 755–758.
64. Harmon, M. E.; Kuckling, D.; Frank, C. W., Photo-cross-linkable PNIPAAm copolymers. 5. Mechanical properties of hydrogel layers. *Langmuir* **2003**, *19*, 10660-10665.
65. Kuckling, D.; Harmon, M. E.; Frank, C. W., Photo-cross-linkable PNIPAAm copolymers. 1. Synthesis and characterization of constrained temperature-responsive hydrogel layers. *Macromolecules* **2002**, *35*, 6377-6383.
66. Xu, X.-D.; Wei, H.; Zhang, X.-Z.; Cheng, S.-X.; Zhuo, R.-X., Fabrication and characterization of a novel composite PNIPAAm hydrogel for controlled drug release. *Journal of Biomedical Materials Research Part A* **2007**, *81A*, 418-426.
67. Dusek, Responsive gels, volume transition I and. II. . In *Adv. Polym. Sci.*, K., D., Ed. 1993; Vol. 110, pp 1-261.
68. Schild, H. G., Poly (n-isopropylacrylamide) - experiment, theory and application. *Progress in Polymer Science* **1992**, *17*, 163-249.
69. Sershen, S. R.; Mensing, G. A.; Ng, M.; Halas, N. J.; Beebe, D. J.; West, J. L., Independent optical control of microfluidic valves formed from optomechanically responsive nanocomposite hydrogels. *Advanced Materials* **2005**, *17*, 1366-+.
70. Sumaru, K.; Kameda, M.; Kanamori, T.; Shinbo, T., Reversible and Efficient Proton Dissociation of Spirobenzopyran-Functionalized Poly(N-isopropylacrylamide) in

- Aqueous Solution Triggered by Light Irradiation and Temporary Temperature Rise. *Macromolecules* **2004**, *37*, 7854-7856.
71. Sugiura, S.; Sumaru, K.; Ohi, K.; Hiroki, K.; Takagi, T.; Kanamori, T., Photoresponsive polymer gel microvalves controlled by local light irradiation. *Sensors and Actuators A: Physical* **2007**, *140*, 176-184.
 72. Sugiura, S.; Szilagy, A.; Sumaru, K.; Hattori, K.; Takagi, T.; Filipcsei, G.; Zrinyi, M.; Kanamori, T., On-demand microfluidic control by micropatterned light irradiation of a photoresponsive hydrogel sheet. *Lab on a Chip* **2009**, *9*, 196-198.
 73. Sugiura, S.; Szilágyi, A.; Sumaru, K.; Takagi, T.; Zrinyi, M.; Kanamori, T., On-demand fluid control on microchip by micro-patterned light irradiation using photo-responsive hydrogels. In *Twelfth International Conference on Miniaturized Systems for Chemistry and Life Sciences*, San Diego, California, USA, 2008; pp 838-840.
 74. Huang, X. H.; Gordon, M. J.; Zare, R. N., Current-monitoring method for measuring the electroosmotic flow-rate in capillary zone electrophoresis. *Analytical Chemistry* **1988**, *60*, 1837-1838.
 75. Liu, Y.; Fanguy, J. C.; Bledsoe, J. M.; Henry, C. S., Dynamic coating using polyelectrolyte multilayers for chemical control of electroosmotic flow in capillary electrophoresis microchips. *Analytical Chemistry* **2000**, *72*, 5939-5944.
 76. Rathore, A. S.; Horvath, C., Capillary electrochromatography: theories on electroosmotic flow in porous media. *Journal of Chromatography A* **1997**, *781*, 185-195.
 77. Moorthy, J.; Khoury, C.; Moore, J. S.; Beebe, D. J., Active control of electroosmotic flow in microchannels using light. *Sensors and Actuators B-Chemical* **2001**, *75*, 223-229.
 78. Oroszi, L.; Der, A.; Kirei, H.; Ormos, P.; Rakovics, V., Control of electro-osmotic flow by light. *Applied Physics Letters* **2006**, *89*.
 79. Oroszi, L. s.; Der, A. s.; Kirei, H.; Rakovics, V.; Ormos, P. I., Manipulation of microfluidic flow pattern by optically controlled electroosmosis. *Microfluidics and Nanofluidics* **2009**, *6*, 565-569.
 80. Scarmagnani, S.; Walsh, Z.; Benito-Lopez, F.; Macka, M.; Paull, B.; Diamond, D., Incorporation of acrylate based spiropyran monoliths in micro-fluidic devices for photo-controlled electroosmotic flow. *Advances in Science and Technology* **2010**, *76*, 100-105.
 81. Teh, S.-Y.; Lin, R.; Hung, L.-H.; Lee, A. P., Droplet microfluidics. *Lab on a Chip* **2008**, *8*, 198-220.
 82. Chaudhury, M. K.; Whitesides, G. M., How to make water run uphill. *Science* **1992**, *256*, 1539-1541.
 83. Fries, K.; Samanta, S.; Orski, S.; Locklin, J., Reversible colorimetric ion sensors based on surface initiated polymerization of photochromic polymers. *Chemical Communications* **2008**, 6288-6290.
 84. Wang, D.; Jiao, P.; Wang, J.; Zhang, Q.; Feng, L.; Yang, Z., Fast photo-switched wettability and color of surfaces coated with polymer brushes containing spiropyran. *Journal of Applied Polymer Science* **2012**, *125*, 870-875.
 85. Lygeraki, M. I.; Tsiranidou, E.; Anastasiadis, S. H.; Fotakis, C.; Pisignano, D.; Cingolani, R.; Athanassiou, A., Controlling the reversible wetting capability of smart photochromic-polymer surfaces by micro patterning. *Applied Physics a-Materials Science & Processing* **2008**, *91*, 397-401.
 86. Ichimura, K.; Oh, S. K.; Nakagawa, M., Light-driven motion of liquids on a photoresponsive surface. *Science* **2000**, *288*, 1624-1626.
 87. Yang, D.; Piech, M.; Bell, N. S.; Gust, D.; Vail, S.; Garcia, A. A.; Schneider, J.; Park, C.-D.; Hayes, M. A.; Picraux, S. T., Photon control of liquid motion on reversibly photoresponsive surfaces. *Langmuir* **2007**, *23*, 10864-10872.
 88. Berna, J.; Leigh, D. A.; Lubomska, M.; Mendoza, S. M.; Perez, E. M.; Rudolf, P.; Teobaldi, G.; Zerbetto, F., Macroscopic transport by synthetic molecular machines. *Nature Materials* **2005**, *4*, 704-710.

89. Liu, S. L.; Fujihira, M.; Saji, T., Formation of an organic thin-film by photochemical isomerization of a surfactant with a spiropyran moiety. *Journal of the Chemical Society-Chemical Communications* **1994**, 1855-1856.
90. Sakai, H.; Ebana, H.; Sakai, K.; Tsuchiya, K.; Ohkubo, T.; Abe, M., Photoisomerization of spiropyran-modified cationic surfactants. *Journal of Colloid and Interface Science* **2007**, *316*, 1027-1030.
91. Sakai, K.; Imaizumi, Y.; Oguchi, T.; Sakai, H.; Abe, M., Adsorption Characteristics of Spiropyran-Modified Cationic Surfactants at the Silica/Aqueous Solution Interface. *Langmuir* **2010**, *26*, 9283-9288.
92. Takagi, K.; Kurematsu, T.; Sawaki, Y., Photochromic behavior of surfactant spiro 2h-1-benzopyran-2,2' 2,3 -dihydroindole s (spiopyrans) adsorbed into clay interlayers. *Journal of the Chemical Society-Perkin Transactions 2* **1995**, 1667-1671.
93. Takumi, K.; Sakamoto, H.; Uda, R. M.; Sakurai, Y.; Kume, H.; Kimura, K., Photocontrol of anionic micelles containing lipophilic crowned spirobenzopyran. *Colloids and Surfaces a-Physicochemical and Engineering Aspects* **2007**, *301*, 100-105.
94. Eastoe, J.; Dominguez, M. S.; Wyatt, P.; Beeby, A.; Heenan, R. K., Properties of a stilbene-containing gemini photosurfactant: Light-triggered changes in surface tension and aggregation. *Langmuir* **2002**, *18*, 7837-7844.
95. Yang, L.; Takisawa, N.; Hayashita, T.; Shirahama, K., Colloid-chemical characterization of the photosurfactant 4-ethylazobenzene 4'-(oxyethyl)trimethylammonium bromide. *Journal of Physical Chemistry* **1995**, *99*, 8799-8803.
96. Zhang, J.; Wang, S.-C.; Lee, C. T., Jr., Photoreversible Conformational Changes in Membrane Proteins Using Light-Responsive Surfactants. *Journal of Physical Chemistry B* **2009**, *113*, 8569-8580.
97. Bonini, M.; Berti, D.; Di Meglio, J. M.; Almgren, M.; Teixeira, J.; Baglioni, P., Surfactant aggregates hosting a photoresponsive amphiphile: structure and photoinduced conformational changes. *Soft Matter* **2005**, *1*, 444-454.

Chapter 4

Polyaniline Coated Micro-capillaries for Continuous Flow Analysis of Aqueous Solutions

Larisa Florea¹, Dermot Diamond¹ and Fernando Benito-Lopez^{1, 2 *}

Analytica Chimica Acta 759 (2013) 1-7

ISSN: 0003-2670; DOI: 10.1016/j.aca.2012.11.027

¹CLARITY: Centre for Sensor Web Technologies, National Centre for Sensor Research, School of Chemical Sciences, Dublin City University, Dublin, Ireland;

²CIC microGUNE, Arrasate-Mondragón, SPAIN

*Author to whom correspondence should be addressed;



VOLUME 759 8 JANUARY 2013 ISSN 0003-2670

ANALYTICA CHIMICA ACTA

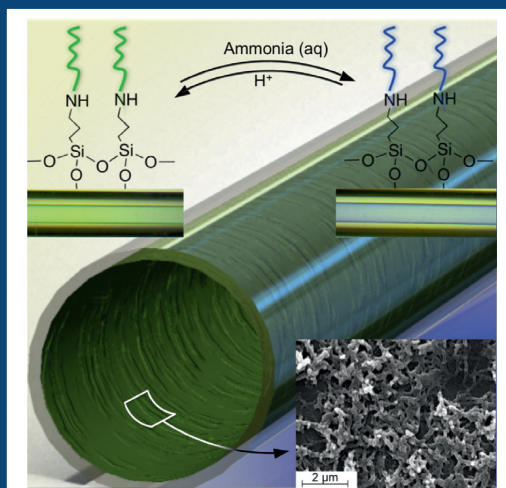
AN INTERNATIONAL JOURNAL DEVOTED TO ALL BRANCHES OF ANALYTICAL CHEMISTRY

EDITORS:

RICHARD P. BALDWIN
NEIL W. BARNETT
WOLFGANG BUCHBERGER
LUTGARDE BUYDENS
PUERNENDU K. DASGUPTA
ULRICH J. KRULL
JAMES P. LANDERS
LIANG LI
JANUSZ PAWLISZYN
PAUL J. WORSFOLD

REVIEW EDITOR:

MANUEL MIRÓ



Featured Article

Polyaniline coated micro-capillaries for continuous flow analysis of aqueous solutions

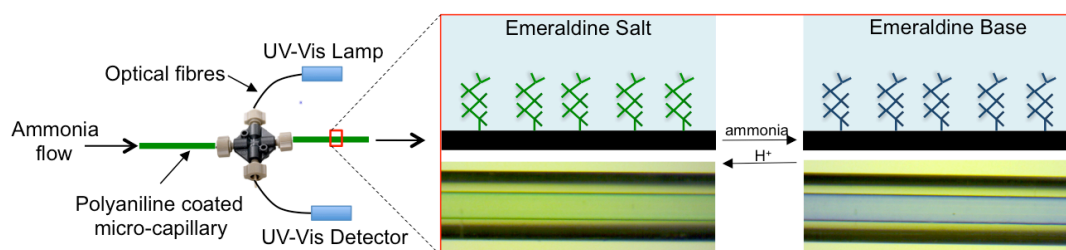
Larisa Florea, Dermot Diamond and Fernando Benito-Lopez

(Published on pp. 1–7 of this issue)

Available online at www.sciencedirect.com

SciVerse ScienceDirect

Abstract: The inner walls of fused silica micro-capillaries were successfully coated with polyaniline nanofibres using the “grafting” approach. The optical response of polyaniline coatings was evaluated during the subsequent redoping–dedoping processes with hydrochloric acid and ammonia solutions, respectively, that were passed inside the micro-capillary in continuous flow. The optical absorbance of the polyaniline coatings was measured and analysed in the wavelength interval of [300–850 nm] to determine its optical sensitivity to different concentrations of ammonia. It was found that the optical properties of polyaniline coatings change in response to ammonia solutions in a wide concentration range from 0.2 ppm to 2000 ppm. The polyaniline coatings employed as a sensing material for the optical detection of aqueous ammonia have a fast response time and a fast regeneration time of less than 5 seconds at room temperature. The coating was fully characterised by Scanning Electron Microscopy, Raman Spectroscopy, absorbance measurements and kinetic studies. The response of the coatings showed very good reproducibility, demonstrating that this platform can be used for the development of micro-capillary integrated sensors based on the inherited sensing properties of polyaniline.



Keywords: polyaniline, continuous flow, sensor, ammonia, micro-capillary;

4.1 Introduction

Sensors providing continuous, direct and immediate analytical information are of great interest for many areas of research as such environmental monitoring [1-6]. In particular, some sectors of the water industry dealing with the detection and characterisation of chemical contaminants in surface water, predominantly rely on the batch sampling technique, where water samples are collected and analysed in the laboratory. This is mainly due to costs or legal constraints around certified methods[7]. Although this technique often offers accurate detection and possesses good sensitivity and limits of detection, it is time consuming, requires manpower and, most importantly, it fails to provide immediate or continuous information, which is of enormous interest when picking a sporadic, but fatal, event in the network. In this context, flow-through sensors have attracted a lot of attention for real time monitoring of water samples [8-12]. Flow-through sensors possess many advantages compared with classical probe-type sensors as such facile sample transport, sensor conditioning, maintenance and regeneration among others [13]. A subclass of flow-through sensors, accomplished through miniaturisation of the “flow-through” unit are micro-capillary integrated optical sensors, in which glass or plastic micro-capillaries are coated on their inner surface with a chemically sensitive layer that changes its optical properties (absorbance [14-17], reflectance [14], fluorescence [15, 16], swelling [16] and refractive index [15, 16]) in response to a particular analyte as it passes through the micro-capillary. Hence, in this type of systems, it is no longer the intrinsic optical properties of the sample as it passes through the detector that are being studied, but rather those of the inner micro-capillary coating, as they are modulated by the sample. Because the optical properties of the coating, instead of the sample itself, are being monitored, micro-capillary integrated optical sensors are virtually independent of the colour and turbidity of the sample, which may interfere with the chemical sensing process in a conventional optical sensor. Moreover, micro-capillary integrated optical sensors offer advantages in terms of size, electrical safety, costs and have no need for a separate reference electrode, as is the case in electrochemical measurements [18]. In particular, several micro-capillary integrated optical sensors have been developed for the optical sensing of metal ions [14], solvent polarity [19], or carbon dioxide [18].

Exploring new means of developing micro-capillary integrated optical sensors capable of continuous flow analysis of water contaminants; we explored the optical properties of the semiconductive polymer polyaniline (PAni), [20-23] for the detection and quantification of aqueous ammonia. In fact, many recent articles describe electrical and optical sensors for ammonia detection with PAni as the sensitive layer, [24-28] or PAni composites [29, 30]. For the detection of aqueous ammonia, however, to our knowledge, only one recent study presents an optical sensor based on PAni. Castellon-Urbe *et al.* [31] used a glass substrate covered with a film of polyaniline produced by the chemical bath method, for which transmittance is measured after immersing the glass slide in aqueous ammonia solutions and subsequently drying the slide. Although the sensor is reported to have good signal linearity over the concentration range 3–100 ppm of ammonia, the sensing method is disruptive, cannot provide immediate or continuous information, and it is not suitable for real-time measurements. Bearing these constraints in mind, we adopted a different approach to produce polyaniline modified sensing micro-capillaries that showed fast response and regeneration times providing with the possibility of working with a wide range of aqueous ammonia concentrations in a continuous flow mode.

4.2 Experimental

4.2.1 Materials and Methods

Aniline (BDH), hydrochloric acid (Fisher Scientific), ammonium persulfate (APS) (Aldrich), *N*-[3-(Trimethoxysilyl)propyl]aniline (Aldrich), ammonium hydroxide solution (28.0-30.0 % NH₃ basis) (Aldrich) were used. The aniline monomer was purified by vacuum distillation before use. Other chemicals were used as received. Fused-silica micro-capillaries (100 μm ID, 375 μm OD) were purchased from Polymicro Technologies (Phoenix, AZ, USA).

Raman Spectroscopy was employed to study the chemical features of the polyaniline coatings inside the micro-capillary. Raman spectra were taken with a

Perkin Elmer RamanStation at 2 cm^{-1} resolution, 3s per scan and 20 collections. A 785 nm laser line was used as it can detect both doped and dedoped features in polyaniline.

UV-Vis Spectroscopy was used to study the pH dependence of the polyaniline coatings. The absorbance spectra were recorded using 2 fiber-optic light guides connected to a Miniature Fiber Optic Spectrometer (USB4000 - Ocean Optics) and aligned using cross shaped cell (see Figure 4.4B). The light source used was DH-2000-BAL UV-NIR deuterium tungsten halogen source (Ocean Optics). Data from the spectrometer was processed using Spectrasuite software provided by Ocean Optics Inc. For clarity, the absorbance spectra recorded were smoothed using Origin software using Savitzky-Golay algorithm.

4.2.2 Fused Silica Micro-Capillaries Coating Protocol

The functionalisation of the inner walls of the micro-capillary with PANi nanofibres was achieved using chemical polymerisation. The protocol used to coat micro-capillaries with polyaniline nanofibres is described in Figure 4.1. Prior to functionalisation the inner micro-capillary surface was quickly washed with acetone and water, then flushed with a solution of NaOH 0.2 M for 30 min at a flow rate of $0.25\text{ }\mu\text{L min}^{-1}$ using a syringe pump and then, rinsed with deionised water. Next, the micro-capillary was flushed with a solution of HCl 0.2 M for 30 min at a flow rate of $0.25\text{ }\mu\text{L min}^{-1}$, rinsed with water, and with ethanol. A 20 % wt solution of *N*-[3-(trimethoxysilyl)propyl]aniline in ethanol was then pumped through the micro-capillaries for 90 min at a flow rate of $0.25\text{ }\mu\text{L min}^{-1}$ (Figure 4.1 – A). Later, the micro-capillaries were washed with ethanol, dried under nitrogen stream, and left at room temperature for 24h.

Fresh solutions of aniline and the oxidant (ammonium persulfate) in 1M HCl were prepared as follow: 82 μL aniline was added to 4 mL 1 M HCl solution; 0.050 g ammonium peroxydisulfate was dissolved in 4 mL 1M HCl solution. Equal volumes of the two solutions were rapidly mixed together in a micro-syringe and immediately used to fill the micro-capillary (Fig. 4 – B), which was after closed at both ends using rubber septa. After about 10 min the solution inside the micro-

Chemical reaction scheme for the synthesis of a polybenzoxazine-coated substrate:

The scheme illustrates the sequential functionalization of a substrate surface (represented by a hatched rectangle) with hydroxyl groups (OH).

Reaction (A): The substrate is reacted with a benzylamine-terminated silane (containing a benzylamine group, $\text{NH-CH}_2\text{-CH}_2\text{-Si}$, and a trimethoxysilyl group, Si-O-CH_3). This results in a monolayer of the silane on the surface.

Reaction (B): The monolayer is further reacted with anhydride-terminated silane (containing an anhydride group, O-CO-O , and a trimethoxysilyl group, Si-O-CH_3) in the presence of APS (Aqueous Potassium Permanganate Solution). This step leads to the formation of a cross-linked polybenzoxazine network on the surface.

Legend: The green wavy line represents the polybenzoxazine chain segment, defined as:

$$\text{Polybenzoxazine} = \left(\text{benzene ring} - \text{HN} - \text{benzene ring} - \text{NH} \right)_m \left(\text{benzene ring} - \text{N} = \text{benzene ring} = \text{N} \right)_n$$

4.2.3 Polyaniline Coatings Imaging Protocol

For imaging purposes, a flat silicon wafer was coated with polyaniline nanofibres using the same procedure as the one employed for the coating of micro-capillaries. For this, a polydimethylsiloxane (PDMS) layer containing a micro-fluidic channel ($100\text{ }\mu\text{m} \times 50\text{ }\mu\text{m} \times 2\text{ cm}$) incorporating one inlet and one outlet was placed on top of a silicon wafer. The obtained micro-channel (PDMS/silicon wafer) was coated with polyaniline following the procedure described above. Prior imaging, the PDMS layer was removed and the silicon wafer containing the polyaniline film was

coated with 10 nm Au layer. The imaging was performed on a Carl Zeiss EVOLS 15 system at an accelerating voltage of 5.75 kV (Figure 4.2B).

4.3 Results and Discussion

4.3.1 Polyaniline Coatings

4.3.1.1 Morphological Analysis

Fused silica micro-capillaries were covalently functionalised with polyaniline as described in the experimental section. Scanning electron microscope (SEM) images showed that using the described polymerisation technique, a 3D arrangement of polyaniline isles, homogeneously distributed along the micro-capillary walls were obtained, in which polyaniline is covalently attached to the inner walls of the micro-capillary (Figure 4.2A). For a better visualisation of the morphology of polyaniline coatings, a flat silicon wafer surface was coated (Figure 4.2B and C) using the same procedure (see Experimental Section 3.3). Figure 4.2C shows that the method employed produces nanofibres that are around 200 nm in diameter and up to several microns in length. The great advantage of nanofiber structured films (*versus* bulk polyaniline) is the high surface area that is exposed to the target molecules and the very short diffusional path lengths [1, 22] which, coupled with rather thick films, produces enhanced sensitivity and fast response times [32-34]. The covalent attachment of the nanofibres ensures good mechanical stability of the coating, moreover no leaching has been observed over a period of three months of use for lab experiments.

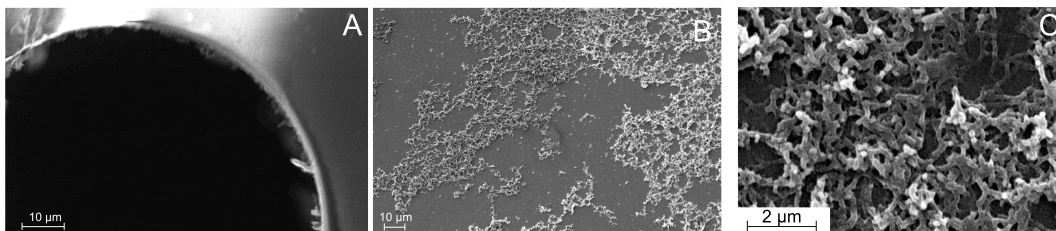


Figure 4.2. SEM images of the polyaniline coated micro-capillary (A) and silicon wafer (B and C).

4.3.1.2 Structural Analysis

Raman spectroscopy was used to characterise the chemical structure of the polyaniline since this technique allows non-invasive, *in situ* analysis of the polyaniline coating inside the micro-capillary. Raman spectroscopy showed that the polyaniline coating is obtained in its half-oxidised emeraldine state [35]. In addition, Raman spectroscopy was also employed to study the changes in the bonding structure of the coatings upon doping-dedoping, as very distinct signature bands appear for the quinoid and benzenoid rings, respectively [36, 37]. Figure 4.3A presents the Raman spectra of the polyaniline coatings in the region of interest ($1000\text{--}1800\text{ cm}^{-1}$) after a solution of hydrochloric acid (HCl) 10^{-2} M and aqueous solution of ammonia (200 ppm), respectively, are passed inside the micro-capillary.

When a solution of 10^{-2} M HCl is passed through the micro-capillary, polyaniline exists in the doped state, emeraldine salt (ES). Passing a solution of 200 ppm aqueous ammonia inside the micro-capillary causes changes in the bonding structure of the material (Figure 4.3B) reflecting the adoption of the dedoped–emeraldine base (EB) state. Signature bands between 1300 and 1400 cm^{-1} appear for the doped material (Fig. 3A – in green). After dedoping of the polymer with ammonia, these bands are less significant, and strong bands between 1400 and 1500 cm^{-1} reflect the dedoped state (Fig. 3A – in blue). Complete characterisation and assignments are listed in Table 4.1.

In particular, in the case of EB, an important peak can be observed at 1456 cm^{-1} and is characteristic to C=N stretching vibration of the quinoid units [35, 37–40]. Other bands at 1592 cm^{-1} and 1162 cm^{-1} , are assigned to C-C stretching [35, 39] and C-H bending modes[35, 38], respectively, centered on the quinoid ring. Another new peak at 1220 cm^{-1} appears in the spectra of polyaniline upon dedoping and is assigned to C–N stretching vibrations of the benzenoid units [35, 39] (the EB form consists of both C=N and C-N bonds). In the case of ES, the most important band appears at 1346 cm^{-1} and can be assigned to a C-N• + polaron stretch [35, 39, 41, 42] while the band at 1170 cm^{-1} is characteristic to the C–H in-plane bending of the benzenoid ring [35, 40]. These studies have been repeated on the same micro-capillary in similar conditions after a period of two months. Raman spectroscopy

indicated no noticeable changes in the chemical structure of polyaniline (ES and EB).

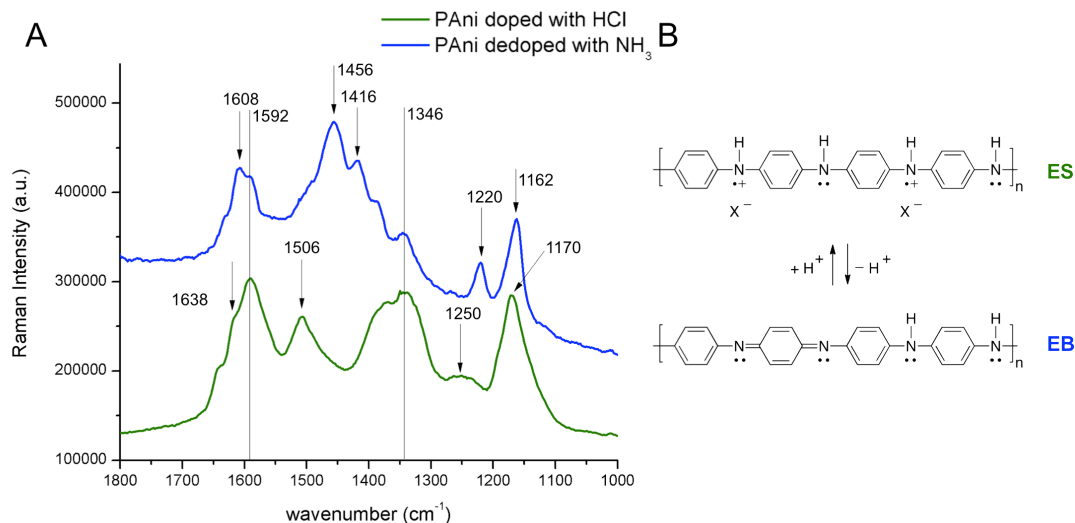


Figure 4.3. (A) Raman Spectra of PANi functionalised micro-capillary after being filled with a HCl solution 10^{-2} M (green) and with NH_3 aqueous solution 200 ppm (blue). (B) Scheme showing the chemical structures of Emeraldine Salt (ES) and Emeraldine Base (EB).

Table 4.1. Assignment of the vibrational bands (cm^{-1}) observed between 1800 and 1000 cm^{-1} in the Raman spectra ($\lambda_{\text{ex}} = 785$ nm) of PANi functionalised micro-capillary after being filled with a HCl solution 10^{-2} M (doped) and PANi functionalised micro-capillary after being filled with NH_3 aqua solution 200 ppm (dedoped).

| Wavenumber (cm^{-1}) | | Assignments | References |
|---------------------------------|----------------------------|-------------------------------------|------------------|
| Doped (HCl) | Dedoped (NH ₃) | | |
| 1170 | 1162 | C–H in-plane bending (Q) | [35, 38-40] |
| - | 1220 | C–N stretching (B) | [35, 39] |
| 1250 | - | C–N ⁺ • stretching (SQR) | [35, 40] |
| 1346 | 1346 | C–N ⁺ • stretching (SQR) | [35, 39, 41, 42] |
| - | 1416 | C–C stretching (Q) | [35, 40] |
| 1506 | 1456 | C=N and CH=CH stretching (Q) | [35, 37-40]. |
| 1590 | 1592 | C=C ring stretching (Q) | [35, 40] |
| - | 1608 | C–C ring stretching (B) | [35, 40] |

The benzenoid, quinoid and semiquinone radical units are denoted by B, Q and SQR, respectively.

4.3.1.3 Optical properties of the coating

To evaluate the optical response of the PANi coatings, hydrochloric acid (10^{-2} M) and aqueous ammonia solution (200 ppm) were alternatively pumped through the micro-capillary at a flow rate of $5 \mu\text{L min}^{-1}$ and the absorbance of the coating was monitored transversally across the micro-capillary over the wavelength interval [350–1100nm] (Figure 4.4A) using the configuration described in Figure 4.3B. When hydrochloric acid is passed through the micro-capillary, the polyaniline coating presents a green colour (ES) as depicted in Figure 4.4A. When the ammonia solution reaches the surface of the coating, the micro-capillary rapidly changes its colour – from green to blue (Figure 4.4A - photos). This is due to the fact that when the emeraldine salt form of polyaniline is exposed to a basic solution, such as ammonia, it undergoes deprotonation and it is converted to the emeraldine base (EB) state which presents a blue color. The process occurs on the imine nitrogen atoms as shown in Figure 4.3B. More specifically, the doped state – emeraldine salt – has a characteristic absorption band at around 360 nm associated to π - π^* transition of the conjugated ring system [23] and an absorption band at ~ 420 nm together with an extended tail at 850 nm assigned to polaron band transition [23]. Dedoping the polymer with ammonia leads to a shift in the absorption lambda maxima of PANi from ~ 360 nm (ES) to ~ 320 nm (EB). The band at 610 nm is ascribed to the exciton formation in the quinonoid rings and this absorption gives rise to the blue colour of the PANi coatings [23]. The UV-Vis spectra of the polyaniline coatings obtained using the setup shown in Figure 4.4B is similar to the absorbance spectra of polyaniline presented in the literature, in the case when polyaniline can be found in the form of dispersions in aqueous solutions [20, 23, 43, 44]. Moreover, the UV-Vis spectra can also provide useful information about the electronic structure of the polymer and its geometric structure such as polymer chain conformation [23]. A number of theoretical studies have examined the influence of PANi chain conformation, in particular the effect of the phenyl and phenyl/quinoid torsional angles along the chain on the electronic structure of polyaniline (and consequently their absorbance spectra) [23, 45, 46]. It was found that the position of the absorption bands of PANi is sensitive to the conformation adopted by the polymer chains as well as the conjugation length. In the case of polyaniline coatings, having the polaron band centered at around 827 nm, suggests that the PANi chains are adopting a

“compact coil” conformation compared with an “extended coil” conformation that is characterised by a red shift in the λ_{max} to 1500-2500 nm [23].

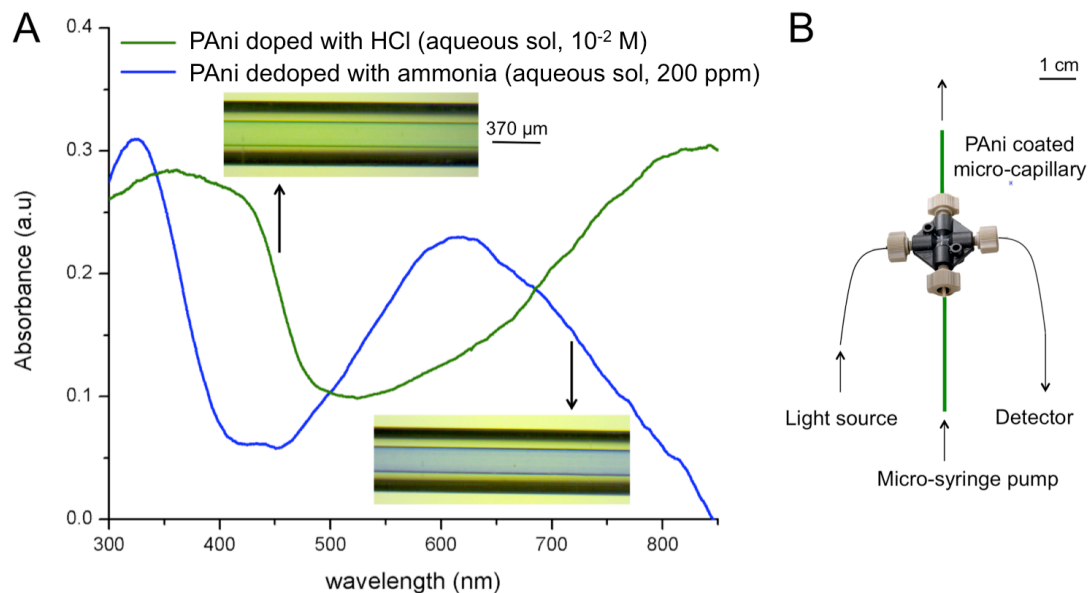


Figure 4.4. (A) Absorbance spectra and photos of PANi functionalised micro-capillary after being filled with a HCl solution 10⁻² M (green) and PANi functionalised micro-capillary after being filled with ammonia aqueous solution (blue). (B) Picture of the UV-Vis flow cell set-up used for UV-Vis characterisation.

The change in colour and absorbance spectra of the coating in response to hydrochloric acid and ammonia solution, respectively, shows the potential of this type of coatings for building micro-capillary integrated micro-sensors capable of working in continuous flow.

To further investigate the reversibility of color change of the micro-capillary sensor during the protonation/deprotonation processes, the absorbance at fixed wavelengths was monitored while pumping HCl 10⁻² M and aqueous ammonia 200 ppm solutions respectively, through the micro-capillary at a flow rate of 5 $\mu\text{L min}^{-1}$. The two wavelengths monitored correspond to typical absorbance of emeraldine salt (827nm – polaron stretch) and emeraldine base (600nm – exciton formation in the quinoid ring). An absorbance reading was taken every 100 ms and no smoothing algorithms were applied for the acquired data (Figure 4.5).

Firstly, a solution of hydrochloric acid is passed through the micro-capillary and the absorbance at 827 nm (Figure 4.5 - in green) and 600 nm (Figure 4.5 – in blue) is recorded in real time. After approximately three to four minutes, aqueous ammonia solution is injected inside the micro-capillary, replacing the previous solution and causing a change in colour of the micro-capillary. The absorbance is continuously monitored, recording the moment when the micro-capillary changes from green to blue (decrease in the absorbance at 827 and increase in the absorbance at 600 nm). The absorbance value stabilises rapidly and after another 3 to 4 minutes the 10^{-2} M hydrochloric acid is injected inside the micro-capillary. The sequence of doping/dedoping/ followed by dedoping/doping process is repeated seven times in total. The results showed excellent reproducibility, with no visible loss in the coating sensitivity. The response time and the recovery time of the PANi coating exposed to aqueous ammonia and hydrochloric acid solutions, respectively, were less than 5 s at room temperature when the solutions are pumped through the micro-capillary at $5 \mu\text{L min}^{-1}$ flow rate (Figure 4.5 – Inset A and B). The response of the PANi coatings, when exposed to aqueous ammonia, is depicted in Figure 4.5 by a decrease in the absorbance at 827 nm and an increase in the absorbance at 600nm. The absorbance values become stable after less than 5 seconds (4.43 ± 0.13 , $n = 4$) and remain stable as long as the solution and the flow passing through the micro-capillary is not modified. In order to ensure a good coating regeneration (doped state), a solution of HCl 10^{-2} M is pumped through the modified micro-capillary. The regeneration of the coating occurs in less than 4 seconds (3.34 ± 0.16 , $n = 3$) and it is characterised by an increase in the absorbance at 827 nm and a simultaneous decrease of the absorbance at 600 nm to their original values (doped state). These results showed that the modified micro-capillary sensor exhibits very rapid response times towards ammonia and HCl solutions with excellent reproducibility.

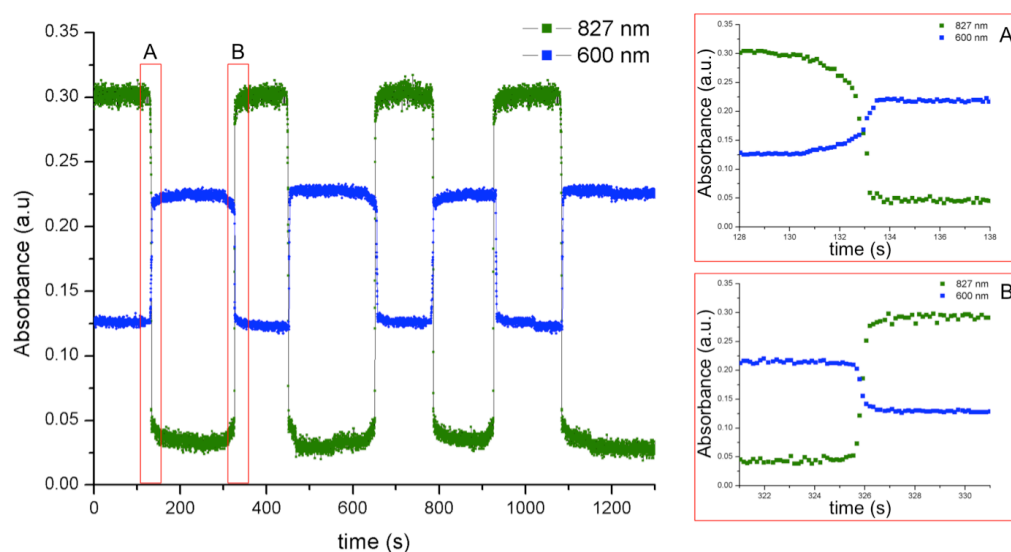


Figure 4.5. Continuous monitoring of the absorbance at 827 nm and 600 nm of the PANi coatings while HCl 10^{-2} M and ammonia (200 ppm) solutions are passed through the PANi coated micro-capillary in continuous flow ($5 \mu\text{L min}^{-1}$). The inset A and B show the response and recovery times of the PANi coatings.

4.3.2 Ammonia Sensing

Different concentrations of aqueous ammonia (from 0.2 ppm - 2000 ppm) were passed through the modified micro-capillary in continuous flow ($5 \mu\text{L min}^{-1}$). The absorbance of the coating was recorded in the interval 300 – 850 nm, using the same methodology presented above, to determine the sensitivity of the PANi coatings to ammonia. Before conducting the experiments, 10^{-2} M hydrochloric acid was passed through the PANi modified micro-capillary to assure the complete doping of the coating. As observed in Figure 4.6, the absorbance intensity of the two absorption bands (350 nm, 600 nm) increases with ammonia concentration. Complete dedoping of the polymeric coating is achieved at 20 ppm ammonia solution, and can be depicted from Figure 4.6 by the disappearance of the absorbance band centered at 420 nm. Moreover, the λ_{max} of the absorbance band, due to the exciton formation in the quinoid rings, shows a gradual shift towards lower wavelength with increasing ammonia concentrations. To further characterise the performance of the polyaniline based micro-capillary sensor towards aqueous ammonia, three sets of aqueous

ammonia solutions (from 0 ppm - 2000 ppm) were passed through the modified micro-capillary in continuous flow ($5 \mu\text{L min}^{-1}$) and this time the absorbance at 600 nm was recorded continuously. The integration time in the Ocean Optics software was set to 1 second and an absorbance reading was recorded every five seconds for three minutes for each of the solutions (see Table A1 – Appendix A). A plot of the absorbance at 600 nm versus concentration of aqueous ammonia is shown in Figure 4.6 - Inset B showing the logarithmic calibration curve. This type of logarithmic response is commonly depicted in the case of ammonia sensors based on polyaniline [28, 31]. However, to further simplify the calibration curve, often in cases of ammonia concentration over a wide range, logarithm of concentration is plotted [28]. In the case of the micro-platform presented here, this approach offers a linear calibration curve ($R^2 = 0.991$) between absorbance at 600 nm and $\log[\text{conc}]$ (Figure 4.6 – Inset B) making the sensor more practical. The limit of detection and limit of quantification were found to be 0.0067 ppm and 0.041 ppm, respectively. The relative standard deviation of the sensor's response lies typically in the range 1-3% over the calibration range. The results indicate that the PANi modified micro-capillary integrated optical sensors could be used for sensing aqueous ammonia over wide concentration range (0.2 – 2000 ppm).

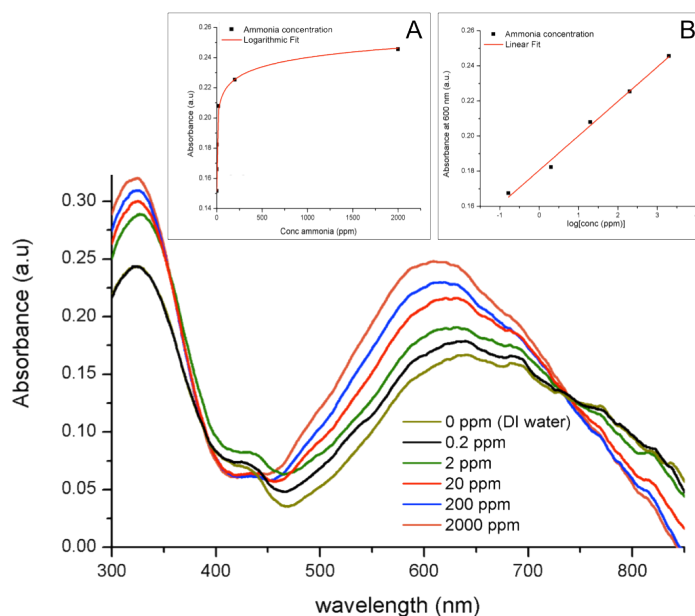


Figure 4.6. Absorbance spectra of the polyaniline coatings exposed to different concentrations of aqueous ammonia. Inset A shows the logarithmic dependency of the absorbance at 600 nm *versus* ammonia concentration. Inset B shows the linear dependency of the absorbance at 600 nm *versus* logarithm of ammonia concentration.

4.4 Conclusions

A micro-capillary integrated optical sensor suitable for the detection of aqueous ammonia has been realised by coating the inner walls of a fused-silica micro-capillary with polyaniline nanofibres. In this approach, the ammonia solution does not need to be pretreated prior entering the micro-capillary, for the incoming optical analysis, as the polymer coating itself acts as the indicator dye. The ability to form nanostructures together with its intrinsically pH-sensitive property makes polyaniline an excellent candidate for the fabrication of optical sensors in the visible-near IR regions, capable for real time continuous-flow measurements of aqueous ammonia. The performance of the PANi modified optical sensor when aqueous ammonia solutions are passed through the micro-capillary in continuous flow, showed that the polyaniline modified micro-capillary optical sensors can operate in a wide range (0.2 – 2000 ppm) of ammonia concentrations. The high surface area of the polymer offers good permeability for the analyte. Very fast response times of less than 5 seconds are achieved. Another distinguishing feature of the PANi-modified micro-capillary optical sensor is the possibility of a fast regeneration process of less than 4 seconds by just pumping hydrochloric acid solutions through the modified micro-capillary. Good reproducibility of the signal was obtained when cycling ammonia and hydrochloric acid solutions, respectively, showing the stability of the polyaniline coating through at least 7 cycles. It was determined that by monitoring the absorbance at 600 nm, the concentration of ammonia can be determined with good linearity. Therefore, we have shown the feasibility of employing polyaniline to develop micro-capillary integrated optical sensors capable of operating in continuous flow mode for the optical detection of aqueous ammonia.

Acknowledgments

The project has been carried out with the support of the Irish Research Council for Science, Engineering and Technology (IRCSET) – Embark Initiative and Science Foundation Ireland under grant 07/CE/I1147 and Science Foundation Ireland under the CLARITY award (07/CE/I1147).

Appendix A. Supplementary Information

Supplementary data associated with this article can be found, in the online version, at <http://dx.doi.org/>

4.5 References

1. Ho, C. K.; Robinson, A.; Miller, D. R.; Davis, M. J., Overview of sensors and needs for environmental monitoring. *Sensors* **2005**, *5*, 4-37.
2. Sequeira, M.; Bowden, M.; Minogue, E.; Diamond, D., Towards autonomous environmental monitoring systems. *Talanta* **2002**, *56*, 355-363.
3. O'Hare, G. M. P.; Diamond, D.; Lau, K. T.; Hayes, J.; Muldoon, C.; O'Grady, M. J.; Tynan, R.; Rancourt, G.; Kolar, H. R.; McCarthy, R. J., The adaptive environment: Delivering the vision of in situ real-time environmental monitoring. *Ibm Journal of Research and Development* **2009**, *53*.
4. Fay, C.; Doherty, A. R.; Beirne, S.; Collins, F.; Foley, C.; Healy, J.; Kiernan, B. M.; Lee, H.; Maher, D.; Orpen, D.; Phelan, T.; Qiu, Z. W.; Zhang, K.; Gurrin, C.; Corcoran, B.; O'Connor, N. E.; Smeaton, A. F.; Diamond, D., Remote Real-Time Monitoring of Subsurface Landfill Gas Migration. *Sensors* **2011**, *11*, 6603-6628.
5. Lechuga, L. M.; Prieto, F.; Calle, A.; Llobera, A.; Dominguez, C., Immunological biosensors based on integrated optical sensors for environmental applications. *Quimica Analitica* **1999**, *18*, 144-146.
6. Lapresta-Fernandez, A.; Capitan-Vallvey, L. F., Environmental monitoring using a conventional photographic digital camera for multianalyte disposable optical sensors. *Analytica Chimica Acta* **2011**, *706*, 328-337.
7. Berna, J.; Leigh, D. A.; Lubomska, M.; Mendoza, S. M.; Perez, E. M.; Rudolf, P.; Teobaldi, G.; Zerbetto, F., Macroscopic transport by synthetic molecular machines. *Nature Materials* **2005**, *4*, 704-710.
8. Morais, I. P. A.; Miro, M.; Manera, M.; Estela, J. M.; Cerda, V.; Souto, M. R. S.; Rangel, A., Flow-through solid-phase based optical sensor for the multisyringe flow injection trace determination of orthophosphate in waters with chemiluminescence detection. *Analytica Chimica Acta* **2004**, *506*, 17-24.
9. Pulido-Tofino, P.; Barrero-Moreno, J. M.; Perez-Conde, M. C., A flow-through fluorescent sensor to determine Fe(III) and total inorganic iron. *Talanta* **2000**, *51*, 537-545.
10. Taurozzi, J. S.; Tarabara, V. V., Silver nanoparticle arrays on track etch membrane support as flow-through optical sensors for water quality control. *Environmental Engineering Science* **2007**, *24*, 122-137.
11. Perez-Palacios, D.; Armenta, S.; Lendl, B., Flow-Through Fourier Transform Infrared Sensor for Total Hydrocarbons Determination in Water. *Applied Spectroscopy* **2009**, *63*, 1015-1021.
12. Mehta, A.; Shekhar, H.; Hyun, S. H.; Hong, S.; Cho, H. J., A micromachined electrochemical sensor for free chlorine monitoring in drinking water. *Water Science and Technology* **2006**, *53*, 403-410.
13. Valcarcel, M.; Decastro, M. D. L., Flow-through (bio)chemical sensors - Plenary lecture. *Analyst* **1993**, *118*, 593-600.
14. Kuswandi, B.; Narayanaswamy, R., Capillary optode: Determination of mercury(II) in aqueous solution. *Analytical Letters* **1999**, *32*, 649-664.

15. Borecki, M.; Korwin-Pawłowski, M. L.; Beblowska, M.; Szmidt, J.; Jakubowski, A., Optoelectronic Capillary Sensors in Microfluidic and Point-of-Care Instrumentation. *Sensors* **2010**, *10*, 3771-3797.
16. McCurley, M. F., An optical biosensor using a fluorescent, swelling sensing element. *Biosensors & Bioelectronics* **1994**, *9*, 527-533.
17. Florea, L.; Hennart, A.; Diamond, D.; Benito--Lopez, F., Synthesis and characterisation of spiropyran-polymer brushes in micro-capillaries: Towards an integrated optical sensor for continuous flow analysis. *Sensors and Actuators B: Chemical* **2011**.
18. Weigl, B. H.; Wolfbeis, O. S., Capillary optical sensors. *Analytical Chemistry* **1994**, *66*, 3323-3327.
19. Florea, L.; Benito-Lopez, F.; Hennart, A.; Diamond, D., Photo-detection of solvent polarities using non--invasive coatings in capillaries. *Procedia Engineering* **2011**, *25*, 1545 – 1548.
20. Epstein, A. J.; Ginder, J. M.; Zuo, F.; Bigelow, R. W.; Woo, H. S.; Tanner, D. B.; Richter, A. F.; Huang, W. S.; Macdiarmid, A. G., Insulator-to-metal transition in polyaniline. *Synthetic Metals* **1987**, *18*, 303-309.
21. Genies, E. M.; Boyle, A.; Lapkowski, M.; Tsintavis, C., Polyaniline - a historical survey. *Synthetic Metals* **1990**, *36*, 139-182.
22. Huang, J. X., Syntheses and applications of conducting polymer polyaniline nanofibers. *Pure and Applied Chemistry* **2006**, *78*, 15-27.
23. Wallace, G. G.; Spinks, G. M.; Kane-Maguire, L. A. P.; Teasdale, P. R., *Conductive electroactive polymers*. CRC Press LLC: 2003.
24. Asijati, E. K., B.; Arifah, N.F.; Kurniawati, Y.I.; Gani, A.A.; , Non-invasive optical chemical sensor based on polyaniline films for detection of ammonia and acetic acid solutions. *Sensors and the International Conference on new Techniques in Pharmaceutical and Biomedical Research, 2005 Asian Conference on* **2005**, 111 - 114.
25. Crowley, K.; O'Malley, E.; Morrin, A.; Smyth, M. R.; Killard, A. J., An aqueous ammonia sensor based on an inkjet-printed polyaniline nanoparticle-modified electrode. *Analyst* **2008**, *133*, 391-399.
26. Manigandan, S.; Jain, A.; Majumder, S.; Ganguly, S.; Kargupta, K., Formation of nanorods and nanoparticles of polyaniline using Langmuir Blodgett technique: Performance study for ammonia sensor. *Sensors and Actuators B-Chemical* **2008**, *133*, 187-194.
27. Stamenov, P.; Madathil, R.; Coey, J. M. D., Dynamic response of ammonia sensors constructed from polyaniline nanofibre films with varying morphology. *Sensors and Actuators B-Chemical* **2012**, *161*, 989-999.
28. Kebiche, H.; Debarnot, D.; Merzouki, A.; Poncin-Epaillard, F.; Haddaoui, N., Relationship between ammonia sensing properties of polyaniline nanostructures and their deposition and synthesis methods. *Analytica Chimica Acta* **2012**, *737*, 64-71.
29. He, L.; Jia, Y.; Meng, F.; Li, M.; Liu, J., Gas sensors for ammonia detection based on polyaniline-coated multi-wall carbon nanotubes. *Materials Science and Engineering: B* **2009**, *163*, 76-81.
30. Blighe, F. M.; Diamond, D.; Coleman, J. N.; Lahiff, E., Increased response/recovery lifetimes and reinforcement of polyaniline nanofiber films using carbon nanotubes. *Carbon* **2012**, *50*, 1447-1454.
31. Castrellon-Urbe, J.; Nicho, M. E.; Reyes-Merino, G., Remote optical detection of low concentrations of aqueous ammonia employing conductive polymers of polyaniline. *Sensors and Actuators B-Chemical* **2009**, *141*, 40-44.
32. Huang, J.; Virji, S.; Weiller, B. H.; Kaner, R. B., Nanostructured polyaniline sensors. *Chemistry-a European Journal* **2004**, *10*, 1315-1319.
33. Virji, S.; Fowler, J. D.; Baker, C. O.; Huang, J. X.; Kaner, R. B.; Weiller, B. H., Polyaniline manofiber composites with metal salts: Chemical sensors for hydrogen sulfide. *Small* **2005**, *1*, 624-627.

34. Huang, J. X.; Virji, S.; Weiller, B. H.; Kaner, R. B., Polyaniline nanofibers: Facile synthesis and chemical sensors. *Journal of the American Chemical Society* **2003**, *125*, 314-315.
35. Berrada, K.; Quillard, S.; Louarn, G.; Lefrant, S., Polyanilines and substituted polyanilines - A comparative-study of the Raman-spectra of leucoemeraldine, emeraldine and pernigraniline. *Synthetic Metals* **1995**, *69*, 201-204.
36. Bartonek, M.; Sariciftci, N. S.; Kuzmany, H., Resonance Raman-spectroscopy of the emeraldine insulator-to-metal phase-transition. *Synthetic Metals* **1990**, *36*, 83-93.
37. Hugotlegoff, A.; Bernard, M. C., Protonation and oxidation processes in polyaniline thin-films studied by optical multichannel analysis and in-situ Raman-spectroscopy. *Synthetic Metals* **1993**, *60*, 115-131.
38. Furukawa, Y.; Hara, T.; Hyodo, Y.; Harada, I., Vibrational-spectra of polyaniline and its N-15-substituted and H-2-substituted derivatives in as-polymerized, alkali-treated and reduced states. *Synthetic Metals* **1986**, *16*, 189-198.
39. Laska, J.; Girault, R.; Quillard, S.; Louarn, G.; Pron, A.; Lefrant, S., Raman spectroscopic studies of polyaniline protonation with bis(2-ethylhexyl) hydrogen phosphate. *Synthetic Metals* **1995**, *75*, 69-74.
40. Lindfors, T.; Ivaska, A., Raman based pH measurements with polyaniline. *Journal of Electroanalytical Chemistry* **2005**, *580*, 320-329.
41. Liu, C.; Zhang, J. X.; Shi, G. Q.; Chen, F. E., Doping level change of polyaniline film during its electrochemical growth process. *Journal of Applied Polymer Science* **2004**, *92*, 171-177.
42. Mazeikiene, R.; Statino, A.; Kuodis, Z.; Niaura, G.; Malinauskas, A., In situ Raman spectroelectrochemical study of self-doped polyaniline degradation kinetics. *Electrochemistry Communications* **2006**, *8*, 1082-1086.
43. Chen, S. A.; Hwang, G. W., Water-soluble self-acid-doped conducting polyaniline - Structure and properties. *Journal of the American Chemical Society* **1995**, *117*, 10055-10062.
44. Chiang, J. C.; Macdiarmid, A. G., Polyaniline - Protonic acid doping of the emeraldine form to the metallic regime. *Synthetic Metals* **1986**, *13*, 193-205.
45. Barta, P.; Kugler, T.; Salaneck, W. R.; Monkman, A. P.; Libert, J.; Lazzaroni, R.; Bredas, J. L., Electronic structure of emeraldine and pernigraniline base: a joint theoretical and experimental study. *Synthetic Metals* **1998**, *93*, 83-87.
46. de Oliveira, Z. T.; dos Santos, M. C., Semi-empirical study of chain conformation and absorption spectra of polyanilines: size, solvent and disorder effects. *Chemical Physics* **2000**, *260*, 95-103.

Chapter 5

Dynamic pH mapping in micro-fluidic devices by integrating adaptive coatings based on polyaniline with colorimetric imaging techniques

Larisa Florea ¹, Cormac Fay ¹, Emer Lahiff ¹, Thomas Phelan ¹, Noel E.
O'Connor ¹, Brian Corcoran ¹, Dermot Diamond ¹
and Fernando Benito-Lopez ^{1, 2, *}

Lab on a Chip 13 (2013) 1079-1085

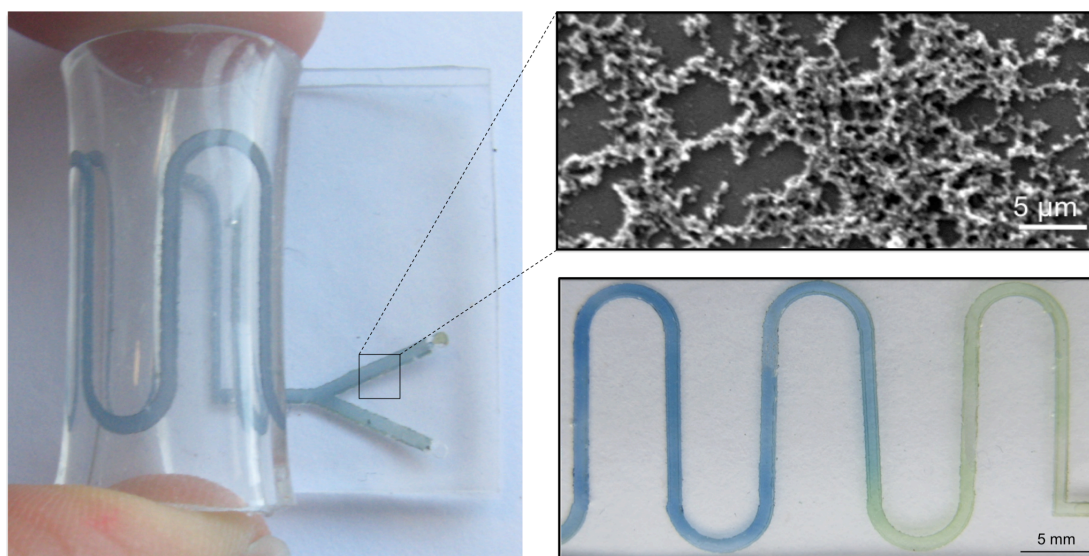
ISSN: 1473-0197; <http://dx.doi.org/10.1039/C2LC41065F>

¹CLARITY: Centre for Sensor Web Technologies, National Centre for Sensor Research, School of Chemical Sciences, Dublin City University, Dublin, Ireland;

²CIC microGUNE, Arrasate-Mondragón, SPAIN

*Author to whom correspondence should be addressed;

Abstract: In this chapter we present a micro-fluidic device that has integrated pH optical sensing capabilities based on polyaniline. The optical properties of polyaniline coatings change in response to the pH of the solution that is flushed inside the micro-channel offering the possibility of monitoring pH in continuous flow over a wide pH range throughout the entire channel length. This work also features an innovative detection system for spatial localisation of chemical pH gradients along micro-fluidic channels through the use of a low cost optical device. Specifically, the use of a micro-fluidic channel coated with polyaniline is shown to respond colorimetrically to pH and that effect is detected by the detection system, even when pH gradients are induced within the channel. This study explores the capability of detecting this gradient by means of imaging techniques and the mapping of the camera's response to its corresponding pH after a successful calibration process. The provision of an inherently responsive channel means that changes in the pH of a sample moving through the system can be detected dynamically using digital imaging along the entire channel length in real time, without the need to add reagents to the sample. This approach is generic and can be applied to other chemically responsive coatings immobilised on micro-channels.



5.1 Introduction

Conventional glass-type electrodes have been widely used for pH measures for many years in both industry and academic areas. However, in terms of specific applications (*e.g.* in vivo, food industry, or for clinical applications), they possess several disadvantages due to their size constraints, rigidity, and the inflexibility of the glass electrode. In recent years, a wide number of pH sensors have been developed to overcome these limitations, including ion sensitive field-effect transistor (iSFET) pH sensors [1-4], optical pH sensors based on pH responsive dyes [5-8], hydrogel film pH sensors [9, 10], and solid-state metal oxides pH sensors [11-13]. In particular, optical pH sensors present several advantages over the traditional pH electrodes as such their low costs, immunity from electromagnetic field, absence of electric contacts, possibility of reference electrode removal and a high degree of miniaturisation [14]. Optical fiber-based pH sensors have been particularly popular, as the fibre allows the optical signal to be transported over long distances, which can facilitate applications in remote sensing [15].

Usually, these optical pH sensors (or optrodes) employ a dye or an indicator that requires immobilisation onto a solid support material. There are several critical issues related to this approach: firstly, the dye should retain its optical properties after the immobilisation process [16] and secondly, it should not leach into the solution [17]. A third issue of practical importance is their inherently narrow dynamic response range which is usually around 3-4 pH-units centred on the dye's pKa [18].

Therefore, the further improvement of such sensors focuses on the search for new materials that can overcome these issues. An alternative approach is to use the inherent optical response of certain polymers like the conducting polymer polyaniline (PAni) rather than a conventional pH-sensitive dye. PAni displays striking changes in the visible/NIR spectrum upon proton-mediated doping-dedoping of the polymer backbone, thus offering the possibility of developing optical sensors with extended pH ranges. The polymer itself, therefore, acts as both the matrix support and the indicator dye. In this way, leaching is prevented, thereby enhancing the long-term stability and reproducibility.

PAni is an excellent candidate for the fabrication of optical sensors in the visible-near IR detection since it is an intrinsically pH-sensitive polymer with good environmental stability [19, 20]. Furthermore, by focusing on PAni nanofibres we can dramatically increase the surface area of the material [21], which in turn can manifest in improved response times and sensitivity.

A relatively new and promising approach to produce sensors of this kind involves optofluidics wherein optical and fluidic functionalities are integrated at the micro- and nano-scale to leverage their combined advantages by functionalising the inner walls of a micro-channel with a responsive material [22, 23]. For example, functionalisation with antibodies for flow-through cell separation have been reported [24], as have florescent dyes for optical sensing of acidity [25] and monolayers that exhibit metal ion sensing properties [26, 27].

Nowadays, a wide variety of detectors can be employed to transduce the colorimetric analytical signal, such as light dependent resistors [28, 29], photodiodes [30-32], phototransistors [33-35] and even reverse-biased LEDs [36-38]. More specific to this study is the use of digital imaging cameras for the detection of colorimetric reactions. Up to now, almost all of the studies carried out have been based on the RGB colour model, probably because this is readily accessible via a number of popular image processing packages [39-43]. The major challenge with this approach is that the RGB colour space is inherently sensitive to changes in ambient lighting, and measurements therefore have to be made under strictly controlled light conditions. Recently, studies such as those by *Fay et al.* [44] (qualitatively) and *Cantrell et al.* [45] (quantitatively) explored the use of a different colour model (HSV) for colorimetric chemical analysis which has shown to be more tolerant of ambient light variations [46].

Based on this concept, we present an innovative, robust, simple and fast method to measure pH simultaneously at all locations across an entire micro-fluidic system using polyaniline nanofibres modified micro-channel coupled with HSV-based digital image color analysis.

5.2 Experimental

5.2.1 *Micro-fluidic Device Fabrication*

The fabrication of the master mold was carried out using a laser ablation system-excimer/CO₂ laser (Optec Laser Micro-machining Systems, Belgium) by cutting the micro-fluidic structures in a 50 μm double-sided pressure sensitive adhesive film, PSA, (AR8890, Adhesives Research, Ireland) and pasting one of the PSA sides to a petri dish [47].

For PDMS casting, the precursor was prepared by mixing PDMS elastomer with the curing agent from Sylgard 184 kit at a weight ratio of 10:1, poured onto a master mould, and cured in an oven at 80 °C for 2 h. Following curing, the PDMS layer is peeled from the master. The inlets and outlets (800 μm in diameter) were made using a manual puncher (Technical Innovations, Inc., Brazoria, TX). The PDMS replica (~ 1 mm height) was thoroughly washed with isopropanol and exposed to oxygen plasma to seal the chip to a clean glass slide (35 mm x 64 mm, Agar Scientific Limited, England) or another flat PDMS layer (~ 2 mm height). Silicon tubes were employed to further connect the main inlets with a syringe pump (PHD 2000 Syringe, Harvard Apparatus) for sample delivery and washing.

5.2.2 *Micro-fluidic Device Functionalisation*

The functionalisation of the inner walls of the micro-fluidic channel with PANi nanofibres was achieved using the procedure described in Figure 5.1. The detailed micro-channel functionalisation process and the corresponding characterisation of the coating are listed in the Appendix B. Briefly, immediately after exposure of the PDMS chips to oxygen plasma for 60 s (Harrick Plasma) and sealing to the glass slide/PDMS layer, the activated channels (1000 \times 100 μm) were flushed with a 20 % wt solution of *N*-[3- (trimethoxysilyl) propyl]aniline in ethanol for 60 min at a flow rate of 0.5 $\mu\text{L min}^{-1}$. Using this technique, a monolayer of silane-bearing aniline was formed on the substrate via molecular self-assembly. Chemical deposition of the

PAni on the modified micro-channel walls was performed by filling the micro-channel with freshly prepared 1 M HCl solution containing the oxidant (ammonium peroxydisulfate) and aniline in a molar ratio of 0.25:1. This molar ratio was chosen as it has been previously shown that polymerisation of aniline in these experimental conditions produces nanofibres [48]. The pendant aniline on the surface served as an initiation site for polymerisation and was also used to covalently anchor the PAni chain on the substrate [49]. The polymerisation time was fixed to 20 h. After polymerisation, the channels were washed extensively with water to remove any unattached polyaniline nanofibres. The resulting films had good adhesion due to the chemical bonding between the substrate and polymer film. Homogeneous PAni coatings were obtained, covalently attached to the internal walls of micro-channels made of PDMS/PDMS or PDMS/glass, see Figure 5.2.

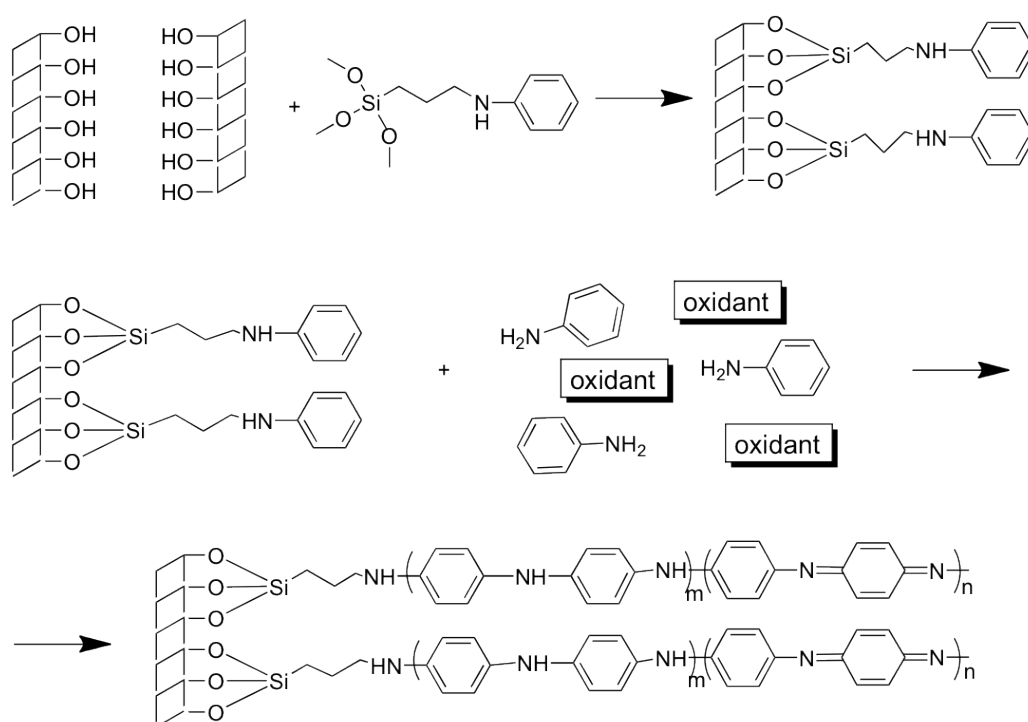


Figure 5.1. Chemical functionalisation of micro-channel surface with polyaniline chains.

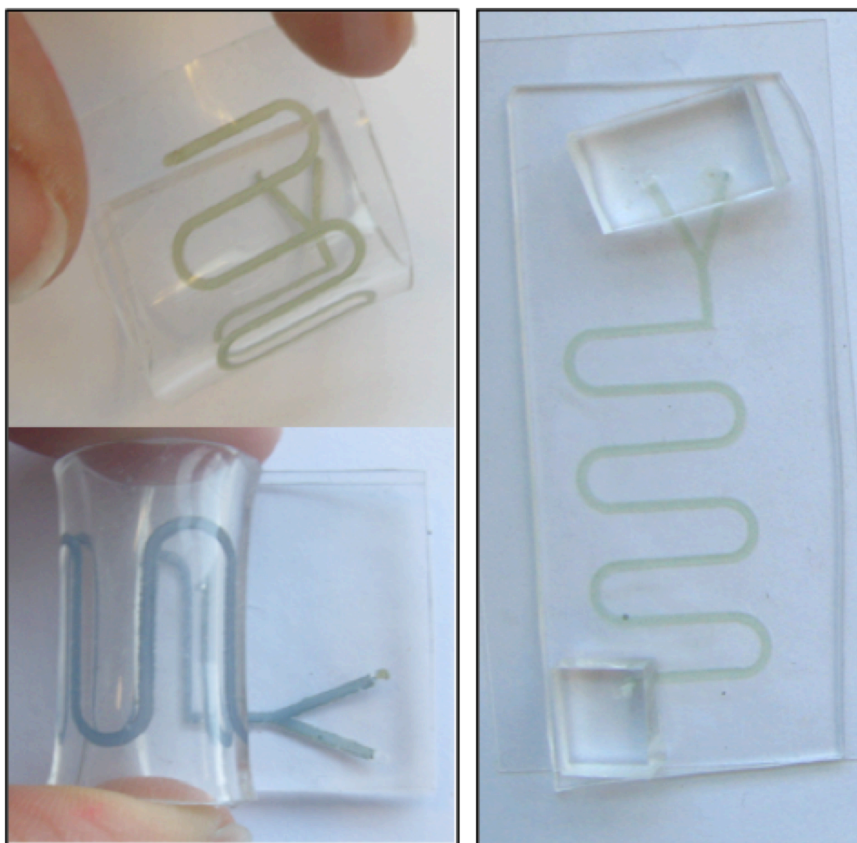


Figure 5.2. Pictures of polyaniline functionalised PDMS/PDMS (left), acidic on the top and basic on the bottom, and glass/PDMS (right) micro-fluidic devices. The picture on the right shows the PDMS extensions that were attached to the PDMS layer by oxygen plasma. These extensions were configured to secure the connections between the silicon tubes and the inlets of the micro-channel and to facilitate sample delivery.

5.2.3 Measurement of Absorbance Spectra of PAni Coatings

Changes in the absorbance spectra of the PAni coatings as different pH solutions flushed inside the micro-channel were recorded using two fiber-optic light guides connected to a Miniature Fiber Optic Spectrometer (USB4000 - Ocean Optics) and aligned using an in-house made holder. The in-house-designed holder was fabricated using a three-dimensional space (3D) printer (Dimension SST 768) in black acrylonitrile butadiene styrene co-polymer (ABS) plastic in order to minimise interferences from ambient light. The two parts of the holder (2 identical parts, one to be placed on top of the micro-fluidic chip, the other underneath) were designed using

ProEngineer CAD/CAM software package and fixed together with screws ensuring precise alignment between the two fiber-optics (appendix B, Fig. B1).

The Absorbance spectra recorded with Miniature Fiber Optic Spectrometer (USB4000). For clarity, all absorbance spectra recorded were smoothed using Origin software using Savitzky-Golay algorithm.

5.2.4 Digital Image Capture

After the fabrication of the flow channels and subsequent analysis using reference instrumentation (spectrophotometer) the channels were then subjected to analysis via digital imaging techniques. The channel was placed within the field of view of a standard colour camera (Panasonic DMC-FZ38) along with a white background for subsequent image processing. An XRite professional colour reference chart was also placed within the camera's field of view (see Appendix B - Figure B2) as this experiment was performed under variable ambient lighting conditions.

Solutions of known pH produced by mixing appropriate amounts of hydrochloric acid or sodium hydroxide (pH 2 to 12) were then flushed through the micro-channel at a flow rate of $50 \mu\text{L min}^{-1}$. At each pH unit step, an image was captured using the colour camera. This process was repeated and multiple images gathered at each unit step to investigate reproducibility.

An additional set of images were similarly captured, in which the flow channel was first filled with a solution of pH 3 and then a droplet of pH 6.5 aqueous solution placed at the opposite inlet where it was encouraged along the micro-channel via an applied negative pressure using a microsyringe. This generated a pH gradient inside the micro-channel along the channel's length. Therefore, the channel showed two extreme colours at either end coupled with a colour gradient connecting them. The ability to detect this pH gradient point through image processing and analysis was then investigated.

5.2.5 Image Processing

A number of image processing steps were employed in order to analyse the overall channel pH for the calibration procedure, and subsequently additional steps were undertaken to detect the pH gradient along the channel. After capturing an image (see Appendix B - Figure B2 left) a segmentation process identified regions of interest from background areas (see appendix B - Figure B2 right). The regions were identified based on their spatial coordinates and were matched between progressive calibration images on this basis. The average Hue component of each region was taken to represent the colour of the channel and reference patches, which were then used for normalisation, and later to generate a calibration plot. Following this, a similar approach was employed to analyse the pH gradient along the channel in which the pH analysis was localised at every point along the channel. A more detailed account of these processing steps can be found in Appendix B (Figure B2 and B3).

5.3 Results and Discussion

5.3.1 Characterisation of the PAni Coatings

The PAni coatings were characterised by Raman spectroscopy as it permits in situ analysis [50] of PAni coating inside the micro-channel (see Appendix B - Figure B4). Raman spectroscopy showed that PAni is obtained in its half-oxidised emeraldine state [51]. In addition, Raman spectroscopy was also employed to study the changes in the bonding structure of the coatings upon doping-dedoping, as very distinct signature bands appear for the quinoid and benzenoid rings, respectively [52, 53]. When a solution of pH 2 is passed through the micro-channel, PAni presents the typical bands for the emeraldine salt (ES). When a solution of pH 12 is flushed through the micro-channel, the ES bands decrease and the specific quinoid ring bands appear in the spectra, reflecting the dedoped state – emeraldine base (EB).

Scanning electron microscope (SEM) images showed that using the polymerisation technique described in the experimental section, PANi nanofibres were obtained, covalently attached to the inner walls of the micro-channels, (Figure 5.3). The immediate advantages of having nanofibres (*versus* bulk PANi) are the high surface area that is exposed to the target molecules and the very short diffusional path lengths [54] which produces enhanced sensitivity coupled with fast response times [21, 55, 56].

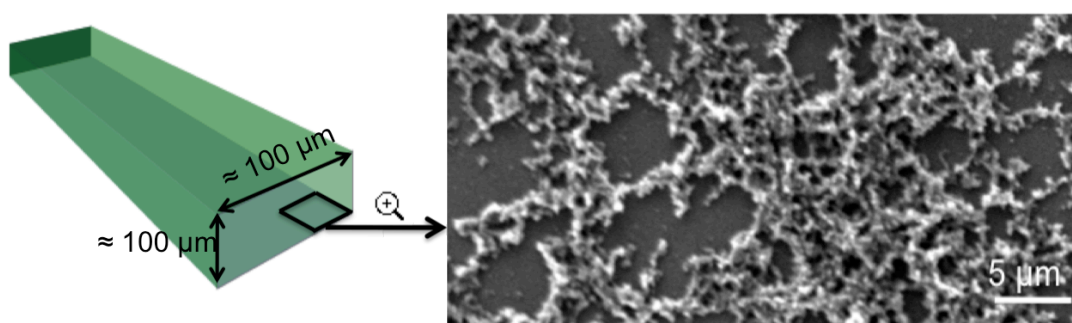


Figure 5.3. Representation of the polyaniline functionalised micro-channel (left). SEM image of the polyaniline functionalised glass bottom layer showing a homogeneously covered surface with polyaniline nanofibres (right).

5.3.2 *pH Measurements*

Polyaniline's sensitivity towards pH has been extensively used in recent years for the development of pH sensors due to its intrinsic doping-dedoping pH response [57, 58]. However, to the best of our knowledge this is the first example of the use of polyaniline nanofibres as a pH optical sensor in a micro-fluidic device, wherein the whole inner wall of the micro-channel acts as a sensor enabling the pH to be measured simultaneously at all points within the channel.

The reversible protonation/deprotonation reaction of PANi is of particular interest during the development of the pH sensor. The process occurs on the imine nitrogen atoms as shown in Appendix B - Figure B5. The transformation of Emeraldine Salt (ES) to Emeraldine Base (EB) by deprotonation is accompanied by significant changes in colour. This phenomenon is observed in the case of the PANi

coatings when colourless solutions of at varying pH are passed through the micro-channel, showing the ability of the covalently bonded PANi nanofibres to rapidly respond to changes in their environment (see Appendix B - Figure B5).

The changes in the absorbance spectra of the PANi coatings in response to different pH solutions flushed inside the micro-channel were recorded using two fiber-optic light guides connected to a Miniature Fiber Optic Spectrometer and aligned using an in-house made cell.

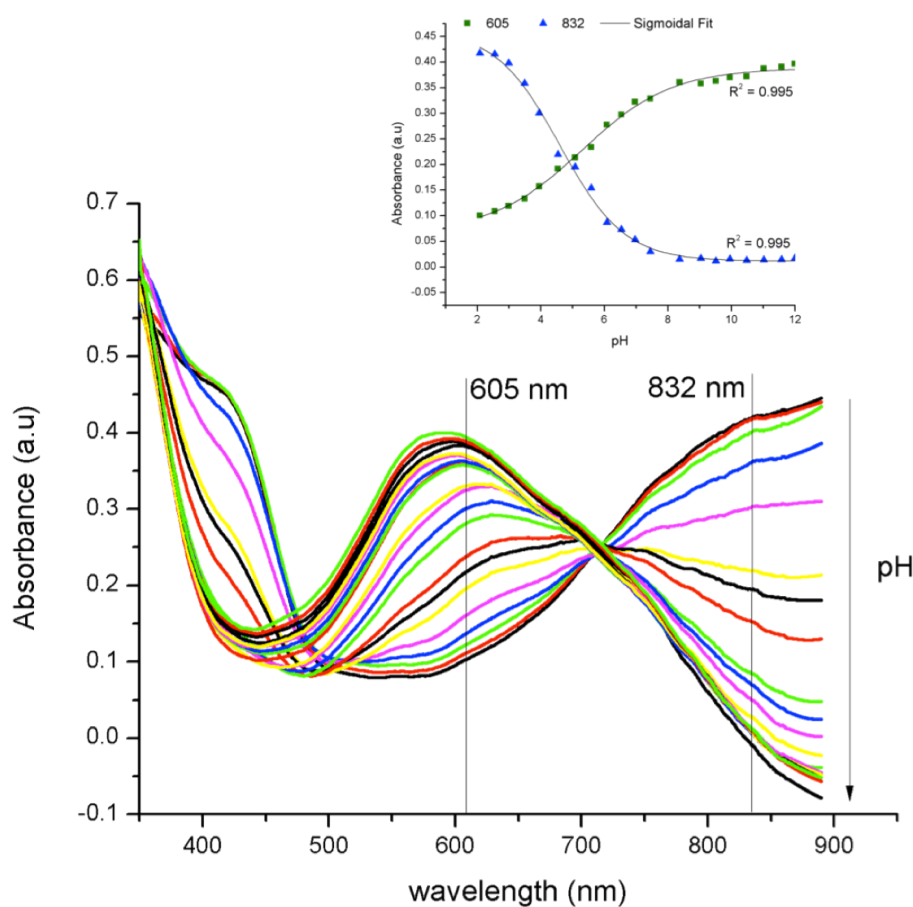


Figure 5.4. Absorbance spectra of the polyaniline coatings in the channel when solutions at different pH are passed through (pH 2-12). Inset - Graph of the absorbance change of polyaniline coatings vs. pH at 605 nm and 832 nm.

The UV–VIS absorption spectra of PANi films were measured for each pH solution passed through the channel at a flow rate of $50 \mu\text{L min}^{-1}$, see Figure 5.4. It is important to note that the absorbance spectrum changes very rapidly after the solution reaches the detection area (approx. 2 s), thereby ensuring a very fast

response of the device (see ESI† - videos 1 and 2). Moreover, the signal remains stable during the timescale of the experiment, which was set to 5 minutes. The measurements were done in triplicates with a standard deviation of the absorbance value over the calibration range of 0.001.

As depicted in Figure 5.4 the spectrum of the PANi coatings is highly pH dependent and changes in colour from the green (ES) to blue (EB). Increasing the pH from 2 to 12 leads to a shift in the absorption λ_{max} of PANi in the visible region from 420 nm (at pH 2) to 605 nm (at pH 12). This shift is due to doping–dedoping of PANi coatings and can be explained by the different degree of protonation of the imine nitrogen atoms in the polymer chain [59]. More specifically, in a low pH environment, PANi exhibits strong absorbances at approximately 420 nm and 830 nm assigned to polaron and bipolaron transitions. Upon dedoping these transitions disappear and a new absorbance band appears at approximately 600 nm. This new band is ascribed to the exciton formation in the quinonoid rings [60] and it is responsible for the blue colour of the PANi coatings. The pH dependence of the absorptions at 605 nm and 832 nm were plotted in Figure 5.4 – Inset. The characteristic PANi sigmoid shape curve ($R^2 = 0.996$) was obtained for the absorbance change *versus* pH, similar to the previous reported results in the case of PANi [19, 51]. The curve is broad, ensuring that the pH dependence of the PANi occurs over a wide range of pH. Therefore, this type of coating can be used for pH sensing across a reasonably broad range, constituting an important advantage over common pH indicator dyes. Since PANi does not fit the expected response curve for an indicator, because of its broad range, the Henderson-Hasselbach equation cannot be applied⁷. In the literature, there have been attempts to introduce an adjusted exponent to fit PANi doping- dedoping behaviour using Henderson-Hasselbach equation, although these attempts were proven to be unsuccessful [58]. Therefore, only an apparent pK_a value can be used to describe the sensor response. As depicted from Figure 5.4 – Inset, the apparent pK_a value of PANi coatings is approximately 5, representing the pH value where the two sigmoidals intersect (concentration of ES is approximately equal with the concentration of EB). Most probably this value represents a distribution of pK_a 's of PANi units with differing chain length and local environments [57]. Nevertheless, since important changes in λ_{max} and absorbance were observed in the pH range from 2 to 8, it should be possible to use these PANi

coated micro-channels for monitoring the pH of, for instance, physiological fluids (gastric juice, saliva, blood) which are important applications for micro-fluidics at this time.

5.3.3 pH Determination via Colorimetric Imaging Analysis

It has been shown that the channels respond accurately to changes in pH when analysed using a spectrophotometer. However, this work also explored the possibility of performing colorimetric analysis without the need for specialised instrumentation *i.e.* through the use of a standard digital colour camera. This has the potential to extend the applicability of the sensor, for instance, to point of care micro-fluidic devices and to low cost diagnostics for the developing world using mobile phones with integrated digital cameras to capture analytical information [61]. The steps taken to extract colorimetric information from the captured images are outlined in detail in the Appendix B.

Processing of the images began with the application of a white balance algorithm. This was possible as the image setting/scene was relatively similar in each case, and included a white region specifically for this purpose. As this study took place in an ambient lighting environment, normalisation of the images in this way was necessary to compensate for shifts in ambient light intensity. For further robustness, the Hue value representing the colour of the channel underwent a colour normalisation process using two of the array of invariant reference patches (*i.e.* the purple and yellow patches as presented in Figure B2). Next, the average and standard deviation of the channel's normalised Hue value across each of the captured images at corresponding pH unit steps were calculated ($RSD \leq 2.06\%$). Following this, a calibration plot of the camera's response to different pH solutions was achieved and a sigmoidal model was applied to the data points, see Appendix B - Figure B6. It can be seen from the figure that an excellent fit was achieved ($R^2 = 0.998$, $n = 18$) and subsequently, the resulting mathematical model was used to map the camera response to pH concentration values for gradient analysis.

While spectrophotometer and the camera generate the pH estimations on the basis of 'colour' measurements, the way in which this is achieved is different for

both devices. The spectrophotometer can generate a calibration plot at any effective wavelength (*i.e.* regions of the absorbance spectrum of the dye that change with pH) within its measurement range. For this study, the most dominant peak changes were selected; 605 nm and 832 nm, see Figure 5.4. In contrast, the camera measures colour across the entire available spectrum, and wavelength specific measurements are not possible except through the rather crude RGB division of the spectrum into three ‘Red’, Green’ and ‘Blue’ (RGB) channels. When conversion into the HSV colour space is applied, the H (Hue) component quantitatively represents the most dominant ‘colour’ based on the transformation from the captured RGB data to the target HSV colour space[46], see Figure B6.

Although, individually, each approach generated good quality fits to the calibration data, it was important to establish whether a correlation existed between both detection methods. One way of achieving this was to compare the predicted pH at each unit using the derived mathematical regression models. Figure B7 presents a plot of the predicted pH using the camera model against the UV-vis model at 832 nm. Clearly, a linear correlation exists when comparing both approaches with a good fit resulting ($R^2 = 0.98$, $n = 18$). Moreover, the difference in slope between this linear fit and the ideal slope (slope = 1) is relatively small at 0.021, suggesting there is little bias or skewness between the two data sets. The correlation between the camera and the UV-Vis model at 605 nm was also investigated. Similar accuracies were achieved with $R^2 = 0.98$ and a difference to the ideal slope of 0.025. From Figure B7 it can be seen that the goodness of fit of the correlation decreases above c.a. pH 7. This arises from the increasingly small absorbance (colour changes) occurring above this value, see Figure 5.4 (inset). Despite this, it is interesting to note that the camera and the spectrometer data remain reasonably well correlated above pH 7, although the scatter is understandably greater, see Appendix B - Figure B7.

5.3.4 Gradient pH Measurements

The main advantage of the digital camera over the spectrometer lies in its ability to rapidly generate spatially distributed information. This should enable the camera to dynamically track changes in pH along the entire length of the fluidic channel. To test this thesis, the micro-channel was filled with a pH 3 solution and a second

solution of pH 6.5 was introduced at one end, as described in the experimental section and appendix B. The solutions were allowed to diffuse until a pH gradient visually appeared whereupon an image was captured (Figure 5.5).

Following the image processing and data extraction as described above, the images were white balanced and the Hue values at each localised point normalised with respect to the colour reference patches, as described previously for the calibration process. Using the calibration model derived from the sigmoidal regression analysis, the localised Hue values were mapped to their corresponding pH concentrations and a plot of pH concentration over the length of the channel was derived. To reduce noise, a smoothing algorithm based on the Savitzky-Golay filter [62] was applied to the data set. For both Figure 5.5b and Figure 5.5c, labels are present to denote discrete points along the flow path *i.e.* points of maximum curvature along the four considered flow bends.

It can be seen visually from Figure 5.5b that the pH varies significantly between points '2' and '3' as reflected in the colour gradient. Correspondingly, the analysis presented (Figure 5.5c) shows a dramatic change in pH from *ca.* pH 3 at '2' to *ca.* pH 6.5 at, and beyond, point '3'. Figure 5.5c shows the resulting pH gradient as estimated by processing the colour image with the digital camera algorithm. Close examination of the image reveals the presence of small bubbles, which manifest as slight inconsistencies in the unsmoothed pH data in Figure 5.5c.

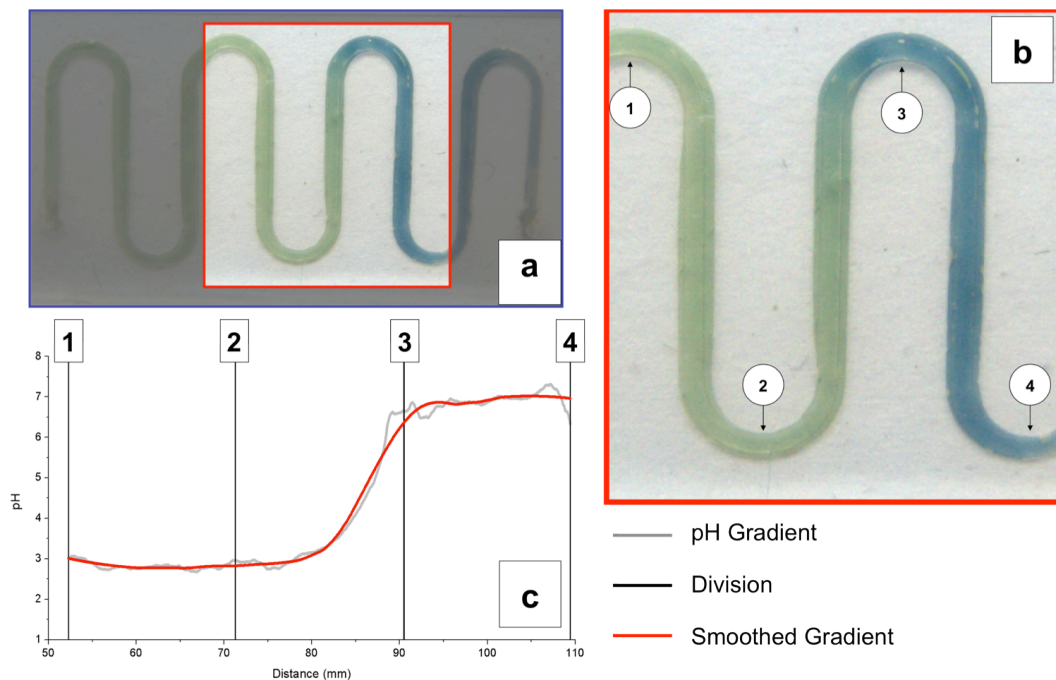


Figure 5.5. (a) Images showing a pH gradient along the micro-fluidic channel reflected in the changing colour of the PAni coating, red box shows a magnified section in (b), which also identifies specific locations (1-4) highlighted in (c), Plot of the pH gradient along the flow channel generated from the image. The grey line is the raw data from the analysis; the red line has been smoothed using the Savitsky-Golay algorithm.

To demonstrate the capabilities of the digital imaging approach, changes in the pH along the entire channel were tracked using low-cost digital video imaging, see supplementary information (ESI† – Video 3). In this example, the image section under analysis is bounded by a red square and also enlarged (shown in the top left corner). In addition, a dynamic plot is presented on the right hand side of the video showing the change in pH along the channel. Although the data in Figure 5.5a and ESI† – Video 3 represents the pH dynamics of the channel at a single point in time, this process can be easily expanded to enable pH variations to be tracked dynamically along the entire micro-fluidic system as a function of time.

This capability could have a substantial impact in many areas. For instance, a number of chemical reactions are time critical and require precision when introducing a reagent. By coupling a micro-fluidic system, PAni and a low cost colour camera, a miniaturised and cost effective solution can be achieved for many chemical and biochemical sensing scenarios that rely on a localised pH to drive the reaction. The speciation state of multi-basic acids, or of amino acids could be inferred from knowledge of pH gradients. Mixing processes involving buffers could be tracked to identify locations of optimum pH for particular processes, and to explore how these locations can be moved, expanded or contracted prior to addition of active reagents. Furthermore, the rapid improvement in price-performance in digital photography through the development of sophisticated, miniaturised and low cost CCD sensors [63-65] and its increasing integration with mobile phones, provides a powerful technology platform for many new applications. However, while tremendous potential impact of integration of chemical/biological measurements with digital imaging and communications is compelling, for example, in tele-health and personal (point-of-need) diagnostics, the route to winning applications is not clear. Hence, companies like Nokia are sponsoring global competitions with very significant prizes to generate ideas from which they will select the best possible

candidate applications [66]. This activity emphasises the rising importance of applying digital imaging to analytical measurements.

5.4 Conclusions

A new, simple, and fast photometric method to measure pH using PANi based coatings in micro-fluidic devices is presented. pH measurements were performed in continuous flow mode using fiber-optic light guides aligned to the device using an in-house made cell. The main advantage of these sensors is that no reagent indicator is needed to measure the pH, because the PANi acts as the indicator itself, reducing the complexity of pH detection inside micro-channels. The functionalisation process is easy and highly reproducible from microdevice to microdevice and over the whole micro-channel length. Moreover, it can be easily achieved using different materials as such glass, PDMS or any other material that allows the introduction of hydroxyl groups on the surface, necessary for the present silanisation procedure. Although the time for functionalisation is rather long (~ 22 h), the polyaniline functionalised micro-channels are suitable for multiple uses since the coating can be easily regenerated by passing an acidic solution (HCl solution, pH 2) inside the channel. PANi coated micro-channels present long-term stability and reproducibility, can be stored at room temperature, exposed to air, empty or filled with a pH 2 solution for over two months without any deterioration in sensor performance.

Since this technique is based on pH responsive coatings, at present, it is not suitable for 3D pH sensing in micro-channels but rather bi-dimensional space (2D) (along the length and width of the channel) pH sensing. However, when coupled with imaging techniques, this approach offers a low cost, accurate approach for the tracking of the 2D temporal and spatial dynamics of pH changes along an entire micro-fluidic channel in real-time, without the need to add a pH sensitive dye to the liquid phase in the channel. The approach of using the colour camera for pH mapping is generic and could be applied for a wide variety of pH responsive systems.

Acknowledgements

The project has been carried out with the support of the Irish Research Council (IRC) - Embark Initiative and Science Foundation Ireland under the CLARITY initiative, grant 07/CE/I1147.

Appendix B. Supplementary Information

Electronic Supplementary Information (ESI) available: Video 1 and Video 2 are showing the rapid colour change of the polyaniline coating when solutions of different pHs are passed through the micro-channel. In Video 3, using image processing techniques, pH is successfully mapped when a pH gradient is induced inside the polyaniline modified micro-channel. See DOI: 10.1039/b000000x/

5.5 References

1. Pasztor, K.; Sekiguchi, A.; Shimo, N.; Kitamura, N.; Masuhara, H., Iridium oxide-based microelectrochemical transistors for pH sensing. *Sensors and Actuators B-Chemical* **1993**, *12*, 225-230.
2. Khanna, V. K., Fabrication of ISFET microsensor by diffusion-based Al gate NMOS process and determination of its pH sensitivity from transfer characteristics. *Indian Journal of Pure & Applied Physics* **2012**, *50*, 199-207.
3. Nemeth, B.; Tsuda, S.; Busche, C.; Cronin, L.; Cumming, D. R. S., ISFET sensor system for real-time detection of extracellular pH oscillations in slime mould. *Electronics Letters* **2012**, *48*, 143-U120.
4. Chin, Y. L.; Chou, J. C.; Sun, T. P.; Chung, W. Y.; Hsiung, S. K., A novel pH sensitive ISFET with on chip temperature sensing using CMOS standard process. *Sensors and Actuators B-Chemical* **2001**, *76*, 582-593.
5. Cheng, Y.; Luo, X.; Betz, J.; Buckhout-White, S.; Bekdash, O.; Payne, G. F.; Bentley, W. E.; Rubloff, G. W., In situ quantitative visualization and characterization of chitosan electrodeposition with paired sidewall electrodes. *Soft Matter* **2010**, *6*, 3177-3183.
6. Gunnlaugsson, T.; Kruger, P. E.; Jensen, P.; Tierney, J.; Ali, H. D. P.; Hussey, G. M., Colorimetric "naked eye" sensing of anions in aqueous solution. *Journal of Organic Chemistry* **2005**, *70*, 10875-10878.
7. Klauke, N.; Monaghan, P.; Sinclair, G.; Padgett, M.; Cooper, J., Characterisation of spatial and temporal changes in pH gradients in microfluidic channels using optically trapped fluorescent sensors. *Lab on a Chip* **2006**, *6*, 788-793.
8. Ge, X.; Kostov, Y.; Tolosa, L.; Rao, G., Study on low-cost calibration-free pH sensing with disposable optical sensors. *Analytica Chimica Acta* **2012**, *734*, 79-87.
9. Richter, A.; Paschew, G.; Klatt, S.; Lienig, J.; Arndt, K.-F.; Adler, H.-J. P., Review on hydrogel-based pH sensors and microsensors. *Sensors* **2008**, *8*, 561-581.
10. Trinh, Q. T.; Gerlach, G.; Sorber, J.; Arndt, K.-F., Hydrogel-based piezoresistive pH sensors: Design, simulation and output characteristics. *Sensors and Actuators B-Chemical* **2006**, *117*, 17-26.

11. Cheng, Y.; Xiong, P.; Yun, C. S.; Strouse, G. F.; Zheng, J. P.; Yang, R. S.; Wang, Z. L., Mechanism and Optimization of pH Sensing Using SnO₂ Nanobelt Field Effect Transistors. *Nano Letters* **2008**, *8*, 4179-4184.
12. Tsai, C. N.; Chou, J. C.; Sun, T. P.; Hsiung, S. K., Study on the sensing characteristics and hysteresis effect of the tin oxide pH electrode. *Sensors and Actuators B-Chemical* **2005**, *108*, 877-882.
13. Huang, W.-D.; Cao, H.; Deb, S.; Chiao, M.; Chiao, J. C., A flexible pH sensor based on the iridium oxide sensing film. *Sensors and Actuators a-Physical* **2011**, *169*, 1-11.
14. S. Martellucci; A.N. Chester; Mignani, A. G., Optical Sensors and Microsystems - New Concepts, Materials, Technologies. *Springer, New York, USA* **2000**.
15. Wolthuis, R. M., D. Saaski, E. Hartl, J. Mitchell, G., Development of a medical fiber-optic pH sensor based on optical absorption. *IEEE Transactions on Biomedical Engineering* **1992**, *39*, 531 - 537.
16. Buchholz, F.; Buschmann, N.; Cammann, K., A fiberoptic sensor for the determination of sodium with a reversible response. *Sensors and Actuators B-Chemical* **1992**, *9*, 41-47.
17. Kuswandi, B.; Narayanaswamy, R., Polymeric encapsulated membrane for optrodes. *Fresenius Journal of Analytical Chemistry* **1999**, *364*, 605-607.
18. Sabnis, R. W.; Sanders, S.; Dempsey, L., *Handbook of Acid-Base Indicators*. CRC Press: 2007.
19. Ge, Z. F.; Brown, C. W.; Sun, L. F.; Yang, S. C., Fiberoptic ph sensor-based on evanescent-wave absorption-spectroscopy. *Analytical Chemistry* **1993**, *65*, 2335-2338.
20. Asijati, E. K., B.; Arifah, N.F.; Kurniawati, Y.I.; Gani, A.A., Non-invasive optical chemical sensor based on polyaniline films for detection of ammonia and acetic acid solutions. *Sensors and the International Conference on new Techniques in Pharmaceutical and Biomedical Research, 2005 Asian Conference on* **2005**, 111 - 114
21. Huang, J. X.; Virji, S.; Weiller, B. H.; Kaner, R. B., Polyaniline nanofibers: Facile synthesis and chemical sensors. *Journal of the American Chemical Society* **2003**, *125*, 314-315.
22. Florea, L.; Hennart, A.; Diamond, D.; Benito-Lopez, F., Synthesis and characterisation of spiropyran-polymer brushes in micro-capillaries: Towards an integrated optical sensor for continuous flow analysis. *Sensors and Actuators B: Chemical* **2012**, *175*, 92-99.
23. Florea, L.; Benito-Lopez, F.; Hennart, A.; Diamond, D., Photo-detection of solvent polarities using non-invasive coatings in capillaries. *Procedia Engineering* **2011**, *25*, 1545 – 1548.
24. Miwa, J., Suzuki, Y., Kasagi, N., Adhesion-Based Cell Sorter With Antibody-Coated Amino-Functionalized-Parylene Surface. *Journal of Microelectromechanical Systems Journal of* **2008**, *17*, 611-622.
25. Mela, P.; Onclin, S.; Goedbloed, M. H.; Levi, S.; Garcia-Parajo, M. F.; van Hulst, N. F.; Ravoo, B. J.; Reinhoudt, D. N.; van den Berg, A., Monolayer-functionalized microfluidics devices for optical sensing of acidity. *Lab on a Chip* **2005**, *5*, 163-170.
26. Basabe-Desmonts, L.; Benito-Lopez, F.; Gardeniers, H. J. G. E.; Duwel, R.; van den Berg, A.; Reinhoudt, D. N.; Crego-Calama, M., Fluorescent sensor array in a microfluidic chip. *Analytical and Bioanalytical Chemistry* **2008**, *390*, 307-315.
27. Benito-Lopez, F.; Scarmagnani, S.; Walsh, Z.; Paull, B.; Macka, M.; Diamond, D., Spiropyran modified micro-fluidic chip channels as photonically controlled self-indicating system for metal ion accumulation and release. *Sensors and Actuators B-Chemical* **2009**, *140*, 295-303.
28. Lau, K. T.; Shepherd, R.; Diamond, D.; Diamond, D., Solid state pH sensor based on light emitting diodes (LED) as detector platform. *Sensors* **2006**, *6*, 848-859.

29. Matias, F. A. A.; Vila, M.; Tubino, M., A simple device for quantitative colorimetric diffuse reflectance measurements. *Sensors and Actuators B-Chemical* **2003**, 88, 60-66.
30. Schmidt, G. J.; Scott, R. P. W., Simple and sensitive ion chromatograph for trace-metal determination. *Analyst* **1984**, 109, 997-1002.
31. Clinch, J. R.; Worsfold, P. J.; Casey, H., An automated spectrophotometric field-monitor for water-quality parameters - determination of nitrate. *Analytica Chimica Acta* **1987**, 200, 523-531.
32. Hauser, P. C.; Tan, S. S.; Cardwell, T. J.; Cattrall, R. W.; Hamilton, I. C., Versatile manifold for the simultaneous determination of ions in flow-injection analysis. *Analyst* **1988**, 113, 1551-1555.
33. Johnson, K. S.; Beehler, C. L.; Sakamotoarnold, C. M., A submersible flow-analysis system. *Analytica Chimica Acta* **1986**, 179, 245-257.
34. Betteridge, D.; Cheng, W. C.; Dagless, E. L.; David, P.; Goad, T. B.; Deans, D. R.; Newton, D. A.; Pierce, T. B., An automated viscometer based on high-precision flow-injection analysis 1. Apparatus for high-precision flow-injection analysis. *Analyst* **1983**, 108, 1-16.
35. Feres, M. A.; Reis, B. F., A downsized flow set up based on multicommutation for the sequential photometric determination of iron(II)/iron(III) and nitrite/nitrate in surface water. *Talanta* **2005**, 68, 422-428.
36. Lau, K. T.; Baldwin, S.; Shepherd, R. L.; Dietz, P. H.; Yerzunis, W. S.; Diamond, D., Novel fused-LEDs devices as optical sensors for colorimetric analysis. *Talanta* **2004**, 63, 167-173.
37. Lau, K. T.; Baldwin, S.; O'Toole, M.; Shepherd, R.; Yerazunis, W. J.; Izuo, S.; Ueyama, S.; Diamond, D., A low-cost optical sensing device based on paired emitter-detector light emitting diodes. *Analytica Chimica Acta* **2006**, 557, 111-116.
38. O'Toole, M.; Lau, K.-T.; Shazmann, B.; Shepherd, R.; Nesterenko, P. N.; Paull, B.; Diamond, D., Novel integrated paired emitter-detector diode (PEDD) as a miniaturized photometric detector in HPLC. *Analyst* **2006**, 131, 938-943.
39. Barnard, S. M.; Walt, D. R., A fiberoptic chemical sensor with discrete sensing sites. *Nature* **1991**, 353, 338-340.
40. Alexandre, I.; Hamels, S.; Dufour, S.; Collet, J.; Zammattéo, N.; De Longueville, F.; Gala, J. L.; Remacle, J., Colorimetric silver detection of DNA microarrays. *Analytical Biochemistry* **2001**, 295, 1-8.
41. Byrne, L.; Barker, J.; Pennarun-Thomas, G.; Diamond, D.; Edwards, S., Digital imaging as a detector for generic analytical measurements. *Trac-Trends in Analytical Chemistry* **2000**, 19, 517-522.
42. Byrne, L.; Lau, K. T.; Diamond, D., Development of pH sensitive films for monitoring spoilage volatiles released into packaged fish headspace. *Irish Journal of Agricultural and Food Research* **2003**, 42, 119-129.
43. Lapresta-Fernandez, A.; Capitan-Vallvey, L. F., Environmental monitoring using a conventional photographic digital camera for multianalyte disposable optical sensors. *Analytica Chimica Acta* **2011**, 706, 328-337.
44. Fay, C.; Lau, K.-T.; Beirne, S.; Conaire, C. O.; McGuinness, K.; Corcoran, B.; O'Connor, N. E.; Diamond, D.; McGovern, S.; Coleman, G.; Shepherd, R.; Alici, G.; Spinks, G.; Wallace, G., Wireless aquatic navigator for detection and analysis (WANDA). *Sensors and Actuators B-Chemical* **2010**, 150, 425-435.
45. Cantrell, K.; Erenas, M. M.; de Orbe-Paya, I.; Capitan-Vallvey, L. F., Use of the Hue Parameter of the Hue, Saturation, Value Color Space As a Quantitative Analytical Parameter for Bitonal Optical Sensors. *Analytical Chemistry* **2010**, 82, 531-542.
46. Smith, A. R., Color gamut transform pairs. *SIGGRAPH Comput. Graph.* **1978**, 12, 12-19.
47. Shrirao, A. B.; Perez-Castillejos, R., Simple Fabrication of Microfluidic Devices by Replicating Scotch-tape Masters. *Chips & Tips* **17 May 2010**.

48. Qiang, J. F.; Yu, Z. H.; Wu, H. C.; Yun, D. Q., Polyaniline nanofibers synthesized by rapid mixing polymerization. *Synthetic Metals* **2008**, *158*, 544-547.
49. Wu, C. G.; Chen, J. Y., Chemical deposition of ordered conducting polyaniline film via molecular self-assembly. *Chemistry of Materials* **1997**, *9*, 399-&.
50. Dambrine, J.; Geraud, B.; Salmon, J. B., Interdiffusion of liquids of different viscosities in a microchannel. *New Journal of Physics* **2009**, *11*.
51. Berrada, K.; Quillard, S.; Louarn, G.; Lefrant, S., Polyanilines and substituted polyanilines - a comparative-study of the raman-spectra of leucoemeraldine, emeraldine and pernigraniline. *Synthetic Metals* **1995**, *69*, 201-204.
52. Bartonek, M.; Sariciftci, N. S.; Kuzmany, H., Resonance Raman-spectroscopy of the emeraldine insulator-to-metal phase-transition. *Synthetic Metals* **1990**, *36*, 83-93.
53. Hugotlegoff, A.; Bernard, M. C., Protonation and oxidation processes in polyaniline thin-films studied by optical multichannel analysis and in-situ raman-spectroscopy. *Synthetic Metals* **1993**, *60*, 115-131.
54. Huang, J. X., Syntheses and applications of conducting polymer polyaniline nanofibers. *Pure and Applied Chemistry* **2006**, *78*, 15-27.
55. Huang, J.; Virji, S.; Weiller, B. H.; Kaner, R. B., Nanostructured polyaniline sensors. *Chemistry-a European Journal* **2004**, *10*, 1315-1319.
56. Virji, S.; Fowler, J. D.; Baker, C. O.; Huang, J. X.; Kaner, R. B.; Weiller, B. H., Polyaniline nanofiber composites with metal salts: Chemical sensors for hydrogen sulfide. *Small* **2005**, *1*, 624-627.
57. Pringsheim, E.; Terpetschnig, E.; Wolfbeis, O. S., Optical sensing of pH using thin films of substituted polyanilines. *Analytica Chimica Acta* **1997**, *357*, 247-252.
58. Grummt, U. W.; Pron, A.; Zagorska, M.; Lefrant, S., Polyaniline based optical pH sensor. *Analytica Chimica Acta* **1997**, *357*, 253-259.
59. Chiang, J. C.; Macdiarmid, A. G., Polyaniline - Protonic acid doping of the emeraldine form to the metallic regime. *Synthetic Metals* **1986**, *13*, 193-205.
60. Epstein, A. J.; Ginder, J. M.; Zuo, F.; Bigelow, R. W.; Woo, H. S.; Tanner, D. B.; Richter, A. F.; Huang, W. S.; Macdiarmid, A. G., Insulator-to-metal transition in polyaniline. *Synthetic Metals* **1987**, *18*, 303-309.
61. Martinez, A. W.; Phillips, S. T.; Whitesides, G. M.; Carrilho, E., Diagnostics for the Developing World: Microfluidic Paper-Based Analytical Devices. *Analytical Chemistry* **2010**, *82*, 3-10.
62. Savitzky, A.; Golay, M. J. E., Smoothing + differentiation of data by simplified least squares procedures. *Analytical Chemistry* **1964**, *36*, 1627-&.
63. Tamayama, H.; Ito, K.; Nishimura, T. In *Technology trends of high-definition digital still camera systems*, VLSI Circuits Digest of Technical Papers, 2002. Symposium on, 2002, 2002; 2002; pp 100-105.
64. Maxwell, P. In *Test for low cost CMOS image sensors*, Test Symposium, 2005. European, 22-25 May 2005, 2005; 2005; p 222.
65. Xiao, F.; Zhang, X.; Fowler, B. In *Color processing in camera phones: How good does it need to be?*, 2005; Nitin, S.; Jeffrey, M. D.; Ricardo, J. M., Eds. SPIE: 2005; pp 96-104.
66. <http://www.nokiasensingxchallenge.org/>

Chapter 6

Synthesis and characterisation of spiropyran-polymer brushes in micro-capillaries: towards an integrated optical sensor for continuous flow analysis

Larisa Florea¹, Alexandre Hennart¹, Dermot Diamond¹ and Fernando Benito-Lopez^{1*}

Sensors and Actuators B: Chem. 175 (2012) 92-99

ISSN: 0925-4005; [//WOS:000312358700019](#)

¹CLARITY: Centre for Sensor Web Technologies, National Centre for Sensor Research, School of Chemical Sciences, Dublin City University, Dublin, Ireland;

*Author to whom correspondence should be addressed;

Abstract: Fused silica-capillaries were successfully functionalised with spiropyran-polymer brushes using spiropyran functionalised norbornyl derivative as monomer. The polymerisation was achieved by surface-initiated ring-opening metathesis polymerisation. A three-dimensional arrangement, covalently attached to the inner wall of the fused-silica capillary, was obtained. The spiropyran moiety has the freedom to open and close in response to light (ultraviolet, white light) within the polymer brushes. The coating was fully characterised by Scanning Electron Microscopy, absorbance measurements and kinetic studies. The photo-response of the coatings showed very good reproducibility comparable with spiropyran monomers in solution demonstrating that this platform can be used for the develop of capillary integrated sensors based on the inherited sensing proprieties of spiropyran moieties.

Keywords: spiropyran, micro-capillary, ROMP, sensor, continous flow

6.1 Introduction

Previously reported capillary optical sensors have shown numerous advantages compared to planar optical sensors as such a) are suitable for direct sampling, b) cheap fabrication protocols (c) represent an optical waveguide structure that enables various methods of optical interrogation, d) have small internal volumes and e) very rapid response times [1, 2].

The development of capillary optical sensors involves the coating of the inner walls of a capillary (usually glass) with a sensitive layer that can be optically interrogated. Welgl *et al.* [1] reported capillary optical sensors obtained by immobilising a carbon dioxide sensitive layer onto the inner walls of a capillary by “reverse pumping” meanwhile, other research groups have published integrated-optic ammonia sensors based as well in capillaries as the sensor platform [3, 4]. Lippitsch *et al.* [5] showed the use of capillary optical sensors for biomedical applications proving good sensor performance and easy handling by the integration of the sample compartment, the optical sensor, and the light-collecting optics into a single device. However, most of the reported protocols involved non-covalent bonding of the sensitive material to the inner walls of the capillary [3, 5] and required protective coatings [1] to avoid leaching of the immobilised sensitive material over time [6].

An attractive alternative for making capillary integrated optical sensors is the possibility of incorporating active sensing surfaces that can be switched on and off remotely using light. In our laboratories, we are extensively working in the generation of switchable optical sensors based on photo-responsive materials using spiropyran derivatives [7-10].

Spiroyrans are one of the most popular classes of photocromic compounds as they are particularly interesting targets for the development of new approaches for sensing. They offer new routes to multifunctional materials that take advantage of their photo-reversible interconversion between two thermodynamically stable states: a spiropyran (SP) form, and a merocyanine (MC) form, Figure 6.1, which have dramatically different charge, polarity and molecular conformations [11]. Spiroyrans are an attractive starting point in the construction of molecular-level sensors with molecular recognition properties and signal transduction ability due to their unique molecule binding power and signal transduction function [12]. The MC

may interact with the surrounding environment (solvent or analyte) manifesting different photochromic responses [12]. Based on these sensing proprieties, that are only shown by the MC form, spiropyrans have been employed in analytical chemistry as molecular sensors where the sensing behaviour can be remotely switched *ON/OFF* using light of appropriate wavelengths (by switching between the spiro (*OFF*) and the merocyanine (*ON*) form). The sensing capability of spiropyrans in solution have been extensively studied and demonstrated for a wide range of analytes from metal ions [13-17], neutral molecules (such as nucleobases [18], amino acids [19, 20] and DNA [21]), a range of anions [22, 23] and solvents of different polarities [24].

The possibility of fabricating optical sensors that can be photo-activated has significant implications in science since this methodology represents a totally non-invasive manner of controlling and interrogating the response of the sensor. In this respect, a significant amount of effort has been devoted to functionalise surfaces [9] and micro-fluidic platforms [25] with photochromic materials. Rosario *et al.* [26] coated capillary tubes with a photoresponsive monolayer based on spiropyran and showed that the water level inside the capillary rised when the light source was switched from VIS to UV in correlation with the switching of the surface-bound spiropyran molecule between nonpolar and polar forms. Previous work done in our group by Benito-Lopez *et al.* [25] showed that micro-fluidic channels coated with spiropyran monolayers can be used as photonically controlled self-indicating systems for metal ion accumulation and release, based on the metal ion-binding and molecular recognition properties of the MC form. However, the main disadvantage of the monolayer approach is the low concentration of photochromic moieties, which manifests in extremely weak absorbance peaks, where the formation of the MC form cannot be detected by eye [26].

In the context of developing chemical sensors, the use of homopolymers, where each monomer contains the spiropyran unit, is desired as it increases the concentration of the photochromic component in the polymer [27] and enhances the photochromic processes [28]. For instance, Samanta *et al.* [28] showed that when glass slides are coated with spiropyran polymer brushes obtained by surface-initiated ring opening metathesis polymerisation (SI-ROMP), the photochromic behaviour is greatly enhanced compared to the monolayer. Moreover, the color and wettability of the surface can be externally controlled using light as the external stimulus.

In this context, we have focused our research in the synthesis and characterisation of sensing coatings based on spiropyran moieties inside micro-capillaries that can be externally photo-controlled in a non-invasive way. Functionalisation of the inner wall of a fused silica capillary with this photo-responsive molecule provides a convenient small platform for rapid analysis and detection. Furthermore, continuous flow operation facilitates real-time measurements and consequently fast analysis protocols [25].

In this chapter fused-silica micro-capillaries with photochromic polymer brushes based on spiropyran moieties using surface-initiated ring-opening metathesis polymerisation (SI-ROMP) have been successfully coated. Their synthesis offers a transition from a two-dimensional to a three-dimensional arrangement and allows for high density of functional groups to be obtained in a limited area [28]. The photo-responsive behaviour of the spiropyran polymer brushes was fully characterised using acetonitrile (ACN) as the running solvent in the capillary.

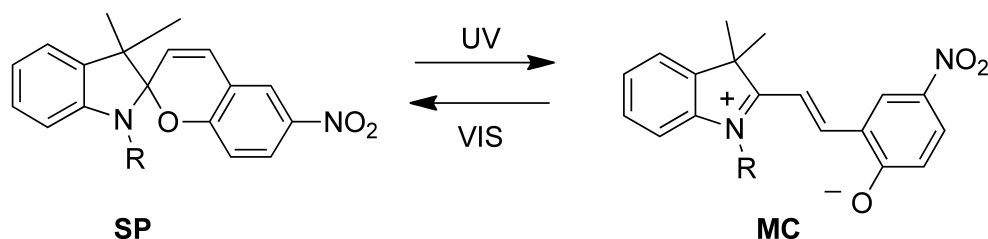


Figure 6.1. Molecular structure of a generic spiropyran moiety irradiated with UV/white light, spiropyran (left) and merocyanine (right).

6.2 Experimental

6.2.1 Materials

7-Octenyltrichlorosilane (Gelest), 5-norbornene-2-carboxylic acid, mixture of isomers (Alfa Aesar), 1-(2-Hydroxyethyl)-3,3-dimethylindolino-6'-nitrobenzopyrrolospiran (SP1) (TCI Europe), *N,N'*-Dicyclohexylcarbodiimide (DCC) (Aldrich), 4-(Dimethylamino)pyridine (DMAP) (Aldrich) and Grubbs Generation-II catalyst (Aldrich) were used as received. Acetone, acetonitrile, dry tetrahydrofuran (THF), dry toluene and dry dichloromethane (CH_2Cl_2) solvents were purchased from

Aldrich and used as received. Fused-silica capillaries (100 μm ID, 375 μm OD) were purchased from Polymicro Technologies (Phoenix, AZ, USA).

6.2.2 Procedures

6.2.2.1 Synthesis of Spiropyran Functionalised Norbornene Monomer

Norbornyl functionalised spiropyran monomer [28] (SP-M) was prepared, as described in Figure 6.2, from the reaction of 5-norbornene-2-carboxylic acid (mixture of isomers) with SP1 in the presence of DCC and DMAP in THF, according to the previously reported method [27]. A representative example of this method is the following: SP1 (0.3 g, 0.851 mmol) and 5-norbornene-2-carboxylic acid (0.104 ml, 0.851 mmol) were placed in a 250 mL round-bottomed flask. After the solution was dissolved in dry THF (20 mL) and cooled to 0 $^{\circ}\text{C}$, a solution of DCC (0.21 g, 1.02 mmol) and DMAP (0.010 g, 0.08 mmol) in THF (5 mL) was added drop-wise over the course of 1 h. The mixture was stirred at 0 $^{\circ}\text{C}$ for an additional 2 h and then gradually warmed to 25 $^{\circ}\text{C}$ over the course of 24 h. During the warming period, a dicyclohexyl urea precipitate formed, which was filtered and washed with THF (3 x 50 mL). After the filtrate was evaporated, the resulting red wax was purified using silica gel column chromatography in the dark with a mixture of hexane/ethylacetate (10/1).

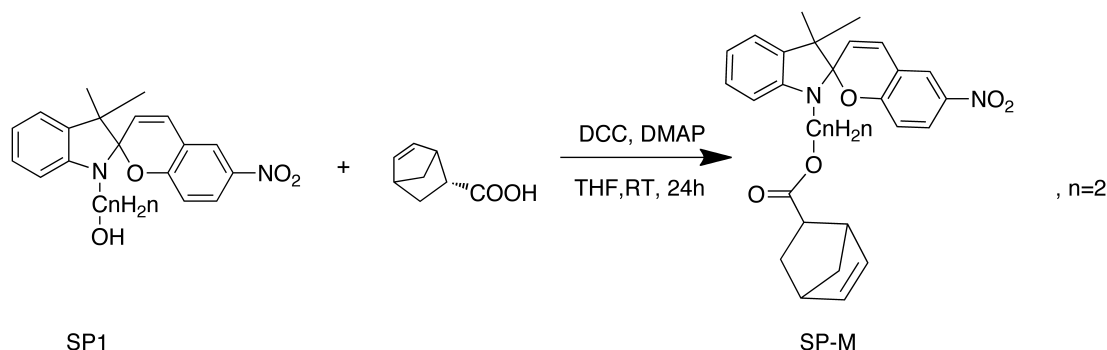


Figure 6.2. Synthesis of the spiropyran functionalised norbornene monomer.

6.2.2.2 Characterisation of Spiropyran Functionalised Norbornene Monomer

Fourier transform-infrared (FT-IR) measurements were taken with a Perkin Elmer Spectrum GX FT-IR System® instrument equipped with an attenuated total reflectance accessory at 264 scans with 4 cm^{-1} resolution. A solution of spiropyran norbornene monomer (10^{-2} M) in acetone was prepared, irradiated for 1 minute with white light and 1 ml of this solution was transfer onto the ATR crystal. The solvent was then evaporated and the spectrum of the spiropyran norbornene monomer in its closed form was recorded. Next, the ATR crystal was exposed to UV light for 20 seconds to allow complete conversion of the spiropyran norbornene monomer to the open merocyanine form and a new spectrum was recorded.

6.2.2.3 Fused Silica Micro-capillaries Coating Protocol

The protocol used to coat micro-capillaries with spiropyran polymer brushes is described in Figure 6.3, steps 1-4. Prior to functionalisation, the inner surface of fused-silica capillaries was first activated with 7-octenyl trichlorosilane. The inner capillary surface was quickly washed with acetone and water, then flushed with a solution of NaOH 0.2 M for 30 min at a flow rate of $0.25\text{ }\mu\text{L min}^{-1}$ using a syringe pump, and then rinsed with deionised water. Next, the capillary was flushed with a solution of HCl 0.2 M for 30 min at a flow rate of $0.25\text{ }\mu\text{L min}^{-1}$, rinsed with water, and with dry toluene. A 0.1 M solution of the silanisation agent (7-octenyl trichlorosilane) 0.1 M in dry toluene was pumped through the capillaries for 90 min at a flow rate of $0.25\text{ }\mu\text{L min}^{-1}$ (Figure 6.3 – step 1). The capillaries were then washed with acetone, dried under nitrogen stream, and left at room temperature for 24h. Later, the capillary was filled with a solution of Grubbs Catalyst Second Generation 0.02 M in degassed CH_2Cl_2 , closed at both ends using rubber septa and put in a water bath for 1h at $45\text{ }^\circ\text{C}$ (Figure 6.3 – step 2). After the catalyst-attached capillary was thoroughly washed with degassed CH_2Cl_2 . Finally, the capillary filled with a solution of spiropyran functionalised monomer, SP-M 0.5 M in degassed CH_2Cl_2 , closed at both ends using rubber septa and put in a water bath for at $50\text{ }^\circ\text{C}$

for 4 h (Figure 6.3 – step 3). The polymerisation was quenched by passing ethyl vinyl ether into the capillary (Figure 6.3 – step 4). Finally the capillary was thoroughly washed with acetone to remove any physisorbed materials.

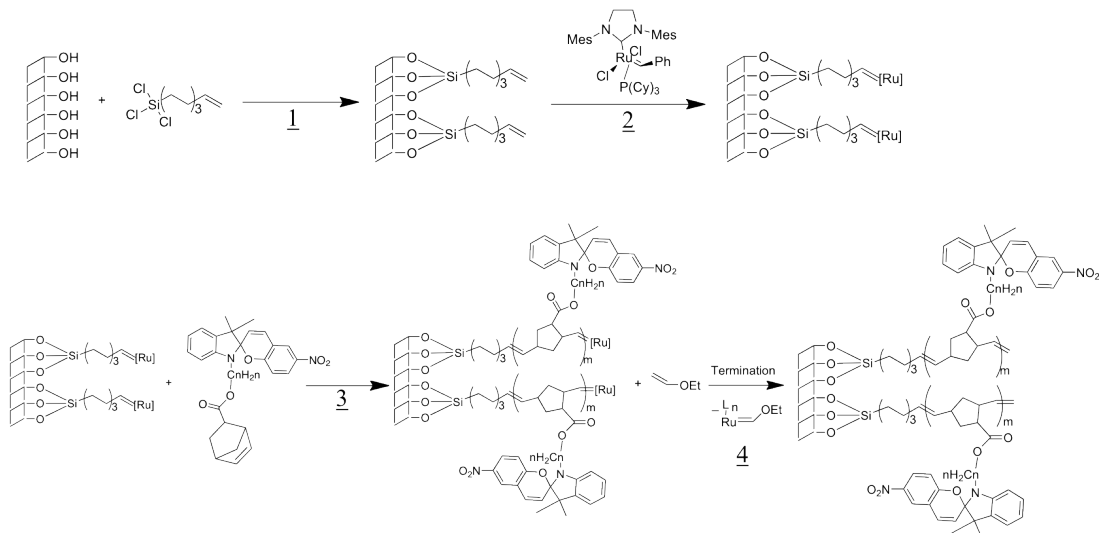


Figure 6.3. Functionalisation protocol of fused silica micro-capillaries with spiropyran based polymeric brushes.

6.2.2.4 Estimation of the Molar Extinction Coefficient of the SP-M

To estimate the molar extinction coefficient (ϵ) of the SP-M in acetonitrile (ACN), 5 solutions of different concentration of SP-M (0.2×10^{-5} , 0.4×10^{-5} , 0.6×10^{-5} , 0.8×10^{-5} and 10^{-4}) were prepared. The solutions were irradiated with UV light for 90 seconds using an array of 9 UV LEDs (365 nm) and the spectra were recorded on a UV–Vis–NIR PerkinElmer Lambda 900 spectrometer. A plot of the Absorbance at λ_{\max} (nm) *versus* concentration showed good linearity ($R^2 = 0.990$). The molar extinction coefficient of SP-M was calculated based on the Lambert-Beer law (eq.1), where the path length, l , was 1 cm (the width of the quartz cuvette).

6.2.2.5 Morphological Characterisation of the Polymer Brushes

Spiropyran polymer brushes were imaged using scanning electron microscopy (SEM) performed on a Carl Zeiss EVOLS 15 system at an accelerating voltage of

4.27 kV. The micro-capillaries were cut using a SGT capillary column cutter with rotating diamond blade (SHORTIX, Nederland) to create a smooth cut of the capillary wall. Then they were placed in vertical position in a custom made metallic capillary holder that has holes of internal diameters equal to the external diameter of the micro-capillary (375 μm). This set-up allows the micro-capillaries to be kept in vertical position. During the imaging process, the stage was tilted of an angle between 0 – 15 ° for better imaging of the inner wall of the micro-capillary.

6.2.2.6 Optical Characterisation of Spiropyran Coatings

The UV irradiation source used to switch the spiropyran based coatings and the spiropyran monomer (SP-M) solution was an array of 9 UV LEDs placed at a distance of 1 cm from the spiropyran solution or the functionalised micro-capillaries, respectively. The LEDs have an emission wavelength peak at 365 nm and an optical output power of 1.2 mW, supplied by Roithner Lasertechnik Austria. The white light irradiation source used for the switching of MC back to SP form (in both solutions and capillary coatings) was a DC-regulated light source supplied by Polytec, USA, and placed at a distance of 1 cm from the illuminated area. The maximum power output of the lamp is 150 W, and the intensity control of the light output was fixed at 50 %. The optical switching of the spiropyran moiety inside the capillary has been studied using USB 4000 Fiber Optic Spectrometer – Ocean Optics, Inc, when the light source was a LS-1 tungsten halogen lamp (white light) obtained from Ocean Optics, Inc. A representation of the set-up used for absorbance measurements is described in Figure 6.4. The solvent acetonitrile (ACN) was passed through the capillary at constant flow rate (0.5 $\mu\text{L min}^{-1}$) using a syringe pump (PHD 2000 Syringe) purchased from Harvard Apparatus. All the absorbance spectra were smoothed using Origin Software (each initial spectra contained 3900 points; the smoothing was realised automatically using an average value for every 50 points).

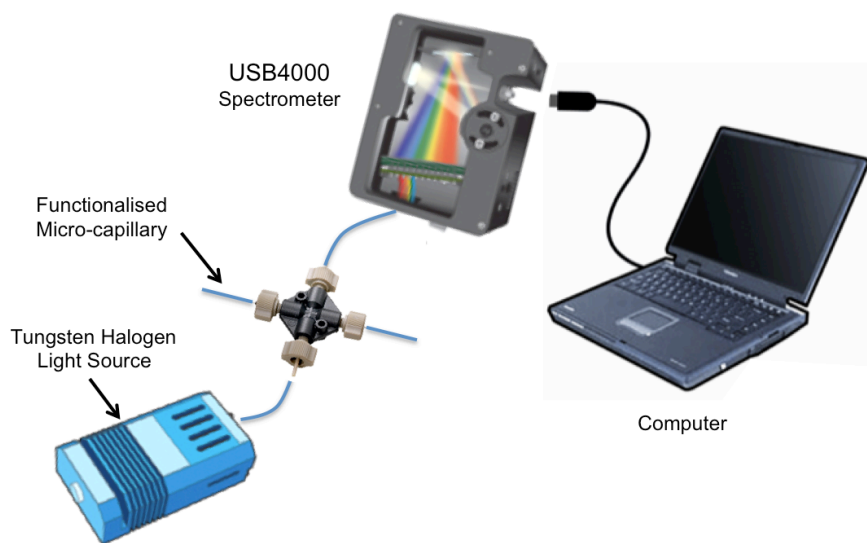


Figure 6.4. Scheme of the set-up used for absorbance measurements.

6.3 Results and Discussion

6.3.1 Structure Characterisation and Photoinduced Conversion of SP to MC

ATR-FT-IR was used to characterise the chemical structure of the spiropyran functionalised monomer as well as the photo-induced conversion of spiropyran to merocyanine in solution. Figure 6.5 shows the ring-closed SP and ring-opened MC form of SP-M after irradiation with UV light. Complete characterisation and assignments are listed in Table 6.1. Bands of particular importance are the C-C-N bend that appears in the spectra of SP-M at 1026 cm^{-1} and the O-C-N stretching emerging at 952 cm^{-1} . These bands disappear upon irradiation with UV light and new bands appear at 1593 , 1426 , and 1307 cm^{-1} assigned to the $\text{C}=\text{N}^+$, $\text{C}-\text{O}^-$ and $\text{C}-\text{N}^+$ stretches, respectively, characteristic to the open merocyanine form [29-35]. Also the symmetrical stretching band of the nitro group is shifted to lower energy from 1520 to 1509 cm^{-1} upon irradiation, due to the increased conjugation brought about in the planar, merocyanine [35].

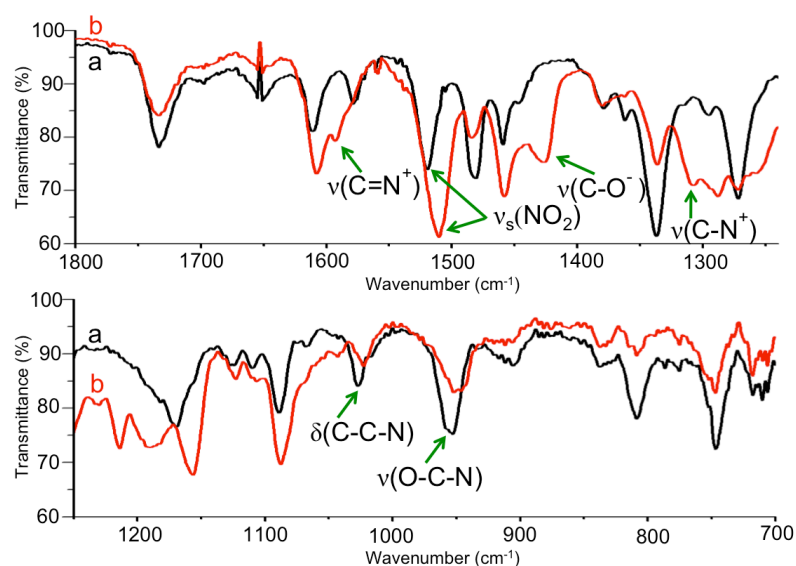


Figure 6.5. FT-IR spectra of spiropyran functionalised norbornene monomer (SP-M) before UV irradiation (a) and after UV irradiation (b). Peaks that indicate the photoconversion of spiropyran to merocyanine are labeled.

Table 6.1. Important FT-IR frequencies for spiropyran functionalised norbornene monomer (SP-M) before (spiropyran) and after (merocyanine) UV irradiation.

| Assignment | Spiropyran | Merocyanine |
|---|--------------------------------|--------------------------------|
| | Wavenumber (cm ⁻¹) | Wavenumber (cm ⁻¹) |
| C=O | 1734 | 1734 |
| C=C stretch | 1610 | 1607 |
| C=N ⁺ | - | 1593 |
| NO ₂ sym stretch | 1520 | 1509 |
| C-C aromatic ring stretch | 1481, 1459 | 1483, 1457 |
| C-O ⁻ | - | 1426 |
| NO ₂ asym stretch | 1336 | 1336 |
| C-N stretch | 1336 | - |
| C-N ⁺ | - | 1307 |
| C-O-C ether sym stretch | 1271 | - |
| C-O-C ether asym stretch | 1169 | - |
| C-O ester stretch | 1169 | 1156 |
| C-O ester stretch | 1086 | 1087 |
| C-C-N bend | 1026 | - |
| O-C-N stretch | 952 | - |
| C=CH; CH out of plane deformation (cis) | 952 | 952 |
| C-H bending | 809 | 809 |
| C-H bending | 746 | 746 |
| C-H bending | 709 | 709 |

6.3.2 Polymer Brushes Length Analysis

Fused silica capillaries were covalently functionalised with spiropyran polymer brushes as described in the experimental section. Scanning electron microscopy of the inner wall of the capillary showed a 3D arrangement of polymer brushes with a thickness of about 1-2 μm as shown in Figure 6.6. Samanta *et al.* [28] also used surface-initiated ring-opening metathesis polymerisation to produce spiropyran polymeric brushes on a flat glass surface, obtaining brushes length of approximately 120 nm which are shorter than the ones obtained by us. This length enhanced effect during the synthesis of polymer brushes inside capillaries was previously reported by Miller *et al.* [36] who showed that when atom transfer radical polymerisation (ATRP) is employed to produce polymer brushes inside a capillary, the length of the brushes is longer than when the same technique was employed on flat surfaces. Although the coatings present good homogeneity over the cross section, certain heterogeneity was observed along the length of the micro-capillary through colourless areas on the capillary walls when irradiation with UV light (coloured MC form should be present). Further investigations are on going to explore ways to synthesise more homogenous coatings.

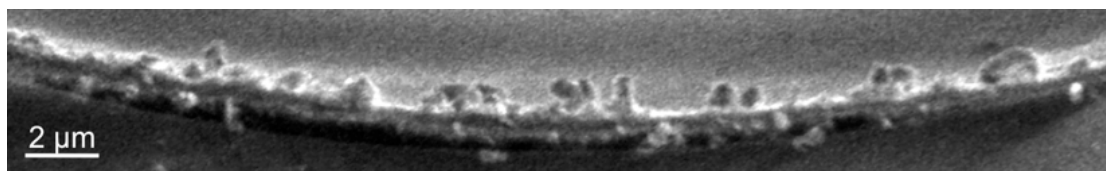


Figure 6.6. Scanning electron microscopy image of the inner wall of a fused silica capillary (100 μm inner diameter) after functionalisation with spiropyran polymer brushes.

6.3.3 Photo-patterning of Spiropyran-merocyanine Forms in the Capillary

SP-M and SP-polymer brushes were optically characterised in acetonitrile (ACN) since it is one of the most common solvents to study the photophysical properties of spiropyran and spiropyran derivatives before and after UV irradiation [37]. In our experimental conditions, ACN was used because it is able to dissolve the monomer and solvate the polymer brushes, while also inhibiting the formation of aggregates.

ACN was passed through the functionalised capillary at a constant flow rate of 5 $\mu\text{L min}^{-1}$ filling the channel completely and avoiding the generation of air bubbles. Then masks formed from metal foil were placed in different positions along the capillary in order to pattern open/closed spiropyran regions along the capillary (see Figure 6.7 a-b). To do this, the capillary was irradiated with UV light (365 nm) for 10 s through the mask. After removing the mask it is clearly visible, even by eye, that the parts of the capillary exposed to UV light irradiation have a strong purple colour characteristic of the merocyanine form while the portions that were covered by the mask remained colourless depicting the presence of the colourless closed form of the spiropyran, Figure 6.7 c. Moreover, when the entire capillary is exposed to white light irradiation, the colour pattern of the capillary recovers the initial colourless spiropyran form, Fig.7 d. This protocol demonstrates that, with the polymer brushes structures, the spiropyran presents no steric hindrance to the kinetics of opening and closing in response to UV and white light irradiation, respectively.

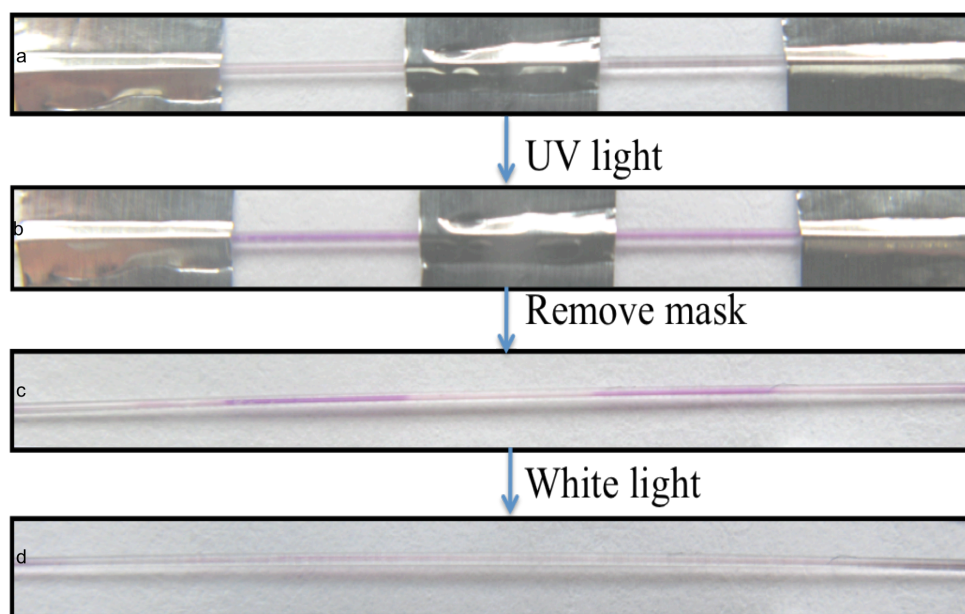


Figure 6.7. Pictures of the spiropyran polymeric brushes functionalised capillaries when filled with acetonitrile (ACN) after irradiation for 10 seconds with UV light through a mask (a and b), c shows the pattern generated by the mask on the capillary. Picture d shows the capillary after irradiation for 1 minute with white light.

6.3.4 Characterisation of SP-monomer in Solution and SP-polymer Brushes in the Capillary by UV-Vis Spectroscopy

UV-Vis spectra of the polymer brushes were taken using the set-up described in the experimental section, Figure 6.4, permitting in-situ spectroscopic characterisation of the coatings inside the capillary. When the capillary is irradiated with UV light for 10 s in the presence of ACN, the absorbance spectra of the coating presents a λ_{max} at about 546 nm. This absorption band disappears after irradiation of the capillary with white light for 1 minute because of the switching of the merocyanine molecule back to the closed spiropyran form (Figure 6.8 A). This behaviour shows a good agreement with the photochromic response of the monomer (10^{-4} M) in ACN solution under identical conditions (Figure 6.8 B), which presents a λ_{max} of 568 nm.

The shift of the λ_{max} in the absorption spectra of the polymer brushes compared to that of the monomer solutions is most likely due to local environmental effects related to the immobilisation of the spiropyran moiety and the integration within the polymer matrix. This effect has been previously observed in different spiropyran-polymer systems, where the shift in the λ_{max} depends on the nature of the polymer and the technique of immobilisation [37-39]. The significant hypsochromic (blue) shift in λ_{max} for the polymer brushes compared to the monomer indicates a more polar micro-environment of the spiropyran in the brushes and it can be explained taking into account the compact organisation of spiropyran units in the polymer brushes, where the conformation of a single spiropyran moiety is not only influenced by the solvent but also by the neighbouring spiropyran units that in response to UV light, are present in their more polar merocyanine form.

Although the UV-Vis spectra were taken directly in the capillary (100 μm , inner diameter) a high absorbance value (0.2 a.u.) of the coating after 10 s UV light irradiation was obtained, indicating a high loading of spiropyran units on the capillary walls.

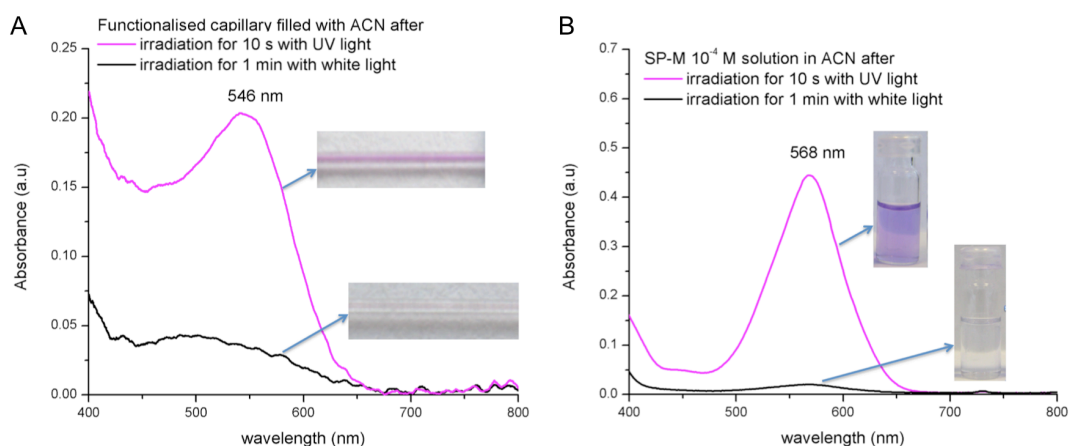


Figure 6.8. (A) Absorbance spectra of spiropyran polymer brushes functionalised in the capillary filled with ACN after irradiation with UV and white light, respectively. (B) Absorbance spectra of spiropyran monomer (SP-M) solution 10^{-4} M in ACN after irradiation with UV and white light, respectively. The spectra are accompanied by photos of the functionalised capillary (A) and monomeric solution (B) under the same experimental conditions.

The concentration of spiropyran units inside the micro-capillary was estimated using the Lambert-Beer law, with the molar extinction coefficient, ϵ , considered to be equal to the molar extinction coefficient of the monomer in ACN, since the polymer brushes are formed from identical monomeric units. The molar extinction coefficient of the SP-M calculated as described in the experimental section was found to be $46000 \pm 10 \text{ M}^{-1}\text{cm}^{-1}$. Consequently the loading of spiropyran units inside the capillary was estimated to be approximately $43 \times 10^{-3} \text{ mol dm}^{-3}$, according to Lambert Beer law presented below,

$$A_{brushes} = \epsilon \cdot l \cdot c \quad \text{Eq. 1}$$

where $A_{brushes}$ is the absorbance of the photochromic coating after exposure for 10 s to UV light (~ 0.2 a.u.), ϵ is the molar extinction coefficient of the monomer in ACN ($46000 \pm 10 \text{ M}^{-1} \text{ cm}^{-1}$), c is the concentration of spiropyran units in the capillary and l is the inner diameter of the capillary ($100 \text{ }\mu\text{m}$).

However, this is the loading of the spiropyran units relative to the capillary and not to the polymeric brushes that represent only 2-4 % of the capillary width. These high values show that this platform can be easily used to produce new types of

sensors based on the inherited spiropyran proprieties where the response of the sensor can be optically interrogated by simple absorbance measurements. The strong response of the coating to the photo-stimulus (manifested in high absorbance values) shows the promise of this platform for the development of optofluidics sensors where optic and fluidic functionalities are integrated at the micro-scale to leverage their combined advantages [40].

6.3.5 Switching Properties of the SP-polymer Brushes in the Capillary by UV-Vis Spectroscopy

When the colourless SP-polymer brushes are illuminated with UV light (365 nm) the capillary become purple-coloured, and the colour change is easily observed by eye. This effect has been intensively investigated by us using other polymeric surfaces like poly(methyl methacrylate) [7-9, 41] and in polystyrene/ silica beads [10], onto which spiropyran derivatives were covalently immobilised.

The capillary, filled with ACN was irradiated with 365 nm UV light for 10 s to convert the SP-polymer brushes to the MC-polymer brushes form, then, the channels were illuminated with white light for 1 min. Absorbance values at 546 nm were recorded immediately after irradiation, Figure 6.9 A. The plot clearly shows a high efficient interconversion of spiropyran units inside the polymer brushes. Therefore, the spiropyran moiety has enough freedom and it is well solvated by ACN, allowing the high degree of conformational flexibility required for efficient switching between the MC and SP forms.

Photo-stability over time has to be considered when dealing with spiropyran photochromic dyes, as a well-documented photo-bleaching process [42-44] occurs when SP is exposed to UV-vis radiation for extended time periods. After 5 switching cycles, the efficiency was found to be constant in the capillary. Figure 6.8 A shows typical results obtained for one location on the capillary. The $A_{SP} = 0.035 \pm 0.003$ a.u. and the $A_{MC} = 0.204 \pm 0.003$ a.u. The $\Delta A_{SP \rightarrow MC} = 0.169 \pm 0.003$ a.u. and the $\Delta A_{MC \rightarrow SP} = -0.169 \pm 0.001$ a.u. for 5 cycles obtaining similar differences in absorbance values, therefore these cycles are reproducible and repeatable, with no hysteresis. This result demonstrates that the capillary could be re-used at least five

times, without significant photo-bleaching, suggesting that it can be photo-switched many more times if required.

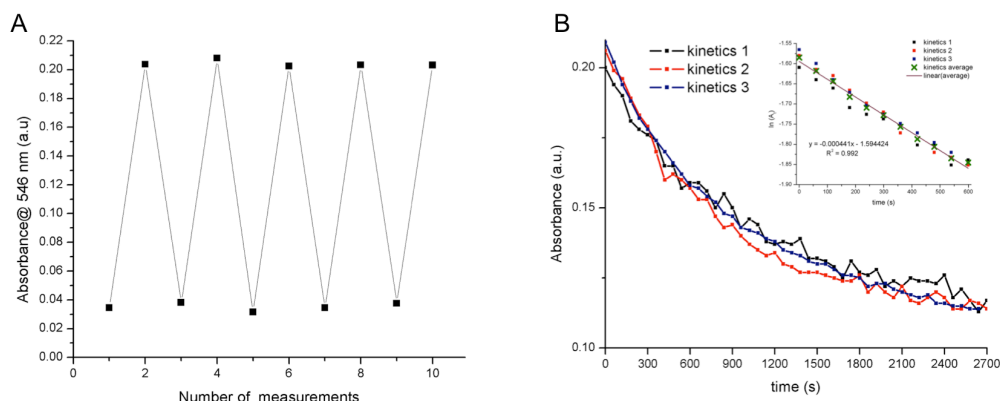


Figure 6.9. (A) Absorbance intensity at 546 nm of spiropyran polymer brushes functionalised in a capillary after repeated switching cycles consisting of 10 seconds UV light exposure followed by 1 minute white light irradiation. (B) Absorbance decreases at the λ_{\max} (546 nm) in acetonitrile as a function of time for the transition of the spiropyran polymeric coating from the merocyanine form, obtained after UV light irradiation, to the closed spiropyran form. Inset – Linear plot of $\ln(A_t)$ vs. time used for the determination of the first order kinetic constant of the spiropyran closing process (MC→SP).

The kinetics of the closing process of the spiropyran moiety inside the polymeric brushes was studied using white light irradiation, Figure 6.9 B. This involved inducing the formation of the MC state by exposure of the capillary to UV light irradiation for 10 s, and then monitoring the decrease of the absorbance value at λ_{\max} (546) at a fixed time interval of 60 s upon removal of the UV light source, as equilibrium is re-established between the SP and MC forms. It is known from solution studies that this process follows first-order kinetics [45], with the thermodynamics and kinetics strongly influenced by the solvent. Figure 6.9 B shows the reduction of the absorbance at the λ_{\max} for the transition from MC form of the polymer brushes to the SP form at 18 °C. From these measurements, the first-order rate constants k for the MC to SP closing process in the presence of white light (coming from LS-1 tungsten halogen lamp) was determined by plotting $\ln(A_t)$ versus time and it was found to be $4.4 \pm 0.5 \times 10^{-4} \text{ s}^{-1}$. This value is similar to other reported values for spiropyran functionalised polystyrene beads in ACN ($1.5 \times 10^{-4} (\pm 2 \%) \text{ s}^{-1}$) [10] or for poly(methyl methacrylate) chains having a single photochromic spiropyran end-group in ACN at 15 °C ($3.03 \times 10^{-3} \text{ s}^{-1}$) [37].

6.4 Conclusions

To the best of our knowledge this is the first time spiropyran based polymer brushes were grafted on the inner walls of a micro-capillary. Using Si-ROMP a three-dimensional arrangement formed of polymeric brushes, covalently attached to the inner wall of the fused-silica capillary, where the spiropyran moiety has the freedom to open and close in response to light (UV, white light) was obtained. It was shown that the photochromic behaviour presents good reproducibility and the switching between SP to MC can be performed at least 5 times with no photobleaching. The spiropyran polymer brushes inherit the spiropyran proprieties, in addition, a good agreement was found between the monomer in solution and photochromic coatings obtained inside the capillary. Based on these promising results, this fabricated and characterised capillary platform based on the spiropyran proprieties will be further investigated as a novel miniaturised integrated optical molecular sensor for real time analysis in continuous flow mode using a variety of analytes.

Acknowledgements

The project has been carried out with the support of the Irish Research Council for Science, Engineering and Technology (IRCSET) - Embark Initiative and Science Foundation Ireland under grant 07/CE/I1147 and Science Foundation Ireland under the CLARITY award (07/CE/ I1147). We would like to thank Dr. Brendan Twamley for providing the custom designed capillary holder used for SEM imaging.

6.5 References

1. Weigl, B. H.; Wolfbeis, O. S., Capillary optical sensors. *Analytical Chemistry* **1994**, *66*, 3323-3327.
2. Tan, W. H.; Shi, Z. Y.; Smith, S.; Birnbaum, D.; Kopelman, R., Submicrometer intracellular chemical optical fiber sensors. *Science* **1992**, *258*, 778-781.
3. Giuliani, J. F.; Wohltjen, H.; Jarvis, N. L., Reversible optical-waveguide sensor for ammonia vapors. *Optics Letters* **1983**, *8*, 54-56.
4. Chernyak V., R. R., Gvishi R, Venezky D. , Oxazine-170 in sol-gel glass and PMMA films as a reversible optical waveguide sensor for ammonia and acids. *Sensors and Materials* **1990**, 117-126.
5. Lippitsch, M. E.; Draxler, S.; Kieslinger, D.; Lehmann, H.; Weigl, B. H., Capillary waveguide optrodes: An approach to optical sensing in medical diagnostics. *Applied Optics* **1996**, *35*, 3426-3431.

6. Kuswandi, B.; Narayanaswamy, R., Polymeric encapsulated membrane for optrodes. *Fresenius Journal of Analytical Chemistry* **1999**, *364*, 605-607.
7. Byrne, R.; Diamond, D., Chemo/bio-sensor networks. *Nature Materials* **2006**, *5*, 421-424.
8. Byrne, R. J.; Stitzel, S. E.; Diamond, D., Photo-regenerable surface with potential for optical sensing. *Journal of Materials Chemistry* **2006**, *16*, 1332-1337.
9. Radu, A.; Scarmagnani, S.; Byrne, R.; Slater, C.; Lau, K. T.; Diamond, D., Photonic modulation of surface properties: a novel concept in chemical sensing. *Journal of Physics D-Applied Physics* **2007**, *40*, 7238-7244.
10. Scarmagnani, S.; Walsh, Z.; Slater, C.; Alhashimy, N.; Paull, B.; Macka, M.; Diamond, D., Polystyrene bead-based system for optical sensing using spiropyran photoswitches. *Journal of Materials Chemistry* **2008**, *18*, 5063-5071.
11. Minkin, V. I., Photo-, thermo-, solvato-, and electrochromic spiroheterocyclic compounds. *Chemical Reviews* **2004**, *104*, 2751-2776.
12. Shao, N.; Zhang, X.; Yang, R., Applications of Spiropyran Derivatives in Analytical Chemistry. *Progress in Chemistry* **2011**, *23*, 842-851.
13. Chernyshev, A. V.; Metelitsa, A. V.; Gaeva, E. B.; Voloshin, N. A.; Borodkin, G. S.; Minkin, V. I., Photo- and thermochromic cation sensitive spiro indoline-pyridobenzopyrans. *Journal of Physical Organic Chemistry* **2007**, *20*, 908-916.
14. Ren, J. Q.; Tian, H., Thermally stable merocyanine form of photochromic spiropyran with aluminum ion as a reversible photo-driven sensor in aqueous solution. *Sensors* **2007**, *7*, 3166-3178.
15. Yagi, S.; Nakamura, S.; Watanabe, D.; Nakazumi, H., Colorimetric sensing of metal ions by bis(spiropyran) podands: Towards naked-eye detection of alkaline earth metal ions. *Dyes and Pigments* **2009**, *80*, 98-105.
16. Han, S. L.; Chen, Y., Mercury ion induced activation of the C-O bond in a photo-responsive spiropyran. *Dyes and Pigments* **2011**, *88*, 235-239.
17. Zhu, J. F.; Yuan, H.; Chan, W. H.; Lee, A. W. M., A colorimetric and fluorescent turn-on chemosensor operative in aqueous media for Zn(2+) based on a multifunctionalized spirobenzopyran derivative. *Organic & Biomolecular Chemistry* **2010**, *8*, 3957-3964.
18. Shao, N.; Jin, J.; Wang, H.; Zheng, J.; Yang, R.; Chan, W.; Abliz, Z., Design of Bis-spiropyran Ligands as Dipolar Molecule Receptors and Application to in Vivo Glutathione Fluorescent Probes. *Journal of the American Chemical Society* **2010**, *132*, 725-736.
19. Liu, Y.; Fan, M.; Zhang, S.; Sheng, X.; Yao, J., Basic amino acid induced isomerization of a spiropyran: Towards visual recognition of basic amino acids in water. *New Journal of Chemistry* **2007**, *31*, 1878-1881.
20. Shao, N.; Jin, J. Y.; Cheung, S. M.; Yang, R. H.; Chan, W. H.; Mo, T., A spiropyran-based ensemble for visual recognition and quantification of cysteine and homocysteine at physiological levels. *Angewandte Chemie-International Edition* **2006**, *45*, 4944-4948.
21. Andersson, J.; Li, S. M.; Lincoln, P.; Andreasson, J., Photoswitched DNA-binding of a photochromic spiropyran. *Journal of the American Chemical Society* **2008**, *130*, 11836-11837.
22. Shao, N.; Wang, H.; Gao, X. D.; Yang, R. H.; Chan, W. H., Spiropyran-Based Fluorescent Anion Probe and Its Application for Urinary Pyrophosphate Detection. *Analytical Chemistry* **2010**, *82*, 4628-4636.
23. Shiraishi, Y.; Itoh, M.; Hirai, T., Colorimetric response of spiropyran derivative for anions in aqueous or organic media. *Tetrahedron* **2011**, *67*, 891-897.
24. Botrel, A.; Aboab, B.; Corre, F.; Tonnard, F., A theoretical investigation of solvatochromism - application to merocyanines similar to colored forms obtained by flash-photolysis of spiropyran. *Chemical Physics* **1995**, *194*, 101-116.
25. Benito-Lopez, F.; Scarmagnani, S.; Walsh, Z.; Paull, B.; Macka, M.; Diamond, D., Spiropyran modified micro-fluidic chip channels as photonically controlled self-

- indicating system for metal ion accumulation and release. *Sensors and Actuators B-Chemical* **2009**, *140*, 295-303.
26. Rosario, R.; Gust, D.; Hayes, M.; Jahnke, F.; Springer, J.; Garcia, A. A., Photon-modulated wettability changes on spiropyran-coated surfaces. *Langmuir* **2002**, *18*, 8062-8069.
 27. Keum, S.-R.; Ahn, S.-M.; Roh, S.-J.; Ma, S.-Y., The synthesis and spectroscopic properties of novel, photochromic indolinobenzospiropyran-based homopolymers prepared via ring-opening metathesis polymerization. *Dyes and Pigments* **2010**, *86*, 74-80.
 28. Samanta, S.; Locklin, J., Formation of photochromic spiropyran polymer brushes via surface-initiated, ring-opening metathesis polymerization: Reversible photocontrol of wetting behavior and solvent dependent morphology changes. *Langmuir* **2008**, *24*, 9558-9565.
 29. Uznanski, P., UV-assisted formation of nanoaggregates from photochromic spiropyran in nonpolar solvents. *Langmuir* **2003**, *19*, 1919-1922.
 30. Dattilo, D.; Armelao, L.; Fois, G.; Mistura, G.; Maggini, M., Wetting properties of flat and porous silicon surfaces coated with a spiropyran. *Langmuir* **2007**, *23*, 12945-12950.
 31. Delgado-Macuil, R.; Rojas-Lopez, M.; Gayou, V. L.; Orduna-Diaz, A.; Diaz-Reyes, J., ATR spectroscopy applied to photochromic polymer analysis. *Materials Characterization* **2007**, *58*, 771-775.
 32. Futami, Y.; Chin, M. L. S.; Kudoh, S.; Takayanagi, M.; Nakata, M., Conformations of nitro-substituted spiropyran and merocyanine studied by low-temperature matrix-isolation infrared spectroscopy and density-functional-theory calculation. *Chemical Physics Letters* **2003**, *370*, 460-468.
 33. Cottone, G.; Noto, R.; La Manna, G.; Fornili, S. L., Ab initio study on the photoisomers of a nitro-substituted spiropyran. *Chemical Physics Letters* **2000**, *319*, 51-59.
 34. Zhao, C. T.; Ribeiro, M. D.; Portela, M. F., Addition polymerisation of 5-vinyl-2-norbornene with nickel bis(acetyl acetonate)/methylaluminoxane system. *Journal of Molecular Catalysis a-Chemical* **2002**, *185*, 81-85.
 35. Fries, K. H.; Driskell, J. D.; Samanta, S.; Locklin, J., Spectroscopic Analysis of Metal Ion Binding in Spiropyran Containing Copolymer Thin Films. *Analytical Chemistry* **2010**, *82*, 3306-3314.
 36. Miller, M. D.; Baker, G. L.; Bruening, M. L., Polymer-brush stationary phases for open-tubular capillary electrochromatography. *Journal of Chromatography A* **2004**, *1044*, 323-330.
 37. Ventura, C.; Byrne, R.; Audouin, F.; Heise, A., Atom Transfer Radical Polymerization Synthesis and Photoresponsive Solution Behavior of Spiropyran End-Functionalized Polymers as Simplistic Molecular Probes. *Journal of Polymer Science Part a-Polymer Chemistry* **2011**, *49*, 3455-3463.
 38. Samoladas, A.; Bikiaris, D.; Zorba, T.; Paraskevopoulos, K. M.; Jannakoudakis, A., Photochromic behavior of spiropyran in polystyrene and polycaprolactone thin films - Effect of UV absorber and antioxidant compound. *Dyes and Pigments* **2008**, *76*, 386-393.
 39. Lin, J. S.; Chiu, H. T., Photochromic behavior of spiropyran and fulgide in thin films of blends of PMMA and SBS. *Journal of Polymer Research-Taiwan* **2003**, *10*, 105-110.
 40. Myers, F. B.; Lee, L. P., Innovations in optical microfluidic technologies for point-of-care diagnostics. *Lab on a Chip* **2008**, *8*, 2015-2031.
 41. Stitzel, S.; Byrne, R.; Diamond, D., LED switching of spiropyran-doped polymer films. *Journal of Materials Science* **2006**, *41*, 5841-5844.
 42. Li, X. L.; Li, J. L.; Wang, Y. M.; Matsuura, T.; Meng, J. B., Synthesis of functionalized spiropyran and spirooxazine derivatives and their photochromic

- properties. *Journal of Photochemistry and Photobiology a-Chemistry* **2004**, *161*, 201-213.
43. Baillet, G.; Giusti, G.; Guglielmetti, R., Comparative photodegradation study between spiro indoline oxazine and spiro indoline pyran derivatives in solution. *Journal of Photochemistry and Photobiology a-Chemistry* **1993**, *70*, 157-161.
44. Baillet, G.; Campredon, M.; Guglielmetti, R.; Giusti, G.; Aubert, C., Dealkylation of N-substituted indolinospironaphthoxazine photochromic compounds under UVirradiation. *Journal of Photochemistry and Photobiology a-Chemistry* **1994**, *83*, 147-151.
45. Gerner, H., Photochromism of nitrospiropyrans: effects of structure, solvent and temperature. *Physical Chemistry Chemical Physics* **2001**, *3*, 416-423.

Chapter 7

Spiropyran polymeric micro-capillary coatings for photo-detection of solvent polarity

Larisa Florea¹, Aoife McKeon¹, Dermot Diamond¹ and Fernando
Benito-Lopez^{1, 2*}

Langmuir 29 (2013) 2790-2797

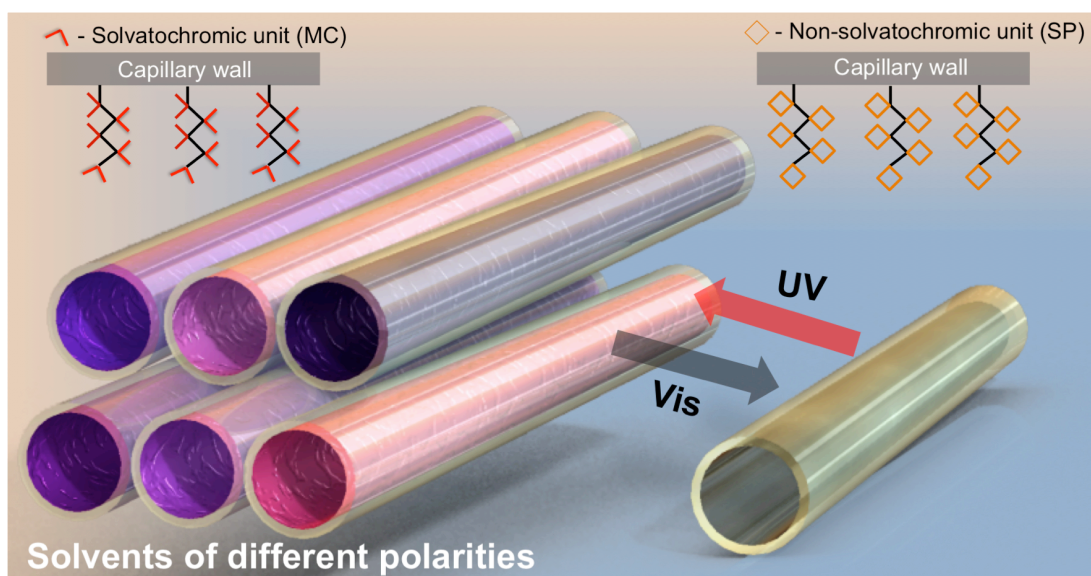
ISSN: 0743-7463, <http://dx.doi.org/10.1021/la304985p>

¹CLARITY: Centre for Sensor Web Technologies, National Centre for Sensor Research, School of Chemical Sciences, Dublin City University, Dublin, Ireland;

²CIC microGUNE, Arrasate-Mondragón, Spain, Tel.: +34 943710212

*Author to whom correspondence should be addressed;

Abstract: Fused silica micro-capillaries were functionalised with spiropyran-polymer brushes using surface-initiated ring-opening metathesis polymerisation. Based on the inherited spiropyran properties, the functionalised capillaries were successfully used to photo-identify solvents of different polarity when passing through the micro-capillary in continuous flow. In the present study, six different solvents (toluene, tetrahydrofuran, acetone, acetonitrile, ethanol and methanol) can be easily detected while passing through the modified micro-capillary by simply irradiating a portion of it with UV light (365 nm). This converts the closed spiropyran moiety to the open merocyanine form and as a consequence, the micro-capillary gains a distinct colour and spectral response depending on the polarity of the solvent. The rate of ring opening of the spiropyran-polymer brushes coatings has been determined in-situ in the presence of different solvents, showing that the coloration rate is also influenced by the solvent polarity and therefore can be used as an additional parameter for solvent sensing.



Keywords: Optical sensor, spiropyran, micro-capillary, continuous flow, solvent sensing;

7.1 Introduction

Optical chemical sensors for liquid phase monitoring (overwhelmingly focused on water-based samples) often employ a dye or indicator that is immobilised onto a solid support material [1-3]. However, this strategy presents two main disadvantages: firstly, the immobilisation process may lead to losses in dye sensitivity [4] and secondly, the stability of the sensor is affected by dye leaching into the sample solution over time [3], making long-term sensor utilisation impractical. Therefore, effective optical-chemical sensors require new materials capable of overcoming all these limitations. In this context, inclusion of photochromic molecules in solid matrices is of particular interest for the development of new approaches for opto-sensing.

Since their discovery by Fisher and Hirshberg in 1952 [5], spiropyrans have become one of the most popular class of photochromic compounds in science due to their potential applicability in new technologies like data recording and storage, optical switching displays and nonlinear optics [6-13]. Spiropyrans offer new routes for the fabrication of multifunctional materials since it is possible to take advantage of their photo-reversible interconversion between the two thermodynamically stable states of the molecule: a spiropyran (SP) form, and a merocyanine (MC) form, which have dramatically different charge, polarity and molecular conformations [14]. The photo-chromic reaction, illustrated in Figure 7.1, occurs because of the photo-cleavage of the C–O spiro-bond of the colourless SP upon UV irradiation. This yields the coloured MC isomer that can return to the SP form by ring closing under visible light irradiation or in the dark through thermal relaxation [7, 15]. Despite the potential applications of photochromic spiropyrans, earlier studies mainly focused on evaluating the utility of monomeric SP systems in solution [16-18]. However, more recently, researchers have tried to use spiropyran for the functionalisation of different types of surfaces. Rosario *et al.* [19] coated capillary tubes with a photoresponsive monolayer based on spiropyran for photo-modulation of surface wettability. Previous work by our group showed that micro-fluidic channels coated with spiropyran monolayers can be used as photonically controlled self-indicating systems for metal ion accumulation and release, based on the metal ion-binding and molecular recognition properties which are only manifested by the MC form [20].

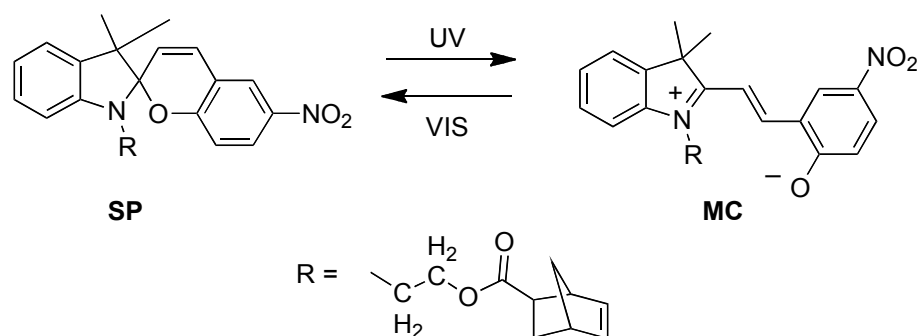


Figure 7.1. Photochromic behaviour of monomeric spiropyrans.

It is well-known that the open-chain merocyanine isomers of nitro-substituted spiropyrans derivatives present negative solvatochromism, meaning that their absorption bands undergo a hypsochromic (blue) shift in solvents of increasing polarity [21]. These changes are caused by intermolecular interactions between the solute and solvent that modify the energy gap between the ground and excited states of the absorbing MC species [22]. Depending on the solvent polarity, the MC form has a tendency to prevail in one of several molecular structures: neutral, cyanine-like, and charge-separated zwitterionic [23]. Based on this property, the MC isomer in solution has been studied for its potential use as an empirical indicator of solvent polarity of typical organic solvents [24, 25], aqueous binary solvent mixtures [26] and even ionic liquids [27, 28]. Monolayers of spiropyran derivatives have been also bound to glass slides to study the polarity of their microenvironment [29]. Although this approach offers interesting information about the interaction of the surface-bound spiropyran with its immediate environment, it is unpractical for studying solvent polarity of a system as a whole. This is because in the monolayer approach only low-resolution fluorescence spectra can be obtained, as the surface concentration of spiropyran molecules tends to be below the detection limit of typical single-pass absorption spectrophotometers.

In this chapter, we present the development of miniaturised analytical platforms wherein solvent polarity can be externally photo-detected in a completely non-invasive manner, through the employment of the colour dependency of the MC form on the solvent polarity. Functionalisation of the inner wall of a fused silica micro-capillary with this photo-responsive molecule provides an excellent platform for rapid analysis and detection of the polarity of solvents. Immobilisation of solvatochromic moieties inside flow-through units (like a micro-capillary) produces

a greatly simplified and flexible platform for achieving these measurements in terms of instrumentation, operational characteristics and reagent/sample handling [30].

Moreover, micro-capillary platforms possess several additional attractive features such as:

- (a) They can act as a mechanical support for optically sensitive materials (coatings) [31];
- (b) They represent an optical waveguide structure and enable various methods of optical interrogation to be employed;
- (c) They are suitable for real-time continuous flow measurements;
- (d) They require very small volumes of analyte [1] and
- (e) They can be easily integrated within commercially available systems (*e.g.* High-performance liquid chromatography (HPLC), capillary electrophoresis (CE), continuous flow and micro-fluidic devices, among others).

In order to assure a high loading of spiropyran, the coating of the capillaries was achieved via photochromic polymer brushes containing the spiropyran moiety. Although several photochromic polymers that incorporate spiropyran or other photochromic derivatives have been reported previously, such systems typically comprise polymer matrices that are either doped or side-chain-modified with photochromes in order to manifest the photochromic behaviour [32-34]. Consequently, the total concentration of photochromic moieties tends to be low in the polymer and consequently the photochromic response is rather weak. In contrast, the micro-capillary coatings presented here are comprised of homopolymeric brushes prepared via surface-initiated ring-opening metathesis polymerisation (SI-ROMP) of a norbornyl functionalised spiropyran monomer (SP-M - Figure 7.1). This approach offers a transition from a two-dimensional to a three-dimensional arrangement, which enables high surface loadings of the stimuli-responsive polymer in a limited area while maintaining the flexibility required for efficient switching of the spiropyran moiety, due to the rather open structure of the brushes which provide very high surface area to bulk characteristics.

7.2 Materials and Methods

7.2.1 Reagents

7-Octenyltrichlorosilane (Gelest), 5-norbornene-2-carboxylic acid, *exo*- (Sigma-Aldrich), 1-(2-Hydroxyethyl)-3,3-dimethylindolino-6'-nitrobenzopyrlospiran (SP1) (TCI Europe), *N,N'*-Dicyclohexylcarbodiimide (DCC) (Sigma-Aldrich), 4-(Dimethylamino)pyridine (DMAP) (Sigma-Aldrich) and Grubbs Generation-II catalyst (Sigma-Aldrich) were used as received. For the SP-M and poly(SP-M) synthesis, dry tetrahydrofuran and dry dichloromethane solvents were purchased from Sigma-Aldrich and used as received. Fused-silica micro-capillaries (100 μm ID, 375 μm OD) were purchased from Polymicro Technologies (Phoenix, AZ, USA). The solvents used for the photo-chromic analyses - toluene, tetrahydrofuran (THF), acetone, acetonitrile (ACN), ethanol (EtOH) and methanol (MeOH), were Sigma-Aldrich HPLC grade, and used without further purification.

7.2.2 Synthesis of Spiropyran Functionalised Norbornene Monomer (SP-M)

The monomer (SP-M) was prepared from the reaction of *exo*-5-norbornyl carboxylic acid with SP1 in the presence of *N,N'*-Dicyclohexylcarbodiimide (DCC) and 4-(Dimethylamino) pyridine (DMAP) [35] as described elsewhere [35, 36]. ^1H NMR (300 MHz, CDCl_3) δ (ppm): 8.05 – 8.01 (m, 2H); 7.22 (t, 1H); 7.12 (d, 1H); 6.94 - 6.90 (m, 2H); 6.78 - 6.76 (d, 1H); 6.73 - 6.71 (d, 1H); 6.15 - 6.14 (m, 1H); 6.09 - 6.06 (m, 1H); 5.93 - 5.90 (d, 1H); 4.32 - 4.11 (m, 2H); 3.57 - 3.39 (m, 2H); 3.00 - 2.91 (m, 2H); 2.19 (s, 1H); 2.19-2.14 (m, 1H); 1.90-1.83 (m, 1H); 1.49 - 1.45 (m, 1H); 1.35 (m, 1H); 1.30 (s, 3H); 1.18 (s, 3H).

7.2.3 *Synthesis of Spiropyran Polymeric Brushes (poly(SP-M))*

Si-ROMP was performed using a modified version of the previously described method [36]. Briefly, prior to functionalisation, the inner surface of the fused-silica micro-capillaries was first activated with 7-octenyl trichlorosilane. The inner capillary surface (internal diameter of 100 μm and 15 cm length) was quickly washed with acetone and water, then flushed with a solution of 0.2 M NaOH for 30 min at a flow rate of 0.25 $\mu\text{L min}^{-1}$ using a syringe pump, and then rinsed with deionised water for 5 times. Next, the micro-capillary was flushed with a solution of 0.2 M HCl for 30 min at a flow rate of 0.25 $\mu\text{L min}^{-1}$, rinsed with water, dry toluene and dried under a N_2 stream. A 0.1 M solution of the silane (7-octenyl trichlorosilane) in dry toluene was pumped through the micro-capillary for 90 min at a flow rate of 0.25 $\mu\text{L min}^{-1}$. The micro-capillary was then washed with acetone, dried under a nitrogen stream, and left at room temperature for 24 h. Later, the micro-capillary was filled with a 0.02 M solution of Grubbs Catalyst Second Generation in degassed CH_2Cl_2 , closed at both ends and put in a water bath for 1 h at 45 $^\circ\text{C}$. After this, the catalyst-attached micro-capillary was thoroughly washed with degassed DCM. Finally, the micro-capillary was exposed to the spiropyran functionalised monomer, SP-M (0.5 M in degassed DCM) at 50 $^\circ\text{C}$ for 1 h. The polymerisation was quenched by passing ethyl vinyl ether into the micro-capillary and finally, it was thoroughly washed with acetone to remove any physisorbed materials.

7.2.4 *Characterisation*

UV-vis spectroscopy for the SP-M solutions in different solvents as well as the kinetic studies of the opening process (SP-M \rightarrow MC-M) were performed using a Cary 50 spectrophotometer (Varian). Morphological studies of poly (SP-M) brushes inside the micro-capillary were performed using scanning electron microscopy (SEM) on a Carl Zeiss EVOLS 15 system at an accelerating voltage of 4.27 kV. The micro-capillaries were cut using a SGT capillary column cutter with rotating diamond blade (Shortix, Nederland) to create a smooth cut of the capillary wall. Then they were placed in vertical position in a custom made metallic capillary holder

that has holes of internal diameters equal to the external diameter of the micro-capillary (375 μm). This set-up allows the micro-capillaries to be kept in vertical position. During the imaging process, the stage was tilted of an angle between 0 – 15° for better imaging of the inner wall of the micro-capillary. Microscopy images of the micro-capillaries were performed on an Aigo digital microscope (The Dolomite Centre Ltd) equipped with a 9X auxiliary objective to give 540X total.

7.2.5 *Light Source*

Photo-conversion of the monomer solutions from SP-M to MC-M was achieved using an in-house fabricated UV light source consisting of three UV LEDs (Roithner LaserTechnik GmbH, emission $\lambda_{\text{max}} = 375 \text{ nm}$). The vials were placed 2 cm from the source and irradiated at a power of 0.4 mW cm^{-2} for 20 s using a 3.75 V supply. The white light irradiation was provided via a LMI-6000 LED Fiber Optic Illuminator obtained from Dolan-Jenner Industries and was used to switch the MC-M monomer solutions and the poly(MC-M) coatings, back to the closed SP-M and poly(SP-M) form, respectively. Also in this case, the vials/capillaries were placed at 2 cm from the light source and were irradiated for 20 s. The maximum light output of the lamp is 780 Lumens, and the intensity control of the light output was fixed at 50 %.

7.2.6 *Photochemical Methods*

UV-Vis Spectroscopy was used to study the solvent dependence of the poly(SP-M) coatings while different solvents were passed through the modified micro-capillary in continuous flow. The absorbance spectra were recorded using two fiber-optic light guides connected to a Miniature Fiber Optic Spectrometer (USB4000 - Ocean Optics) and aligned using a cross-shaped cell (Appendix C - Figure C1). The two fiber-optic light guides were solarization-resistant optical fibers UV/SR-Vis 190-800 nm (aluminum-jacketed, silica-core/silica-clad UV waveguides, 200 μm ID, Ocean Optics). The optical fibers were inserted facing each other across the sample tubing, and secured with t F230 0.015" ID tubing sleeves and fingertight fittings. The light source used was a DH-2000-92 BAL UV-NIR deuterium tungsten halogen source

(Ocean Optics). The six solvents (toluene, tetrahydrofuran, acetone, acetonitrile, ethanol and methanol, respectively) were passed through the micro-capillary at a constant flow rate of $0.5 \mu\text{L min}^{-1}$ using a syringe pump (PHD 2000 Syringe, Harvard Apparatus). Individual absorbance spectra were recorded in-situ after 60 s of irradiation while the kinetics curves for the ring-opening process were obtained by continuously monitoring the absorbance value (acquisition interval of 2 s) for each of the solvents at their characteristic maximum wavelength (λ_{max}) for 190 s, until the absorbance reaches a plateau. The data from the spectrometer were processed using Spectrasuite software provided by Ocean Optics Inc. For better clarity, each recorder absorbance spectra was smoothed using Origin software via the Savitzky-Golay algorithm. A single exponential model (eqn. (1)) was used to determine the ring opening rate constant for the SP-M monomer (see Appendix C) and the poly(SP-M) coatings.

$$y = a (1 - e^{-(kt)}) + b \quad (1)$$

where y is the absorbance at λ_{max} (assumed to be proportional to the concentration of the merocyanine isomer), a is a scaling factor, k is the first order rate constant (s^{-1}), b is the baseline offset and t is time (s).

7.3 Results and Discussion

7.3.1 (SP-M) Polymeric Coatings

Surface-initiated ring-opening metathesis polymerisation (SI-ROMP) of spiropyran norbornene monomers catalysed by Grubbs Catalyst Second Generation has proven to be an efficient method to grow polymer brushes from surfaces [37] and micro-capillaries [36]. This polymerisation technique, allows a 3D arrangement of polymer brushes to be obtained (Figure 7.2), which is very desirable when building micro-capillary-integrated optical sensors, as high concentrations of the sensing unit are necessary to compensate for the micrometre size path length.

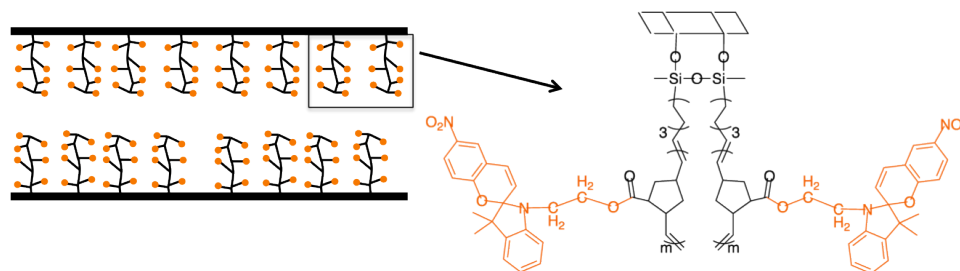


Figure 7.2. Representation of the fused silica micro-capillary functionalised with spiropyran polymeric brushes.

Clear improvements have been obtained when comparing with the previously reported method published by us [36], in the case of poly(SP-M) micro-capillary coatings, by using *exo*-norbornene carboxylic acid as the starting material for the production of the spiropyran *exo*-norbornene monomer (SP-M), instead of a mixture of *exo*- and *endo*- isomers. Several reports on the ROMP of other norbornene derivatives have shown that *exo*- isomers often react faster than the corresponding *endo*- one. The steric interactions between the growing polymer chain and the incoming monomers appear to be the primary cause of this reactivity difference [38]. The time for polymerisation was fixed to one hour. These new conditions allowed better control over the grafting density and therefore more homogenous coatings were obtained along the entire length of the micro-capillary (contrary to the previously reported method). Scanning electron microscopy of the inner wall of the micro-capillary showed a 3D arrangement of the polymer brushes with a thickness of about 2-3 μm as shown in Figure 7.3, thicker than in the previously reported method (1 -2 μm). These results show that by using only the *exo*- isomer of SP-M, both coating homogeneity and thickness are greatly improved while the polymerisation time is reduced to one hour.

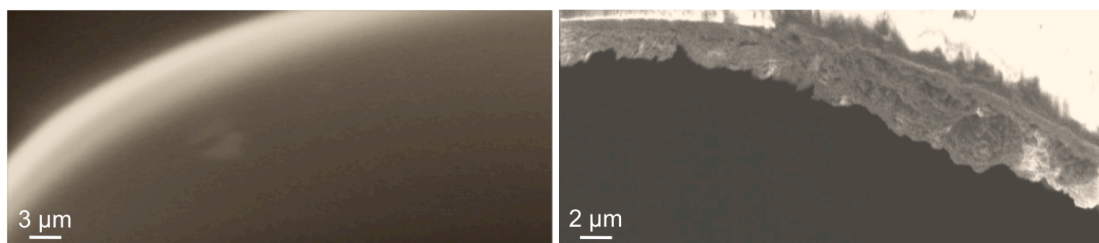


Figure 7.3. Scanning Electron Microscopy (SEM) images of the inner wall of a fused silica micro-capillary before (left) and after (right) functionalisation with spiropyran polymeric brushes.

7.3.2 Solvent Sensing

The solvatochromic properties of SP-M monomer and poly(SP-M) brushes were tested using six solvents of differing polarities: toluene (relative polarity ($p' = 0.099$)) [22], THF ($p' = 0.207$) [22], acetone ($p' = 0.355$) [22], ACN ($p' = 0.460$) [22], EtOH ($p' = 0.654$) [22] and MeOH ($p' = 0.762$) [22].

As previously described, the coloured MC form is well known to undergo solvatochromism [21, 29, 39, 40]. Solvatochromism refers to a strong dependence of the UV-vis absorption bands of a compound on the polarity of the solvent medium. This typically manifests as changes in the position, and intensity of the absorption bands of the molecule when measured in different solvents. These changes are caused by intermolecular interactions between the solute and the solvent, modifying the energy gap between the ground and excited state of the absorbing species. The colour of the MC form depends on the difference in polarity between the photo-excited MC form and the conjugated zwitterionic ground state. The coloured MC form is highly conjugated and characterised by a strong polar character, due to its zwitterionic structure, which strongly contributes to the electronic distribution of the ground state. As a consequence, the ground state of the MC form is stabilised in polar solvents relative to the excited state, leading to larger energy gap than in nonpolar solvents. In non-polar solvents, the energy difference between the ground and the excited state is much lower, because of the high energy level of the ground state. As a result, as the polarity of the solvent increases, the maximum absorbance shifts to shorter wavelengths, higher frequency (hypsochromic or blue shift), while as the polarity decreases the maximum absorbance shifts to longer wavelengths, lower frequency (bathochromic or red shift). When, for instance, a solution of SP-M (10^{-3} M) is irradiated with UV light in MeOH, EtOH, ACN, acetone, THF and toluene (Figure 7.4), the solution shows a strong colour change – from pink to blue. This colour disappears after irradiation of the solution with white light, since the MC form reverts to the non-solvatochromic SP form, and the solution becomes colourless. This behaviour shows that the SP-M monomer inherits the photochromic and solvatochromic properties of the reactant SP1, well known for its solvatochromic properties [21, 29, 39, 40].

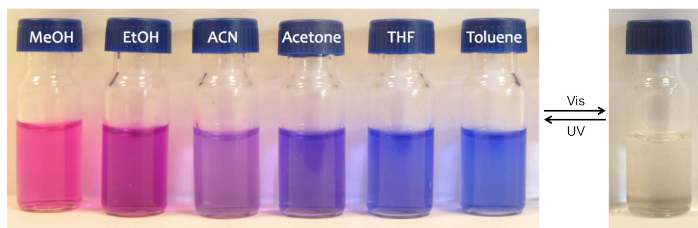


Figure 7.4. Pictures of six vials (left) containing a solution of the SP-M monomer (10^{-3} M) when irradiated for 20 s with UV light in different solvents and after irradiation with white light for 20 s (right).

As seen from Figure 7.5, the absorbance spectra of the monomer open form (MC-R) shows that the λ_{max} of MC-M undergoes red and blue shifts depending on the solvent polarity. Among the solvents analysed, the lowest λ_{max} value was found in the presence of MeOH (540 nm). This value increases to 552 nm in EtOH, 568 in ACN, and 574 nm in acetone, which indicates a significantly more non-polar environment. The highest values are observed for THF (587 nm) and toluene (609 nm) (Figure 7.5). In the absorbance spectra of the MC-M in toluene a shoulder around 565 nm is clearly defined. This can be attributed to the presence of MC aggregates which are known to form in certain non-polar solvents under UV-irradiation [7, 41]. In general two types of aggregates have been identified: *J*-aggregates which have parallel arrangement and present a shift to longer wavelengths, while *H*-aggregates have a head to tail arrangement of the MC dipoles and the spectra are shifted to shorter wavelengths irradiation [7, 41].

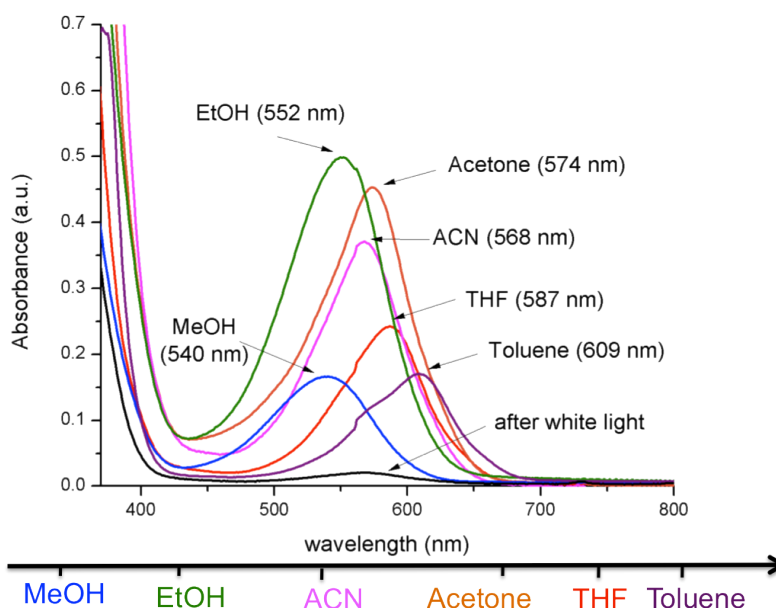


Figure 7.5. Absorption spectra of the SP-M monomer (10^{-3} M) solution in MeOH, EtOH, ACN, acetone, THF and toluene after UV and white light irradiation.

Analysing the absorbance shifts presented by the MC-M isomer in the six different solvents, it was observed that they are in perfect agreement with the Reichardt's empirical $E_T(30)$ polarity scale described in the "Solvents and Solvent Effects in Organic Chemistry" [22]. This scale is based on the solvent-dependent spectral shifts experienced by pyridinium *N*-phenoxide betaine dye $E_T(30)$ and has been shown to take into consideration both the polarity and the hydrogen bond donating acidity of the solvent [22]. The absorption λ_{\max} of the MC-M in different solvents was found to give good linear correlations with the normalised $E_T(30)$ ($R^2 = 0.97$), similarly with other reported spiropyran derivatives [29] (Figure 7.6). Good correlation between the solvatochromic behaviours of the two was expected as both merocyanines and $E_T(30)$ are meropolymethines dyes. The negative slopes of the plots indicate that in polar solvents, the ground state of the MC form is stabilised relatively to the excited state (lower wavelengths means larger energy gap between the ground and excited state) while the linear fit implies that there is a hydrogen bond contribution to this effect [29].

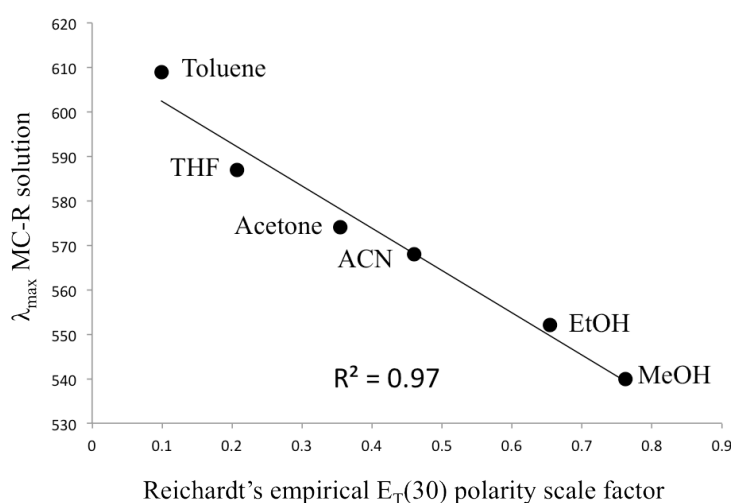


Figure 7.6. Linear correlation between Reichardt's empirical $E_T(30)$ polarity scale factor and the absorption λ_{\max} of SP-M monomeric solutions (10^{-3} M) in different solvents.

When the six different solvents are passed through the micro-capillary functionalised with SP-M polymeric brushes at a flow rate of $0.5 \mu\text{L min}^{-1}$ followed by the exposure of the micro-capillary to UV light (20 s), the colour of the micro-capillary changes according to the polarity of the solvent, from red (highly polar) towards blue (highly non-polar), following a similar behaviour to the SP-M

monomer solutions (Figure 7.7). Moreover, when the micro-capillary is exposed to white light irradiation (20 s), it returns to the initial colourless spiropyran form, Figure 7.7-bottom. This demonstrates that in the polymer brush structures, which are densely packed with spiropyran moieties, there is no evidence of steric hindrance of the characteristic SP to MC photo-switching in response to UV and white light irradiation, and that the merocyanine unit maintains its solvatochromic properties intact.

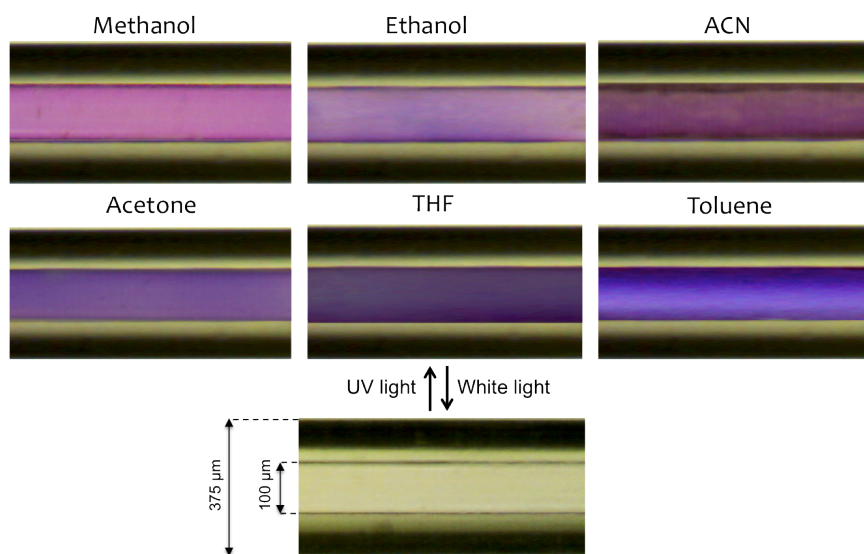


Figure 7.7. Pictures of the poly(SP-M) coated micro-capillary when irradiated for 20 s with UV light while different solvents are passed through the micro-capillary in continuous flow ($0.5 \mu\text{L min}^{-1}$) and after irradiation with white light for 20 s.

UV-vis spectra of the polymer brushes were taken using the set-up described in the Appendix C, Figure C1, permitting *in situ* spectroscopic characterisation of the coatings inside the micro-capillary. When in the merocyanine form, the polymer coatings show an absorbance band with a λ_{max} of 558 nm when the solvent is MeOH, 565 nm in the case of EtOH, 567 nm for ACN, 571 nm for acetone, 575 nm for THF and 576 nm for toluene, respectively (Figure 7.8). Therefore, the poly(SP-M) coatings indicate negative solvatochromism, similar to that shown by the SP-M monomer in solution. These absorption bands disappear after irradiation of the micro-capillary with white light for 20 s due to interconversion to the non-solvatochromic spiropyran form. This process is completely reversible, implying that the platform can be switched between sensing and non-sensing modes entirely using light [36]. The shift of the λ_{max} in the absorption spectra of the polymer brushes

compared to that of the monomer in solution is most likely due to the local environmental effects that are related to the immobilisation of the spiropyran moiety [42] and to the swelling effect of the polymer brushes when in presence of different solvents [43]. It can be explained taking into account the compact organisation of spiropyran units in the polymer brushes, wherein the conformation of a single spiropyran moiety is not only influenced by the solvent but also by the neighbouring spiropyran units that may be present in their polar merocyanine form. The lower dynamic range of the λ_{\max} in the case of polymeric brushes compared with the SP in solution is most probably due to the architecture of the coating and can be explained by taking into consideration two factors: the much higher concentration of spiropyran units inside the polymeric brushes compared with the solution as well as steric hindrances inside the coating, that restricts the conformational freedom of the spiropyran moiety. Nevertheless, the shifts in the absorption λ_{\max} of the poly(SP-M) coatings are also, in this case, in good agreement with the Reichardt's empirical $E_T(30)$ polarity scale, showing reasonably good linear correlations between the absorption λ_{\max} of the poly(SP-M) coatings and the normalised $E_T(30)$, just like in the case of SP-M solutions ($R^2 > 0.95$) (Figure 7.9).

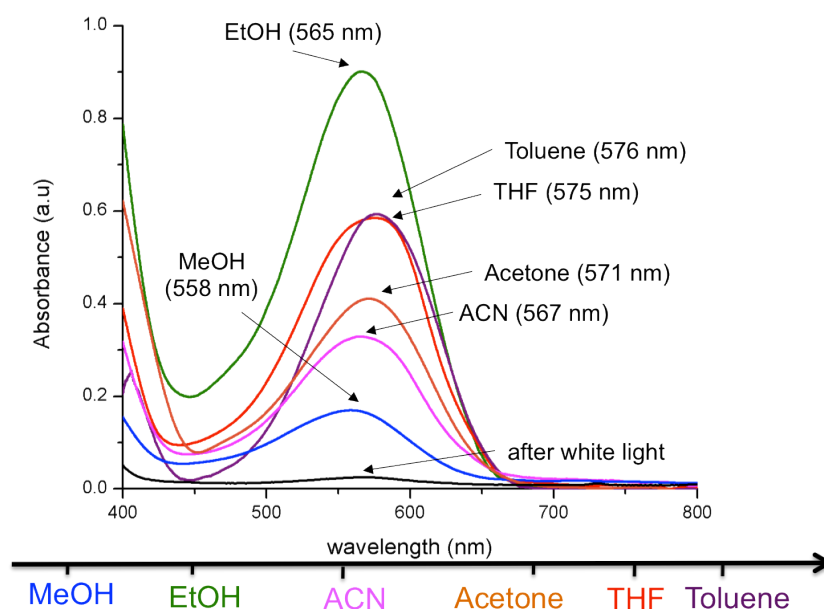


Figure 7.8. Absorption spectra of the poly(SP-M) functionalised capillary when MeOH, EtOH, ACN, acetone, THF and toluene, respectively are passed through the micro-capillary, after UV and white light irradiation.

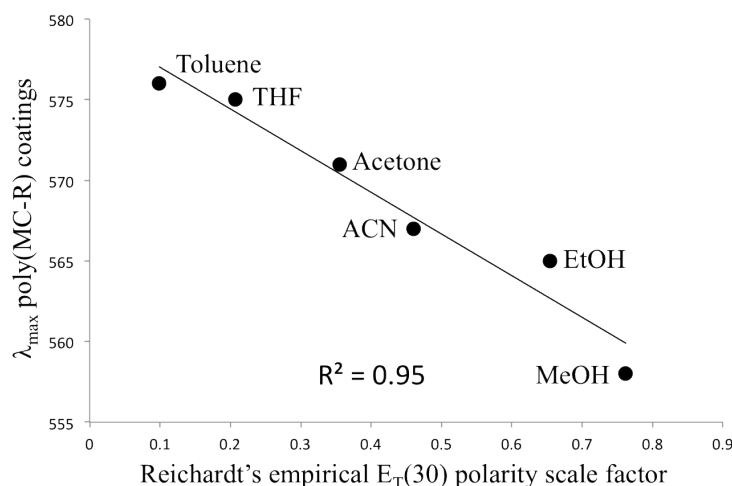


Figure 7.9. Linear correlation between Reichardt's empirical $E_T(30)$ polarity scale factor and the absorption λ_{\max} of poly(SP-M) coatings in the presence of different solvents.

These results indicate that poly(SP-M) coated micro-capillary could be used for the detection of solvents of different polarities based on the colour (absorption λ_{\max}) of the micro-capillary after UV irradiation. This is the first time such a micro-capillary integrated polarity sensor has been reported, capable of performing in continuous flow mode. Moreover, this sensing behaviour can be switched on/off remotely by using light, either along the entire length of the micro-capillary, or at patterned locations using appropriate masks [36]. In addition, these colour changes could be easily quantified using digital image processing techniques [44, 45], or by simple visual observation.

7.3.3 Kinetics of Photo-induced Ring Opening

As the system described in Figure C1 (Appendix C) allows in-situ monitoring of the ring opening process of the poly(SP-M) coatings, kinetic studies were performed in order to evaluate how the different solvents may affect the ring opening kinetics of the poly(SP-M) and so, provide an additional parameter for solvent sensing. This involved, inducing the formation of the poly(MC-M) state by continuous exposure of the micro-capillary to UV light and recording the absorbance value of the MC-M, at the corresponding λ_{\max} in each solvent at fixed time intervals (1 s), until the absorbance value reaches a plateau (approximately 180 s). During these measurements, the micro-capillary is kept in a fixed position, in the dark, inside the

cross-shaped detection cell as shown in Figure C1 (Appendix C) in order to avoid the influence of the ambient light.

The λ_{max} absorbance values in each solvent were obtained from Figure 7.8 and modelled according to eqn. (1). Figure 7.10 shows the absorbance increase over time at the λ_{max} (293 K) for each of the solvents (MeOH, EtOH, ACN, acetone, THF and toluene, respectively) for the poly(SP-M) coating, using the first-order kinetics model [46]. The first-order rate constants were estimated by fitting the absorbance values at λ_{max} using Microsoft Excel Solver and eqn.(1). All the ring-opening kinetics were estimated in triplicate, and at different locations on the micro-capillary, for all the six solvents, showing great reproducibility (See Appendix C– Figure C2). Moreover, the fact that the absorbance at λ_{max} stabilises at the same absorbance values in different positions on the micro-capillary for each individual solvent, demonstrates the excellent homogeneity of the coatings.

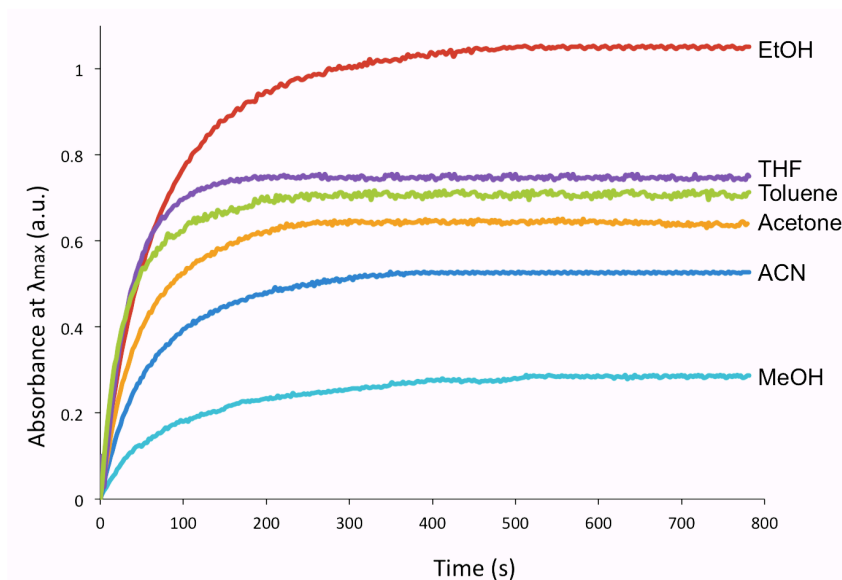


Figure 7.10. Ring opening kinetics of the spiropyran polymeric coatings in different solvents showing the conversion of poly(SP-M) to poly(MC-M). The values of the absorbance were taken at $\lambda_{\text{max}} = 558$ nm for MeOH, $\lambda_{\text{max}} = 565$ nm for EtOH, $\lambda_{\text{max}} = 567$ nm for ACN, $\lambda_{\text{max}} = 571$ nm for acetone, $\lambda_{\text{max}} = 575$ nm for THF and $\lambda_{\text{max}} = 576$ nm for toluene at 293 K.

The ring opening process analysed using eqn. (1) occurs about 1.3 times faster for EtOH compared to MeOH and about 1.5 times faster for ACN and acetone compared to MeOH. The fastest ring-opening kinetics were obtained for THF and toluene at about 2.7 and 2.8 times faster, respectively, than in MeOH. Under these

conditions, the ring opening kinetics of poly(SP-M) show that for poly(MC-M) formation in toluene, the steady-state (ca. 0.7 a.u.) is reached in about 200 s while for the formation of poly(MC-M) steady-state in Acetone and ACN, the absorbance becomes relatively constant at *ca.* 0.6 a.u. and 0.5 a.u. after about 300 and 400 s, respectively. This may be due to the faster ring-opening rate obtained in non-polar solvents compared to polar solvents. Although the influence of the solvent on the ring-opening kinetics has been considered to be weak [39], in the present circumstances, the pattern that emerges is clear and convincing: as the polarity of the solvent decreases the rate of the ring opening process increases. A possible explanation for this behaviour lies in the mechanism of the ring-opening of the spiropyran moiety itself. The interconversion between SP and MC involves an intermediate, which is formed as the bond between the spiro carbon atom and the pyran oxygen atom is ruptured while the orthogonal topology is retained. As shown before, this step is the rate-determining step in the coloration reaction (SP to MC) [40]. As the intermediate, a *cis-cisoid* isomer of MC, has a non-polar character, it is expected to be stabilised in less polar solvents causing faster ring-opening kinetics in solvents of decreasing polarity. Further indications supporting this statement have been found by comparing the ring opening kinetics of poly(SP-M) coatings with the ring opening kinetics of SP-M in solution (See Appendix C – Figure C3). The ring-opening process in solution also followed first order kinetics, and therefore the first-order rate constants were estimated by fitting the absorbance values at λ_{max} using Microsoft Excel Solver via eqn. (1) (See Appendix C – Figure C4). The results obtained for the SP-M in solution are in close agreement with those obtained for the poly(SP-M) coatings, reinforcing the view that the ring-opening rate increases as the solvent polarity decreases (See Appendix C – Table C1). The estimated rate of ring opening of SP-M to MC-M in solution is about 1.1 times higher for EtOH compared to MeOH and about 3 times higher for acetone compared to ACN. The fastest ring-opening kinetics were obtained for THF and toluene where the SP-M coloration occurs approximately 2.5 times faster in toluene than in THF. Table 7.1 lists the solvents and values of the relevant solvent polarity scales used for the analysis of the solvatochromic behavior of the poly(SP-M) coatings.

Table 7.1. poly(MC-M) λ_{max} values in different solvents reported together with the normalised Reichardt's empirical $E_{\text{T}}(30)$ polarity scale factor. These values are followed by the rate constants (\pm absolute error, $n = 3$), for the ring opening equilibrium obtained from the best-fit curves of the absorbance-time curves (Figure C2, Appendix C) recorded at the corresponding poly(MC-M) λ_{max} in each solvent.

| Solvent | $E_{\text{T}}(30)$ | λ_{max} (nm) | k (s^{-1}) |
|----------|--------------------|--------------------------------|--|
| Methanol | 0.762 | 558 | $1.04 \times 10^{-2} \pm 0.9 \times 10^{-3}$ |
| Ethanol | 0.654 | 565 | $1.34 \times 10^{-2} \pm 0.3 \times 10^{-3}$ |
| ACN | 0.460 | 567 | $1.52 \times 10^{-2} \pm 0.8 \times 10^{-3}$ |
| Acetone | 0.355 | 571 | $1.56 \times 10^{-2} \pm 1.8 \times 10^{-3}$ |
| THF | 0.207 | 575 | $2.73 \times 10^{-2} \pm 1.1 \times 10^{-3}$ |
| Toluene | 0.099 | 576 | $2.84 \times 10^{-2} \pm 1.7 \times 10^{-3}$ |

7.4 Conclusions

Spiropyran based polymer brushes grafted onto the inner walls of a micro-capillary have been used for rapid and sensitive solvent polarity detection. The micro-capillary can be functionalised in a highly homogeneous manner along its entire length since the functionalisation is performed in a continuous flow mode. We have demonstrated the feasibility of a self-diagnosing tool for sensing based on a micro-capillary, which can be operated in continuous flow, and is capable of detecting and reporting variations in the local polarity of the medium in contact with the spiropyran polymeric coatings of the micro-capillary through changes in the surface coating. *In-situ* ring-opening kinetics of the spiropyran polymeric coatings have demonstrated highly reproducible performance of the coatings while the rate constant of the ring-opening process have been shown to be influenced by the solvent polarity and could serve as an additional parameter for solvent sensing. ROMP chemistry provides a route to the formation of rather thick, yet highly open brush-type coatings with high SP-M loading, which provide the basis for colourimetric measurements that combine

high sensitivity with rapid kinetics. The photoswitchable nature of the sensing molecule means that this function can be turned on/off in a temporal and spatially controllable manner using UV/visible light, respectively.

Acknowledgment

The project has been carried out with the support of the Irish Research Council (IRC) - Embark Initiative and Science Foundation Ireland under the CLARITY award (07/CE/ I1147).

Appendix C. Supporting Information

A schematic of the set-up used for absorbance and kinetics measurements for the poly(SP-M) capillary coatings is provided (Figure C1) as are experimental and fitted kinetic curves of the photo-induced ring opening of poly(SP-M) coatings in different solvents (Figure C2). Kinetics of photo-induced ring opening equilibrium of SP-M monomer in solution - experimental and fitted kinetic curves are given (Figures C3 and C4) along with associated values of the rate constants, for the photo-induced ring opening process of SP-M monomer solutions (10^{-3} M), in different solvents (Table C1). This material is available free of charge via the Internet at <http://pubs.acs.org>.

7.5 References

1. Weigl, B. H.; Wolfbeis, O. S., Capillary optical sensors. *Analytical Chemistry* **1994**, *66*, 3323-3327.
2. Kuswandi, B.; Narayanaswamy, R., Capillary optode: Determination of mercury(II) in aqueous solution. *Analytical Letters* **1999**, *32*, 649-664.
3. Kuswandi, B.; Narayanaswamy, R., Polymeric encapsulated membrane for optrodes. *Fresenius Journal of Analytical Chemistry* **1999**, *364*, 605-607.
4. Buchholz, F.; Buschmann, N.; Cammann, K., A fiberoptic sensor for the determination of sodium with a reversible response. *Sensors and Actuators B-Chemical* **1992**, *9*, 41-47.
5. Fischer, E.; Hirshberg, Y., Formation of coloured forms of spirans by low-temperature irradiation. *Journal of the Chemical Society* **1952**, 4522-4524.
6. Zhu, M. Q.; Zhu, L. Y.; Han, J. J.; Wu, W. W.; Hurst, J. K.; Li, A. D. Q., Spiropyran-based photochromic polymer nanoparticles with optically switchable luminescence. *Journal of the American Chemical Society* **2006**, *128*, 4303-4309.
7. Minkin, V. I., Photo-, thermo-, solvato-, and electrochromic spiroheterocyclic compounds. *Chemical Reviews* **2004**, *104*, 2751-2776.
8. Uchida, K.; Takata, A.; Saito, M.; Murakami, A.; Nakamura, S.; Irie, M., A novel photochromic film by oxidation polymerization of a bisbenzothienylethene with phenol groups. *Advanced Materials* **2003**, *15*, 785-788.

9. Zhang, Y.; Shao, N.; Yang, R.; Li, K. a.; Liu, F.; Chan, W.; Mo, T., Utilization of a spiropyran derivative in a polymeric film optode for selective fluorescent sensing of zinc ion. *Science in China Series B-Chemistry* **2006**, *49*, 246-255.
10. Ma, Y.; Niu, C.; Wen, Y.; Li, G.; Wang, J.; Li, H.; Du, S.; Yang, L.; Gao, H.; Song, Y., Stable and reversible optoelectrical dual-mode data storage based on a ferrocenylspiropyran molecule. *Applied Physics Letters* **2009**, *95*, 183307.
11. Vollmer, H. P., Investigations on quantum yield and stability of coloration of uv-sensitive spiropyran layers used as a recording material for optical data storage. *Zeitschrift Fur Naturforschung Section a-a Journal of Physical Sciences* **1975**, *30*, 1425-1432.
12. Bobrovsky, A. Y.; Boiko, N. I.; Shibaev, V. P., Photosensitive cholesteric copolymers with spiropyran-containing side groups: Novel materials for optical data recording. *Advanced Materials* **1999**, *11*, 1025-1028.
13. Jiang, G.; Song, Y.; Guo, X.; Zhang, D.; Zhu, D., Organic functional molecules towards information processing and high-density information storage. *Advanced Materials* **2008**, *20*, 2888-2898.
14. Tian, H.; Feng, Y., Next step of photochromic switches? *Journal of Materials Chemistry* **2008**, *18*, 1617-1622.
15. Hirshberg, Y., Reversible formation and eradication of colors by irradiation at low temperatures - a photochemical memory model. *Journal of the American Chemical Society* **1956**, *78*, 2304-2312.
16. Berkovic, G.; Krongauz, V.; Weiss, V., Spiroyrans and spirooxazines for memories and switches. *Chemical Reviews* **2000**, *100*, 1741-1753.
17. Preigh, M. J.; Stauffer, M. T.; Lin, F. T.; Weber, S. G., Anodic oxidation mechanism of a spiropyran. *Journal of the Chemical Society-Faraday Transactions* **1996**, *92*, 3991-3996.
18. Zhu, J.-F.; Yuan, H.; Chan, W.-H.; Lee, A. W. M., A colorimetric and fluorescent turn-on chemosensor operative in aqueous media for Zn(2+) based on a multifunctionalized spirobenzopyran derivative. *Organic & Biomolecular Chemistry* **2010**, *8*, 3957-3964.
19. Rosario, R.; Gust, D.; Hayes, M.; Jahnke, F.; Springer, J.; Garcia, A. A., Photon-modulated wettability changes on spiropyran-coated surfaces. *Langmuir* **2002**, *18*, 8062-8069.
20. Benito-Lopez, F.; Scarmagnani, S.; Walsh, Z.; Paull, B.; Macka, M.; Diamond, D., Spiropyran modified micro-fluidic chip channels as photonically controlled self-indicating system for metal ion accumulation and release. *Sensors and Actuators B-Chemical* **2009**, *140*, 295-303.
21. Keum, S. R.; Hur, M. S.; Kazmaier, P. M.; Buncel, E., Thermochromic and photochromic dyes - indolino-benzospiropyrans .1. uv-vis spectroscopic studies of 1,3,3-spiro(2H-1-benzopyran-2,2'-indolines) and the open-chain merocyanine forms - solvatochromism and medium effects on spiro ring formation. *Canadian Journal of Chemistry-Revue Canadienne De Chimie* **1991**, *69*, 1940-1947.
22. Reichardt, C., *Solvents and Solvent Effects in Organic Chemistry*. Fourth Edition ed.; Wiley-VCH Verlag GmbH & Co. KGaA: 2010.
23. Murugan, N. A.; Chakrabarti, S.; Agren, H., Solvent Dependence of Structure, Charge Distribution, and Absorption Spectrum in the Photochromic Merocyanine-Spiropyran Pair. *Journal of Physical Chemistry B* **2011**, *115*, 4025-4032.
24. Botrel, A.; Aboab, B.; Corre, F.; Tonnard, F., A theoretical investigation of solvatochromism - application to merocyanines similar to colored forms obtained by flash-photolysis of spiropyrans. *Chemical Physics* **1995**, *194*, 101-116.
25. Shirinian, V. Z.; Besugliy, S. O.; Metelitsa, A. V.; Krayushkin, M. M.; Nikalin, D. M.; Minkin, V. I., Novel photochromic spirocyclic compounds of thienopyrroline series: 1 Spiropyrans. *Journal of Photochemistry and Photobiology a-Chemistry* **2007**, *189*, 161-166.

26. Keum, S.-R.; Roh, S.-J.; Ahn, S.-M.; Lim, S.-S.; Kim, S.-H.; Koh, K., Solvatochromic behavior of non-activated indolinobenzospiropyran 6-carboxylates in aqueous binary solvent mixtures. Part II. *Dyes and Pigments* **2007**, *74*, 343-347.
27. Byrne, R.; Coleman, S.; Gallagher, S.; Diamond, D., Designer molecular probes for phosphonium ionic liquids. *Physical Chemistry Chemical Physics* **2010**, *12*, 1895-1904.
28. Byrne, R.; Coleman, S.; Fraser, K. J.; Raduta, A.; MacFarlane, D. R.; Diamond, D., Photochromism of nitrobenzospiropyran in phosphonium based ionic liquids. *Physical Chemistry Chemical Physics* **2009**, *11*, 7286-7291.
29. Rosario, R.; Gust, D.; Hayes, M.; Springer, J.; Garcia, A. A., Solvatochromic study of the microenvironment of surface-bound spiropyranes. *Langmuir* **2003**, *19*, 8801-8806.
30. Bosch Ojeda, C.; Sanchez Rojas, F., Recent development in optical chemical sensors coupling with flow injection analysis. *Sensors* **2006**, *6*, 1245-1307.
31. Florea, L.; Diamond, D.; Benito-Lopez, F., Polyaniline Coated Micro-capillaries for Continuous Flow Analysis of Aqueous Solutions. *Analytica Chimica Acta*.
32. Gonzalez-de los Santos, E. A.; Lozano-Gonzalez, M. J.; Johnson, A. F., Photoresponsive polyurethane-acrylate block copolymers. I. Photochromic effects in copolymers containing 6'-nitro spiropyranes and 6'-nitro-bis-spiropyranes. *Journal of Applied Polymer Science* **1999**, *71*, 259-266.
33. Marsella, M. J.; Wang, Z. Q.; Mitchell, R. H., Backbone photochromic polymers containing the dimethyldihydropyrene moiety: Toward optoelectronic switches. *Organic Letters* **2000**, *2*, 2979-2982.
34. Guo, X. F.; Zhang, D.; Gui, Y.; Wax, M. X.; Li, J. C.; Liu, Y. Q.; Zhu, D. B., Reversible photoregulation of the electrical conductivity of spiropyran-doped polyaniline for information recording and nondestructive processing. *Advanced Materials* **2004**, *16*, 636-640.
35. Keum, S.-R.; Ahn, S.-M.; Roh, S.-J.; Ma, S.-Y., The synthesis and spectroscopic properties of novel, photochromic indolinobenzospiropyran-based homopolymers prepared via ring-opening metathesis polymerization. *Dyes and Pigments* **2010**, *86*, 74-80.
36. Florea, L.; Hennart, A.; Diamond, D.; Benito-Lopez, F., Synthesis and characterisation of spiropyran-polymer brushes in micro-capillaries: Towards an integrated optical sensor for continuous flow analysis. *Sensors and Actuators B: Chemical* **2012**, *175*, 92-99.
37. Samanta, S.; Locklin, J., Formation of photochromic spiropyran polymer brushes via surface-initiated, ring-opening metathesis polymerization: Reversible photocontrol of wetting behavior and solvent dependent morphology changes. *Langmuir* **2008**, *24*, 9558-9565.
38. Rule, J. D.; Moore, J. S., ROMP reactivity of endo- and exo-dicyclopentadiene. *Macromolecules* **2002**, *35*, 7878-7882.
39. Zhou, J. W.; Li, Y. T.; Tang, Y. W.; Zhao, F. Q.; Song, X. Q.; Li, E. C., Detailed investigation on a negative photochromic spiropyran. *Journal of Photochemistry and Photobiology a-Chemistry* **1995**, *90*, 117-123.
40. Song, X. Q.; Zhou, J. W.; Li, Y. T.; Tang, Y. W., Correlations between solvatochromism, Lewis acid-base equilibrium and photochromism of an indoline spiropyran. *Journal of Photochemistry and Photobiology a-Chemistry* **1995**, *92*, 99-103.
41. Uznanski, P., UV-assisted formation of nanoaggregates from photochromic spiropyranes in nonpolar solvents. *Langmuir* **2003**, *19*, 1919-1922.
42. Fries, K. H.; Driskell, J. D.; Samanta, S.; Locklin, J., Spectroscopic Analysis of Metal Ion Binding in Spiropyran Containing Copolymer Thin Films. *Analytical Chemistry* **2010**, *82*, 3306-3314.

- 43. Kong, B.; Lee, J. K.; Choi, I. S., Surface-initiated, ring-opening metathesis polymerization: Formation of diblock copolymer brushes and solvent-dependent morphological changes. *Langmuir* **2007**, *23*, 6761-6765.
- 44. Byrne, L.; Barker, J.; Pennarun-Thomas, G.; Diamond, D.; Edwards, S., Digital imaging as a detector for generic analytical measurements. *Trac-Trends in Analytical Chemistry* **2000**, *19*, 517-522.
- 45. Fay, C.; Lau, K.-T.; Beirne, S.; Conaire, C. O.; McGuinness, K.; Corcoran, B.; O'Connor, N. E.; Diamond, D.; McGovern, S.; Coleman, G.; Shepherd, R.; Alici, G.; Spinks, G.; Wallace, G., Wireless aquatic navigator for detection and analysis (WANDA). *Sensors and Actuators B-Chemical* **2010**, *150*, 425-435.
- 46. Zanoni, M.; Coleman, S.; Fraser, K. J.; Byrne, R.; Wagner, K.; Gambhir, S.; Officer, D. L.; Wallace, G. G.; Diamond, D., Physicochemical study of spiropyran-terthiophene derivatives: photochemistry and thermodynamics. *Physical Chemistry Chemical Physics* **2012**, *14*, 9112-9120.

Chapter 8

Photo-activated Chemopropulsion of Organic Droplets

Larisa Florea ¹, Klaudia Wagner ², Pawel Wagner ², David L. Officer ^{2*},
Gordon W. Wallace ², Fernando Benito-Lopez^{1,3*} and
Dermot Diamond¹

Manuscript in preparation

¹CLARITY: Centre for Sensor Web Technologies, National Centre for Sensor Research, School of Chemical Sciences, Dublin City University, Dublin, Ireland;

² ARC Centre of Excellence for Electromaterials Science and Intelligent Polymer Research Institute University of Wollongong, Wollongong, NSW 2522, Australia

³CIC microGUNE, Arrasate-Mondragón, Spain, Tel.: +34 943710212

*Authors to whom correspondence should be addressed;

Abstract: Photo-activated chemopropulsion at the liquid/liquid interface is a new concept in droplet actuation that involves the photo-generation of surface tension gradients high enough to cause rapid propulsion of organic liquid droplets present on the surface of an aqueous solution. The “fuel” of the propulsion is a gradient in surface tension, generated by the local release of surfactants from the droplet to the aqueous solution upon photo-stimulation. The propulsion type movement presented here involves high-speed movements of organic droplets ($\sim 4000 \mu\text{m s}^{-1}$), 14 times faster than any other photo-induced movement of droplets reported previously. In addition, this movement is reversible, and since it is based on surface tensions effects can be used for the manipulation of multiple droplets simultaneously.

Keywords: chemopropulsion, photo-manipulation, surface tension, photochemistry, pH gradient

8.1 Introduction

The idea of developing inanimate chemical machineries capable of propulsion upon photo-stimulation could open a new area of research due to their potential applicability in fields like microfluidics [1, 2], cargo transport [3-5] and drug-delivery [6]. The possibility of using photo-stimulus to control directional movement of microliter size droplets is very appealing, as light can provide contactless stimulation, is biocompatible and can be applied in a non-invasive and highly precise manner. The most common strategy toward this goal uses solid surfaces with specific photosensitive properties able to produce changes in wettability or surface tension upon photo-stimulation [7]. When a liquid droplet is deposited on such substrates, asymmetrical illumination by light induces a gradient of wettability that results in a low-speed motion (*ca.* $35 \mu\text{m s}^{-1}$) of the droplet over distances of about 3 mm [7]. Other approach [8] involves the photo-induced movement of oil droplets on aqueous solutions containing photo-sensitive surfactants. In this approach, a 3 μL oleic acid droplet is photo-manipulated at the surface of an aqueous solution containing the cationic photosensitive azobenzene trimethylammonium bromide surfactant (AzoTAB). The apolar tail of AzoTAB contains a photosensitive azobenzene group, which photoisomerises into *trans* (less polar) and *cis* (more polar) configurations upon visible and UV light illumination, respectively. This photo-dependent polarity allows the interfacial tension between the floating oil droplet and the aqueous solution to be modulated, thus inducing an interfacial tension gradient at the liquid (aq.)/liquid (oil) interface, which results in droplet motion in the opposite direction to the gradient. Under these conditions, droplet motions with speeds of about $300 \mu\text{m s}^{-1}$ can be obtained. Although this process is reversible and allows precise photo-manipulation of oil droplets, the photo-induced difference in surface tension is rather small, *ca.* 1 mN m^{-1} . Thus for continuous droplet movement the light source must follow the droplet in order to maintain an acceptable interfacial tension gradient. Herein, this chapter describes a new concept that can be used for the photo-manipulation of liquid droplets within open channels at high speeds ($\sim 4000 \mu\text{m s}^{-1}$).

8.2 Materials and Methods

8.2.1 Materials

The spiropyran sulfonic acid (SP-SO₃H) was synthesised by sulfonation of *N*-(2-hydroxybenzylidene) aniline according to a previously reported method [9].

8.2.2 Channel Fabrication

The fabrication of the channels was carried out using a laser ablation system-excimer/CO₂ laser (Optec Laser Micro-machining Systems, Belgium) by cutting the fluidic structures in a 1 mm polymethylmethacrylate (PMMA) sheet attached to a 50 µm double-sided pressure sensitive adhesive film, PSA, (AR8890, Adhesives Research, Ireland). After the channels removal, the PSA protective layer was detached and the PMMA/PSA template was laminated with another 1 mm PMMA sheet or subsequently replicated into poly(dimethyl siloxane) (PDMS, Sylgard 184, Dow Corning, Michigan USA). The channels obtained were 2 mm wide, 1 mm high and were filled with 1 mM solution of spiropyran sulfonic acid (SP-SO₃H) in deionised water.

8.3 Results and Discussion

The photo-activated chemopropulsion of the organic droplet on the aqueous solution is powered by the combination of photo-induced pH changes and surface tension gradients at the liquid/liquid interface and can be used for simultaneous manipulation of multiple droplets. Generation of photo-activated chemopropulsion involves the following steps:

- initial conditions: droplet formulation is stable on the aqueous solution which has a predetermined pH value.
- local pH of the aqueous solution decreases upon photo-stimulation;

- the pH decrement induces localised release of a surfactant type molecules (“fuel”) from the organic droplet to the aqueous solution in the low pH region;
- the release of the surfactants causes a spontaneous drop in the surface tension, enough to propel the droplet in the opposite direction, as dictated by the generated surface tension gradient;
- the droplet stops when it reaches a region of higher pH, similar to the initial conditions, under which the initial state of the droplet is re-established.

To achieve the conditions for photo-activated propulsion mechanism presented above, the following formulations for the aqueous solution and the organic droplet were developed.

The aqueous solution contains a spiropyran derivative dissolved in deionised (DI) water (10^{-3} M). Spiropyrans are one of the most useful photochromic compounds due to their applicability in various fields like data recording and storage [10, 11], optical switching displays [10], liquid crystals [12] and sensing technologies [13]. The photochromism of spiropyran (SP) is due to the photo-cleavage of the C-O spiro bond upon irradiation with UV light [14]. This cleavage allows a conformational rearrangement between a closed, colourless SP form and an opened, colourful merocyanine (MC) form which has a significant absorption band in the visible spectral region. Exposure of the MC form to visible light induces the reversion to its closed SP form, and therefore it is possible to modulate which species are in excess using light irradiation. Another interesting property of the SP is its sensitivity towards pH [9, 15, 16]. By adding acid, the opened MC becomes protonated (MC-H^+). This form can be reverted to the SP form by irradiation with visible light, releasing H^+ in the process (Figure 8.1A).

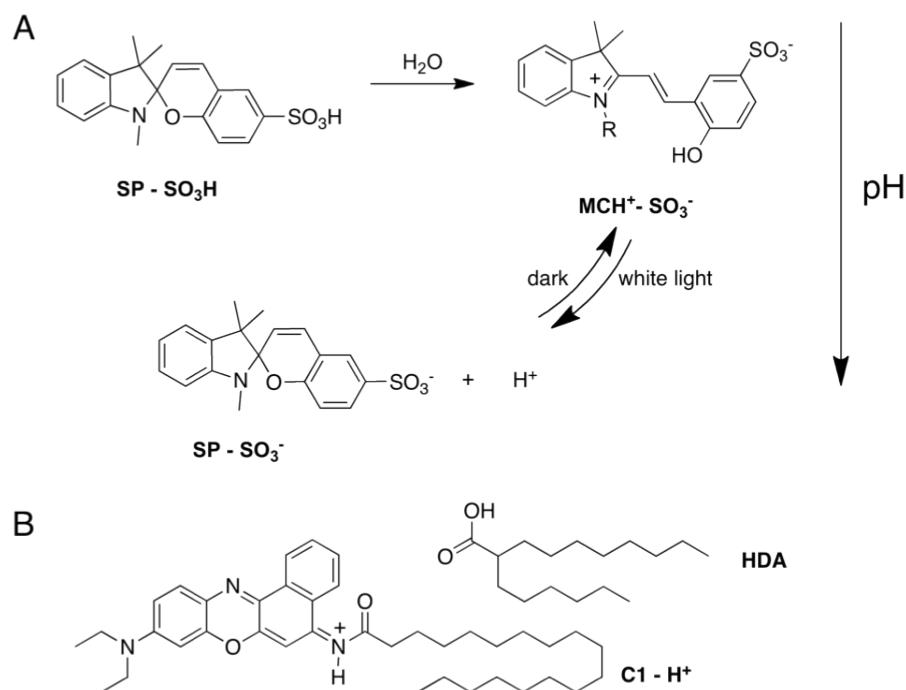


Figure 8.1. Chemical composition of the aqueous solution (A) and the droplet (B). A - Reversible structural transformations of SP-SO₃H derivative in response to white light; B - Chemical structures of protonated Chromoionophore 1 (C1-H⁺) and Hexyldecanoic acid (HDA).

The spiropyran derivative used in this study contains a sulfonic acid group (SP-SO₃H), which makes the whole unit water-soluble. Upon solubilisation in water, the sulfonic acid group of the spiropyran dissociates and the proton is taken by the phenolic group to form the protonated merocyanine (MC-H⁺) (Figure 8.1A). The colour of the resulting solution is yellow (absorption at 408 nm) (see Appendix D), indicative of the presence of MC-H⁺ and the pH is approximately 5.0. Upon white light irradiation, the protonated merocyanine reverts to the closed spiropyran form (Figure 8.1A) and the proton is released in the solution. This causes a decrease of the pH, in the irradiated area, to ~ 3.4. Therefore the spiropyran solution allows photo-modulation of pH in the range 5.0 - 3.4. To ensure the pH-activated propulsion of organic droplets, the “fuel” surfactants of the propulsion should only be released from the droplet at the lowest extreme of this pH range. At the highest extreme (pH ~ 5.0 or higher) the surfactants remain stable inside the droplet, and no mobility of the droplet occurs.

The droplet contains Chromoionophore I in dichloromethane (DCM) (0.02 M). Chromoionophore I is protonated (C1-H⁺) inside the droplet by hexyldecanoic

acid (HDA) which is present at a much higher concentration (DCM:HDA = 1:1 v:v). This droplet formulation is stable in the pH interval from 6 to 4 having self-healing abilities (*i.e.* if physically disturbed or distorted, the droplet spontaneously re-established its initial form, observe the big droplet in video D1). The self-healing properties are most likely due to the HDA present at the liquid-liquid interface (droplet-solution) that increases the hydrophobicity of the droplet at the interface, the weak hydrogen bonds formed between HDA molecules presented in large excess inside the droplet (HDA:C1 \approx 170:1) and the hydrophobicity and insolubility of DCM in water. In a smaller extend the self-healing properties of the droplet might be also due to the interactions between the Chromoionophore I (weak base) and the HDA (weak acid) willing to form long chain ion pairs. Moreover, it was experimentally observed that at pH values below 4, some of the protonated chromoionophore (CI-H⁺) becomes soluble in the aqueous solution and can therefore leave the droplet, see video D1 and Figure D5 and D6, Appendix D). This might be due to the fact that, as the H⁺ concentration increases outside the droplet, some of the DA⁻ present at the interface gets protonated to the neutral HDA, causing it to migrate back into the droplet. This phenomenon disturbs the C1-H⁺-DA⁻ ion pairs, forcing the charged C1-H⁺ species to leave the droplet.

When a microliter size droplet of this formulation is placed in a channel filled with the spiropyran solution (Figure 8.2A), and locally the aqueous solution is subjected to white light irradiation, the pH of the aqueous solution drops due to the white light irradiation (Figure 8.2B). Therefore the protonated chromoionophore present at the droplet interface becomes more soluble in the region of lower pH and leaves the droplet (Figure 8.2C). As long as the droplet is in a pH gradient region (lower than 4), the CI-H⁺ will continuously leave the droplet in the direction facing the white light source (lower pH), see Figure 8.2C. This asymmetric distribution of CI-H⁺ in the aqueous solution translates to a gradient of surface tension, at the liquid-air interface, determined by the pending droplet method (see surface tension measurements, Appendix D). These surface tension gradients generate convective flows [2, 17], which are ultimately responsible for the motion of the droplet. In these conditions, as soon as the surfactant CI-H⁺ is released from the droplet in the white light irradiated area, the droplet starts to move away from the light, stopping in the higher pH region (spiropyran solution not affected by light), where the initial droplet steady-state is re-established (Figure 8.2D). The local surface tension of the aqueous

solution decreases from $75.7 \pm 0.5 \text{ mN m}^{-1}$ ($n = 5$) to about $60.7 \pm 0.3 \text{ mN m}^{-1}$ ($n = 5$) which is sufficient to propel a microliter size droplet away from the illuminated area with a speed of $4000 \text{ } \mu\text{m s}^{-1}$.

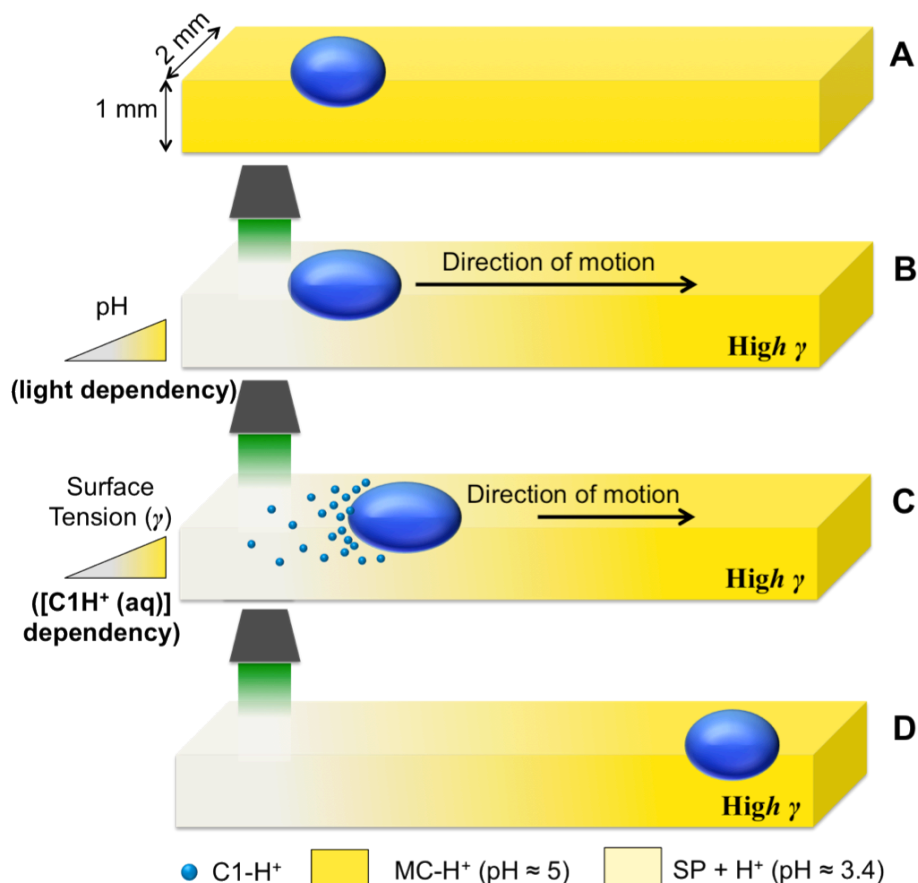


Figure 8.2. Schematic representation of the droplet movement on the aqueous solution. From top to bottom: A – droplet is stable in the initial pH conditions ($\text{pH} \approx 5$, MC-H^+ solution); B – upon irradiation with white light, MC-H^+ reverts to SP, causing the generation of free H^+ ($\text{pH} \approx 3.4$); C – as a consequence, C1-H^+ present at the interface becomes soluble in the aqueous solution and can now leave the droplet; as soon as this happens, the surface tension of the solution dramatically drops, causing the droplet to spontaneously move to the opposite direction of the light source. D – The droplet stops in the region of high surface tension, where it encounters the initial conditions (MC-H^+ , $\text{pH} \approx 5$).

Experiments involving multiple droplets were performed by using several fluidic structures of different configurations (see Appendix D). Figure 8.3 shows a sequence of snapshots taken from a video (see Appendix, video D3) in which five different droplets with volumes between $0.2\text{--}1 \text{ } \mu\text{L}$ were placed in central positions of a cross-shaped fluidic structure (Figure 8.3A). Upon illumination with a white

light irradiation source from the right side of the frame (Figure 8.3B), the droplets start moving away from the white light irradiated area, in accordance with the mechanism described above. Figure 8.3C clearly shows the spreading of the droplet closest to the light illumination area, due to the solubilisation of C1-H⁺ into the aqueous solution. Once this droplet reaches its final position (initial conditions), it self-heals, recovering its circular shape (Figure 8.3D). All five droplets are clearly present in the final snapshot (Figure 8.3D) at locations far from the white light source.

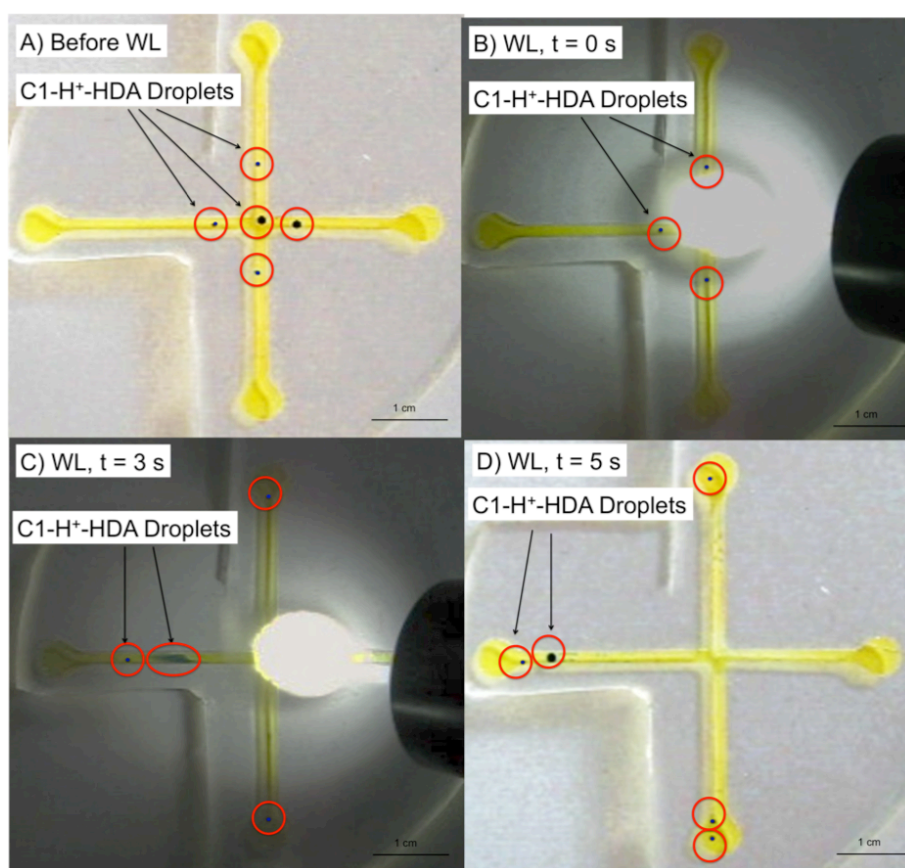


Figure 8.3. Snapshots showing the photo-activated chemopropulsion of five different droplets in a cross-shaped open fluidic structure. A - five different droplets of different dimensions at the initial conditions; B –white light irradiation source; C – After three seconds, of white light irradiation, the droplets have already moved to the opposite directions, far from the light source, by the generated surface tension gradient. D – The droplets stop in the region of high surface tension where the droplet composition is stable (initial conditions).

White light irradiation sources of different intensities were also examined to determine the optimal irradiation intensity. It was found that even with a single white light emitting LED (*ca.* 1mW cm⁻²), droplet propulsion was still observed (see Appendix, video D5). Under these conditions, the impact on the MC-H⁺/SP equilibrium is more moderate, and the proton release is less abrupt, which translates into a slower movement of the droplet (speed $\approx 100 \mu\text{m s}^{-1}$). Therefore it is possible to modulate the speed of the drop by changing the intensity of the light used for propulsion.

We emphasise that in all of these experiments, the presence of both HDA and C1-H⁺ inside the droplet as well as SP-SO₃H in the aqueous solution is crucial for the “photopropulsion” of the droplets: when the droplets lacked HDA or C1-H⁺, or when the pH of the aqueous solution was uniformed throughout the channel, no directional motion of the droplets was observed.

8.4 Conclusions

In conclusion, we have demonstrated the photo-activated chemopropulsion of organic droplets at a liquid/liquid interface. This phenomenon was exploited for easy and fast manipulation of single or multiple droplets in channels of different configurations. Although the system developed here uses specific chemicals like HDA, C1 and SP-SO₃H, it illustrates the essence of this new concept of photo-activated chemopropulsion.

We believe that, in general, when a pH difference can be photo-induced around a “fuel” droplet, able to release a surface-active chemical, this pH difference translates into the chemopropulsion of the droplet due to surface tension gradients at the liquid air interface. This property suggests that other formulations involving materials with similar characteristics to those used here could be employed to achieve photo-activated chemopropulsion of organic droplets. However, it must be appreciated that appropriate illumination conditions are essential to generate a pH gradient suitable for initiating and controlling droplet propulsion [2].

The principle of photo-activated chemopropulsion offers new possibilities to use light as an external stimulus for controlling droplet motion at the liquid-air interface. This new concept is generic and can be applied to various organic/ aqueous

systems, making photo-manipulation of microliter-size droplets relatively easy to implement. We anticipate that photo-activated chemopropulsion will help to the development of new alternatives for light-driven fluidics, molecular cargo-transport and drug-delivery.

Acknowledgment

The project has been carried out with the support of Science Foundation Ireland under the CLARITY award (07/CE/ I1147), and the Australian Research Council.

Appendix D. Supporting Information

Detailed descriptions of the materials characterisation, surface tension measurements and videos showing photo-activated chemopropulsion are provided in Appendix D.

8.5 References

1. Teh, S.-Y.; Lin, R.; Hung, L.-H.; Lee, A. P., Droplet microfluidics. *Lab on a Chip* **2008**, *8*, 198-220.
2. Lagzi, I.; Soh, S.; Wesson, P. J.; Browne, K. P.; Grzybowski, B. A., Maze Solving by Chemotactic Droplets. *Journal of the American Chemical Society* **2010**, *132*, 1198-+.
3. Sinz, D. K. N.; Darhuber, A. A., Self-propelling surfactant droplets in chemically-confined microfluidics - cargo transport, drop-splitting and trajectory control. *Lab on a Chip* **2012**, *12*, 705-707.
4. Sander, J. S.; Erb, R. M.; Denier, C.; Studart, A. R., Magnetic Transport, Mixing and Release of Cargo with Tailored Nanoliter Droplets. *Advanced Materials* **2012**, *24*, 2582-2587.
5. Wang, J., Cargo-towing synthetic nanomachines: Towards active transport in microchip devices. *Lab on a Chip* **2012**, *12*, 1944-1950.
6. Nastasa, V.; Samaras, K.; Andrei, I. R.; Pascu, M. L.; Karapantsios, T., Study of the formation of micro and nano-droplets containing immiscible solutions. *Colloids and Surfaces a-Physicochemical and Engineering Aspects* **2011**, *382*, 246-250.
7. Ichimura, K.; Oh, S. K.; Nakagawa, M., Light-driven motion of liquids on a photoresponsive surface. *Science* **2000**, *288*, 1624-1626.
8. Diguët, A.; Guillermic, R. M.; Magome, N.; Saint-Jalmes, A.; Chen, Y.; Yoshikawa, K.; Baigl, D., Photomanipulation of a Droplet by the Chromocapillary Effect. *Angewandte Chemie-International Edition* **2009**, *48*, 9281-9284.
9. Sunamoto, J.; Iwamoto, K.; Akutagawa, M.; Nagase, M.; Kondo, H., Rate control by restricting mobility of substrate in specific reaction field - Negative photochromism of water-soluble spiropyran in AOT reversed micelles. *Journal of the American Chemical Society* **1982**, *104*, 4904-4907.
10. Berkovic, G.; Krongauz, V.; Weiss, V., Spiroyrans and spirooxazines for memories and switches. *Chemical Reviews* **2000**, *100*, 1741-1753.
11. Evans, R. A.; Hanley, T. L.; Skidmore, M. A.; Davis, T. P.; Such, G. K.; Yee, L. H.; Ball, G. E.; Lewis, D. A., The generic enhancement of photochromic dye switching speeds in a rigid polymer matrix. *Nature Materials* **2005**, *4*, 249-253.

12. Kosa, T.; Sukhomlinova, L.; Su, L. L.; Taheri, B.; White, T. J.; Bunning, T. J., Light-induced liquid crystallinity. *Nature* **2012**, *485*, 347-349.
13. Byrne, R.; Diamond, D., Chemo/bio-sensor networks. *Nature Materials* **2006**, *5*, 421-424.
14. Hirshberg, Y., Reversible formation and eradication of colors by irradiation at low temperatures - a photochemical memory model. *Journal of the American Chemical Society* **1956**, *78*, 2304-2312.
15. Lee, C. W.; Song, Y. H.; Lee, Y.; Ryu, K. S.; Chi, K. W., Reversible photochromic switch ensemble and its photoimaging using H⁺ transfer between spiropyran and fluorescein in a polymer matrix. *Chemical Communications* **2009**, 6282-6284.
16. Yu, Q.; Bauer, J. M.; Moore, J. S.; Beebe, D. J., Responsive biomimetic hydrogel valve for microfluidics. *Applied Physics Letters* **2001**, *78*, 2589-2591.
17. Soh, S.; Bishop, K. J. M.; Grzybowski, B. A., Dynamic self-assembly in ensembles of camphor boats. *Journal of Physical Chemistry B* **2008**, *112*, 10848-10853.

Chapter 9

Self-assembled Solvato-morphologically Controlled Photochromic Crystals

Larisa Florea ¹, Silvia Scarmagnani ¹, Fernando Benito-Lopez^{1, 2}* and
Dermot Diamond ¹

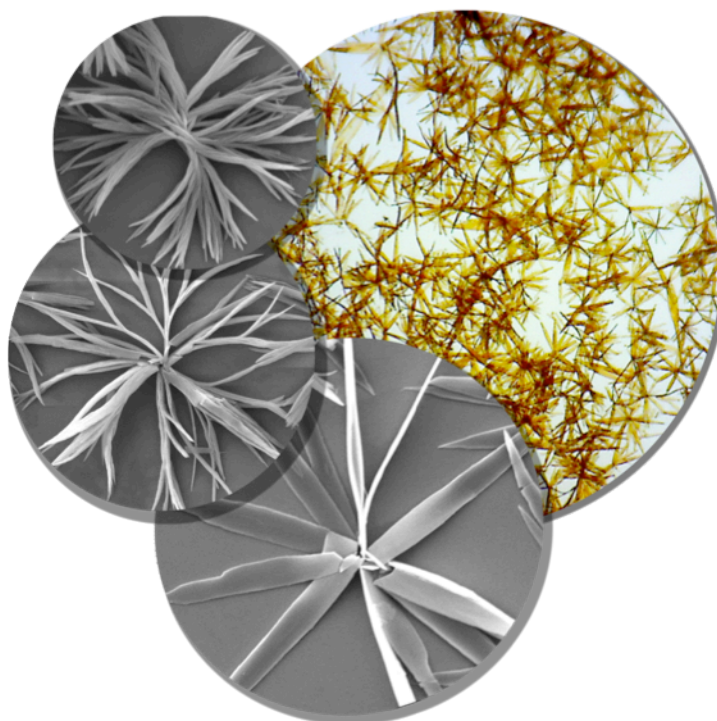
Angewandte Chemie Angewandte Chemie International Edition,
submitted

¹CLARITY: Centre for Sensor Web Technologies, National Centre for Sensor Research, School of Chemical Sciences, Dublin City University, Dublin, Ireland;

²CIC microGUNE, Arrasate-Mondragón, Spain, Tel.: +34 943710212

*Author to whom correspondence should be addressed;

Abstract: Here it is described, for the first time, intriguing solvato-morphological control of photochromic micro-structures based on spiropyran. By simply changing the ratio of the solvents forming the aqueous phase, selective control of the formation of molecular assemblies at the liquid/air interface as well as the morphology (flat crystals to ribbon-like structures) and the dimensions ($\sim 10\text{-}80\text{ }\mu\text{m}$) of the resulting 3D structures can be easily achieved. Moreover, these microstructures exhibit reversible photoisomerization upon light irradiation in the solid state. Finally, guided aggregation of these micro-structures was also demonstrated.



Keywords: self-assembly, photochromism, spiropyran, microstructure, solvato-morphological control

9.1 Introduction

Self-assembly is omnipresent in nature as components of any size (from molecules to galaxies) can self-assemble in a favorable environment [1-5]. From the assembly of a school of fish in the ocean or an ant colony in the underground to the lipid bilayer membrane of a cell or the folding of a polypeptide chain into a protein, self-assembly is inspiring scientists (chemists, physicists, biologists, materials scientists, nanoscientists, and materials engineers), in using this approach as a “bottom-up” tool to create intriguing structures for different applications [4-11]. Although, until recently, much of the work in self-assembly has been focused on molecular components, the development of supramolecular chemistry and the direction of technology toward micrometer- and nanometer- scale structures have broaden this focus to include larger structures [3, 7, 12, 13]. New types of aggregates, especially those with potential applications in microelectronics [14, 15], photonics [16-18], biomedicine [19, 20] and nanoscience [19, 21-24] are becoming increasingly important technologically. In these conditions, self-assembly serves as a solution to the challenges brought by the continued shrinking of device features [25] but also shows great potential in building three-dimensional (3D) microstructures in a practical way [4, 12, 26]. Many scientists believe that the key towards the assembly of nano- to micro-scale components into ordered arrays relies on self-assembly [3, 4, 7].

Besides molecular aggregation in solution, such as micelles, liposomes, vesicles and liquid crystals, various nano- and micro- structures may also be formed at interfaces [27, 28]. Interfacial self-assembly has attracted great interest in the recent years mainly because of the creative and unique principles of this method for constructing materials, such as self-assembled monolayers, Langmuir–Blodgett films, nanocrystals, clusters, and capsules [27]. Among the self-assembly architectures, a nano- or micro- structure with photo-responsive properties presents special interest as a promising candidate for optical memories, optical switches and displays [29-31]. It is becoming increasingly obvious that the next generation of these materials will incorporate intelligent design of externally addressable photo-responsive units that posses self-assembly properties, as these can produce highly pre-organised nano- or microstructures.

Among the various classes of photochromic compounds, spiropyrans are one of the most studied, and derivatives have been successfully used in applications such as non-linear optics, data recording, optical and electrical switching, and chemical sensing, among others [32-34]. The photochromic behavior of spiropyrans is due to the reversible heterolytic cleavage and rebinding of the C_{spiro}-O bond upon irradiation with UV light and white light, respectively [35, 36] (Figure 9.1). UV irradiation results in the formation of the highly colored merocyanine (MC) form that reverts back to the closed spiropyran (SP) form upon visible-light irradiation, or thermodynamically (*i.e.*; spontaneously, usually much slower) in the dark. These characteristics offer the possibility to modulate or switch various functions at the molecular or supramolecular level using light as a trigger.

Several assemblies of spiropyran derivatives and relevant photomodulation have been reported showing the great potential of MC to be used as a self-assembly unit. Krongauz and coworkers described the formation of MC aggregates composed of tiny-globules (0.1-0.4 μm) referred to as “quasicrystals” obtained after UV irradiation of SP-long chain derivatives in aliphatic hydrocarbons or when exposed to constant external electric field ($V = 25 \text{ kV cm}^{-1}$) [37-41]. Larger MC crystals (10-100 μm) were obtained from aliphatic hydrocarbons and non-polar solvents upon prolong UV irradiation (30 min) [42, 43] or when MC functionalised polymers were used [44, 45]. Other assemblies include Langmuir-Blodgett films [46, 47] and aggregates of spiropyran-functionalised dendrons [48].

This chapter reports, for the first time, the spontaneous formation of photochromic spiropyrans aggregates of 1'-(3-carboxypropyl)-3,3'-dimethyl-6-nitrospiro-1-benzopyran-2,2'-indoline (SP-COOH, Figure 9.1) at the liquid-air interface when the aqueous phase is an ethanol/water mixture. In a very effective manner, this process produces highly organised assemblies composed of three-dimensional daisy-like microstructures. By changing the ratio of the solvents forming the aqueous phase (ethanol:water), selective control of the formation of molecular assemblies as well as the morphology (flat crystals to ribbon-like structures) and the dimensions ($\sim 10\text{-}80 \text{ }\mu\text{m}$) of the resulting 3D structures can be easily achieved. Moreover, these microstructures exhibit reversible photoisomerisation upon light irradiation in the solid state. To our knowledge, such structures and behavior have never been observed before, and is in clear contrast to “quasicrystals” and larger-sized aggregates through their high degree of organisation

at the microscopic level, morphological complexity, facile solvato-morphological control and the absence of residual amorphous material. This study provides the first direct measurement of the structural, spectroscopic, and photochromic properties of such SP-COOH microstructures.

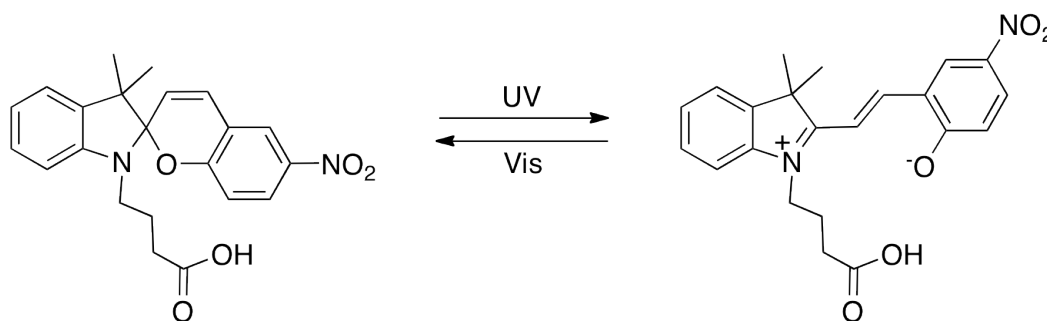


Figure 9.1. Photochromism of SP-COOH spiropyran derivative.

9.2 Experimental

Experimental details, including the synthesis procedures, characterisation methods, and all relevant characterisation data, are available in Appendix E.

9.3 Results and Discussion

To prepare the aggregates, SP-COOH was dissolved in ethanol (EtOH), which is a good solvent for most benzospiropyrans, at a concentration of 10^{-3} M. The resulting solution had a strong purple color due to the absorbance of MC centered at 550 nm (see Appendix E, Fig. E2). To this solution, DI water was added so that the final EtOH volume percent (V %) in the water/EtOH solution was 15 % (SP-COOH 15 %), 20 % (SP-COOH 20 %) and 25 % (SP-COOH 25 %), respectively. After this, the solution was left to rest in the dark for 12 h. Immediately after mixing the two solvents, and following the exothermic reaction (due to mixing of water with EtOH), the solution is clear and has a pale red color. However, over time the solution becomes turbid. This phenomenon is due to the formation of MC-COOH individual micro-size structures caused by the poor solubility of MC-COOH in water. The only water-soluble species is $\text{MCH}^+\text{-COO}^-$ formed throughout the partial dissociation of

carboxylic acid ($pK_a \sim 4.9$ [49]) in DI water ($pH \sim 6$) and successive protonation of the SP-COO⁻ form (typical pK_a for MCH⁺ is $\sim 6-7$ [50]), see Appendix E - Figure E4. Moreover, depending on the water/EtOH ratio, the formed structures have different morphologies and sizes. These microscopic structures are in the MC form (indicated by their red color) and remain stable inside the aqueous solution most likely due to the stabilisation of individual structures in such a highly polar environment. Previously, aggregation of MC derivatives was always observed due to photo-induced formation of MC units surrounded by a non-polar environment. This caused spontaneous association of MC in order to minimise the overall energy of the system [42, 43, 48, 51]. In the case presented here however, these conditions are not satisfied, no spontaneous association is observed, and the turbidity of the solution exhibits good homogeneity (Appendix E, Figure E3). Following this, the solution was poured in a Petri dish in order to ensure a high surface area for the liquid/air interface and the solution was exposed to daylight. This caused fast switching of the EtOH/water solution from reddish to light yellow due to the switching of the remaining dissolved spiropyran from the MC/MCH⁺ to the SP/MCH⁺ forms in response to white light (Appendix E, Figure E5). This process was accompanied by spontaneous assembly of aggregates at the air/liquid interface. The proposed mechanism for this process relies on the fact that, as the polarity of the aqueous solution decreases due to the switching of the polar MC unit to the less polar SP form, the MC solid structures start to aggregate due to their polar nature, minimising their surface energy. Another important observation is that evaporation of EtOH from the surface facilitates the movement of the assembled structures towards the liquid/air interface. This process was very rapid, as a continuous aggregation film forms at the interface within minutes. A video showing this spontaneous assembly can be seen in Appendix E- Video E1 and Figure E6, in the case of SP-COOH 25 %. Very similar behavior is found however in the case of all the other solutions studied (Figure E7 and E8). Furthermore, it was observed that the morphology of the obtained structures and their dimensions are different and very dependent on the percentage of water used. Scanning electron microscopy images of these structures (Figure 9.2) show that the morphology of the assembled one-unit structures varies from ribbon-like shape in the case of SP-COOH 15 % (Figure 9.2, left) to daisy-like shaped structures composed of flat crystals in the case when SP-COOH 25 % is used (Figure 9.2, right). The structures obtained for SP-COOH 20 % resemble the daisy-

like shape of SP-COOH 25 %, however the endings of the single units are hyper branched and twisted (Figure 9.2, center).

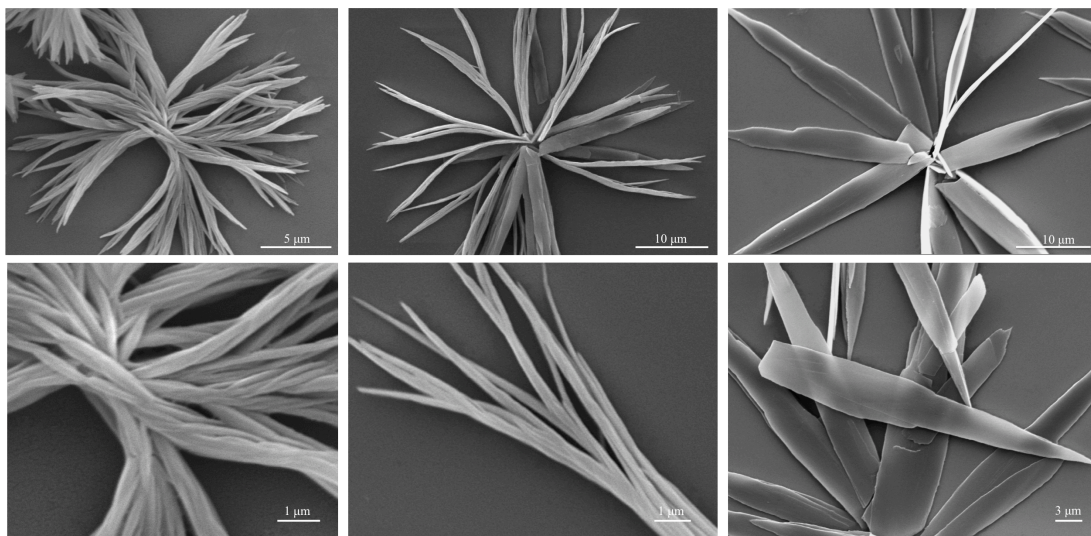


Figure 9.2. Scanning electron microscopy images of spiropyran self-assembled microstructures obtained at the air-liquid interface when the aqueous solution is SP-COOH 15 % (left), SP-COOH 20 % (centre) and SP-COOH 25 % (right), respectively. The figures on the bottom show particular details of each type of microstructures.

These structures present good homogeneity across the entire aggregated film obtained at the liquid-air interface and closely maintain their morphology with great reproducibility from structure to structure as well as from solution to solution (Figure 9.3). For better resolution images of the aggregates, please refer to Appendix E (Figures E9-E11). Analysis of the diameter of the individual self-assembled structures shows that by varying the water content of the solutions, structures with average diameters from $\sim 24 \mu\text{m}$ (SP-COOH 15 %) to $\sim 71 \mu\text{m}$ (SP-COOH 25 %) can be easily achieved (Figure 9.3). For SP-COOH 15 % and 20 %, the width of the fiber-like structures is about 300 nm while for the SP-COOH 25 % the width of the flat crystal-like structures is about 5 μm (at the assembling point) and their height is about 200 nm or less and partially transparent (Figure 9.2-right). Moreover, it was found that the morphology of the photochromic structures is not dependent on the concentration of the SP-COOH in the final solution but rather dependent on the ratio between the two solvents: water/EtOH. Identical morphologies were obtained for the spiropyran structures generated using different SP-COOH concentrations and after different times (12 h to several months) as long as the ratio of water/EtOH was kept

constant. It should be appreciated however, that the water/EtOH ratios in which this type of complex, highly symmetrical structures were obtained is quite small. At % EtOH > 40 % or < 10 %, such structures were hardly observed due to high content of EtOH, ensuring total solubility of the spiropyran derivative or low overall concentration of spiropyran dissolved in water due to the formation of $\text{MCH}^+\text{-COO}^-$ respectively (data not shown). In most of those cases the interfacial aggregation was minimum and the analysis of the solid material obtained after evaporation of the solution showed a rather amorphous solid. It is most likely that the self-assembly of individual structures (“petals”) in the “daisy-shaped structure” is governed by intermolecular forces between MC-COOH units including the π - π stacking and hydrogen-bonding between individual MC-COOH (SP-COOH) units (through the carboxylic acid group) and between MC-COOH (SP-COOH) molecules and water [18, 29, 48, 51].

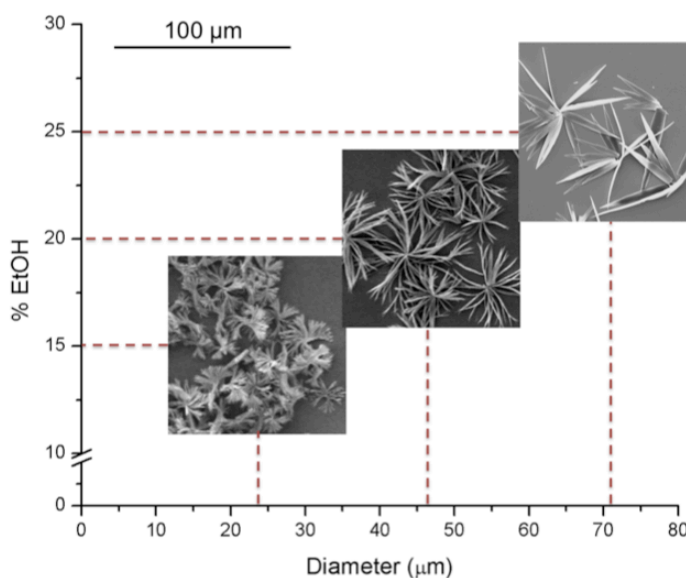


Figure 9.3. The size of the SP-COOH self-assembled microstructures strongly depends on the V% EtOH in the EtOH/water mixture.

Microanalysis of the dried structures have shown that all the microstructures – SP-COOH 15 %, SP-COOH 20 % and SP-COOH 25 %, respectively, have very similar % content of C ($66 \% \pm 0.17$, $n = 7$), H ($5.5 \% \pm 0.05$, $n = 7$) and N ($6.8 \% \pm 0.06$, $n = 7$), corresponding to the pure SP-COOH derivative, indicating no significant composition differences between the different structures.

Further studies have revealed that all microstructures obtained present photochromic properties not only at the liquid/air interface (Appendix E, Figure E12), but also in the dried state, see Figure 9.4 (SP-COOH 25 %). After irradiation with UV light for 5 min these crystals change their color from yellow to red, due to an absorbance band centered around 550 nm. Although until recently, it was believed that spiropyrans do not typically show photochromism in the solid state, recent results have shown that in some cases this behavior can be found in spiropyran or spirooxazine crystals even at room temperature [52]. These results indicate that there is enough free volume inside the structures to facilitate the transformation between the two isomers [52]. Photo-stability over time has to be considered when dealing with spiropyran photochromic dyes, as a well-documented photo-bleaching process [53, 54] occurs when SP is exposed to UV-white light radiation for extended periods of time. After four switching cycles (Figure 9.5), the efficiency was found to be constant in the case of the SP-COOH 25 % microstructures. The $A_{SP} = 0.233 \pm 0.003$ a.u. and the $A_{MC} = 0.054 \pm 0.004$ a.u. The differences in the absorbance values of the two isomers at 550 nm (corresponding to the λ_{max} for MC) showed good reproducibility over four cycles ($\Delta A_{SP \rightarrow MC} = -0.178 \pm 0.005$ a.u. and $\Delta A_{MC \rightarrow SP} = 0.179 \pm 0.004$ a.u.) indicating that these cycles are repeatable, with no detectable hysteresis. Moreover, microscopy imaging between irradiation cycles showed that the microstructures do not suffer any obvious physical degradation.

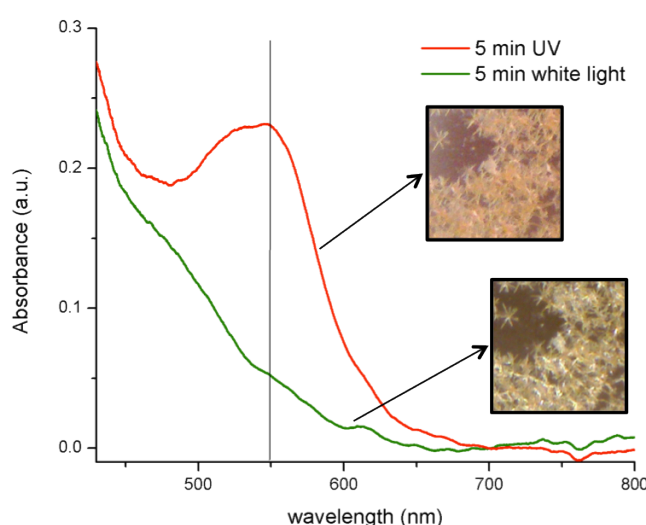


Figure 9.4. Absorbance spectra of SP-COOH 25 % self-assembled microstructures under different illumination conditions (5 min UV and 5 min white light, respectively).

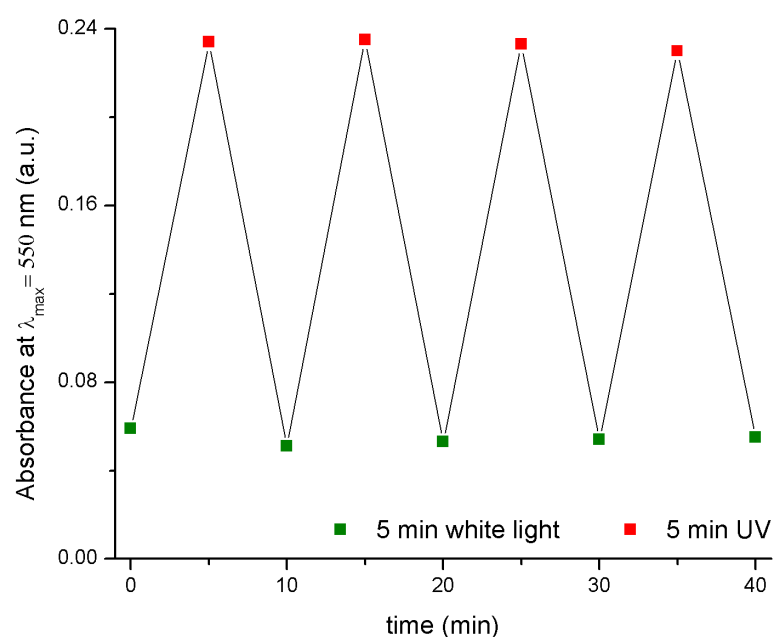


Figure 9.5. Absorbance intensity at 550 nm of SP-COOH 25 % after repeated switching cycles consisting of 5 min UV light exposure followed by 5 min white light irradiation.

Further imaging investigation of SP-COOH 25 % microstructures have shown that these structures look bright under crossed-polarizers (in contrast with SP-COOH 15 % and 20 %) indicating optical anisotropy of the material and their crystalline structure (Figure E13). Further investigation including determination of the structures of the self-assembling units for both species (SP and MC) using X-ray crystallography is in progress.

Moreover, as it was experimentally found that the interfacial aggregation is driven by the evaporation of EtOH, guided assembly was realised at the liquid-air interface by using a Halogen lamp, 150W DDL Polytec GmbH Waldbronn (Video S2). The heating effect produced by this lamp ($\sim 4^\circ\text{C}$) caused the assembly of the SP-COOH 25 % microstructures largely in the vicinity of the irradiated area (where there is predominant EtOH evaporation). The “crystal moths” (in that the crystals appear to spontaneously migrate towards the light source) behavior can be very useful for fast harvesting of the self-assembled microstructures.

9.4 Conclusions

In conclusion, we have demonstrated a convenient protocol to fabricate dimensionally controlled micrometer structures of carboxylic acid functionalised spiropyran (SP-COOH) at the liquid-air interface and their thermal guided aggregation throughout the use of a high power halogen lamp. The material has been characterised by spectroscopic and imaging methods in order to derive structural and photochromic information on the aggregates. A mechanism for the association is proposed. The process described here permits efficient production of highly organised aggregates that present reversible photochromic properties. The good optical properties and the ease of formation suggest that the self-assembled aggregates can be used for optical memory, non-linear optics and Langmuir-Blodgett films while the organised architecture could be of high potential for smart materials and devices.

Acknowledgment

The project has been carried out with the support of Science Foundation Ireland under the CLARITY award (07/CE/I1147).

Appendix E. Supporting Information

Experimental details, including the synthesis procedures, characterisation methods, and all relevant characterisation data, are available in Appendix E.

9.5 References

1. Mlot, N. J.; Tovey, C. A.; Hu, D. L., Fire ants self-assemble into waterproof rafts to survive floods. *Proceedings of the National Academy of Sciences* **2011**, *108*, 7669-7673.
2. Sanchez, C. m.; Arribart, H.; Guille, M. M. G., Biomimetism and bioinspiration as tools for the design of innovative materials and systems. *Nature Materials* **2005**, *4*, 277-288.
3. Whitesides, G. M.; Grzybowski, B., Self-assembly at all scales. *Science* **2002**, *295*, 2418-2421.
4. Grzybowski, B. A.; Wilmer, C. E.; Kim, J.; Browne, K. P.; Bishop, K. J., Self-assembly: from crystals to cells. *Soft Matter* **2009**, *5*, 1110-1128.
5. Robert, F., How far can we push Chemical Self Assembly? *Science* **2005**, *309*, 95.
6. Cai, C.; Wang, L.; Lin, J., Self-assembly of polypeptide-based copolymers into diverse aggregates. *Chemical Communications* **2011**, *47*, 11189-11203.

7. Jones, M. R.; Mirkin, C. A., Materials science: Self-assembly gets new direction. *Nature* **2012**, *491*, 42-43.
8. Prins, L. J.; De Jong, F.; Timmerman, P.; Reinhoudt, D. N., An enantiomerically pure hydrogen-bonded assembly. *Nature* **2000**, *408*, 181-184.
9. Crego-Calama, M.; Reinhoudt, D. N.; Garcia-Lopez, J. J.; Kerckhoffs, J. M., Nanostructured Hydrogen-Bonded Rosette Assemblies Self-Assembly and Self-Organization. In *Nanoscale Assembly*, Springer: 2005; pp 65-78.
10. Klok, H.-A.; Jolliffe, K. A.; Schauer, C. L.; Prins, L. J.; Spatz, J. P.; Möller, M.; Timmerman, P.; Reinhoudt, D. N., Self-assembly of rodlike hydrogen-bonded nanostructures. *Journal of the American Chemical Society* **1999**, *121*, 7154-7155.
11. Piermattei, A.; Giesbers, M.; Marcelis, A.; Mendes, E.; Picken, S. J.; Crego-Calama, M.; Reinhoudt, D. N., Induction of Liquid Crystallinity by Self-Assembled Molecular Boxes. *Angewandte Chemie International Edition* **2006**, *45*, 7543-7546.
12. Whitesides, G. M.; Boncheva, M., Beyond molecules: Self-assembly of mesoscopic and macroscopic components. *Proceedings of the National Academy of Sciences* **2002**, *99*, 4769-4774.
13. Whitesides, G. M. In *Self-assembly and nanotechnology*, 1996 Symposium on Smart Structures and Materials, 1996; International Society for Optics and Photonics: 1996; pp 307-308.
14. Sirringhaus, H.; Kawase, T.; Friend, R.; Shimoda, T.; Inbasekaran, M.; Wu, W.; Woo, E., High-resolution inkjet printing of all-polymer transistor circuits. *Science* **2000**, *290*, 2123-2126.
15. Black, C.; Ruiz, R.; Breyta, G.; Cheng, J.; Colburn, M.; Guarini, K.; Kim, H.-C.; Zhang, Y., Polymer self assembly in semiconductor microelectronics. *Ibm Journal of Research and Development* **2007**, *51*, 605-633.
16. Jenekhe, S. A.; Chen, X. L., Self-assembly of ordered microporous materials from rod-coil block copolymers. *Science* **1999**, *283*, 372-375.
17. Xia, Y.; Gates, B.; Yin, Y.; Lu, Y., Monodispersed colloidal spheres: old materials with new applications. *Advanced Materials* **2000**, *12*, 693-713.
18. Liao, Q.; Fu, H.; Wang, C.; Yao, J., Cooperative Assembly of Binary Molecular Components into Tubular Structures for Multiple Photonic Applications. *Angewandte Chemie-International Edition* **2011**, *50*, 4942-4946.
19. Schnitzler, T.; Herrmann, A., DNA Block Copolymers: Functional Materials for Nanoscience and Biomedicine. *Accounts of Chemical Research* **2012**, *45*, 1419-1430.
20. Otsuka, H.; Nagasaki, Y.; Kataoka, K., Self-assembly of poly (ethylene glycol)-based block copolymers for biomedical applications. *Current Opinion in Colloid & Interface Science* **2001**, *6*, 3-10.
21. Klimov, V.; Mikhailovsky, A.; Xu, S.; Malko, A.; Hollingsworth, J.; Leatherdale, C.; Eisler, H.-J.; Bawendi, M., Optical gain and stimulated emission in nanocrystal quantum dots. *Science* **2000**, *290*, 314-317.
22. Sun, S.; Murray, C.; Weller, D.; Folks, L.; Moser, A., Monodisperse FePt nanoparticles and ferromagnetic FePt nanocrystal superlattices. *Science* **2000**, *287*, 1989-1992.
23. Bisoyi, H. K.; Kumar, S., Liquid-crystal nanoscience: an emerging avenue of soft self-assembly. *Chemical Society Reviews* **2011**, *40*, 306-319.
24. Wu, D.; Zhi, L.; Bodwell, G. J.; Cui, G.; Tsao, N.; Müllen, K., Self-Assembly of Positively Charged Discotic PAHs: From Nanofibers to Nanotubes. *Angewandte Chemie International Edition* **2007**, *46*, 5417-5420.
25. Jeong, M.; Doris, B.; Kedzierski, J.; Rim, K.; Yang, M., Silicon device scaling to the sub-10-nm regime. *Science* **2004**, *306*, 2057-2060.
26. Madou, M. J., *Fundamentals of microfabrication: the science of miniaturization*. CRC Press LLC: 2002.

27. Ma, H.; Hao, J., Ordered patterns and structures via interfacial self-assembly: superlattices, honeycomb structures and coffee rings. *Chemical Society Reviews* **2011**, *40*, 5457-5471.
28. Smith, R. K.; Lewis, P. A.; Weiss, P. S., Patterning self-assembled monolayers. *Progress in Surface Science* **2004**, *75*, 1-68.
29. Zhou, X.; Duan, Y.; Yan, S.; Liu, Z.; Zhang, C.; Yao, L.; Cui, G., Optical modulation of supramolecular assembly of amphiphilic photochromic diarylethene: from nanofiber to nanosphere. *Chemical Communications* **2011**, *47*, 6876-6878.
30. Hirose, T.; Matsuda, K.; Irie, M., Self-assembly of photochromic diarylethenes with amphiphilic side chains: reversible thermal and photochemical control. *The Journal of Organic Chemistry* **2006**, *71*, 7499-7508.
31. Patra, A.; Métivier, R.; Brisset, F. o.; Nakatani, K., Photochromic one-dimensional nanostructures based on dithienylethene: fabrication by light-induced precipitation and reversible transformation in the nanoparticle state. *Chemical Communications* **2012**, *48*, 2489-2491.
32. Florea, L.; Diamond, D.; Benito-Lopez, F., Photo-Responsive Polymeric Structures Based on Spiropyran. *Macromolecular Materials and Engineering* **2012**, *297*, 1148-1159.
33. Delaire, J. A.; Nakatani, K., Linear and nonlinear optical properties of photochromic molecules and materials. *Chemical Reviews* **2000**, *100*, 1817-1845.
34. Berkovic, G.; Krongauz, V.; Weiss, V., Spiropyrans and spirooxazines for memories and switches. *Chemical Reviews* **2000**, *100*, 1741-1753.
35. Aldoshin, S. M., Spiropyrans - structural features and photochemical properties. *Molecular Crystals and Liquid Crystals Science and Technology Section a-Molecular Crystals and Liquid Crystals* **1994**, *246*, 207-214.
36. Hirshberg, Y., Reversible formation and eradication of colors by irradiation at low temperatures - a photochemical memory model. *Journal of the American Chemical Society* **1956**, *78*, 2304-2312.
37. Meirovitch, E.; Shvartsman, F. P.; Krongauz, V. A.; Zimmermann, H., An electron spin resonance study of spiropyran-merocyanine quasi-liquid crystals. *The Journal of Physical Chemistry* **1985**, *89*, 5522-5525.
38. Shvartsman, F. P.; Cabrera, I. R.; Weis, A. L.; Wachtel, E. J.; Krongauz, V. A., Investigation of the quasi-liquid crystal structure. *The Journal of Physical Chemistry* **1985**, *89*, 3941-3946.
39. Cabrera, I.; Shvartsman, F.; Veinberg, O.; Krongauz, V., Photocontraction of Liquid Spiropyran-Merocyanine Films. *Science* **1984**, *226*, 341-343.
40. Hsiung, H.; Rasing, T.; Shen, Y.; Shvartsman, F.; Cabrera, I.; Krongauz, V., Polar ordering of quasiliquid crystals - An optical second harmonic generation study. *The Journal of chemical physics* **1987**, *87*, 3127.
41. Krongauz, V.; Fishman, S.; Goldburt, E., Quasi-crystals. Growth from photochromic spiropyrans on irradiation in a constant electric field. *The Journal of Physical Chemistry* **1978**, *82*, 2469-2474.
42. Onai, Y.; Mamiya, M.; Kiyokawa, T.; Okuwa, K.; Kobayashi, M.; Shinohara, H.; Sato, H., Colored merocyanine aggregates: long-lived crystals of large size (10-100. mu. m) and deaggregation of small aggregates in solutions. *The Journal of Physical Chemistry* **1993**, *97*, 9499-9505.
43. Uznanski, P., From spontaneously formed aggregates to J-aggregates of photochromic spiropyran. *Synthetic Metals* **2000**, *109*, 281-285.
44. Kotharangannagari, V. K.; Sánchez-Ferrer, A.; Ruokolainen, J.; Mezzenga, R., Photoresponsive reversible aggregation and dissolution of rod-coil polypeptide diblock copolymers. *Macromolecules* **2011**, *44*, 4569.
45. Wismontski-Knittel, T.; Krongauz, V., Self-assembling of spiropyran polymers by zipper crystallization. *Macromolecules* **1985**, *18*, 2124-2126.

46. Ando, E.; Moriyama, K.; Arita, K.; Morimoto, K., Photochromic behaviors of long alkyl chain spiropyrans at the air-water interface and in LB films. *Langmuir* **1990**, *6*, 1451-1454.
47. Tachibana, H.; Yamanaka, Y.; Sakai, H.; Abe, M.; Matsumoto, M., J-aggregate formation of amphiphilic merocyanine in Langmuir-Blodgett films. *Journal of Luminescence* **2000**, *87*, 800-802.
48. Chen, Q.; Feng, Y.; Zhang, D.; Zhang, G.; Fan, Q.; Sun, S.; Zhu, D., Light-Triggered Self-Assembly of a Spiropyran-Functionalized Dendron into Nano, Micrometer- Sized Particles and Photoresponsive Organogel with Switchable Fluorescence. *Advanced Functional Materials* **2010**, *20*, 36-42.
49. Bacarella, A. L.; Grunwald, E.; Marshall, H. P.; Purlee, E. L., The potentiometric measurement of acid dissociation constants and pH in the system methanol-water - pKa values for carboxylic acids and anilinium ions. *Journal of Organic Chemistry* **1955**, *20*, 747-762.
50. Sumaru, K.; Kameda, M.; Kanamori, T.; Shinbo, T., Characteristic phase transition of aqueous solution of poly(N-isopropylacrylamide) functionalized with spiropyrans. *Macromolecules* **2004**, *37*, 4949-4955.
51. Uznanski, P., UV-assisted formation of nanoaggregates from photochromic spiropyran in nonpolar solvents. *Langmuir* **2003**, *19*, 1919-1922.
52. Harada, J.; Kawazoe, Y.; Ogawa, K., Photochromism of spiropyran and spirooxazines in the solid state: low temperature enhances photocoloration. *Chemical Communications* **2010**, *46*, 2593-2595.
53. Baillet, G.; Giusti, G.; Guglielmetti, R., Comparative photodegradation study between spiro indoline oxazine and spiro indoline pyran derivatives in solution. *Journal of Photochemistry and Photobiology a-Chemistry* **1993**, *70*, 157-161.
54. Baillet, G.; Campredon, M.; Guglielmetti, R.; Giusti, G.; Aubert, C., Dealkylation of N-substituted indolinospironaphthoxazine photochromic compounds under UVirradiation. *Journal of Photochemistry and Photobiology a-Chemistry* **1994**, *83*, 147-151.

Chapter 10

Future Work and Perspectives

*The Development of Integrated Opto-molecular
Systems as Sensors and Actuators in Micro-fluidic
Devices, a View to the Future*

The role of materials science has never been more critical. It is believed that the technologies of the near future will depend on the efforts of talented researchers working with novel and fascinating materials concepts. Few of these concepts include stimuli-responsive polymers for sensing and actuation purposes, chemo- and photo-actuation of droplets and self-assembly of stimuli-responsive units at the micro- and nano-scale. In the area of micro-fluidics, stimuli-responsive polymers have the potential to become fully integrated into micro-fluidic platforms that will possess multiple functionalities including actuation and sensing.

The work presented in Chapters 4 to 9 of this thesis opens new strategies for the development of novel miniaturised sensing platforms or new means of droplet/micro-gel actuation.

If Chapter 4 and 5 describe the potential of using polyaniline coated micro-platforms for pH and ammonia sensing based on the inherited doping-dedoping properties of polyaniline, here we propose, as future work, the use of these coatings for studying mixing and diffusion processes in micro-channels (section 10.1).

Other exciting future work possibilities rely on the use of the micro-platform presented in Chapters 6 and 7 for the development of micro-analytical platforms for functions such as light-activated guest uptake and release and optical reporting on status (passive form, free active form, guest bound to active form) based on the inherited spiropyran binding properties. In this context, future work explores the use of spiropyran-polymeric brushes coated micro-capillaries for photo-activated sensing, accumulation, release and extraction of target metal ions (Section 10.2).

Further development of the concept described in Chapter 8 could produce new means of photo-actuation for micro-fluidic applications. Surfactant powered actuation at the liquid/air interface and Marangoni's effect are not by any means new concepts in science and paper boats have been "powered" through the use of soaps for decades [1, 2]. However, having the key components required for the propulsion-type movement confined into one "vesicle" and having that vesicle activated only upon photo-stimulation represents a great step forward for actuation at the liquid/air interface. Therefore several means of generating photo-actuation of ionogel micro-boats on the surface of aqueous solutions are proposed (Section 10.3).

10.1 Sensing the Flow: Adaptive Coatings based on Polyaniline for Direct Observation of Mixing Processes in Micro-fluidic Systems

10.1.1 Introduction

The small characteristic dimensions of micro-fluidics results in small internal volumes and high surface-to-volume ratios, leading to improved heat and mass transfer rates, and affecting chemical reactions. This in turn is exponentially increasing their applicability in real life since the last decade, and make micro-fluidics an attractive alternative to conventional systems [3]. The continuing growing trends in microfluidics highlight the importance of understanding the mechanisms and fundamental differences involved in fluid flow and mixing at the micro-scale [4].

Mixing solutions in micro-channels can be difficult. Physically, flows of common liquids at practical pressures in microfluidic channels (typical cross-sectional dimension, 1-100 μm) are characterised by low values of the Reynolds number ($Re = Ul/\nu < 100$, where U is the average flow speed, l is the cross-sectional dimension of the channel and ν is the kinematic viscosity of the fluid). At low Re , in simple channels (*i.e.*, with smooth walls), pressure flows are laminar and uniaxial, so the mixing of material between streams in the flow is purely diffusive. Different approaches like using bas-relief structures on the floor of the channel are used to create chaotic mixing in micro-fluidic devices and so improving mixing [5].

Mixing of fluids flowing through a micro-channel is very important for various applications of micro-fluidic systems: homogenisation of solutions of reagents used in chemical reactions or various biomedical and biochemical processes that involve the mixing of two fluids, including DNA purification, polymerase chain reaction (PCR), enzyme reaction, and protein folding. The performance of such processes relies on effective and rapid mixing of samples and reagents [5, 6].

In addition, on-chip detection techniques are essential for the continuous monitoring of the mixing behaviour of confluent streams. For this purpose many spectroscopic detection methods have been employed: laser-induced fluorescence [7,

8], confocal fluorescence microscopy [9], ultraviolet absorption [10, 11], chemiluminescence [12, 13], providing good opportunities for the detection of chemical species and so they are suitable for studying mixing in micro-fluidic devices. However, these techniques typically require the addition of a dye or pre-treatment of a solute species with fluorescent tags to allow on-chip detection. Consequently, in these approaches one follows the bulk behaviour of an added solute, rather than the solvent/liquid itself.

We have shown in Chapter 5 that polyaniline functionalised micro-channels have the ability to sense solutions of different pHs that are passing through the micro-channel manifesting in changes in colour of the polyaniline coatings, due to the doping-dedoping of the polymer backbone.

Future work could explore the possibility of quantitatively evaluating the mixing process under label/dye free conditions, using adaptive coatings based on polyaniline. Moreover, this label free approach could be employed both in cases of non-reactive fluids (*e.g.*, hydrochloric acid and water) that have shown good agreement with theoretical values calculated using conventional diffusion [14], and in the case of reactive fluids (*e.g.*, hydrochloric acid and sodium hydroxide) wherein rapid proton diffusion might be achieved [14].

10.1.2 Direct Observation of Mixing Processes in Micro-fluidic Systems

To probe the viability of using PANi coatings for studying mixing in this micro-fluidic device (Figure 10.1), colourless hydrochloric acid (10^{-2} M, pH = 2) and sodium hydroxide (10^{-2} M, pH = 12) solutions were pumped into the two arms of a Y-shaped micro-channel, 1000 x 100 μ m and 112 mm long. The two liquid streams meet at the Y-junction, and have an interaction time defined by the flow rate, which was varied between 2-12 μ L min⁻¹ for each of the flows. Due to their different pH, the two confluent streams in contact with the polyaniline coating, cause different degrees of doping in the polymer, manifesting in different colours of the coating (Figure 10.1). In this way, the two laminar flows can be easily distinguished in a label/dye free manner and the mixing point can be recorded (Figure 10.2).

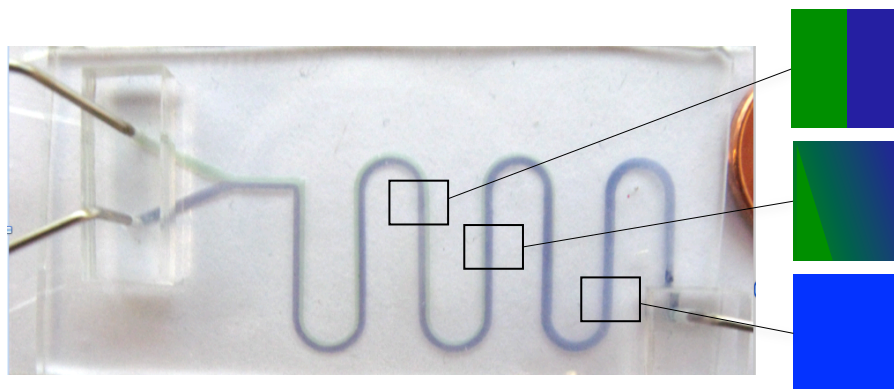


Figure 10.1. Photo of the micro-channel when the 2 solutions ($\text{HCl} = 10^{-2} \text{ M}$ and $\text{NaOH} = 10^{-2} \text{ M}$) had a flow rate of $10 \mu\text{L min}^{-1}$ each.

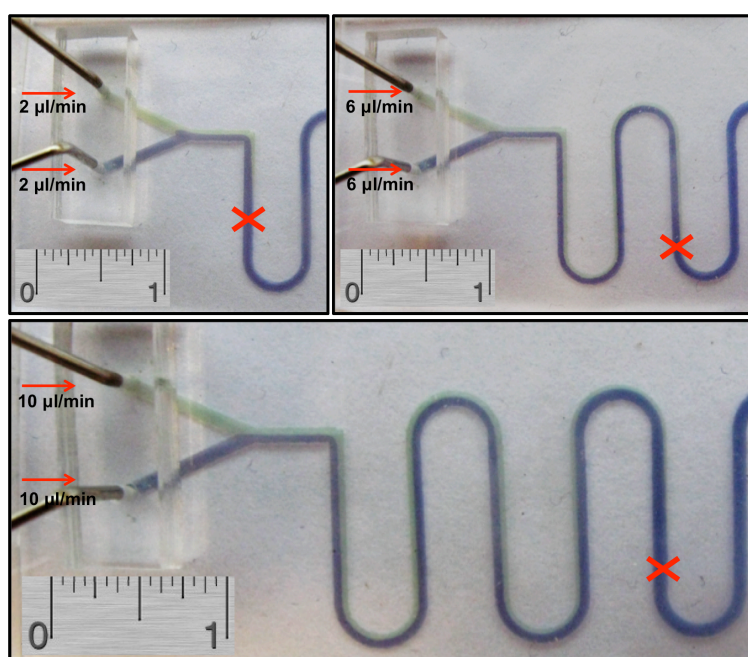


Figure 10.2. Photo of the micro-channel when the 2 different solutions ($\text{HCl} = 10^{-2} \text{ M}$ and $\text{NaOH} = 10^{-3} \text{ M}$) are passed through the micro-channel at different flow rates (2, 6 and $10 \mu\text{L min}^{-1}$, respectively). The photo indicates that the point of complete mixing changes according to the flow rate.

Figure 10.3a, shows a scheme of a micro-fluidic device with the mixing positions indicated by letters when different flows are applied. A plot of the mixing point (*i.e.* the point at which the green colour disappears relative to the meeting point at the Y- junction) against flow rate presents good linearity (Figure 10.3b) showing the utility of this approach for investigating diffusion and mixing processes of solutions in micro-channels by simply using colourless solutions of different pH.

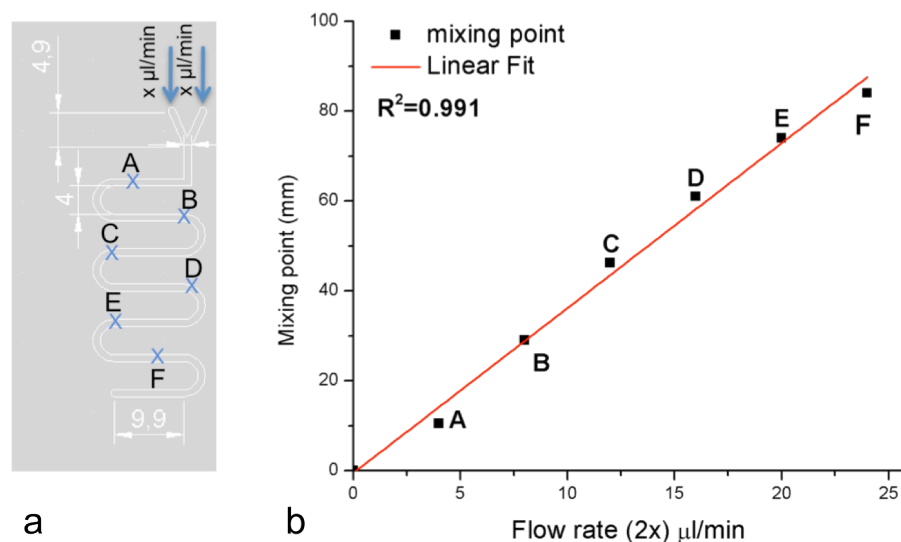


Figure 10.3. a- Scheme of the micro-channel when the two different solutions ($\text{HCl } 10^{-2} \text{ M}$ and $\text{NaOH } 10^{-2} \text{ M}$) are passed through the micro-channel. Points marked A-F indicate the mixing point of the two flows having different flow rates ($x= 2, 4, 6, 8, 10$ or $12 \mu\text{L min}^{-1}$ respectively); b-Plot of the mixing point (reported from the Y-junction point) against total flow rate ($2x$).

Further work should focus on the use of microscopy imaging techniques to record in a precise manner the mixing point of two or multiple confluent streams of different pH. As it can be seen from Figure 10.4, by using microscopy imaging it is clearly observable the laminar flow of two fluids of different pH, $\text{pH} = 2$ ($\text{HCl sol. } 10^{-2} \text{ M}$) and $\text{pH} = 12$ ($\text{NaOH sol. } 10^{-2} \text{ M}$) flowing at a total flow rate of $20 \mu\text{L min}^{-1}$.

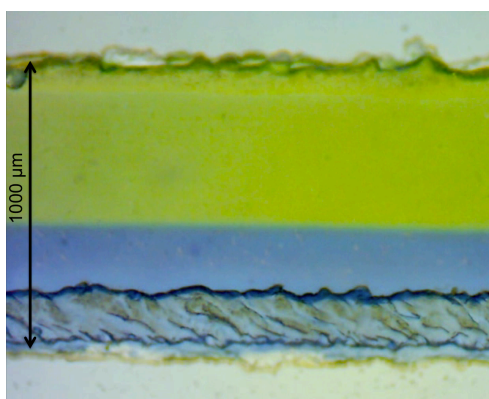


Figure 10.4. Photo of a polyaniline functionalised micro-channel taken with a digital microscope when two different streams of liquid having different pH ($\text{pH } 2 - \text{HCl sol. } 10^{-2} \text{ M}$ and $\text{pH } 12 - \text{NaOH sol. } 10^{-2} \text{ M}$) are passed through the micro-channel at a total flow rate of $20 \mu\text{L min}^{-1}$.

The final goal of this work could be to build up experimental models of the mixing behaviour of reactive and non-reactive fluids in micro-fluidic devices and compare the results with the theoretical models. Moreover, our approach could be used for investigating proton diffusion with or without a chemical reaction and also for obtaining useful information for the optimal design of micro-reactors for chemical synthesis applications.

10.2 Spiropyran Functionalised Micro-capillaries for Metal Ion Sensing, Accumulation, Release and Extraction

The use of spiropyran polymer brushes functionalised capillaries, which were described in detail in Chapter 6 and 7, could potentially be used for sensing, accumulation, release and extraction of target metal ions.

10.2.1 Introduction

The real-time analysis of metal ions is important for chemical monitoring as well as environmental and clinical applications [15]. Recently, great scientific efforts have been focused on producing sensors that are capable of detecting metal ions in a fast and reversible manner [16]. Building arrays of sensors composed of multiple ligands specific for the detection of different metal ions is difficult to realise and rather time-consuming. In this respect, a single material that is capable of binding multiple metal ions and give a unique spectral response to each metal ion-ligand complex would be preferred. Moreover, if the chelator itself could be switched between a passive and an active state, then very simple, reusable and cost-effective sensors could be developed. As described in Chapter 1, spiropyrans are organic photochromic compounds that have been widely studied [17, 18]. Upon irradiation with UV or visible light, spiropyrans isomerise between the closed and open forms, in which the open form is comparatively more polar. Metal ions can influence this isomerisation process by complexing with the open form through the electron-rich oxygen atom (Figure 10.5). In contrast, visible light produces a high concentration of the closed form, and thus hinders metal-binding. Spiropyrans, therefore, show great potential as

photo-reversible metal-complexation agents. Based on this coordination-induced photochromism characteristic of the MC form (Figure 10.5). Further investigations should focus on the photo-controlled detection, accumulation and release of target metal ions passing through the modified micro-capillary in a continuous flow regime.

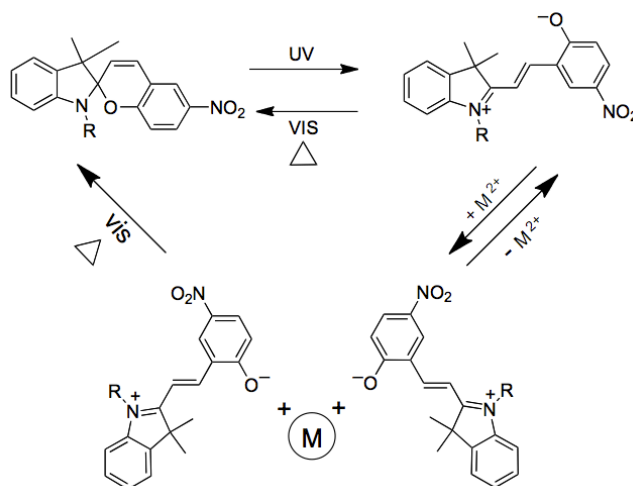


Figure 10.5. Metal ion binding propriety of spiropyran derivatives.

Metal ion uptake can be triggered using UV light and subsequently reversed on demand by shining white light on the coloured complex, which regenerates the inactive spiropyran form resulting in the release of metal ions [17]. The use of light to trigger the chelator offers unique opportunities as the binding/releasing process is now reversible and can be controlled externally in a non-invasive manner.

Through the integration of the beneficial characteristics of both micro-fluidic platforms and photochromic dyes, a simple and innovative micro-capillary capable of metal ion detection, accumulation and release could be realised. The functionalised micro-capillary acts as photonicallly controlled self-indicating system for metal ion detection that operates in continuous flow facilitating real-time measurements and fast analysis protocols.

10.2.2 Metal Ions Sensing – Qualitative Studies

Preliminary studies have shown that the open merocyanine form of the spiropyran norbornene functionalised monomer (MC-M), described in Chapter 6 and 7, presents metal ion binding proprieties in solution (Figure 10.6).

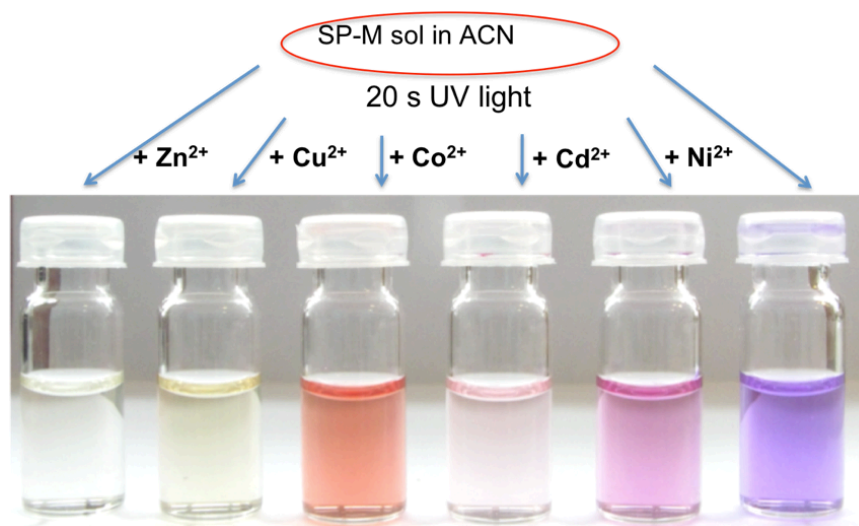


Figure 10.6. Photos of the spiropyran-monomer (MC-M) solutions in ACN (10^{-3}M) in the presence of different divalent metal ions (molar ratio: MC-M: Me^{2+} 2:1) after irradiation with UV light for 20 seconds.

The MC-M- Me^{2+} complexes have been successfully characterised in solution using UV-Vis spectroscopy (Figure 10.7).

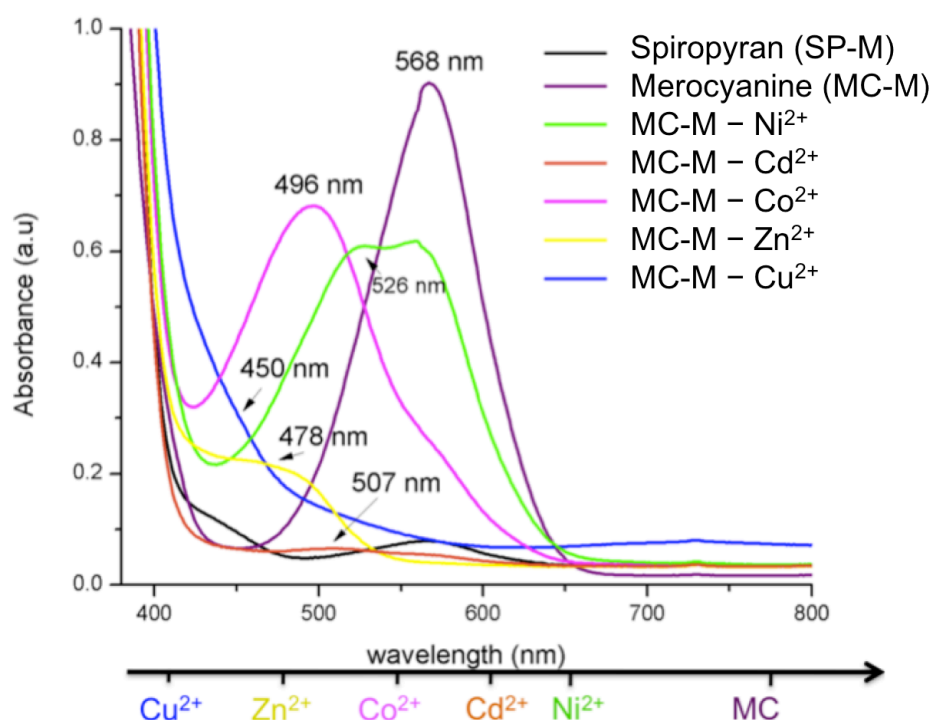


Figure 10.7. Absorption spectra of spiropyran-monomer (SP-M) solutions in ACN (10^{-3}M) in the presence of different divalent metal ions (molar ratio: MC-M: Me^{2+} 2:1) after irradiation with UV light for 20 seconds.

As depicted from Figure 10.7, in the presence of the MC-M form, different metal ions will form complexes that absorb at different wavelengths in solution. The colourless, ring-closed spiropyran (SP-M) is characterised by an absorption shoulder at around 430 nm and an absorption tail below 400 nm. After irradiation of the solution with UV light for 20 s, the ring-opened merocyanine (MC-M) is obtained, characterised by an intense absorption band at 568 nm. Upon complexation with Ni^{2+} , Cd^{2+} , Co^{2+} , Zn^{2+} and Cu^{2+} , the absorption band is shifted at lower wavelengths which is metal-ion dependent. The MC-M- Ni^{2+} (2:1), complex yields the smallest blue shift of only 40 nm ($\lambda_{\text{max}} = 559$ nm), but the MC-M- Co^{2+} (2:1) and MC-M- Zn^{2+} (2:1) complexes give blue shifts of 72 nm ($\lambda_{\text{max}} = 496$ nm) and 90 nm ($\lambda_{\text{max}} = 478$ nm), respectively. This shift to higher energy accompanying binding is attributed to the disruption of planarity in trans-MC that occurs upon complexation [18]. However, as it can be seen from Figure 10.7, in the case of the presence of some metal ions (Ni^{2+} , Co^{2+}), the absorbance band characteristic to the MC-M is still present. Therefore, in the same experimental conditions, MC-M presents different binding abilities towards different metal ions. These results also suggest that the MC-M unit might be capable of binding simultaneously to multiple metal ions as it has been shown in the case of other spiropyran derivatives [16].

Preliminary studies have shown SP-M polymer brushes modified micro-capillaries are capable of detecting different metal solutions when passing through the micro-capillary and this detection is based on changes in colour of the coating after irradiation with UV light (Figure 10.8). Further studies will be necessary to fully characterise these changes in colour of the micro-capillary coating in the presence of different metal ions. However, these are promising results suggesting that metal ion photo-detection in continuous flow is possible using the SP-M polymer brushes coated micro-capillaries.

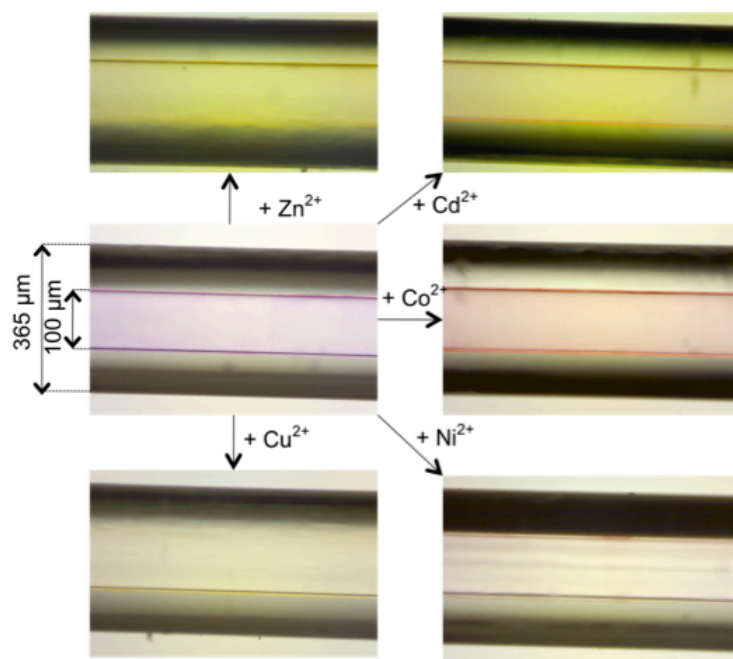


Figure 10.8. Photos of the spiropyran-polymer brushes coated micro-capillaries when solutions of different divalent metal ions in ACN (10^{-3}M) are passed through the capillary after irradiation for 20 s with UV light.

Following the same way of thinking that in the case of the solvent sensing presented in the Chapter 7, the sensing behaviour of the SP-M polymer brushes micro-capillaries can be switched *ON/OFF* using light at appropriate wavelengths. After the metal ion binding process, which is manifested by a change in colour of the micro-capillary coating, the micro-capillary is irradiated with white light for 1 min, MC-M will go back to the closed SP-M form and the metal ion previously bound will be released. As a consequence, the micro-capillary goes back to colourless. This process is depicted in the case of Co^{2+} in Figure 10.9.

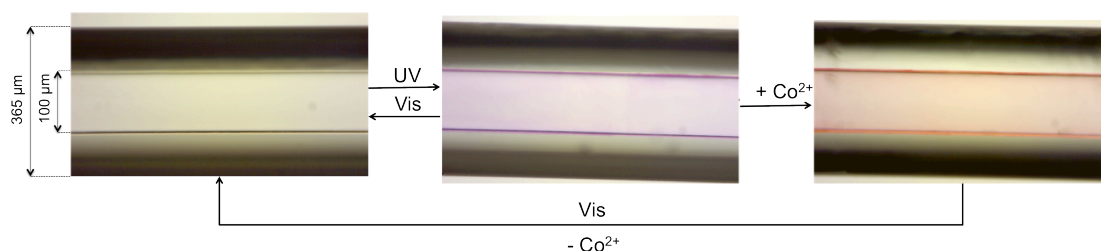


Figure 10.9. Photos of a section of a micro-capillary modified with spiropyran polymer brushes before (left) and after irradiation for 20 s with UV light (middle) followed by the addition of Co^{2+} (right). The micro-capillary goes back to colourless (due to the conversion of the MC to SP) after irradiation for 1 min with white light (left) and Co^{2+} is released.

10.2.3 Metal Ions Accumulation and Release – Quantitative Studies

The results presented above suggest that metal ion photo-accumulation (UV light) and photo-release (white light) in the modified micro-capillaries is possible. As a consequence of these promising results, future investigations could focus on the study of how to quantitatively measure the capacity of our modified micro-capillaries for metal ion photo-accumulation. For this work, two different approaches are suggested.

10.2.3.1 Detection of the Photo-Release of Metal Ions using Capacitively Coupled Contactless Conductivity Detection

Capacitively Coupled Contactless Conductivity Detection (C⁴D) is a well documented technique that has been more extensively used as a method of detection in capillary electrophoresis [19, 20]. The advantage of C⁴D over conventional conductivity detection for chromatography is that the cell design is extremely robust and there is a lack of physical contact with the eluent. This eliminates possible fouling of the electrodes and reduces to zero the extra-column band broadening that would be observed with a conventional conductivity flow cell. A typical C⁴D cell consists of two ring electrodes through which a 365 µm OD micro-capillary is introduced. The electrodes are placed a fixed distance apart, and an alternating current is applied to the first electrode at a particular optimised frequency. The two electrodes act as capacitors and so there is a passage of electrons which flow through the solution between the electrodes in order to complete the circuit. The presence of conducting groups between these electrodes will result in a higher signal being collected by the second pickup electrode, the size of which is proportional to the conductivity [20]. In this way, metal ions released from the modified micro-capillary after irradiation with white light could be easily detected post column, in a non-invasive manner.

For this, the following scheme of the installation, depicted in Figure 10.10., is proposed. Here, a metal ion solution is pumped through the micro-capillary using a micro-syringe pump. The micro-capillary is irradiated with UV light for a certain period of time to ensure binding of the metal ion to the micro-capillary coating

through the open MC-M form. Following this, the metal ion solution inside the micro-syringe is replaced with the solvent only (no metal ions present) and pumped through the system until no response is recorded by the C^4D detector. This is done to ensure that there are no more free metal ions present in the system. Next, the pump is turned off and the UV source is replaced by a white light source until full conversion of the MC-M polymer brushes to SP-M is optically observed. At this point, the micro-syringe pump (pumping the solvent) is turned back on so that the photo-released metal ions are passing through the C^4D detector and exit the system in a concentrated plug. The presence of metal ions should increase the conductivity of the solution (compared to the solvent) and this effect, should be recorded by the C^4D detector. Following a series of calibrations, this approach should provide quantitative data regarding the metal ions loading capacity of the SP-M micro-capillary coating.

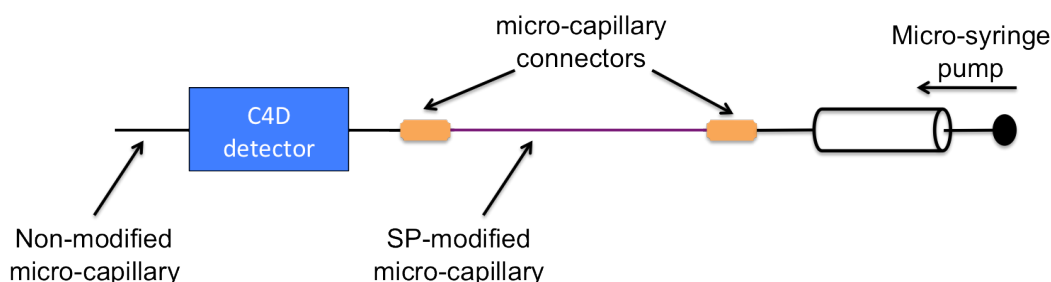


Figure 10.10. Scheme of the set-up used for C^4D measurements

10.2.3.2 Detection of the Photo-release of Metal Ions using Post-column Derivatisation

Post column derivatisation is a widely used technique in HPLC chromatography for the detection of analytes after exiting the column. According to IUPAC it is defined as a version of reaction chromatography in which the separated components eluting from the column are derivatised prior to entering in the detector. This is accomplished by performing a chemical reaction on the eluted components that gives them an easily detectable physical property. As the most popular HPLC detectors use either UV/VIS light absorption, or fluorescence, typically the post-column reaction

produces a strong colour or makes a fluorescent product. If used correctly, the post column reaction can increase the sensitivity of detection by several orders of magnitude in favourable cases. Most reagents are selective for a particular class of substances, so analytes of that class are more easily seen against a complex background. So, post-column reaction is used to increase sensitivity and selectivity in HPLC analysis [21].

A similar approach could be employed in a capillary system as the one presented above, where the “column” is considered to be the SP-M modified micro-capillary. It is expected that, by using the proper post-column reagent, the detection of the photo-released metal ions coming from the MC-M polymeric coating will be possible.

The post-column reagent suggested for this study is the 4-(2-Pyridylazo)resorcinol (PAR). PAR has the reactive groups (a heterocyclic nitrogen group, azo group, and *o*-hydroxyl group as shown in Figure 10.11-left) available for possible coordination to metal ions [22, 23] (Figure 10.11 - right). PAR has been used before for metal determination in the case of Ni^{2+} , Cd^{2+} , Zn^{2+} among others [22, 23].

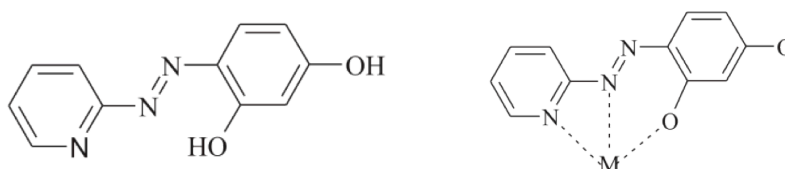


Figure 10.11. Chemical structures of 4-(2-pyridylazo) resorcinol (left) and metal complexed resorcinol (right).

The post column reaction of Co^{2+} metal solution (solvent: ACN) with PAR could be investigated following the steps proposed below and the set-up depicted in Figure 10.12:

1. The SP-M modified micro-capillary is irradiated with UV light for 20 s.
2. The pump (left) is turned on (flow rate = $20 \mu\text{L min}^{-1}$; mobile phase = ACN).
3. The syringe pump is turned on (flow rate = $20 \mu\text{L min}^{-1}$; mobile phase = post column reagent PAR 0.1 M).

4. Co^{2+} solution (various concentrations) from the injection loop is injected in the system at a flow rate of $\approx 20 \mu\text{L min}^{-1}$ for approximately 5 min.
5. When all the expected Co^{2+} solution leaves the detection area, both pumps (ACN and PAR) are turned *OFF* and the white light is turned *ON*.
6. After about 5 min, both pumps (ACN and PAR) are turned back *ON*.
7. Absorbance spectra are recorded during the entire experiment. Collection rate: 1 spectrum every 5 s.

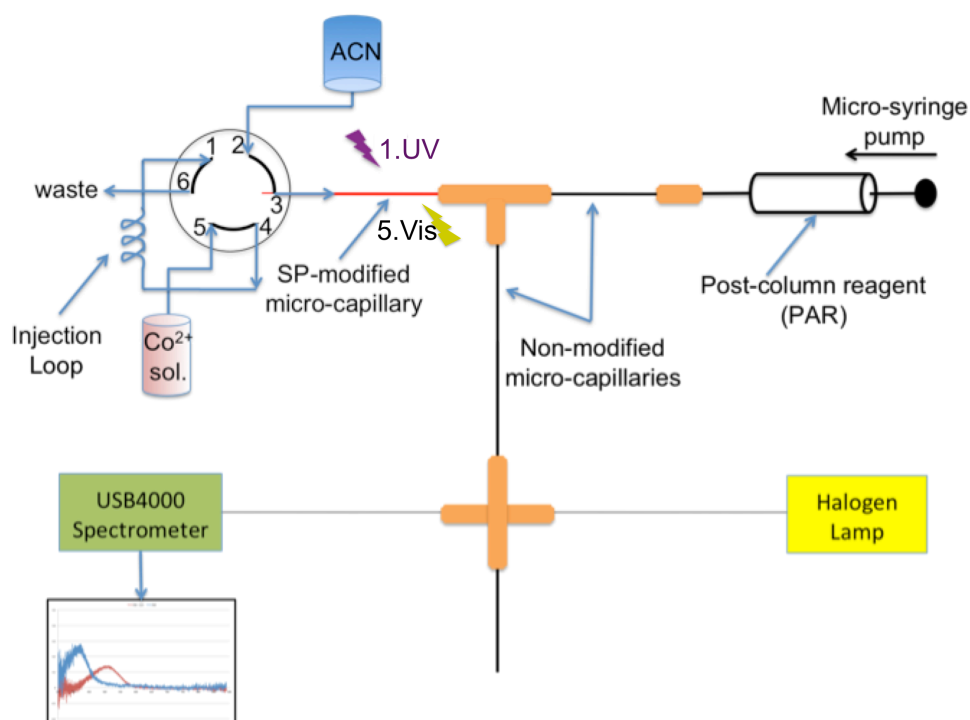


Figure 10.12. Scheme of the set-up used for the determination of metal ions photo-released from the spiropyran modified micro-capillary using post-column derivatisation.

It is expected that, after the irradiation of the micro-capillary with white light, metal ions will be released first and then, when the two pumps will be turned on, the two confluent flows will react and PAR-Co^{2+} will be formed. When reaching the detection area, PAR-Co^{2+} will generate a change in absorbance spectra compared to PAR and the response could be used to quantitatively measured the photo-released metal ions.

10.2.4 Metal Ions Extraction

Fries *et al.* [16] have shown that when methacrylate-based spiropyran copolymer films are exposed to several binary metal ion solutions, based on the binding affinity of the merocyanine to each metal ion - merocyanine binds with either one or both metal ions. These results suggest that, at least in some cases, the micro-capillary platform presented above could be used for targeting metal ion extraction, based on the relative binding preference of the MC-M. Therefore, future work could explore the possibility of using the spiropyran polymer brushes micro-capillary for metal ion extraction in continuous or semi-continuous flow. Spiropyran chemistry could be applicable for extraction of metal ions by first, chelating the ions by using UV light, and subsequently exposing the metal-spiropyran complex to visible light to elute metals efficiently in a concentrated plug as explained in Figure 10.13.

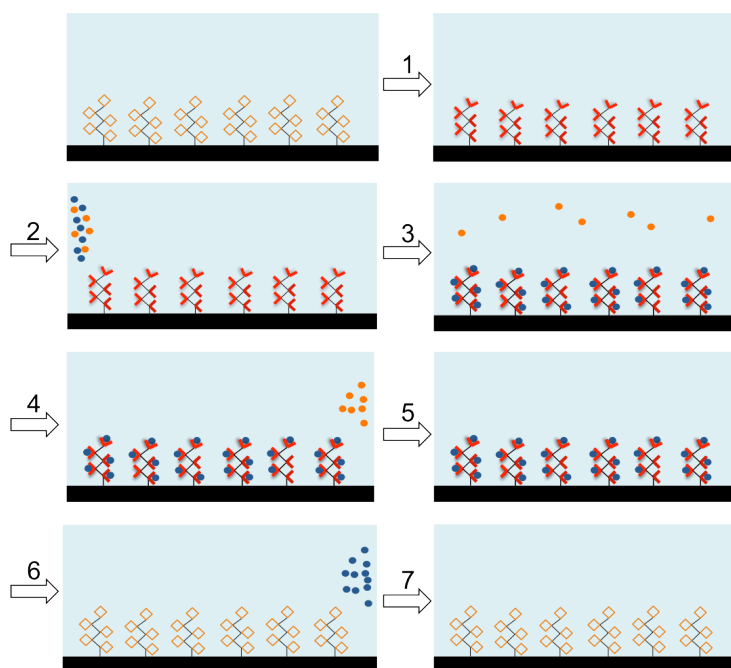


Figure 10.13. Extraction of target metal ions from a binary metal ion solution; non-binding form (\diamond), binding form (\checkmark), targeted metal ions (\bullet), non-targeted metal ions (\bullet); 1 – Opening of the spiropyran to the merocyanine form by irradiation with UV light; 2 – Introduction of target and non-target metal ions inside the micro-capillary; 3 – Binding of the target metal ions to the merocyanine form; 4 – Elution of non-target metal ions; 5 – Only target metal ions are present in the micro-capillary; 6 – Target metal ions are released by irradiation with white light; 7 – The micro-capillary goes back to its initial state.

This process could be used in environmental and industrial processes to remove metals from aqueous solutions [24], where the metals are released from the ligands upon irradiation with visible light in a safe and controlled manner. The use of light to trigger the chelator offers unique opportunities that minimise waste generation and power requirements. In addition, advances in the integration of LED (light emitting diode) sources in the system hold promise for the production of low cost miniaturised systems.

10.3 Photo-activated Propulsion of Ionogel Boats

10.3.1 Introduction

Ionic liquids (ILs) are a class of novel solvents with very interesting properties which are attracting the attention of a growing number of researchers [25]. ILs are organic salts composed of anions and cations that are in the liquid state at ambient conditions and many show negligible volatility and non-flammability [25]. They have also been labeled as ‘designer solvents [25, 26], because it is possible to tailor anions and/or cations for specific functions such as catalysis, solubility and viscosity. Incorporating ILs into polymer gels is also attractive as it may generate materials with the inherent advantages of ILs within a solid or semi- solid gel-type structure [27, 28]. This property could lead to a new era in “vesicle” actuation as the required components for actuation could now be incorporated in the polymer-IL gels matrix without the need to consider solvent evaporation. Moreover, due to the vast library of polymers and ILs available, ionogels could be designed for specific applications with very particular physico-chemical characteristics. Incorporation of a photo-initiator in the monomer-IL mixture could lead to facile fabrication of micro-structured ionogels. In the case of using this type of structure for photo-actuation at the liquid-air interface, the key components could be incorporated in both the polymer matrix (through the use of a compatible monomer) but also dissolved in the ionic liquid, in the case of organic components, that are rather not water-soluble.

10.3.2 From Organic Droplets to Ionogels

If in Chapter 8 of this thesis was demonstrated the photo-activated chemopropulsion of organic droplets, here it is suggested that similar behaviour could be obtain for gel-type structures by the incorporation of the key components inside ionogels. According to the working principle of photo-activated chemopropulsion described in Cahpter 8, those components are:

1. pH sensitive surfactant-type molecule, that shows water-solubility just at low pH conditions;
2. photo-initiator for chemopropulsion (spiropyran).

If in Chapter 8 these key components were dissolved in a dichloromethane (DCM) droplet, next, different compositions of ionogels are suggested in order to achieve similar behaviour. One of the main advantages of this approach is that the ionogels will present improved stability compared to the DCM droplets: negligible evaporation and high thermal stability [25]. Moreover, these ionogels could be polymerised in a variety of two-dimensional structures, including bars, circles, boats, *etc.*

Several chemical compositions are suggested for ionogel “boats” capable of photo-driven actuation at the liquid/air interface. The first generation of ionogel “boats” could have similar composition to the droplet described in Chapter 8, while a more innovative composition could be suggested in a second generation.

10.3.2.1 Ionogel boats – First generation

These ionogel boats have similar composition to the droplet presented in Chapter 8 with the exception that the acid used for the chromoionophore protonation is incorporated inside the polymer matrix. This can be easily achieved through the use of the appropriate monomer or co-monomer. A possible suggestion could be the co-polymerisation of *N*-isopropylacrylamide (NIPAAm) and methacrylic acid, acrylic acid, propylacrylic acid or other appropriate acids from their homologous series. The purpose of the acid is the protonation of the Chromionophore 1 (C1) to C1-H⁺. As C1 is not water-soluble and has long alkyl chains it is not hard to imagine that it will dissolve in the ionic liquids [P₆₆₆₁₄][Tos⁻] and [P₆₆₆₁₄][Dca⁻] due to similar

hydrophobic character. As the IL library is incredibly vast, solubility of organic species like C1 should not be considered an impediment. Having the main conditions fulfilled, actuation of a microstructure ionogel boat on top of the spiropyran –sulfonic acid (SP-SO₃H) aqueous solution could be realised by means of photo-stimulation. Figure 10.14 shows the schematic composition of the ionogel.

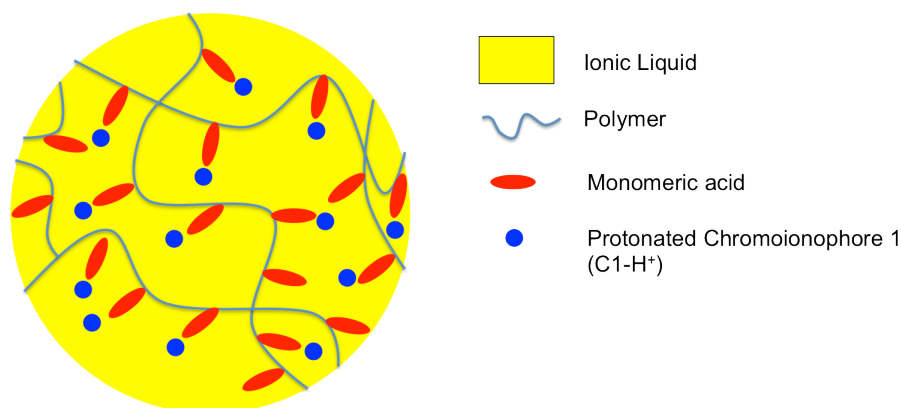


Figure 10.14. Schematic composition of the ionogel suggested for the first generation of photo-actuated ionogel boats.

10.3.2.2 Ionogel boats – Second generation

Second generation of ionogel boats comprises a more innovative approach where the SP-SO₃H solution will no longer be required (see Chapter 8) and photo-actuation of the ionogel boat could be possible in water. For this purpose, spiropyran derivatives (photo-initiator for chemopropulsion) could be incorporated inside the ionogel through polymerisation or co-polymerisation (e.g. acrylated spiropyran derivative)

In this case, both the acid (pH source) and the spiropyran (photo-initiator for chemopropulsion) will be immobilised inside the ionogel, where the only mobile species will be the pH sensitive surfactant molecule (Figure 10.15).

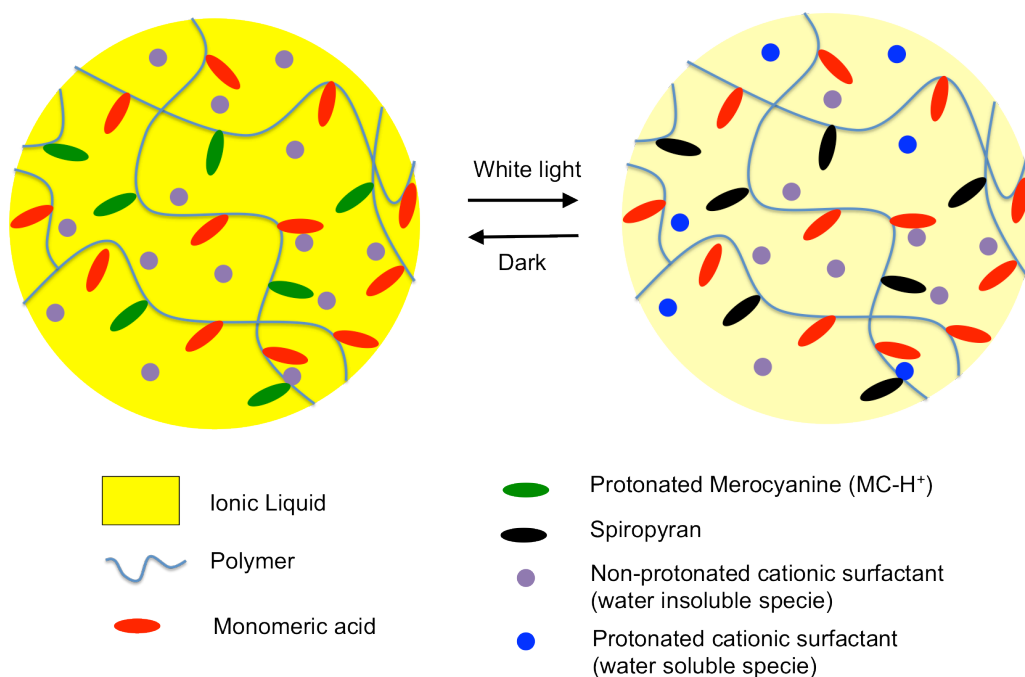


Figure 10.15. Schematic of the composition of the ionogel suggested for the second generation of photo-actuated ionogel boats.

The photo-actuation will follow a cascade of events:

1. The weak acid (suggested $pK_a \sim 4-5$, *e.g.* methacrylic acid, acrylic acid, propylacrylic acid) incorporated inside the polymer should ensure protonation of the spiropyran comonomer to the MC-H⁺ form (Figure 10.15, left).
2. The concentration of the acid and spiropyran monomer inside the ionogel should be high enough to ensure a drop, after photo-stimulation, of at least one pH unit. (*e.g.* ideally, from pH 5 to 3) due to the isomerisation of the MC-H⁺ to SP + H⁺ (Figure 10.15, right).
3. The drop in pH should cause protonation of a cationic surfactant type molecule (dissolved inside the IL), increasing its solubility in water (Figure 10.15, right). Examples of ideal surfactants include betaines that have shown to present cationic surfactant type properties at pH values below 3 [29, 30].
4. The release of the cationic surfactant should cause a localised decrease in the water's surface tension enough to propel the ionogel boat in the opposite direction to the white light irradiated region. Such a movement is described in Figure 10.16.

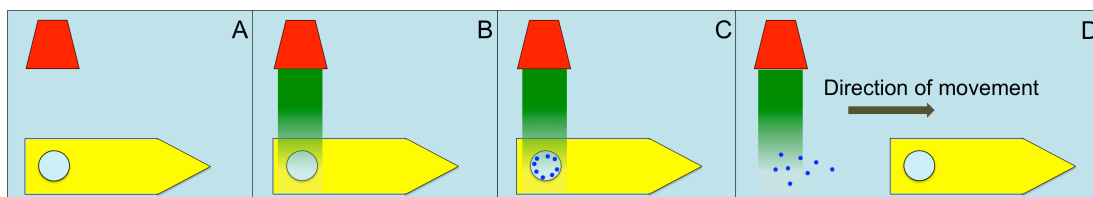


Figure 10.16. Schematic representation of the ionogel “boat” movement on water. A – the boat is stable in the initial conditions; B – upon irradiation with white light, the monomeric MC-H⁺ reverts to SP, causing the generation of free H⁺. C – as a consequence, the free H⁺ protonates the surfactant-type molecule (dissolved inside the IL) generating the cationic surfactant (blue dots), that are soluble in the aqueous solution and can now leave the droplet; D – as soon as this happens, the surface tension of the solution dramatically drops, causing the “boat” to spontaneously move to the opposite direction of the light source.

10.4 Conclusions

Micro-fluidics has shown great potential to revolutionise chemical synthesis and biological analysis by providing automation, high accuracy, low time and energy consumption, and great reconfigurability [31, 32]. However, despite enormous efforts in the area, many microfluidic systems still depend on optical analysis systems or electrical power supply systems, making these devices still large and bulky, and inhibiting their use from real practical applications. Therefore, there is a general scientific effort to develop innovative systems capable of preparing, actuating and/or analysis of samples “on-chip” [33].

In this thesis, there have been several strategies investigated to develop ways to provide functional microfluidic platforms where fluid actuation and chemical sensing of target species could be controlled externally by means of photo-stimulation. This key objective has been driven by the immediate need of non-ambiguous micro-fluidics integrated chemical sensors for medical purposes, self-diagnostic and wearables, among others. The author believes that the possibility of controlling flow and sensing in micro-fluidics using opto-stimulus will offer new platforms with unprecedented flexibility and improved versatility. In these regards, several approaches for photo-actuation of flow have been proposed including the photo-operation of polymeric valves, photo-control of electro-osmotic flows or photo-manipulation of discrete microliter-sized droplets.

Regarding sensing, the possibility of having the sensing material covalently attached on the inner walls of the micro-fluidic platform (micro-channel, micro-capillary) offers the possibility of dynamic and continuous sensing of changing flows. In addition, the use of polymeric sensing materials, rather than the monolayer approach ensures high density of the sensing unit, which is ideal when dealing with micro-fluidic platforms as they involve extremely short path lengths. In these conditions, optical sensing can be simply realised using conventional spectroscopic/optical techniques without the need of complicated micro-fluidic designs.

The examples presented in this thesis give some indication of the potential of using an optical stimulus for photo-modulation of flow behavior in micro-fluidics by incorporating photo-responsive units into polymeric actuators, coatings, or surfactants. Although these examples can only hint at the possibilities, such as photo-modulation of flows or photo-induced droplet formation in micro-fluidics, the reader can gain some knowledge of the tools now available to achieve these effects. Incorporation of photo-responsive or phononic-responsive molecules in micro-fluidics together with smart engineering of the opto-functional unit can provide switchable characteristics that have great potential for many target applications. Opto-controlled micro-fluidics can open new possibilities based on exceptional flexibility, versatility, reduced costs and simplicity. Moreover, advanced features such as parallel manipulation of multiple spatially resolved photo-responsive units through the use of patterned light exposure, variable light intensities, selectable wavelengths, and excellent temporal control, become practically achievable.

The ideas presented in this last chapter represent just few of the possible following paths of the work presented in this thesis. The success of these suggested approaches is still to be confirmed and they should be seen as opportunities for future research. The author believes that the concept of stimuli-responsive materials for micro-fluidic purposes is an extremely important area to be explored and autonomous, easily manipulated, facile and cheap micro-fluidic platforms with multiple functionalities can only be achieved through the use of innovative materials, original designs and outside-the-box approaches.

However, the future of opto-manipulated micro-fluidics relies on convincing demonstrations of their application to real scenarios in which their unique photo-controlled characteristics lead to truly disruptive platforms for studying chemical or biological processes compared to existing technologies.

This last chapter serves also as guidance for future students willing to explore the area of stimuli-responsive materials and their applications in micro-fluidics devices.

10.5 References

1. Luo, C.; Li, H.; Liu, X., Propulsion of microboats using isopropyl alcohol as a propellant. *Journal of Micromechanics and Microengineering* **2008**, *18*, 067002.
2. Walton, G., Propulsion process for lightweight miniature toy boats. In Google Patents: 1993.
3. West, J.; Becker, M.; Tombrink, S.; Manz, A., Micro total analysis systems: Latest achievements. *Analytical Chemistry* **2008**, *80*, 4403-4419.
4. Kumar, V.; Paraschivoiu, M.; Nigam, K. D. P., Single-phase fluid flow and mixing in microchannels. *Chemical Engineering Science* **2011**, *66*, 1329-1373.
5. Stroock, A. D.; Dertinger, S. K. W.; Ajdari, A.; Mezic, I.; Stone, H. A.; Whitesides, G. M., Chaotic mixer for microchannels. *Science* **2002**, *295*, 647-651.
6. Liu, Y. Z.; Kim, B. J.; Sung, H. J., Two-fluid mixing in a microchannel. *International Journal of Heat and fluid flow* **2004**, *25*, 986-995.
7. Ocvirk, G.; Tang, T.; Harrison, D. J., Optimization of confocal epifluorescence microscopy for microchip-based miniaturized total analysis systems. *Analyst* **1998**, *123*, 1429-1434.
8. Melanson, J. E.; Lucy, C. A., Violet (405 nm) diode laser for laser induced fluorescence detection in capillary electrophoresis. *Analyst* **2000**, *125*, 1049-1052.
9. Park, T.; Lee, M.; Choo, J.; Kim, Y. S.; Lee, E. K.; Kim, D. J.; Lee, S. H., Analysis of passive mixing behavior in a poly(dimethylsiloxane) microfluidic channel using confocal fluorescence and Raman microscopy. *Applied Spectroscopy* **2004**, *58*, 1172-1179.
10. Salimi-Moosavi, H.; Jiang, Y. T.; Lester, L.; McKinnon, G.; Harrison, D. J., A multireflection cell for enhanced absorbance detection in microchip-based capillary electrophoresis devices. *Electrophoresis* **2000**, *21*, 1291-1299.
11. Lu, H.; Schmidt, M. A.; Jensen, K. F., Photochemical reactions and on-line UV detection in microfabricated reactors. *Lab on a Chip* **2001**, *1*, 22-28.
12. Greenway, G. M.; Nelstrop, L. J.; Port, S. N., Tris(2,2-bipyridyl)ruthenium (II) chemiluminescence in a microflow injection system for codeine determination. *Analytica Chimica Acta* **2000**, *405*, 43-50.
13. Xu, Y.; Bessoth, F. G.; Eijkel, J. C. T.; Manz, A., On-line monitoring of chromium(III) using a fast micromachined mixer/reactor and chemiluminescence detection. *Analyst* **2000**, *125*, 677-683.
14. Shinohara, K.; Sugii, Y.; Hibara, A.; Tokeshi, M.; Kitamori, T.; Okamoto, K., Rapid proton diffusion in microfluidic devices by means of micro-LIF technique. *Experiments in Fluids* **2005**, *38*, 117-122.
15. Oehme, I.; Wolfbeis, O. S., Optical sensors for determination of heavy metal ions. *Mikrochimica Acta* **1997**, *126*, 177-192.
16. Fries, K. H.; Driskell, J. D.; Sheppard, G. R.; Locklin, J., Fabrication of Spiropyran-Containing Thin Film Sensors Used for the Simultaneous Identification of Multiple Metal Ions. *Langmuir* **2011**, *27*, 12253-12260.
17. Benito-Lopez, F.; Scarmagnani, S.; Walsh, Z.; Paull, B.; Macka, M.; Diamond, D., Spiropyran modified micro-fluidic chip channels as photonically controlled self-indicating system for metal ion accumulation and release. *Sensors and Actuators B-Chemical* **2009**, *140*, 295-303.

18. Fries, K. H.; Driskell, J. D.; Samanta, S.; Locklin, J., Spectroscopic Analysis of Metal Ion Binding in Spiropyran Containing Copolymer Thin Films. *Analytical Chemistry* **2010**, *82*, 3306-3314.
19. Zemann, A. J., Capacitively coupled contactless conductivity detection in capillary electrophoresis. *Electrophoresis* **2003**, *24*, 2125-2137.
20. Tanyanyiwa, J.; Hauser, P. C., High-voltage contactless conductivity detection of metal ions in capillary electrophoresis. *Electrophoresis* **2002**, *23*, 3781-3786.
21. de Castro, M. L.; Fernandez-Romero, J., Post-Column On-Line HPLC Measurement of Reaction Rates by using an Open, Closed Derivatizing System. *Journal of Chromatographic Science* **1991**, *29*, 377-381.
22. Ghasemi, J.; Niazi, A.; Maeder, M., Spectrophotometric studies on the protonation and nickel complexation equilibria of 4-(2-pyridylazo) resorcinol using global analysis in aqueous solution. *Journal of the Brazilian Chemical Society* **2007**, *18*, 267-272.
23. Ghasemi, J.; Peyman, H.; Meloun, M., Study of complex formation between 4-(2-pyridylazo) resorcinol and Al^{3+} , Fe^{3+} , Zn^{2+} , and Cd^{2+} ions in an aqueous solution at 0.1 m ionic strength. *Journal of Chemical and Engineering Data* **2007**, *52*, 1171-1178.
24. Lichtfouse, E.; Schwarzbauer, J.; Didier, R., *Environmental Chemistry: Green Chemistry and Pollutants in Ecosystems* Springer: 2004; p 780.
25. Rogers, R. D.; Seddon, K. R., Ionic liquids--solvents of the future? *Science* **2003**, *302*, 792-793.
26. Marsh, K.; Boxall, J.; Lichtenthaler, R., Room temperature ionic liquids and their mixtures, A review. *Fluid Phase Equilibria* **2004**, *219*, 93-98.
27. Le Bideau, J.; Viau, L.; Vioux, A., Ionogels, ionic liquid based hybrid materials. *Chemical Society Reviews* **2011**, *40*, 907-925.
28. Kavanagh, A.; Byrne, R.; Diamond, D.; Fraser, K. J., Stimuli Responsive Ionogels for Sensing Applications, An Overview. *Membranes* **2012**, *2*, 16-39.
29. Danov, K.; Kralchevska, S.; Kralchevsky, P.; Ananthapadmanabhan, K.; Lips, A., Mixed solutions of anionic and zwitterionic surfactant (Betaine): Surface-tension isotherms, adsorption, and relaxation kinetics. *Langmuir* **2004**, *20*, 5445-5453.
30. Vialle, J.; Kolosky, M.; Rocca, J., Determination of betaine in sugar and wine by liquid chromatography. *Journal of Chromatography A* **1981**, *204*, 429-435.
31. Ohno, K. A.; Tachikawa, K.; Manz, A., Microfluidics: applications for analytical purposes in chemistry and biochemistry. *Electrophoresis* **2008**, *29*, 4443-4453.
32. Whitesides, G. M., The origins and the future of microfluidics. *Nature* **2006**, *442*, 368-373.
33. Byrne, R.; Benito-Lopez, F.; Diamond, D., Materials science and the sensor revolution. *Materials Today* **2010**, *13*, 9-16.

Appendix A

Supporting Information for **Polyaniline Coated Micro-capillaries for Continuous Flow Analysis of Aqueous Solutions**

Larisa Florea¹, Dermot Diamond¹ and Fernando Benito-Lopez^{1,2,*}

Analytica Chimica Acta 759 (2013) 1-7

ISSN: 0003-2670; DOI: 10.1016/j.aca.2012.11.027

Available free of charge at <http://dx.doi.org/>

¹CLARITY: Centre for Sensor Web Technologies, National Centre for Sensor Research, School of Chemical Sciences, Dublin City University, Dublin, Ireland;

²CIC microGUNE, Arrasate-Mondragón, SPAIN

*Author to whom correspondence should be addressed;

Table A1. Average absorbance reading and their standard deviation different concentration of aqueous ammonia.

| Concentration (ppm) | Average absorbance at 600 nm (a.u.) | Standard Deviation | Number of measurements (n) |
|---------------------|-------------------------------------|--------------------|----------------------------|
| 0 | 0.1510 | 0.0006 | 108 |
| 0.2 | 0.1670 | 0.0006 | 108 |
| 2 | 0.1820 | 0.0006 | 108 |
| 20 | 0.2080 | 0.0006 | 108 |
| 200 | 0.2250 | 0.0006 | 108 |
| 2000 | 0.2450 | 0.0007 | 108 |

Appendix B

Supporting Information for **Dynamic pH mapping in micro-fluidic devices by integrating adaptive coatings based on polyaniline with colorimetric imaging techniques**

Larisa Florea ¹, Cormac Fay ¹, Emer Lahiff ¹, Thomas Phelan ¹, Noel E.
O'Connor ¹, Brian Corcoran ¹, Dermot Diamond ¹ and
Fernando Benito-Lopez^{1, 2, *}

Lab on a Chip 13 (2013) 1079-1085

ISSN: 1473-0197; <http://dx.doi.org/10.1039/C2LC41065F>

(Available free of charge at DOI: 10.1039/b000000x/)

¹CLARITY: Centre for Sensor Web Technologies, National Centre for Sensor Research, School of Chemical Sciences, Dublin City University, Dublin, Ireland;

²CIC microGUNE, Arrasate-Mondragón, SPAIN

*Author to whom correspondence should be addressed;

B.1 Materials and Methods

Aniline (BDH), HCl (Fisher Scientific), ammonium persulfate (Aldrich), *N*-[3-(Trimethoxysilyl)propyl]aniline (Aldrich), sodium hydroxide (Aldrich) were used. The aniline monomer was purified by vacuum distillation before use. Other chemicals were used as received.

Raman Spectroscopy was employed to study the chemical features of the polyaniline coatings inside the micro-channel. Raman spectra were taken with a Perkin Elmer RamanStation at 2 cm⁻¹ resolution, 3s per scan and 10–20 collections. A 785 nm laser line was used as it can detect both doped and dedoped features in polyaniline.

Scanning Electron Microscopy (SEM) was carried out at an accelerating voltage of 20kV on a S-4300 Hitachi system. For imaging purposes the PDMS layer of the PDMS/glass micro-channel was removed. The glass layer containing the polyaniline film was coated with 10 nm Au prior to imaging.

UV-Vis Spectroscopy was used to study the pH dependence of the polyaniline coatings. The absorbance spectra were recorded using two fiber-optic light guides connected to a Miniature Fiber Optic Spectrometer (USB4000 - Ocean Optics) and aligned using an in-house made cell (see Figure B1). The light source used was a Deuterium – Halogen light source (Top Sensor Systems).

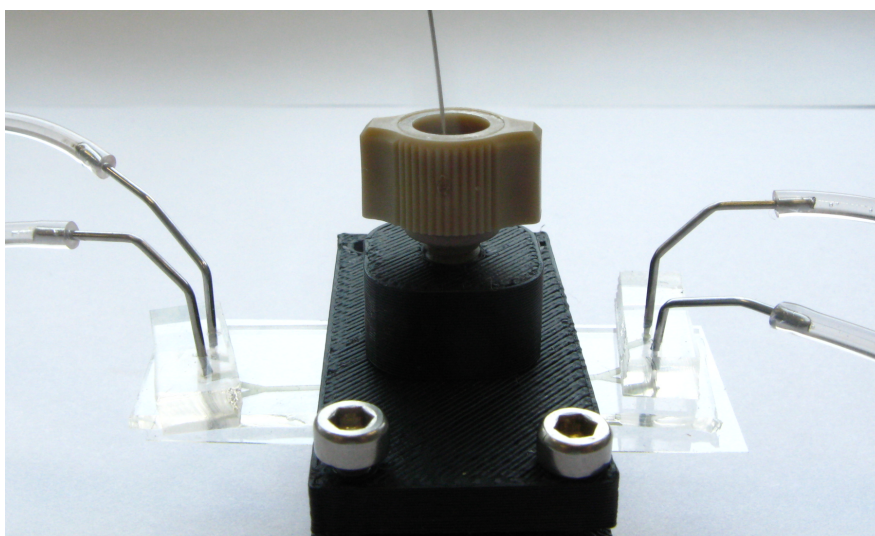


Figure B1. In house designed holder used for absorbance measurements of the PANi coatings.

B.2 Digital Image Capture

Throughout the calibration routine, the images were captured using a Panasonic DMC-FZ38 digital colour camera which was held in a fixed position via a retort stand at a distance of 7 cm from the micro-channel / reference chart to fully capture the image scene, see Figure B2 left. The camera was set to capture in RAW format to eliminate possible image artefacts and at a resolution of 4016x 3016 (12 MPixels). The other camera settings were as follows: F-Number (2.8), Max aperture (F2.8), No Flash and a Focal Length of 4.8 mm.

Once the images were captured, they underwent a segmentation process where pixels representing the flow channel and reference patches were identified and separated into image regions. This was achieved through the use of an Interactive Segmentation Toolkit [1]. Although an unsupervised/automatic segmentation algorithm was possible, it was felt that this supervised approach was more robust to misclassifications and as a result, it fully ensured the location and determination of the reference patches and channel regions. A binary mask image resulted from this process with black pixels representing areas of non interest (*e.g.* the background) and white regions representing the reference colour patches and the flow channel. Finally, a binary erosion algorithm was applied to remove possible boundary pixels and also any isolated white pixels *i.e.* to ensure robustness for subsequent processing steps, see Figure B2 right.



Figure B2. Picture of a captured image (left) during the experimental procedure showing the colour reference chart/patches and flow channel. Mask image (right) after image processing algorithms are applied.

Next, it was necessary to identify each region separately for correct analysis. Therefore, a connected component analysis step was applied to the binary mask image, which assigned a unique region identification number to each image area with connected white pixels. This allowed for each of the reference patches and flow channel to be analysed separately at a later stage. Subsequently, due to the consistency across all images (from the experimental constraints) it was possible to easily identify each region based on their spatial coordinates within the image. As a result, each patch was identified correctly in all instances via their calculated centroid locations in each subsequent image.

After that, the calibration images were taken and processed. Initially, the original images underwent a white balance process in order to compensate for possible changes in the ambient lighting environment. This involved generation of the histograms for each of the Red, Green and Blue channels of the captured sRGB colour space. Next, a bin threshold was determined at either end of each histogram. Pixel counts that used less than 0.05 % of the total image pixels were discarded at each histogram ends and the histograms were stretched to the boundary *i.e.* 0 and 255. The images were then reconstructed. Next, a copy of this image was made and transformed from the captured sRGB colour space into the Hue, Saturation and Value colour space (HSV) [2]. Following this, the binary mask image was applied to the HSV image through a simple pixel-by-pixel binary AND operation on the Hue channel alone. Finally, the colour of each region was ascertained by calculating its Hue average and saving it to an external file in CSV (comma separated value) format for all regions within each image for later analysis.

The gradient analysis step took place in much the same way as with the calibration image processing. However, instead of calculating the Hue average over the entire flow channel region, a localised average was considered at discrete points along the channel's path. This was achieved by firstly isolating the flow channel region alone via its bounding box and using that to crop the image thereby removing the reference patches. Here, a medial axis transformation was applied to this singular binary region resulting in an 8-connected contour line along the centre of the channel at a width of 1 pixel [3], see Figure B3. After this, the starting point was identified to be at the most extreme upper left white pixel of the contour. Next, a binary circular mask image with a diameter of 35 pixels was created and combined (binary AND

operation) with the binary mask image of the channel at the starting point. The resulting mask was, in turn, applied to the Hue channel at the same location. Finally, the average Hue value at this sub region was calculated and saved to a CSV file. The process was repeated at every pixel location along the contour with all values saved to file.

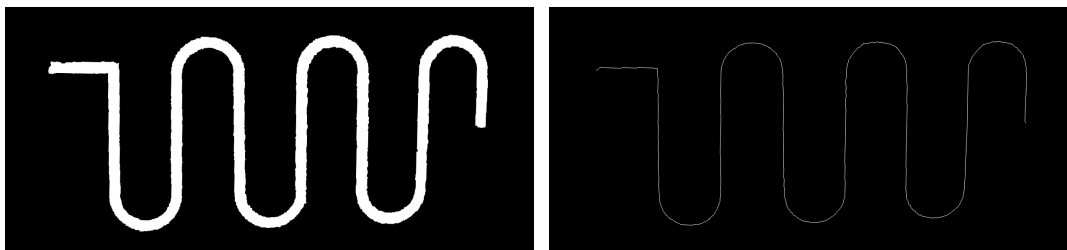


Figure B3. Processed images showing the mask region of the flow channel (left) and the result of applying a medial axis transformation (right).

B.3 Characterisation of Polyaniline (PAni) Coating by Raman Spectroscopy

Raman spectroscopy is a very powerful technique for the analysis of intrinsically conducting polymers. Here, Raman spectroscopy is employed to study the chemical structure of the coating as this technique permits in situ analysis of the polyaniline coating inside the micro-channel. In the case of polyaniline, Raman spectroscopy can also be used to study its doping-dedoping behaviour as very distinct signature bands appear for the quinoid and benzenoid rings respectively.

Figure B4 presents the Raman spectra of a polyaniline functionalised micro-channel taken after a solution of pH 2 (HCl, 10^{-2} M) and pH 12 (NaOH, 10^{-2} M), respectively are passed inside the micro-channel. For comparison, the spectrum of a bare PDMS micro-channel is also shown (black). For low pH values the polymer exists in the doped state, emeraldine salt (ES). Increasing the pH causes a change in the bonding structure of the material, and at high pH values PAni is present in its dedoped state – emeraldine base (EB). Signature bands between 1300 and 1400 cm^{-1} appear for the doped material (Figure B2 – in green). These are less significant at

higher pH values, and strong bands between 1400 and 1500 cm^{-1} reflect the dedoped state (Figure B4 – in blue).

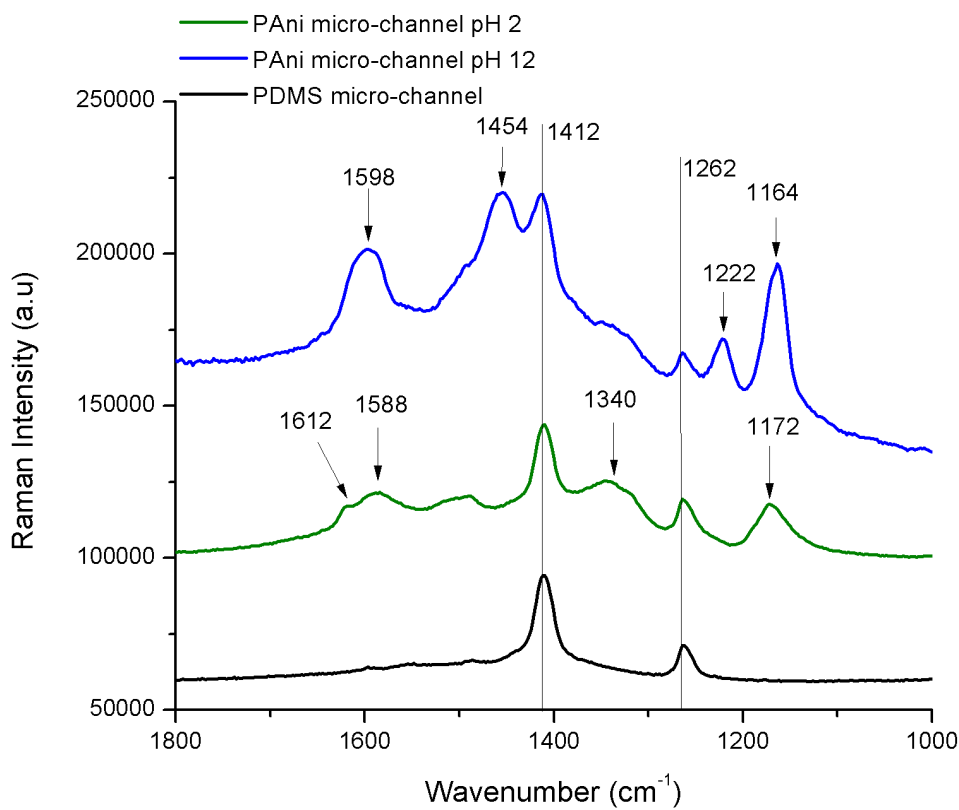


Figure B4. Raman Spectra of unfunctionalised PDMS micro-channel (black), PANi functionalised micro-channel after being filled with a pH2 HCl solution (green) and PANi functionalised micro-channel after being filled with a pH12 NaOH solution (blue).

In particular, in the case of EB, an important peak can be observed at 1454 cm^{-1} and is characteristic to C=N stretching vibration of the quinoid units [4-8]. Other bands at 1596 cm^{-1} and 1164 cm^{-1} , are assigned to C-C stretching [4, 7] and C-H bending modes [4, 5], respectively, centered on the quinoid ring. Another new peak at 1221 cm^{-1} appears in the spectra of polyaniline upon dedoping and is assigned to C-N stretching vibrations of the benzenoid units [4, 7] (the EB form consists of both C=N and C-N bonds). In the case of ES, the most important band appears at 1340 cm^{-1} and can be assigned to a C-N• + polaron stretch [4, 7, 9, 10] while the band at 1172 cm^{-1} is characteristic to the C-H in-plane bending of the benzenoid ring [4, 8]. Both C - C stretching vibrational modes, in the benzenoid and quinoid rings, are seen at 1612 cm^{-1} and 1588 cm^{-1} , respectively [7], in the case of

polyaniline spectra taken at pH 2. This suggests that minor fractions of non protonated quinoid rings are still present in the structure. It has been shown before that the Raman Intensity is enhanced in the case of EB compared with ES when a 785 nm laser is used [8]. The PANi coating may also be partially excited to the EB form by the incoming laser radiation resulting in resonant enhancement of the lines originating from the quinoid ring [7]. The specific vibrations of PDMS can also be found in the spectra of polyaniline coatings since polyaniline is attached to the inner walls of the PDMS/ glass micro-channel. The CH₃ bending vibrations appear at 1263 cm⁻¹ and 1412 cm⁻¹ [11]. Other bands specific to the PDMS layer are also present: Si-O-Si symmetric stretching (490 cm⁻¹), Si-C symmetric stretching (708 cm⁻¹), CH₃ symmetric stretching (2904 cm⁻¹), and CH₃ asymmetric stretching (2964 cm⁻¹)[11], but not shown here.

B.4 pH Measurements

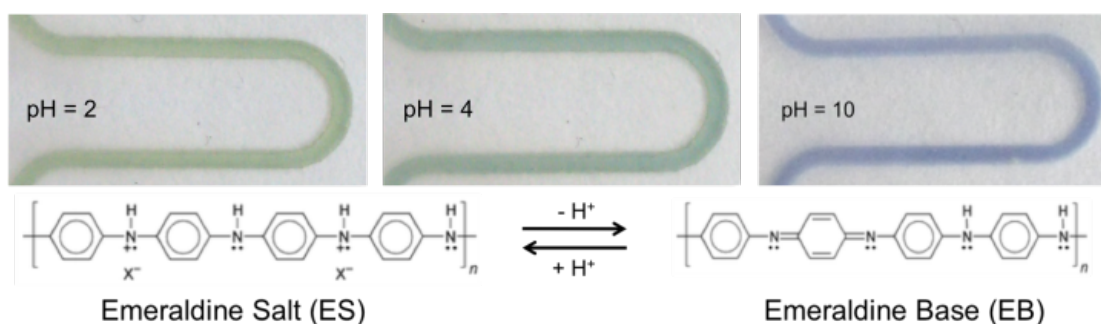


Figure B5. Photos of a micro-channel loop when solutions of different pHs are flushed through the channel. The photos are accompanied by a scheme showing the differences in the chemical structure of polyaniline (two different states: Emeraldine Salt and Emeraldine Base).

B.5 pH Determination via Colorimetric Imaging Analysis

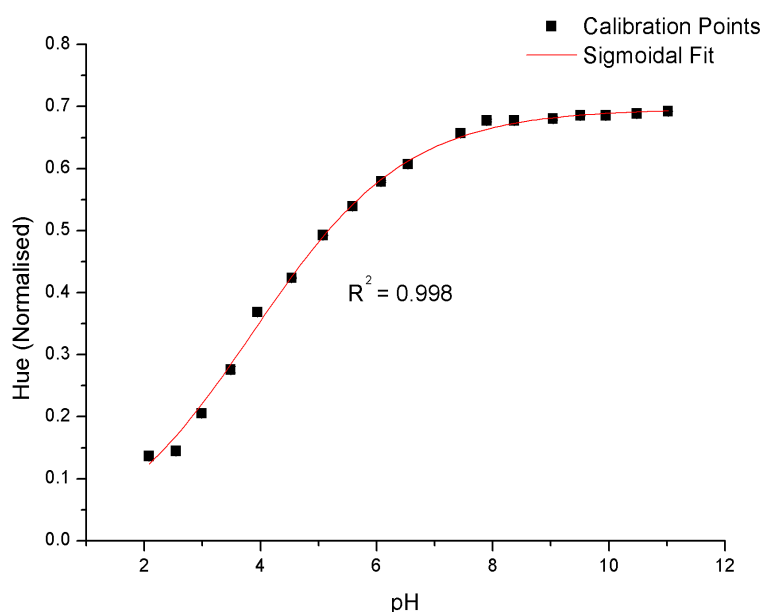


Figure B6. Calibration plot of the camera and channel to changing pH. Points represent the normalised average Hue value of the channel's colour across multiple images and the error bars (occluded by the points) represent their standard deviation. The line is a sigmoidal fit after applying Boltzmann's regression technique ($R^2 = 0.998$, $n = 18$).

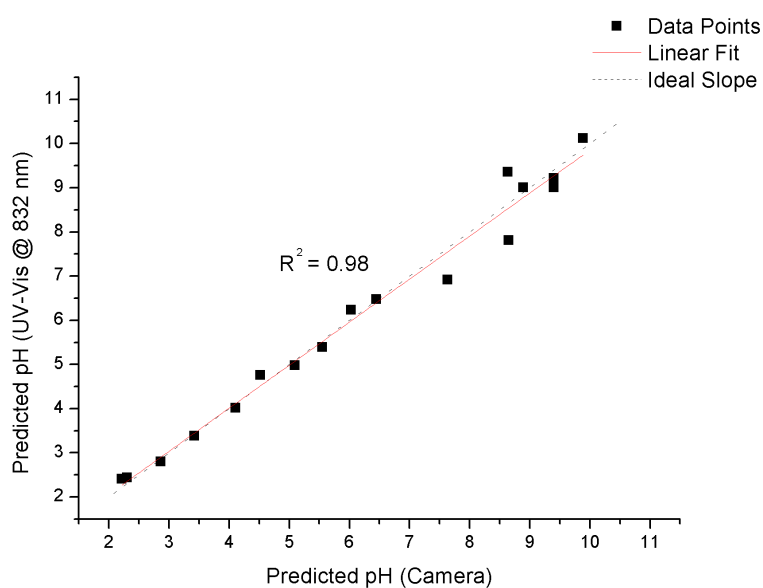


Figure B7. Plot showing the correlation between predicted pH using the camera and UV-Vis at 832 nm. The line represents a linear fit ($R^2 = 0.98$, $n = 18$).

B.6 References

1. McGuinness, K.; O'Connor, N. E., A comparative evaluation of interactive segmentation algorithms. *Pattern Recognition* **2010**, *43*, 434-444.
2. Smith, A. R., Color gamut transform pairs. *SIGGRAPH Comput. Graph.* **1978**, *12*, 12-19.
3. Zhang, T. Y.; Suen, C. Y., A fast parallel algorithm for thinning digital patterns. *Communications of the Acm* **1984**, *27*, 236-239.
4. Berrada, K.; Quillard, S.; Louarn, G.; Lefrant, S., Polyanilines and substituted polyanilines - A comparative-study of the Raman-spectra of leucoemeraldine, emeraldine and pernigraniline. *Synthetic Metals* **1995**, *69*, 201-204.
5. Furukawa, Y.; Hara, T.; Hyodo, Y.; Harada, I., Vibrational-spectra of polyaniline and its N-15-substituted and H-2-substituted derivatives in as-polymerized, alkali-treated and reduced states. *Synthetic Metals* **1986**, *16*, 189-198.
6. Hugotlegoff, A.; Bernard, M. C., Protonation and oxidation processes in polyaniline thin-films studied by optical multichannel analysis and in-situ Raman-spectroscopy. *Synthetic Metals* **1993**, *60*, 115-131.
7. Laska, J.; Girault, R.; Quillard, S.; Louarn, G.; Pron, A.; Lefrant, S., Raman spectroscopic studies of polyaniline protonation with bis(2-ethylhexyl) hydrogen phosphate. *Synthetic Metals* **1995**, *75*, 69-74.
8. Lindfors, T.; Ivaska, A., Raman based pH measurements with polyaniline. *Journal of Electroanalytical Chemistry* **2005**, *580*, 320-329.
9. Liu, C.; Zhang, J. X.; Shi, G. Q.; Chen, F. E., Doping level change of polyaniline film during its electrochemical growth process. *Journal of Applied Polymer Science* **2004**, *92*, 171-177.
10. Mazeikiene, R.; Statino, A.; Kuodis, Z.; Niaura, G.; Malinauskas, A., In situ Raman spectroelectrochemical study of self-doped polyaniline degradation kinetics. *Electrochemistry Communications* **2006**, *8*, 1082-1086.
11. Bae, S. C.; Lee, H.; Lin, Z. Q.; Granick, S., Chemical imaging in a surface forces apparatus: Confocal Raman spectroscopy of confined poly(dimethylsiloxane). *Langmuir* **2005**, *21*, 5685-5688.

Appendix C

Supporting Information for **Spiropyran polymeric micro-capillary coatings for photo-detection of solvent polarity**

Larisa Florea¹, Aoife McKeon¹, Dermot Diamond¹ and
Fernando Benito-Lopez^{1, 2*}

Langmuir 29 (2013) 2790-2797

ISSN: 0743-7463, <http://dx.doi.org/10.1021/la304985p>

(Available free of charge at <http://pubs.acs.org>.)

¹CLARITY: Centre for Sensor Web Technologies, National Centre for Sensor Research, School of Chemical Sciences, Dublin City University, Dublin, Ireland;

²CIC microGUNE, Arrasate-Mondragón, Spain, Tel.: +34 943710212

*Author to whom correspondence should be addressed;

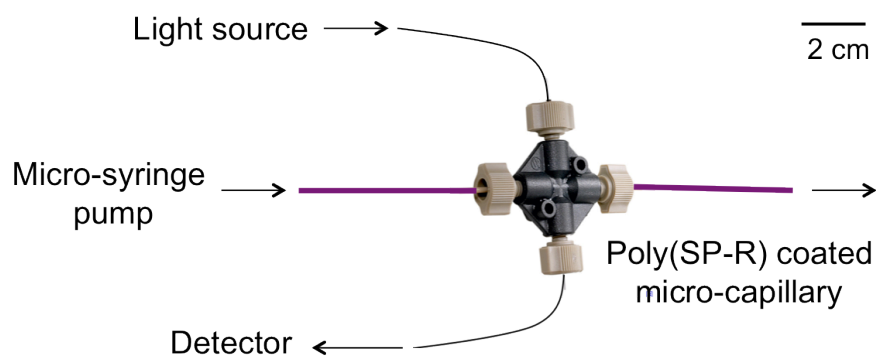


Figure C1. Set-up used for absorbance and kinetics measurements for the poly(SP-M) capillary coatings.

C.1 Kinetics of Photo-induced Ring Opening of Poly(SP-M) Coatings

The first order rate constants were estimated by fitting the absorbance values at λ_{max} using single exponential model (eqn. (1)). The used software was Microsoft Excel Solver. The kinetic curves obtained and the fitting models are presented in Figure C2.

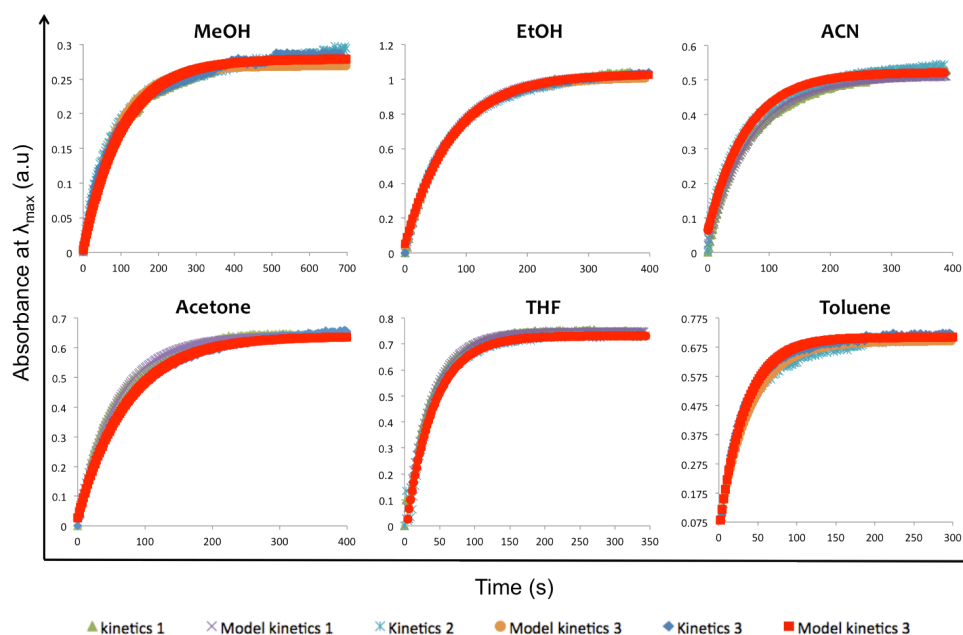


Figure C2. Experimental and fitted kinetic curves of the photo-induced ring opening of poly(SP-M) coatings in different solvents (toluene, tetrahydrofuran (THF), acetone, acetonitrile (ACN), ethanol (EtOH) and methanol (MeOH)) ($n = 3$).

C.2 Kinetics of Photo-induced Ring Opening of SP-M Monomer in Solution

To obtain the rate constants of the ring opening process for SP-M monomer, solutions of the monomer (10^{-3} M) in the six different solvents (toluene, THF, acetone, ACN, EtOH and MeOH) were continuously monitored during UV irradiation at 365 nm. The absorbance value of the MC-M was recorded at the corresponding λ_{\max} in each solvent at fixed time intervals (1 s) for 400 s (Figure C3 and C4). To minimise diffusion effects, the cuvette used in this study was 1 mm wide, with the UV LED array (365 nm) placed above the cuvette at a distance of 2 cm. The temperature on the temperature controller of the Varian Cary 100 UV-Visible Spectrophotometer was set to 20.0 ± 0.1 °C.

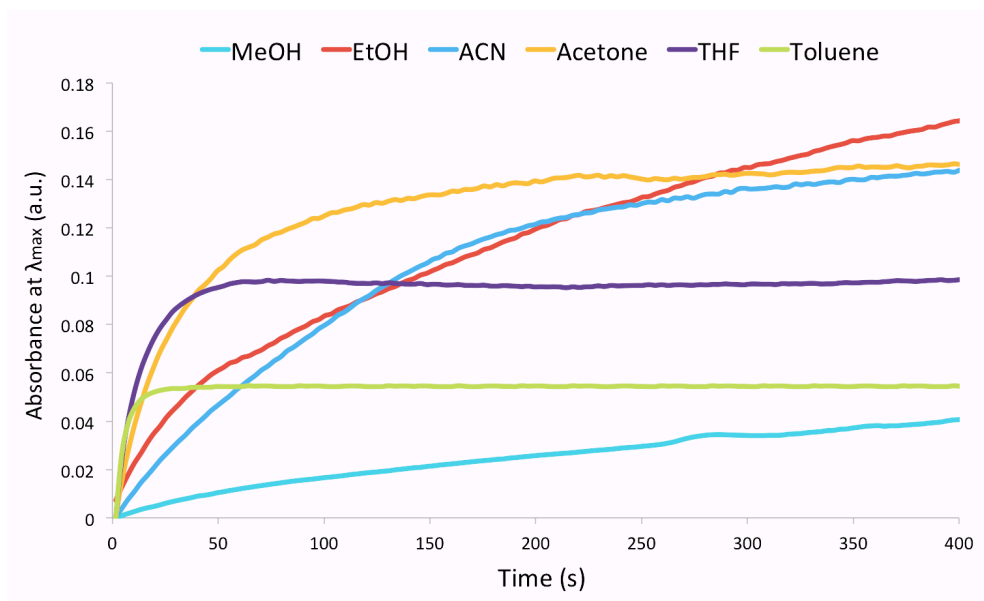


Figure C3. Ring opening kinetics of the spiropyran monomer (SP-M) solutions (10^{-3} M) in different solvents showing the conversion of SP-M to MC-M under continuous irradiation at 365 nm. The values of the absorbance were taken at $\lambda_{\text{max}} = 540$ nm for MeOH, $\lambda_{\text{max}} = 552$ nm for EtOH, $\lambda_{\text{max}} = 568$ nm for ACN, $\lambda_{\text{max}} = 574$ nm for acetone, $\lambda_{\text{max}} = 587$ nm for THF and $\lambda_{\text{max}} = 609$ nm for toluene.

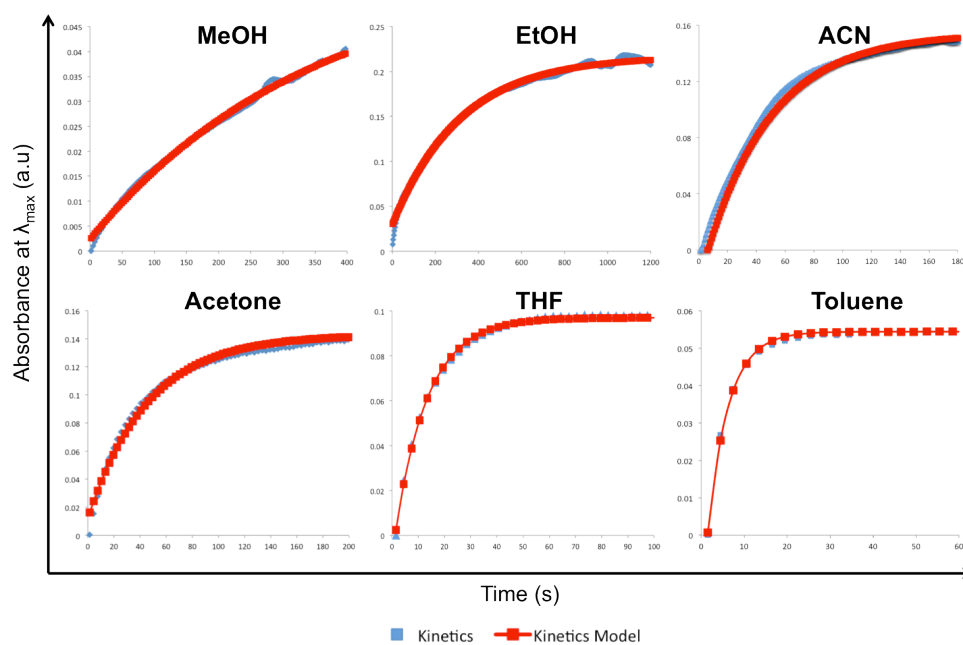


Figure C4. Experimental and fitted kinetic curves of the photo-induced ring opening of SP-M monomer solutions (10^{-3} M) in different solvents.

Table C1. Rate constants for the photo-induced ring opening process of SP-M monomer solutions (10^{-3} M) in different solvents obtained from the fitted kinetic curves (Figure C3).

| Solvent | Ring-opening Kinetics (<i>k</i>) (s⁻¹) | Absolute error (%) |
|----------------|--|-------------------------------|
| Methanol | 2.89×10^{-3} | 2.9 % |
| Ethanol | 3.15×10^{-3} | 2.8 % |
| ACN | 7.32×10^{-3} | 3.0 % |
| Acetone | 2.18×10^{-2} | 2.8 % |
| THF | 8.05×10^{-2} | 1.8 % |
| Toluene | 2.04×10^{-1} | 0.5 % |

Appendix D

Supporting Information for **Photo-activated Chemopropulsion of Organic Droplets**

Larisa Florea ¹, Klaudia Wagner ², Pawel Wagner ², David L. Officer ^{2*},
Gordon W. Wallace ², Fernando Benito-Lopez^{1,3*}
and Dermot Diamond¹
(Manuscript in preparation)

¹CLARITY: Centre for Sensor Web Technologies, National Centre for Sensor Research, School of Chemical Sciences, Dublin City University, Dublin, Ireland;

² ARC Centre of Excellence for Electromaterials Science and Intelligent Polymer Research Institute University of Wollongong, Wollongong, NSW 2522, Australia

³CIC microGUNE, Arrasate-Mondragón, Spain, Tel.: +34 943710212

*Author to whom correspondence should be addressed;

D.1 Characterisation of Spiropyran Sulfonic Acid (SP-SO₃H)

¹H NMR (DMSO): 11.34 (s, 1H, -HSO₃), 8.51-8.47 (d, 1H), 8.26-8.25 (d, 1H), 7.91 (m, 1H), 7.86-7.84 (m, 1H), 7.78-7.73 (d, 1H), 7.70-7.67 (m, 1H), 7.63-7.60 (m, 2H), 7.00-6.98 (d, 1H), 4.09 (s, 3H, N-CH₃), 1.77 (s, 6H, CH₃).

D.2 Photoirradiation

White light irradiation for the photo-activated chemopropulsion of droplets was provided via a LMI-6000 LED Fiber Optic Illuminator obtained from Dolan-Jenner Industries, Massachusetts, or via a single white light LED (emissions centred at 450 and 550 nm, respectively) Radionics, Ireland.

D.3 Spectral Measurements

UV-Vis spectroscopy for the SP-SO₃H solution (10⁻³ M, 10⁻⁴ M) as well as the kinetic studies of the closing process (MCH⁺-SO₃⁻ → SP-SO₃⁻ + H⁺) were performed using a Cary 50 spectrophotometer (Varian).

D.4 Pending Droplet Method

The pending droplet method was used to measure the surface tension of the spiropyran solutions. The experiments were performed on an optical tensiometer (Teclis Tracker – Wilten Instruments). The surface tension values were calculated automatically by the software of the tensiometer using the Young-Laplace equation.

D.5 UV-Vis Spectroscopy of SP-SO₃H

As seen from Figure D1, the absorbance spectra of SP-SO₃H aqueous solution (10⁻⁴ M) shows that, upon solubilisation in water, the sulfonic acid group of the spiropyran gets deprotonated and the acidic proton is uptaken by the negative phenolic oxygen,

causing the formation of the protonated merocyanine ($\text{MC-H}^+\text{-SO}_3^-$), characterised by an absorption centered at $\lambda_{\text{max}} = 408 \text{ nm}$. The absorption centered at 508 nm is specific to the open merocyanine form (MC-SO_3^-), that is in equilibrium with $\text{MC-H}^+\text{-SO}_3^-$ (Figure D2), although present in a much smaller amount. The band intensities decrease upon irradiation with white light, due to the formation of the closed spiropyran form (SP-SO_3^-) that presents no absorption in the visible region of the spectrum. As seen from Figure D1, upon irradiation with white light the absorption centered at 508 nm, specific to MC-SO_3^- , fully disappears, while a small absorption shoulder due to $\text{MC-H}^+\text{-SO}_3^-$ is still present and this is due to high proton concentration. In these conditions, the equilibrium between $\text{MC-H}^+\text{-SO}_3^-$ (protonated form) and SP-SO_3^- (deprotonated form) cannot be pushed all the way towards SP-SO_3^- by means of white light irradiation.

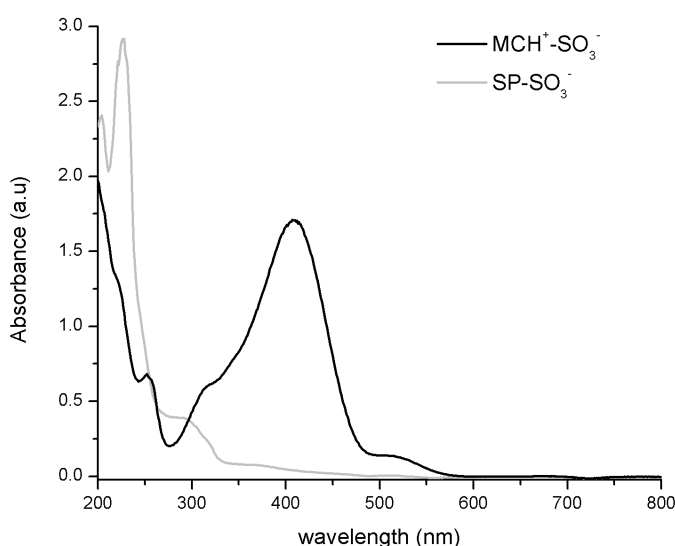


Figure D1. Absorbance spectra of $\text{SP-SO}_3\text{H}$ solution (10^{-4}M), before ($\text{MCH}^+\text{-SO}_3^-$) and after white light irradiation (SP-SO_3^-).

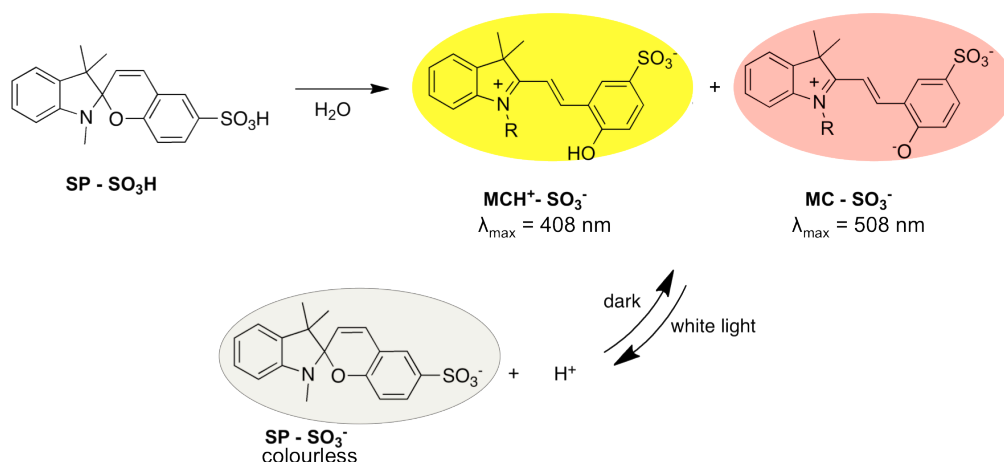


Figure D2. Reversible structural transformations of SP-SO₃H aqueous solution in response to light.

D.6 Kinetics of Photo-Induced Ring Closing

This process involved the formation of the SP-SO₃[−] state by continuous exposure to white light irradiation (LMI-6000 LED Fiber Optic Illuminator obtained from Dolan-Jenner Industries, max. light output = 780 Lumens, used at 30 % of its power and placed at 2 cm distance from the top of the cuvette) and recording the absorbance value of the MCH⁺-SO₃[−], at the corresponding λ_{max} (408 nm) at fixed time intervals (0.1 s) for 2 min. The temperature on the temperature controller of the Varian Cary 50 UV-Visible Spectrophotometer was set to 20.0 ± 0.1 °C.

As seen from Figure D3, as soon as the white light is turned ON ($t = 50 \text{ s}$) the MCH⁺-SO₃[−] starts closing to form SP-SO₃[−]. Equilibrium is achieved after less than 20 s of white light irradiation indicating very fast closing kinetics of the photochromic unit under these specific illumination conditions. The stabilisation of the absorbance value at around 0.18 a.u. shows that in these illumination conditions, at equilibrium, there is still MCH⁺-SO₃[−] present. Once this equilibrium is reached, the concentration of MCH⁺-SO₃[−] remains constant during the measurement.

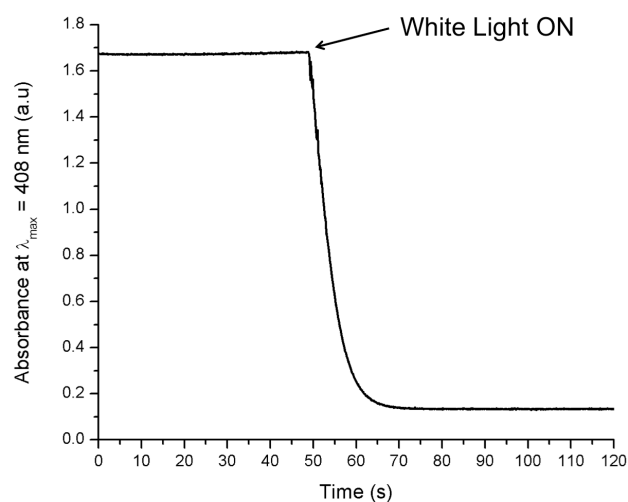


Figure D3. Experimental kinetic curve of the photo-induced ring closing process of SP-SO₃H aqueous solution (10^{-4} M) under continuous white light irradiation.

D.7 UV-Vis Spectroscopy of Chromoionophore I (C1)

As seen from Figure D4, the deprotonated chromoionophore (C1) in DCM (0.03 mM) presents an absorbance band at 540 nm. Upon protonation (C1-H⁺), this band is replaced by the newly emerging protonated bands at 615 and 665 nm.[1]

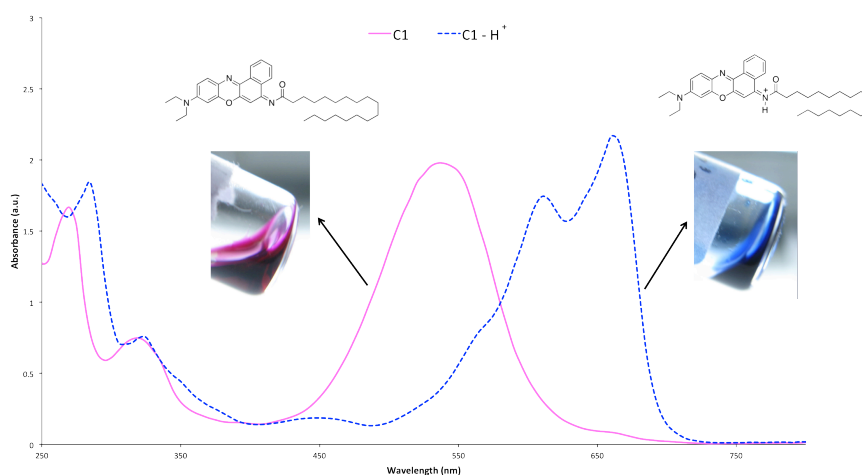


Figure D4. Absorbance spectra of Chromoionophore I solution (0.03 mM) in DCM, in the deprotonated (C1) and protonated (C1-H⁺) states.

D.8 Surface Tension Measurements

Surface tension measurements (see Table D1) done by the pending droplet method indicated that the surface tension (γ) value of the SP-SO₃H after solubilisation in water (MCH⁺-SO₃⁻) is $75.7 \pm 0.5 \text{ mN m}^{-1}$ ($n = 5$) and it remains relatively constant at this value ($\gamma = 75.6 \pm 0.5 \text{ mN m}^{-1}$ ($n = 5$)) after white light irradiation (SP-SO₃⁻). The results indicate that the white light irradiation alone does not change the surface tension of the solution. However, when a microliter size “fuel” droplet is added to the almost colorless (SP-SO₃⁻) solution ($\text{pH} \approx 3.4$), one can see traces of the C1-H⁺ (blue species) getting out of the droplet and dissolving into the aqueous solution (Figure D5 B and D6, meaning that the solubility of C1-H⁺ is now increased in the aqueous solution. This observation is also supported by UV-Vis spectroscopy (Figure D5 C). When the surface tension of the aqueous solution is measured again, it is much smaller ($\gamma = 60.7 \pm 0.3 \text{ mN m}^{-1}$ ($n = 5$)), indicating the presence of the surfactant molecule, in the solution. This difference in surface tension is considerable and can easily explain the propulsion-type movement of the droplet. In these conditions, as soon as the surfactant CI-H⁺ is released from the droplet to the white light irradiated aqueous solution area, the droplet starts moving in the opposite direction to the location of the light, thanks to the surface tension gradient generated.

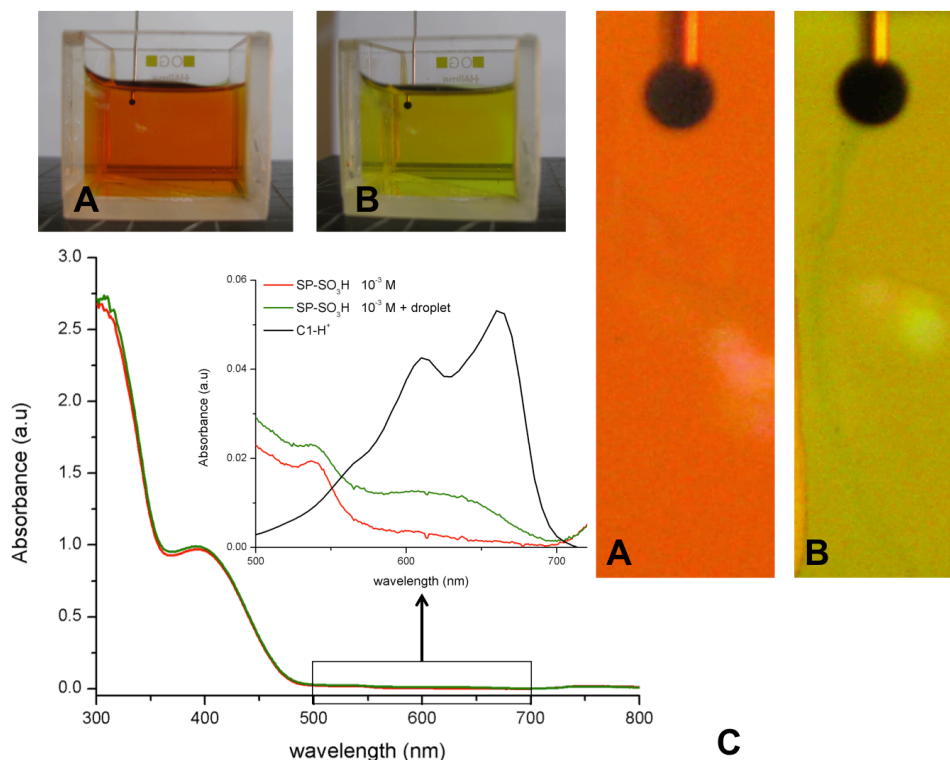


Figure D5. A, B - Photos of the SP-SO₃H solution (10⁻³ M) in which a microliter size “fuel” droplet is placed. The zoom on the photos (right) shows that the solubilisation of C1-H⁺ increases upon white light irradiation. C – UV-Vis spectra of two identical aqueous solutions of SP-SO₃H (10⁻³ M) after irradiation with white light in the absence (red) or presence (green) of the “fuel” droplet. Although the intensity of the new absorbance bands that emerge, in the case when the droplet is present, is small, they match very well the absorbance bands characteristic to C1-H⁺ and the results are reproducible. No other differences in the absorbance spectra between the two solutions were observed.

Table D1. Surface tensions values measured by the pending droplet method for the SP-SO₃H aqueous solution (10⁻³M) in different conditions: before (MCH⁺-SO₃⁻) and after (SP-SO₃⁻ + H⁺) white light irradiation, and after white light irradiation in the presence of C1-H⁺ (SP-SO₃⁻ + H⁺ + C1-H⁺).

| | MCH ⁺ -SO ₃ ⁻ | SP-SO ₃ ⁻ + H ⁺ | SP-SO ₃ ⁻ + H ⁺ + C1-H ⁺ |
|--|--|--|---|
| | pH ≈ 5 | pH ≈ 3.4 | pH ≈ 3.4 |
| Surface Tension (γ) mN m⁻¹ | 75.7 ± 0.5 (n=5) | 75.6 ± 0.5 (n=5) | 60.7 ± 0.3 (n=5) |

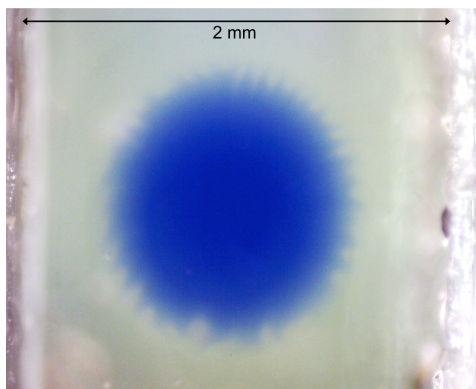


Figure D6. Microscope image of microliter size “fuel” droplet placed in a channel containing the spiropyran solution after white light irradiation. The spiropyran solution is almost colorless (SP-SO_3^-) and its pH has a homogeneous value of about 3.4.

D.9 Droplet Behavior under Different pH Conditions

The behavior of the “fuel” droplet was studied in aqueous solutions of different pHs. It was observed that the droplet presents good stability in a series of aqueous solutions of different pH values: 5.9 (D.I. water), 5.2 (HCl solution), 4.05 (HCl solution). Moreover, in the above conditions, the droplet presented self-healing properties, see video D1. However, at lower pH values (pH 3.4), a microliter size droplet instantly disperses in the aqueous solution (video D2). This is due to the fact that the C1-H^+ , present inside the droplet becomes soluble in the aqueous solution and can leave the droplet. Therefore, the interactions between the two surfactants (C1 and HDA) are destructed and so the droplet is dispersed inside the aqueous solution.

D.10 Mechanism of Photo-propelled Motion of Droplet

The effect of each component produced during white light irradiation and responsible for the droplets propulsion was evaluated. For this purpose, we examined a series of experimental conditions for the photo-propelled organic droplets using different channels geometries and white light irradiation sources at different intensities. The channels geometries used in this study were straight lines, cross-shaped or double-cross shaped channels, 2 mm wide, 1 mm high and with lengths between 5-5.5 cm. The white light irradiation was provided via a LMI-6000 LED Fiber Optic Illuminator obtained from Dolan-Jenner Industries (780 Lumens, 30 % Power) or via a single white light LED (4 Lumens).

On the basis of these results, we interpreted that the movement of the organic droplet in the presence of white light irradiation consists of four stages. Stage 1: the droplet is stable on the aqueous solution containing the spiropyran derivative, present mostly in its protonated merocyanine form ($\text{MCH}^+\text{-SO}_3^-$, 10^{-3} M, $\text{pH} \approx 5$), since none of the droplet components (HDA, C1-H^+) present good solubility in the aqueous solution. Stage 2: irradiation with white light in the proximity of a droplet causes a local drop in solution pH (from approximately 5 to 3.4) due to the conversion of the $\text{MCH}^+\text{-SO}_3^-$ to SP-SO_3^- and release of protons. Stage 3: the localised drop in pH causes protonation of DA^- at the interface converting it to its neutral HDA form. In order to maintain C1-H^+ leaves the interfaces and moves into the aqueous solution (see above), while HDA migrates back into the droplet. The solubilisation of C1-H^+ into the aqueous solution causes a local drop in the surface tension due to the surfactant proprieties of C1-H^+ . Since the concentration of C1-H^+ in the aqueous solution will be always greater in the area facing the irradiation source, this imbalance in surface tension outside the droplet will drive the motion away from the light source. Figure D7 shows the chemical equilibrium reached inside the droplet at Stage 3. Stage 4: the droplet stops in the high pH region away from the illuminated area (initial conditions) where its composition becomes again stable.

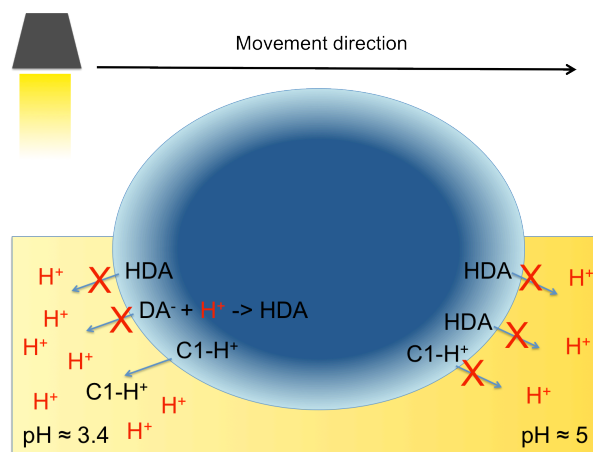


Figure D7. Irradiation with white light causes a localised drop in pH, due to the conversion of $\text{MCH}^+\text{-SO}_3^-$ to SP-SO_3^- , in the aqueous solution (yellow). This triggers the droplet to release C1-H^+ surfactant in the direction facing the light source, producing a decrease in the surface-tension around the droplet, in the region closer to the light irradiation (right side of the droplet). This causes the motion of the droplet away from the low-pH region. Arrows indicate possible or forbidden movements of the droplet components, from the DCM droplet to the aqueous solution.

D.11 Examples of Photoactivated Chemopropulsion

Video D3 shows photo-activated chemopropulsion when five different droplets with volumes between 0.2-1 μL were placed in the central positions of a cross-shaped fluidic structure after which, a white light source is introduced from the right side of the frame.

Video D4 shows photo-activated chemopropulsion when four different droplets with volumes between 0.2-1 μL were placed in the central position of a cross-shaped fluidic structure after which, a white light source is introduced from the center of the frame.

Video D5 shows photo-activated chemopropulsion of a single 0.5 μL size droplet when the white light irradiation source is one single white light LED.

The videos were done under controlled external light conditions. However, since the camera automatically adjusts the white balance of the frame in order to obtain the best picture quality, the light intensity might seem much higher than actually is.

D.12 References

1. Zhu, J.; Zhai, J.; Li, X.; Qin, Y., Applications of hydrophobic room temperature ionic liquids in ion-selective optodes. *Sensors and Actuators B-Chemical* **2011**, 159, 256-260.

Appendix E

Supporting Information for **Self-assembled Solvato-morphologically Controlled Photochromic Crystals**

Larisa Florea ¹, Silvia Scarmagnani ¹, Dermot Diamond ¹ and
Fernando Benito-Lopez ^{1,2 *}

Angewandte Chemie Angewandte Chemie International Edition,
submitted

¹CLARITY: Centre for Sensor Web Technologies, National Centre for Sensor Research, School of Chemical Sciences, Dublin City University, Dublin, Ireland;

²CIC microGUNE, Arrasate-Mondragón, Spain, Tel.: +34 943710212

*Author to whom correspondence should be addressed;

E.1 Synthesis and Characterization of SP-COOH

The spiropyran derivative used in this study, namely 11' -(3-carboxypropyl)-3,3' -dimethyl-6- nitrospiro-[2H-1]-benzopyran-2,2'-indoline (SP-COOH), was produced in a three-step sequence as described elsewhere [1]. ^1H NMR (300 MHz, CDCl_3): 1.19 (3H, s, 3'- CH_3), 1.29 (3H, s, 3'- CH_3), 1.95 (2H, m, N- $\text{CH}_2\text{CH}_2\text{CH}_2$ -), 2.41 (2H, t, J: 7 Hz, N- $\text{CH}_2\text{CH}_2\text{CH}_2$ -), 3.22 (2H, m, N- $\text{CH}_2\text{CH}_2\text{CH}_2$ -), 5.88 (1H, d, J: 10 Hz, H-3), 6.62 (1H, d, J: 8 Hz, H-7'), 6.74 (1H, d, J: 9 Hz, H-8), 6.88 (1H, m, H-5'), 6.89 (1H, d, J: 10 Hz, H-4), 7.09 (1H, d, J: 8 Hz, H-4'), 7.19 (1H, t, J: 8 Hz, H-6'), 7.99 (2H, m, H-5 and H-7). Identical ^1H NMR spectra were obtained in the case of all the microstructures.

IR spectroscopy was employed to study the chemical structure of SP-COOH microstructures in comparison with SP-COOH obtained throughout the evaporation of a homogeneous EtOH solution (Figure E2). IR spectra were recorded on a Perkin Elmer Spectrum GX FT-IR System® using an ATR unit. 64 scans were performed in the spectral range from 4000 cm^{-1} to 600 cm^{-1} with a resolution of 1.00 cm^{-1} . The typical FT-IR bands and their assignments are shown in Table E1 [2, 3]. As presented, no differences were obtained between the FT-IR spectrum of the solid SP-COOH obtained after the evaporation under white light of a homogeneous EtOH solution and of the solid SP-COOH (15 %) microstructures in similar illumination conditions.

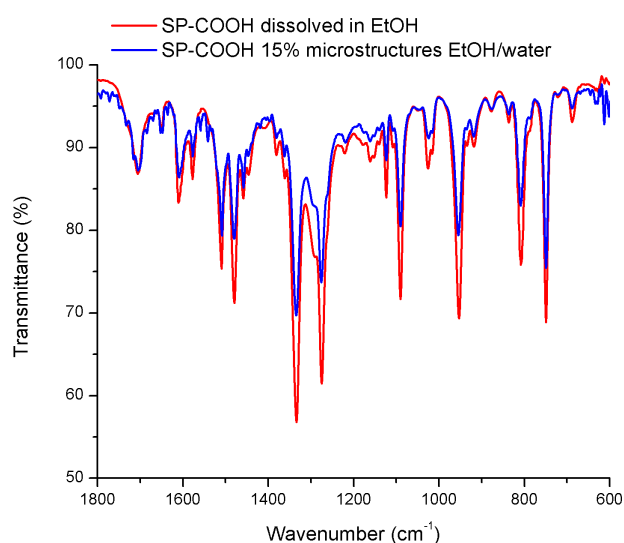


Figure E1. FT-IR spectra of SP-COOH obtained from an EtOH solution and SP-COOH self-assembled microstructures obtained from EtOH/water mixture.

Table E1. Important FT-IR frequencies for SP-COOH from solution and SP-COOH self-assembled microstructures and their assignments.

| Assignment | SP-COOH from solution Wavenumber (cm⁻¹) | SP-COOH microstructures Wavenumber (cm⁻¹) |
|--|---|---|
| C=O | 1705 | 1705 |
| C=C stretch | 1609 | 1609 |
| C=N ⁺ | 1577 | 1576 |
| NO ₂ sym stretch | 1509 | 1508 |
| C-C aromatic ring stretch | 1479, 1458 | 1479, 1457 |
| NO ₂ asym stretch | 1334 | 1334 |
| C-O-C ether sym stretch | 1275 | 1276 |
| C-O ester stretch | 1161 | 1161 |
| C-O ester stretch | 1090 | 1090 |
| C-C-N bend | 1025 | 1024 |
| O-C-N stretch, C=CH; CH out of plane deformation (<i>cis</i>) | 953 | 954 |
| C-H bending | 809 | 808 |
| C-H bending | 749 | 749 |
| C-H bending | 688 | 688 |

E.2 Absorbance Spectra of SP-COOH in EtOH

UV-Vis Spectroscopy was employed to characterize SP-COOH solution in EtOH (10⁻³ M, Figure E2). The UV/Vis absorption spectra were obtained using a Perkin Elmer Lambda 900 UV/Vis/NIR spectrometer. All spectra were obtained in the wavelength region spanning from 300 to 800 nm, using a 1 nm data interval. For the switching of the spiropyran to the merocyanine form, the solution was irradiated for 30 s with UV light. The UV irradiation source was an array of 9 UV LEDs placed at a distance of 1 cm from the spiropyran solution. The LEDs have an emission wavelength peak at 365 nm and an optical output power of 1.2 mW, supplied by

Roithner Lasertechnik Austria. The white light irradiation source used for the switching of MC back to SP form was a LMI-6000 LED 211 Fiber Optic Illuminator obtained from Dolan-Jenner Industries. The irradiation time was also in this case fixed to 30 s.

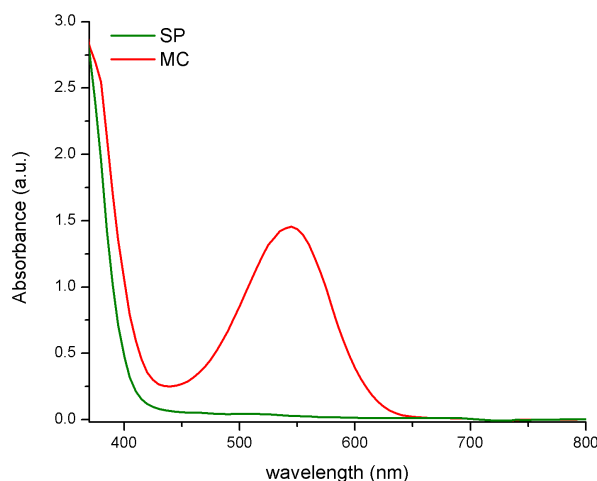


Figure E2. Absorbance spectra of SP-COOH derivative in EtOH (10^{-3} M) in its two forms – closed spiropyran (SP) and open merocyanine (MC).

As it can be seen from Figure E2, the MC-COOH form shows an absorbance band in the visible region centered around 550 nm. In contrast, the SP-COOH form does not show any absorbance band in the visible region.

E.3 Photos of SP-COOH Solution in EtOH (10^{-3} M) and SP-COOH Dispersions in EtOH/Water (25 % EtOH)

Figure E3 shows photos of the SP-COOH solution in EtOH (10^{-3} M) in comparison with the same solution after the addition of 75% deionised water (SP-COOH 25 %) in the dark. One can observe that while SP-COOH solution in EtOH (10^{-3} M) shows good transparency indicating the full solubilisation of SP-COOH in EtOH at 10^{-3} M concentration, the addition of 75 % (V %) deionised water causes a change in colour due to changes in polarity and increased turbidity due to the formation MC-COOH individual micro-size structures caused by the poor solubility of the MC-COOH in water.

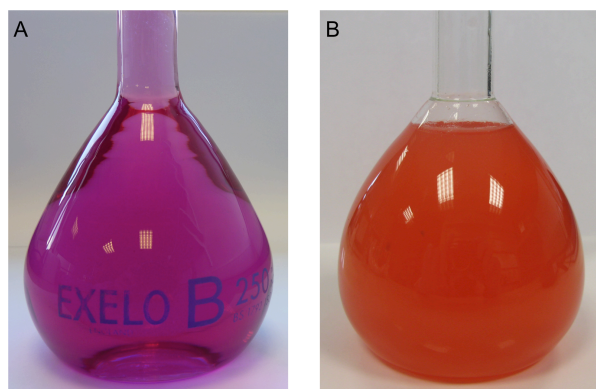


Figure E3. Photos of (A) SP-COOH solution in EtOH (10^{-3} M) in comparison with (B) the same solution after the addition of 75% deionised water, corresponding to SP-COOH 25 %. Both solutions were photograph immediately after they were taken from dark.

E.4 Equilibrium of SP-COOH Derivative in EtOH/Water Solution

Mixing of SP-COOH 10^{-3} M solution in EtOH with water (V % of water – 85 %, 80 % and 75 %, respectively) causes the formation of individual MC-COOH microstructures due to decreased solubility of the SP-COOH derivative in the EtOH/water mixture compared with in pure EtOH. However, a substantial amount of the spiropyran derivative still remains soluble in the solvent mixture. Figure E4 shows the possible reversible structural transformations of SP-COOH in EtOH (A) - water (B) solution in response to light. The corresponding absorbance spectra of SP-COOH in EtOH/water solution are shown in Figure E5 and were realized using the setup described before. Similar spectra were obtained for all of the solutions studied (filtrates obtained from SP-COOH 15 %, SP-COOH 20 % and SP-COOH 25 %, respectively) with the intuitive observation that as the V % of water increases, the absorbance band corresponding to the MC-COOH form decreases. Figure E5 shows a representative example of SP-COOH 25 %.

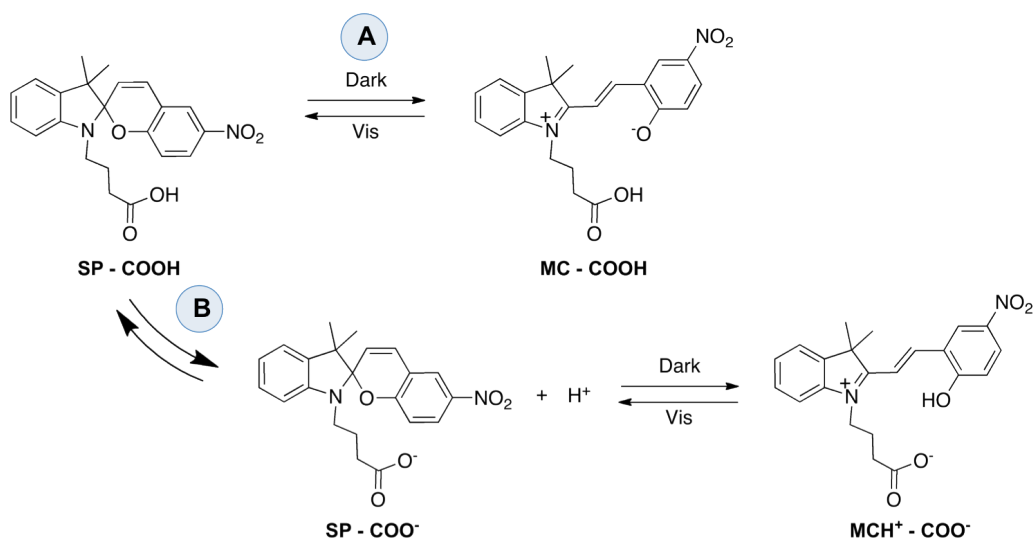


Figure E4. Reversible structural transformations of SP-COOH EtOH (A) / water (B) solution in response to light.

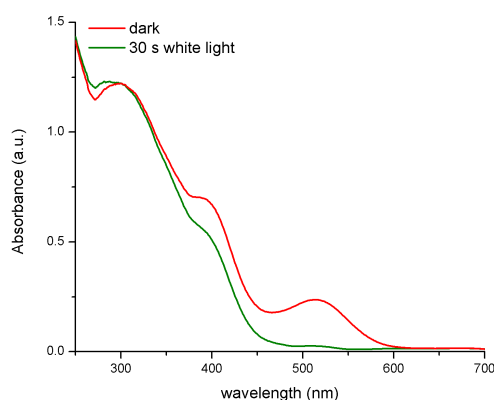


Figure E5. Absorbance spectra of SP-COOH 25 % after the removal of the microstructures under different illumination conditions (dark and 30 s white light irradiation, respectively).

As seen from Figure E5, the solution of SP-COOH in 25 % EtOH/75 % water taken from the dark shows three main absorbance bands. The first absorption band (300 nm) is characteristic of the SP-COOH form (Figure E4). The band centered on 515 nm is specific of the MC-COOH form. This absorption decreases upon irradiation with white light due to the switching of the MC-COOH back to the SP-COOH form (Figure E4 A). The absorption centered around 490 nm is specific of the MCH⁺-COO⁻ specie formed through the protonation of SP-COO⁻ by the H⁺ coming from the partial dissociation of carboxylic acid in water (Figure E4 B). This band also decreases upon irradiation with white light due to the formation of SP-COO⁻.

E.5 Interfacial Self-assembly

Interfacial self-assembly at the liquid/air interface was followed using an Aigo digital microscope, The Dolomite Centre Ltd at a 60X magnification. A representative example is given in Figure E6 for SP-COOH 25 %.

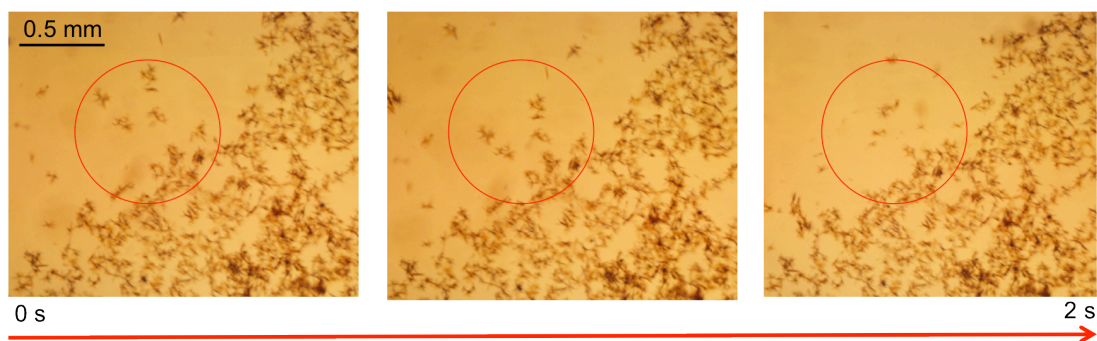


Figure E6. Sequence of microscopy images showing the self-assembly of SP-COOH 25 % microstructures into a single film at the liquid/air interface. For the full video please refer to Video S1.

Pictures of the interfacial self-assembly of SP-COOH 15 % and 25 % are shown in Figure E7 and E8.

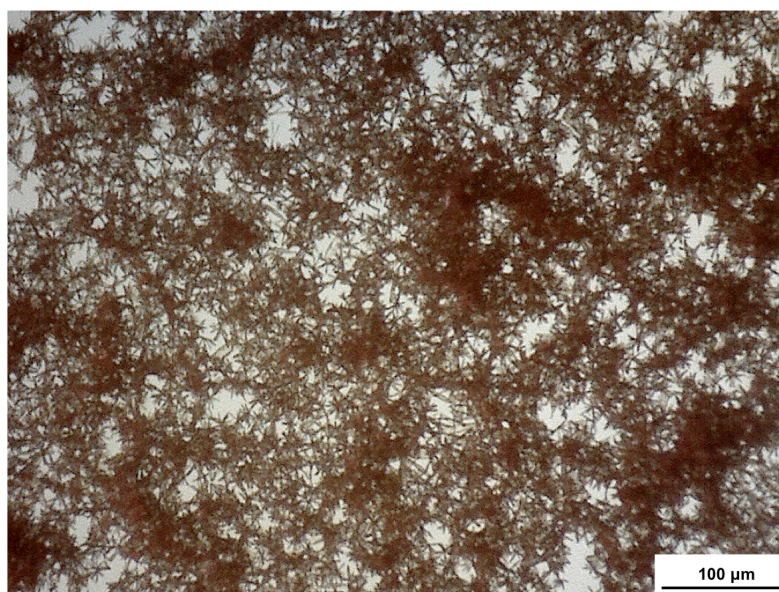


Figure E7. Interfacial agglomeration of SP-COOH 15 %.

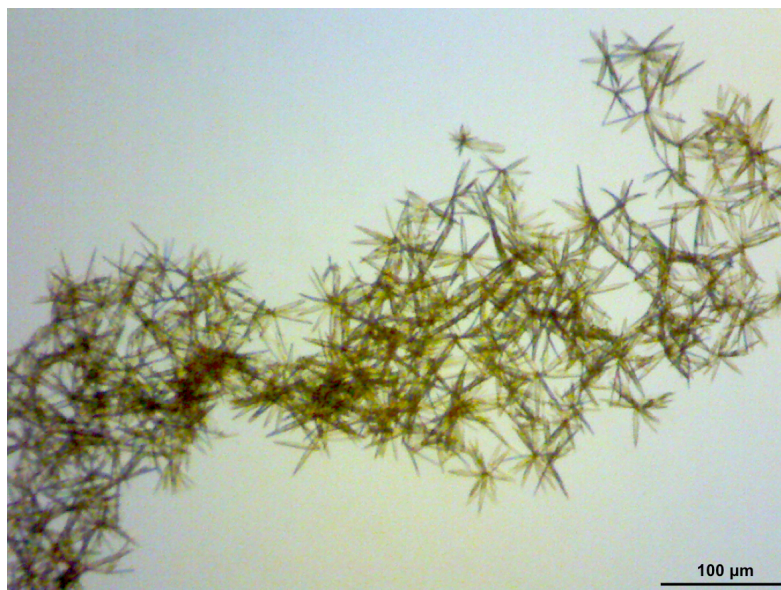


Figure E8. Interfacial agglomeration of SP-COOH 25%.

E.6 Scanning Electron Microscopy

Scanning Electron Microscopy was used to image the self-assembled microstructures corresponding for SP-COOH 25% (Figure E9), SP-COOH 20% (Figure E10) and SP-COOH 15% (Figure E11). The imaging was performed on a Carl Zeiss EVOLS 15 system at an accelerating voltage of ~ 10 kV. Prior to imaging the samples were coated with a 10nm layer gold.

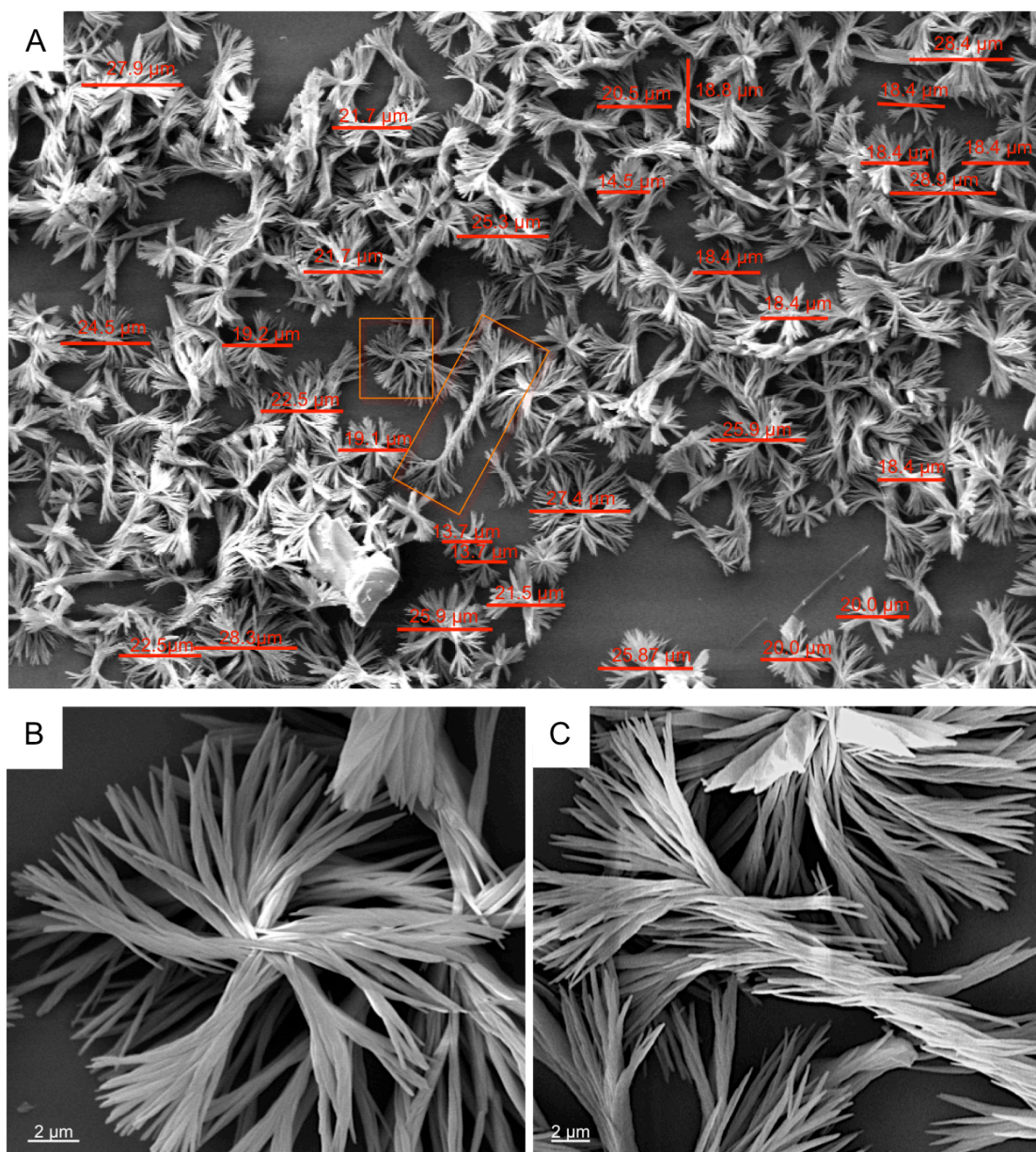


Figure E9. Self-assembled micro-structures of SP-COOH 15 %.

As seen in Figure E9, the assembled microstructures presented diameters ranging from 14 μm to 27 μm . The majority of the structures showed a ribbon-like appearance assembled in a daisy-like structure (Figure E9, B) although few elongated structures (Figure E9, C) were also observed.

Daisy-like structures are obtained for SP-COOH 20 %, having diameters ranging from 34 μm to 53 μm (Figure E10).

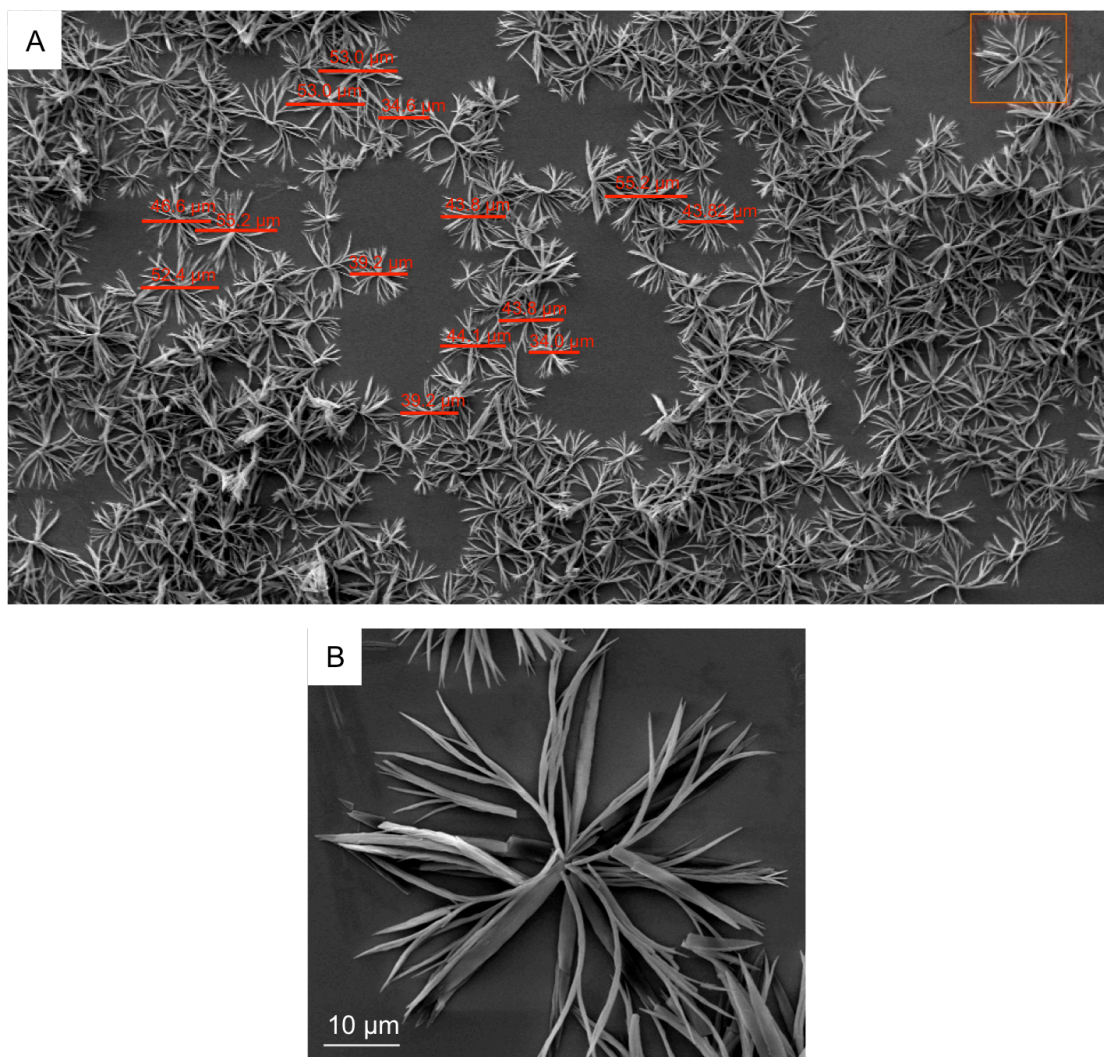


Figure E10. Self-assembled microstructures of SP-COOH 20 %.

Daisy-like structures formed of flat crystals are obtained for SP-COOH 25 %. The diameter of these structures varied from 65 μm to 78 μm , although smaller structures or larger single unit crystals may also be observed (Figure E11).

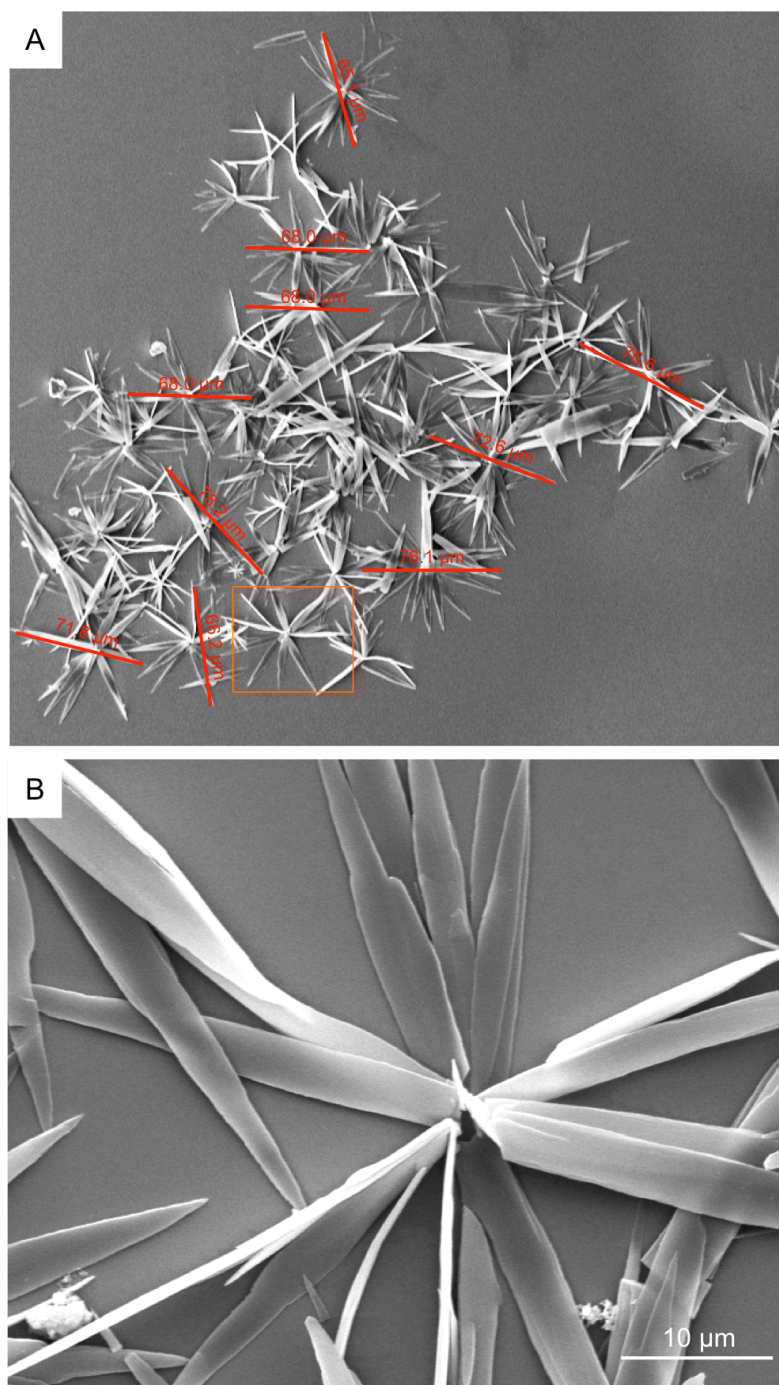


Figure E11. Self-assembled microstructures of SP-COOH 25 %.

E.7 Absorbance Spectra of SP-COOH Microstructures

UV–Vis spectroscopy was used to study the photochromic behavior of spiropyran microstructures (SP-COOH 15 %, SP-COOH 20 % and SP-COOH 25 %). The absorbance spectra were recorded in reflectance mode using a fiber-optic light guide

connected to a Miniature Fiber Optic Spectrometer (USB4000 – Ocean Optics) and a specially designed probe holder. The light source was a LS-1 tungsten halogen lamp (white light) obtained from Ocean Optics, Inc. Data from the spectrometer was processed using Spectrasuite software provided by Ocean Optics Inc. For clarity, the absorbance spectra recorded were smoothed using Origin software using Savitzky–Golay algorithm. Photoconversion of the microstructures from SP to MC form was achieved using an in-house fabricated UV light source consisting of three UV LEDs (Roithner LaserTechnik GmbH, emission $\lambda_{\text{max}} = 375 \text{ nm}$). The microstructures were placed 2 cm from the source and irradiated at a power of 0.4 mW cm^{-2} for 1 min. The white light irradiation was provided via a LMI-6000 LED Fiber Optic Illuminator obtained from Dolan-Jenner Industries and was used to switch the MC form back to the closed SP. The photo-conversion was observed both at the liquid/air interface (Figure E12), but also in the solid state.

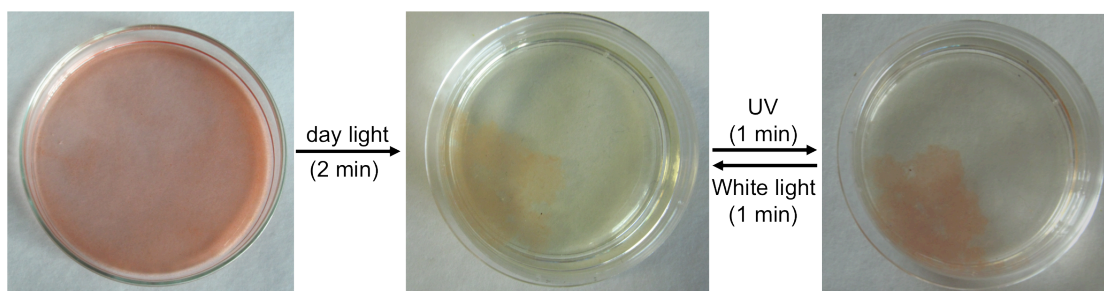


Figure E12. Sequence of photos showing the formation of the self-assembled aggregates at the liquid air/interface and their switching between the SP and MC form.

E.8 Microscopy Imaging of SP-COOH 25 % Microstructures under Cross Polarizers

Spontaneous SP-COOH 25 % assemblies showed a bright image under the microscope with crossed polarizers (Figure E13).

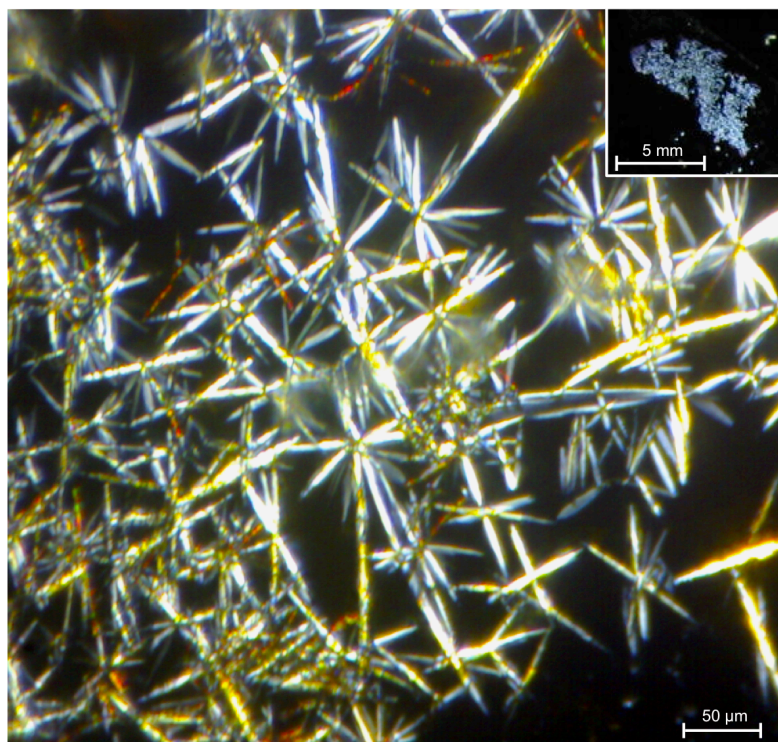


Figure E13. Microscopy image of SP-COOH 25 % under crossed polarizers.

E.9 Guided Interfacial Aggregation

As the assembly of the microstructures towards the liquid/air interface is driven by the evaporation of EtOH, guided evaporation was achieved throughout the use of a 150 W DDL Halogen lamp obtained from Polytec GmbH Waldbronn, Germany. The lamp was placed at a distance of 4 cm from one side of the Petri dish. The process is shown in Video S2. The microstructures form immediately at the interface and they are moving towards the illuminated area. In time, new assemblies of various sizes are formed that will start to migrate in the same direction. The video is presented in real time, showing the fast movement of the structures towards the light. This behavior has given the SP-COOH 25 % crystals the name of “crystal moths”.

E.10 References

1. Rosario, R.; Gust, D.; Hayes, M.; Jahnke, F.; Springer, J.; Garcia, A. A., Photon-modulated wettability changes on spiropyran-coated surfaces. *Langmuir* **2002**, *18*, 8062-8069.

2. Delgado-Macuil, R.; Rojas-Lopez, M.; Gayou, V. L.; Orduna-Diaz, A.; Diaz-Reyes, J., ATR spectroscopy applied to photochromic polymer analysis. *Materials Characterization* **2007**, 58, 771-775.
3. Fries, K. H.; Driskell, J. D.; Samanta, S.; Locklin, J., Spectroscopic Analysis of Metal Ion Binding in Spiropyran Containing Copolymer Thin Films. *Analytical Chemistry* **2010**, 82, 3306-3314.